

Supplementary Information

Enhancing the performance for palladium catalysed *tert*-butyl hydroperoxide-mediated Wacker-type oxidation of alkenes

Matthew N. Blair,^a Meadhbh Murray-Williams,^a Calum Maguire,^a Clare L. Brown,^a Qun Cao,^a Hongxin Chai,^a Yitong Li,^a Róisín L. O'Hagan,^a Paul Dingwall,^a Panagiotis Manesiotis,^a Catherine L. Lyall,^b John P. Lowe,^b Ulrich Hintermair,^c Peter C. Knipe^a and Mark J. Muldoon^{a*}

a. School of Chemistry and Chemical Engineering, Queen's University Belfast
m.j.muldoon@qub.ac.uk

b. Department of Chemistry / Dynamic Reaction Monitoring Facility, University of Bath

c. Department of Chemistry / Dynamic Reaction Monitoring Facility / Institute for Sustainability, University of Bath

Contents

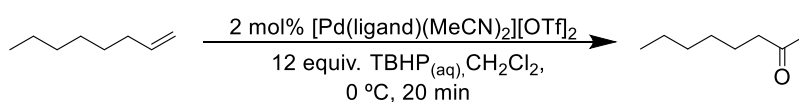
Additional Data and Discussion	4
Initial Screening of Ligands using 1-octene	4
Development of One Step Coupling Method to Second Generation PBO Ligands and Synthesis of Ligand and Catalyst Library	5
<i>In-situ</i> Catalyst Formation Screening using Sigman Conditions (DCM and Ag[SbF ₆])	8
Switching to Trifluoromethanesulfonate (Triflate) Anions	10
Triflate vs bis(trifluoromethanesulfonyl)imide as Counterion.....	13
Solvent Screening and Temperature Effects	14
¹⁹ F DOSY NMR in Toluene with Aqueous TBHP	19
Using Anhydrous TBHP/organic Solvent Mixtures for Wacker Oxidation.....	22
¹⁹ F DOSY Analysis of Wet vs Dry Reaction Mixtures for 1-octene Oxidation in Chlorobenzene.....	26
Monitoring Speciation of Catalyst in Wet vs Dry Acetonitrile	33
Inhibition Studies.....	37
Oxidation of Oct-1-en-3-yl acetate.....	40
Using HFIP to Prevent Substrate/Product Inhibition.....	43
Using HFIP to Reduce Catalyst Deactivation under Aqueous TBHP Conditions.....	46
Comparison of 5-CF ₃ Catalyst at 0.25 mol% Loading under Dry and Aqueous Conditions with HFIP51	
Re-evaluating All Second Generation PBO Catalysts in the Absence of Several Catalyst Deactivation Mechanisms	53
Mechanisms of Catalyst Deactivation	58
Comparison of 5-CF ₃ Ligand vs Quinox Under Optimized Conditions.....	62
Experimental	66
General Considerations	66
Notes on Safety	68
Preparation of Anhydrous TBHP solutions.....	69
Catalytic Reactions	70
General procedure for testing ligand and cationic catalysts formed in-situ with silver salts and aqueous TBHP using 1-octene as substrate:.....	70
General procedure for testing ligand and pre-formed cationic catalysts using aqueous TBHP for both 1-octene and oct-1-en-3-yl acetate:	71
General procedure for testing ligand and pre-formed cationic catalysts using anhydrous TBHP for both 1-octene and oct-1-en-3-yl acetate	72
General procedure for catalyst screening at 0.25 mol% catalyst loading.....	73
General procedure for 1 mol% catalyst loading with aqueous TBHP (Figures 8 & 9 in the main manuscript)	74

“Gram-scale” oxidation of oct-1-en-3-yl acetate	75
Control experiments to examine the potential effect of hexafluoroacetone on catalytic reactions.	76
Figure S56: ¹⁹ F NMR analysis of post-reaction mixture where 20 equiv. of HFIP and 1 equiv. of HFA trihydrate had been added	78
A Note on Reproduceability	79
Job Plot Analysis of HFIP with Oct-1-en-3-yl acetate and 2-oxooctan-3-yl acetate using ¹ H-NMR ...	80
Synthesis of Ligands and Pd(II) Complexes	83
General procedure for the one-step coupling reaction of benzoxazole with aryl pyridines:.....	84
Synthesis of (ligand)PdCl ₂ complexes	91
Synthesis of Substrates and Corresponding Products.....	107
Synthesis of 2-(5-(trifluoromethyl)pyridin-2-yl)benzo[d]oxazole <i>N</i> -oxide.....	108
¹⁹ F DOSY Experimental Details	109
X-Ray Crystallography	110
NMR Spectra.....	112
References	156

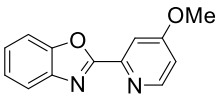
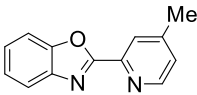
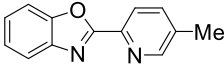
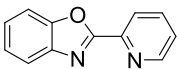
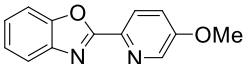
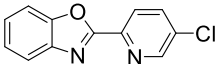
Additional Data and Discussion

Initial Screening of Ligands using 1-octene

Previous work in the Muldoon group had utilized PBO-type complexes for hydrogen peroxide mediated Wacker-type oxidations.^{1,2} We found that while the dicationic PBO catalyst worked well for styrenes, it was not suitable for aliphatic alkenes and quickly isomerized terminal alkenes to internal alkenes. We had tested a number of PBO complexes for aerobic Wacker-type reactions,³ and we wanted to explore such complexes for TBHP mediated wacker reactions. Table S1 shows our initial TBHP tests with some of these complexes.



SUBSTITUTION ON PYRIDINE

Ligand	Yield (%)
	45
	51
	60
	63
	48
	70

SUBSTITUTION ON BENZOXAZOLE

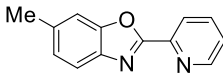
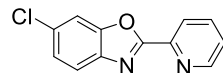
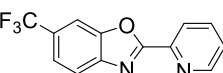
Ligand	Yield (%)
	60
	61
	59

Table S1: Initial screening of ligands under Sigman type conditions.⁴

These initial conditions for the screening were chosen as they are similar to those used by Sigman and co-workers for similar aliphatic olefins in their Quinox work with TBHP.⁴

From these initial tests, it indicated that the electronics of the pyridine portion of the ligand had a greater effect on the performance of the catalyst, while substitution on the benzoxazole moiety did not produce large effect on yield, with both electron withdrawing and electron donating groups giving very similar results to each other and that of the underivatized PBO ligand. Despite variances in yield, all the catalysts showed high selectivity for the 2-octanone and gave very little isomerization (2-5%). This was not the case when [(PBO)Pd(NCMe)][OTf]₂ was previously tested as a catalyst for the oxidation of 1-octene with hydrogen peroxide, where almost exclusive isomerization of the double bond was found in MeCN, DMA and acetone.¹

Development of One Step Coupling Method to Second Generation PBO Ligands and Synthesis of Ligand and Catalyst Library

To further explore the influence of electronics and to try and develop better catalysts, ligands containing groups that are even more electron withdrawing than the 5-Cl were synthesized. The Pd(II) catalyst precursor was also synthesized in one step from commercially available starting materials, using a method which was based on a combination of conditions from previous publications.^{5, 6}

In the first instance we utilized 5 mol% loading of the PdCl(C₃H₅)(dppb) catalyst to prepare ligands (Figure S1). In the case of the 5-CF₃ substituted PBO ligand (which we found to be the best for TBHP Wacker), we demonstrated that the dppb catalyst loading could be dropped to 1 mol% and average yields of 70% and 72% could be obtained using the chloro and bromo pyridine substrates respectively.

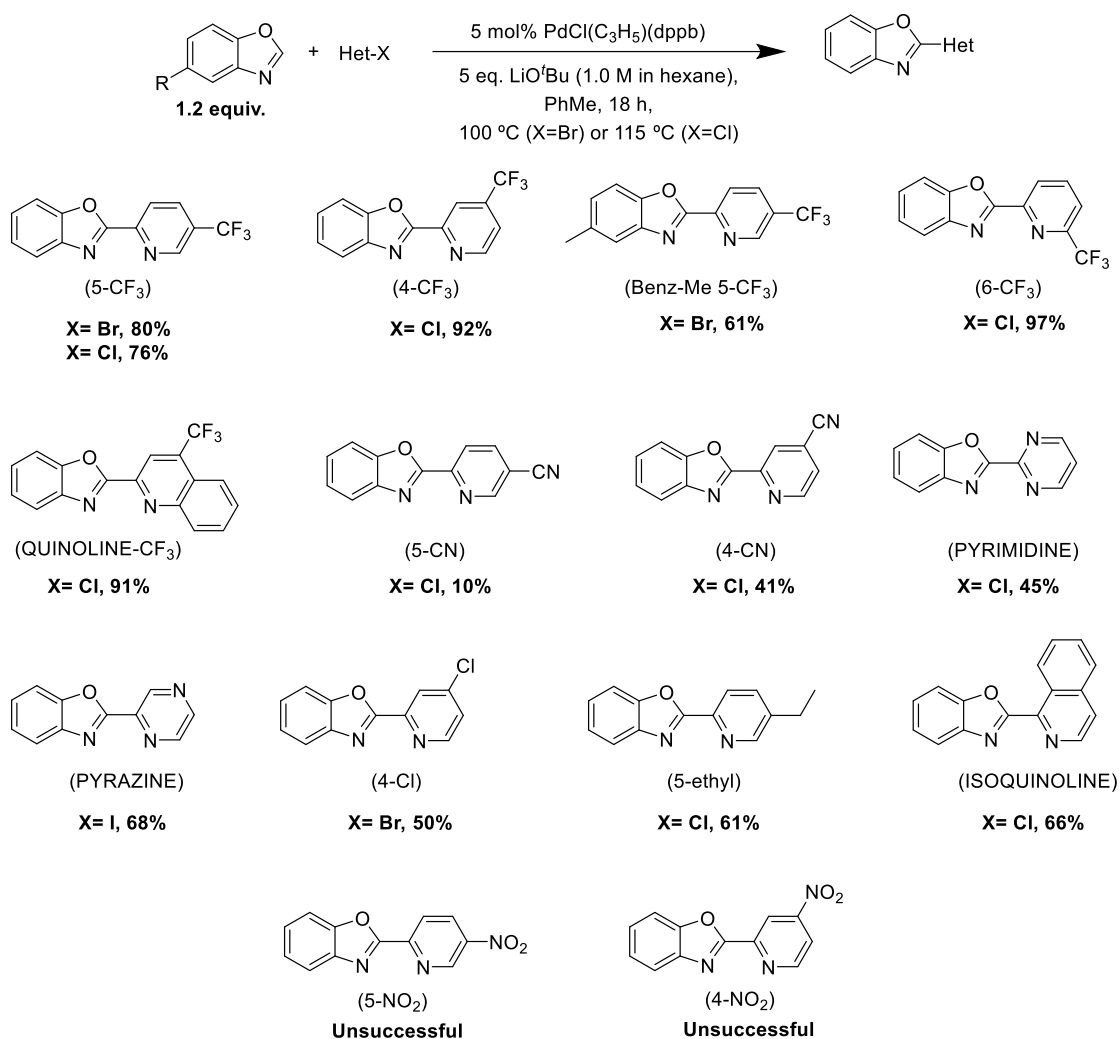


Figure S1: One-step coupling procedure to second generation PBO ligands synthesised over the course of this work with yields in bold. Abbreviations for each ligand shown in brackets.

The active catalysts in these Wacker reactions are cationic species and can be formed in two distinct ways. One method forms the active catalyst *in situ* by halide abstraction of the corresponding chloro complexes with silver salts ($\text{Ag}[\text{SbF}_6]$, $\text{Ag}[\text{Tf}_2\text{N}]$ and $\text{Ag}[\text{OTf}]$). The other method forms an isolated triflate cationic complex, which is made through reaction of the corresponding acetate complexes with triflic acid, $\text{CF}_3\text{SO}_3\text{H}$, or bistriflimidic acid, $(\text{CF}_3\text{SO}_2)_2\text{NH}$ (Figure S2).¹ The dicationic MeCN/H₂O ligated isolated complex can be precipitated out of solution by addition of Et₂O. The *in-situ* method of catalyst formation was applicable to all ligands used in this work except for the 6-CF₃ ligand where the chloro complex could not be formed and so we were unable to obtain any catalytic Wacker data for this ligand. The acid method was found to not be suitable with ligands containing more sensitive functional groups such as nitriles, pyrazines and

pyrimidines where the complexes could not be precipitated from solution, presumably due to adverse reactions in the presence of strong acid.

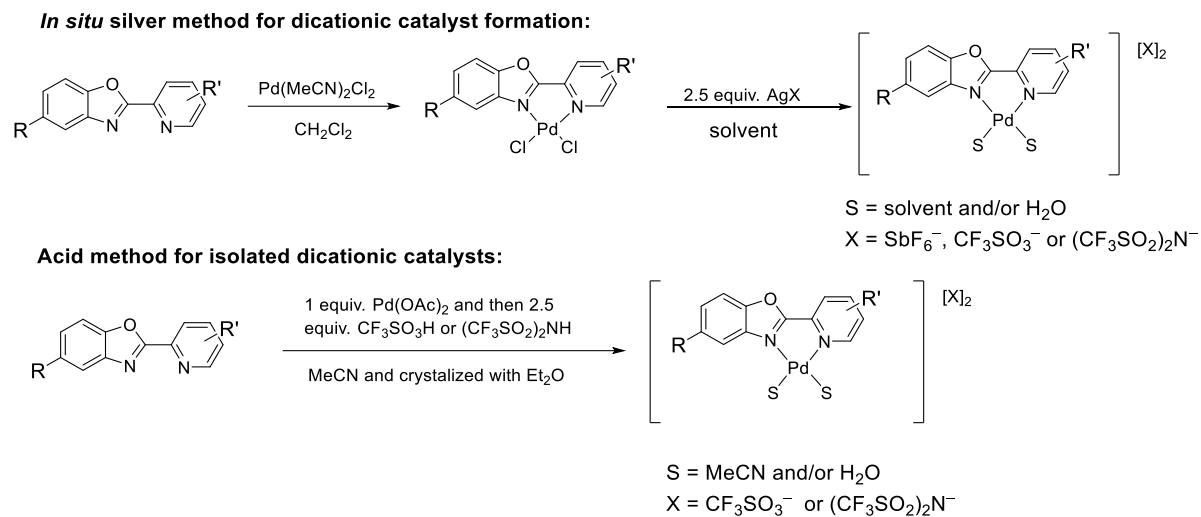


Figure S2: Outline of methods used to form active cationic Pd complexes for Wacker oxidations

***In-situ* Catalyst Formation Screening using Sigman Conditions (DCM and Ag[SbF₆])**

The newly synthesised ligands were evaluated using the literature conditions that were found to be optimum for Quinox, allowing a direct comparison with the literature benchmark.⁴ The reactions were followed by gas chromatography (GC) analysis over a period of 30 minutes and kinetic plots constructed for each ligand (Figure S3).

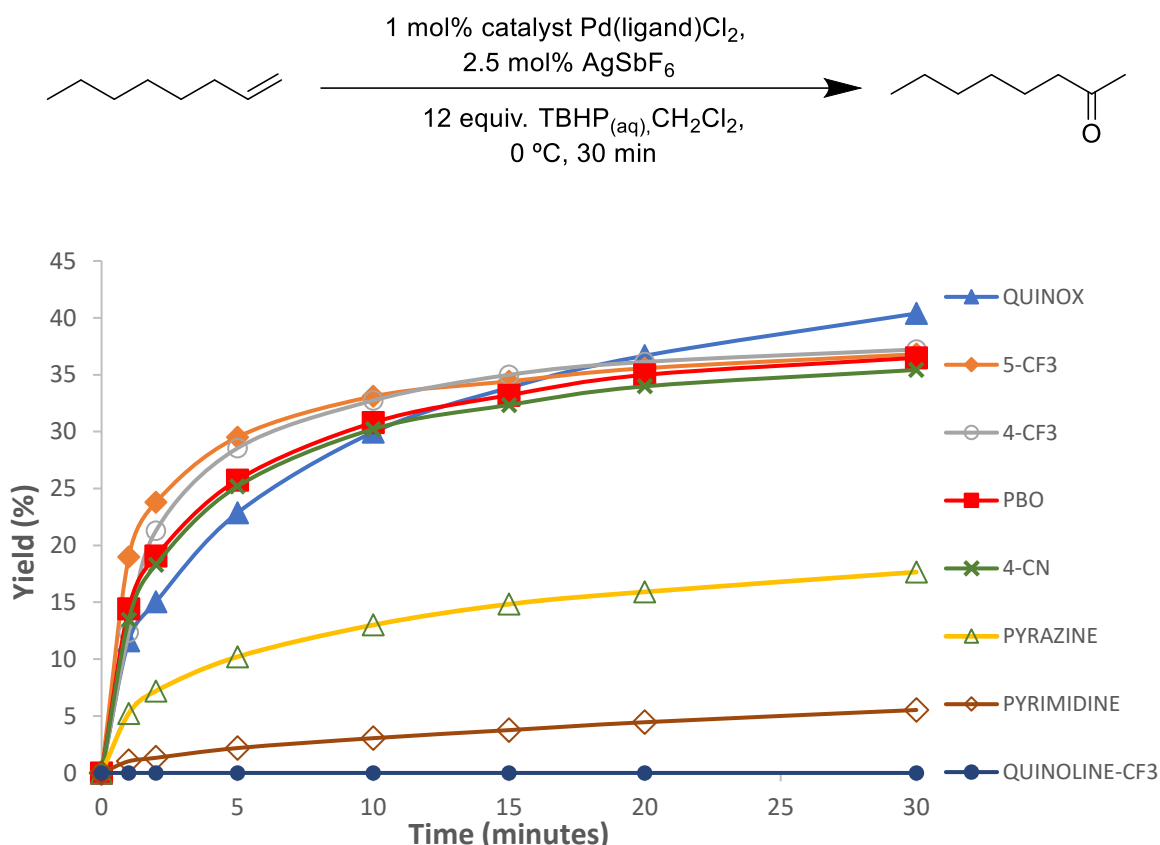


Figure S3: Evaluation of ligands for oxidation of 1-octene using *in situ* catalyst formation with Ag[SbF₆]. Each kinetic plot is an average of two runs.

Overall, ligand structures based on the benzoxazole-pyridine model perform considerably better than those with non-pyridine heterocycles as donors. Ligands bearing the pyrazine and pyrimidine rings both gave low yields for the 2-octanone, possibly due to the ability of the two N-atoms in the rings to bind to more than one electrophilic Pd centre upon formation of the cationic complex. If this was to occur and aggregates were to form, the free sites on the Pd centre to which the alkene and TBHP bind would no longer be available.

Interestingly, the ligand bearing the 4-CF₃-quinoline group gave no product formation and was in fact found to promote rapid isomerization of the double bond. Analysis of the reaction after 1 minute showed complete isomerization of the 1-octene to a mixture of internal alkene isomers. As the reaction progressed, small amounts of these internal alkenes began to be oxidised to the corresponding ketones. This contrasts the performance of the 4-CF₃-PBO ligand which gave fast oxidation of 1-octene (Figure S3). It is also worth noting the similarity to the second generation Quinox-CF₃ ligand synthesized by Sigman and co-workers, which gives the best initial rates for oxidation of oct-1-en-3-yl acetate.⁷ The PNO ligand also shown in Figure S4, which was developed in our lab and gave the best performance for the aerobic Wacker oxidation of styrenes.³ This PNO ligand was tested using TBHP for 1-octene oxidation rapid isomerization of the double bond also occurred. These results illustrate that that relatively small changes to ligand structure result in large differences in performance and that steric factors may promote isomerization.

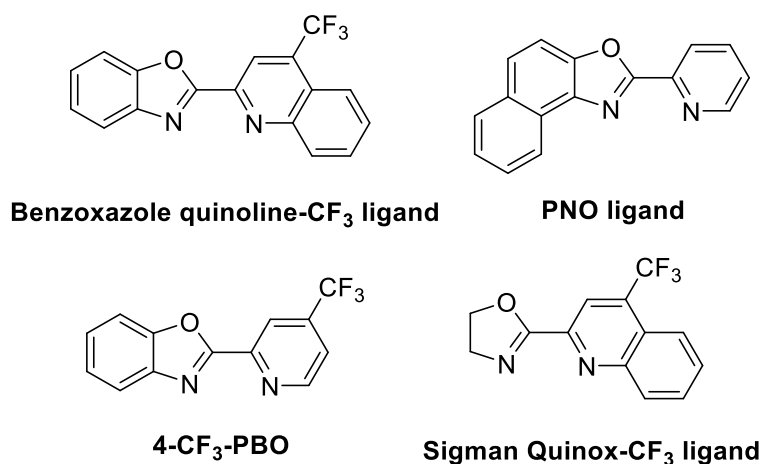


Figure S4: Structures of 4-CF₃-PBO, quinoline-CF₃ and PNO ligands found to give double bond isomerisation and Sigman's second generation Quinox-CF₃ ligand,⁷ that delivered fast initial rates for the oxidation of oct-1-en-3-yl acetate.

For the rest of the pyridine-based catalysts, the 5-CF₃ substituted ligand gave exceptionally fast initial rates of reaction, with 19% yield of 2-octanone formed after only 1 minute. Although differences in initial rates were observed, all the pyridine ring substituted PBO ligands were found to give practically the same catalyst TON. This

finding is in line with what was reported by Sigman and co-workers using these conditions for Quinox and Quinox-CF₃.⁷ Faster initial rates using the Quinox-CF₃ ligand were observed however no significant difference in final catalyst TON was obtained compared with underivatized Quinox. Given these observations, it is reasonable to expect that the principal causes of catalyst deactivation under these conditions are not greatly affected by the ligand being used. The SbF₆⁻ anion is well known to hydrolyse in the presence of water in a stepwise fashion where the first hydrolysis step is described by equation (1).⁸ The SbF₆⁻ anion is a common feature of all the catalysts and water is present in the reactions from the aqueous TBHP solutions being used. The destruction of this counterion could therefore be a significant contributor to catalyst deactivation under these conditions and explain the same TON obtained for many of the catalysts despite differences in initial yields.



Switching to Trifluoromethanesulfonate (Triflate) Anions

Unlike [SbF₆]⁻, the [CF₃SO₃]⁻ ([OTf]⁻) anion is resistant to hydrolysis and has also been found to work well as a counterion for both Quinox and PBO cationic catalysts.^{1, 2, 4} Using triflate as the anion also opens up the possibility of using pre-formed, isolated triflate complexes as well as those formed *in situ* using Ag[OTf]. Kinetic plots for promising ligands were again constructed, using both pre- formed and *in situ* generated triflate catalysts and the results are shown in Figure S5.

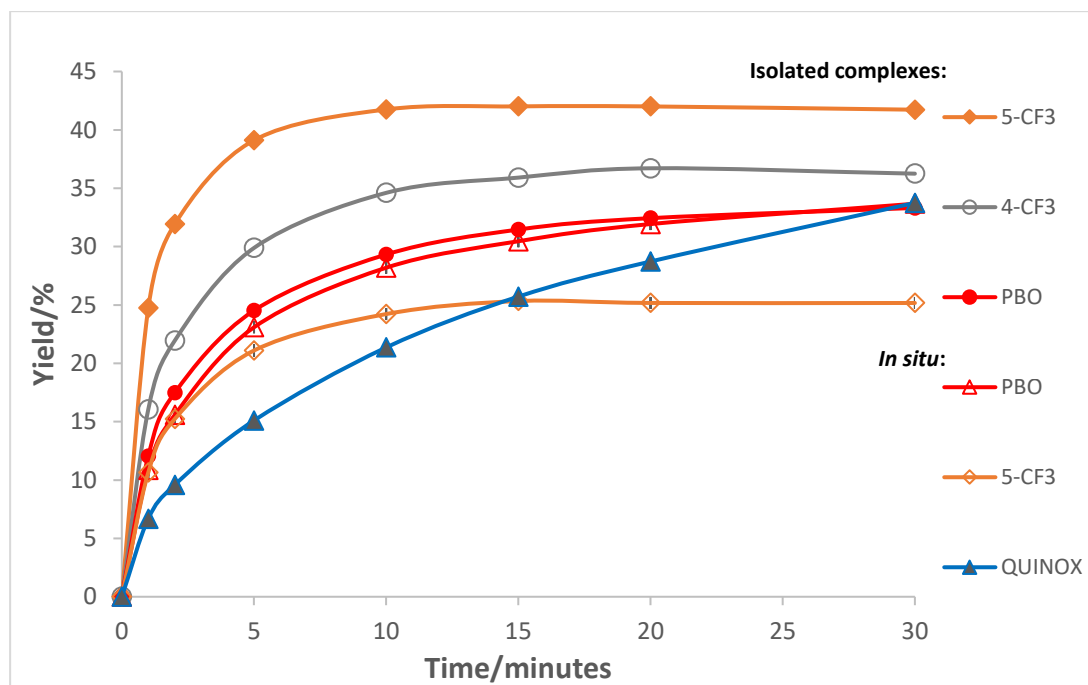
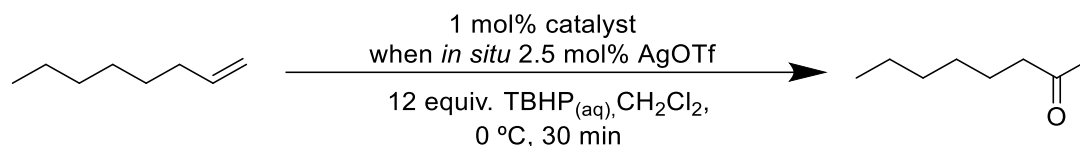


Figure S5: Evaluation of ligands for triflate complexes using isolated and *in situ* generated catalysts. Each kinetic plot an average of two runs.

The 5-CF₃ ligand again gave the best results when the isolated triflate complex is used. This isolated complex gives even faster reaction rates and slightly higher TON than was obtained using the Ag[SbF₆] Sigman conditions. When using the isolated complexes, differences in both initial rates and final TON can now be seen depending on the ligand being used.

Comparing the performance of the pre-formed versus *in situ* generated catalysts for the PBO ligand showed no discernible difference between the two. For the 5-CF₃ ligand however, using the isolated complex leads to improved catalyst performance compared to the *in situ* method. The reason behind this difference in the two ligands is unclear however previous work using hydrogen peroxide and styrenes found that isolated PBO triflate complex gave better yields than the corresponding *in situ* generated method.¹ Forming the cationic catalysts *in situ* produces two equivalents of AgCl salt for every catalyst molecule formed. It is feasible that chloride ions could inhibit performance by

re-forming the catalytically inactive (ligand)PdCl₂ complexes (*i.e.* effectively lowering catalyst loading). The selectivity obtained for the 2-octanone product when using each method of catalyst formation was evaluated, and the results are shown in Figure S6. The other products that are formed in these reactions are a mixture of internal alkene and some internal ketones, from the oxidation of these internal alkenes. It is worth noting that these internal alkenes are significantly slower to oxidise in comparison to the terminal alkene, therefore the majority of the products are internal alkenes. Using the pre-formed catalysts leads to higher selectivity compared with the catalysts formed *in situ* using both Ag[SbF₆] and Ag[OTf]. This is particularly true for the 5-CF₃ catalyst where a 14% increase in selectivity was achieved. Overall, this pre-formed 5-CF₃ catalyst gave the highest selectivity under these conditions with 80%, with the Quinox ligand catalysts giving the worst. Silver triflate has previously been used as a catalyst for the isomerization and subsequent intramolecular addition of carboxylate group to form γ -lactones from unsaturated fatty acids.⁹

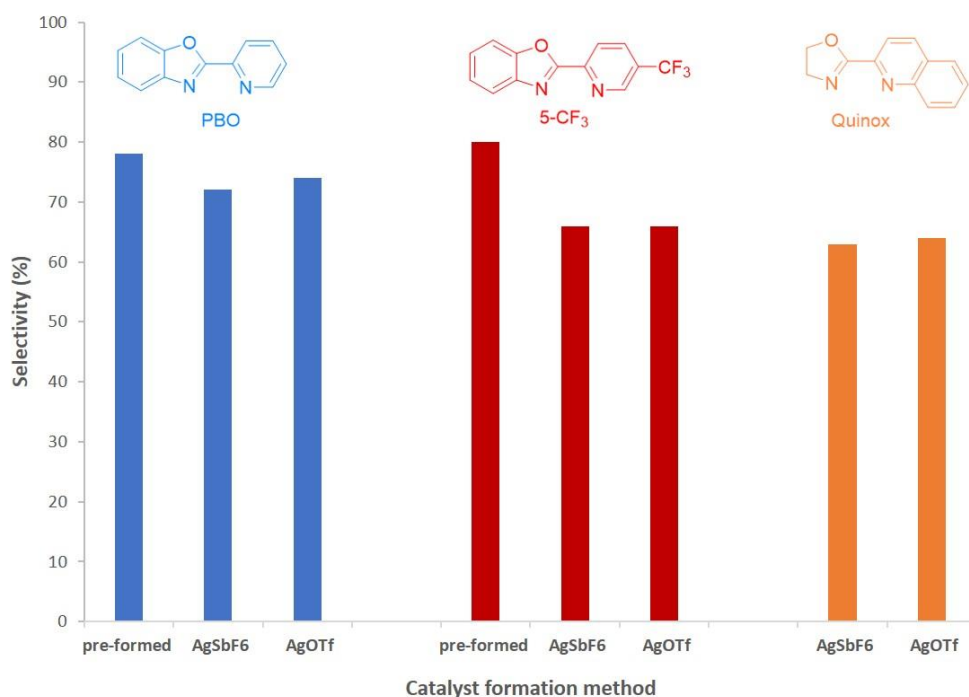
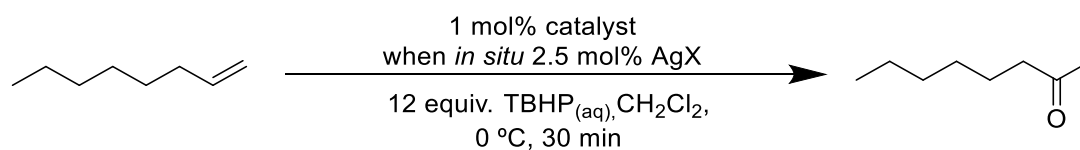


Figure S6: Bar chart showing the selectivity for 2-octanone using different methods of catalyst formation using PBO, 5-CF₃ and Quinox ligands.

Using pre-formed triflate complexes also offers some potential advantages with perhaps the most important being that these pre-formed catalysts can be dissolved in a range of organic solvents to form a homogeneous solution which is applicable to study by spectroscopic methods.

Triflate vs bis(trifluoromethanesulfonyl)imide as Counterion

Bis(trifluoromethanesulfonyl)imide is a structurally related anion to triflate (Figure S7) and like triflate it cannot be hydrolysed by water. It is a weaker coordinating anion than triflate with a conjugate acid pK_a of 0.3 in MeCN compared to 0.7 for triflate.¹⁰

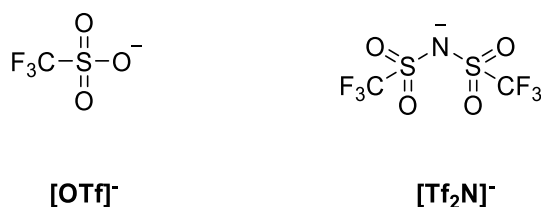


Figure S7: Structures of triflate and bis(trifluoromethanesulfonyl)imide anions.

The triflate anion was substituted for the less coordinating bistriflimide anion,^{11, 12} in an effort to further improve on the catalyst performance. It was found that the isolated bistriflimide cationic catalysts could be formed using an identical procedure to the triflate complexes by swapping triflic acid for triflimidic acid. The best performing 5-CF₃ ligand was used to form the new catalyst and the results using the bistriflimide catalyst are shown in Figure S8. No difference in either initial rate, final yield or selectivity was found when using this bistriflimide catalyst. The studies by Sigman and co-workers found that the weakest anion, [SbF₆]⁻, gave better performance over other anions such as [BF₄]⁻ or [OTf]⁻, however, it is clear that there is no benefit in performance going from [OTf]⁻ to the weaker coordinating [Tf₂N]⁻ in this system. Figure 9 in the main manuscript also showed that for oct-1-en-3-yl acetate, the performance of Ag[OTf] and Ag[Tf₂N] was the same when the *in-situ* method was used with 5-CF₃-PBO ligand.

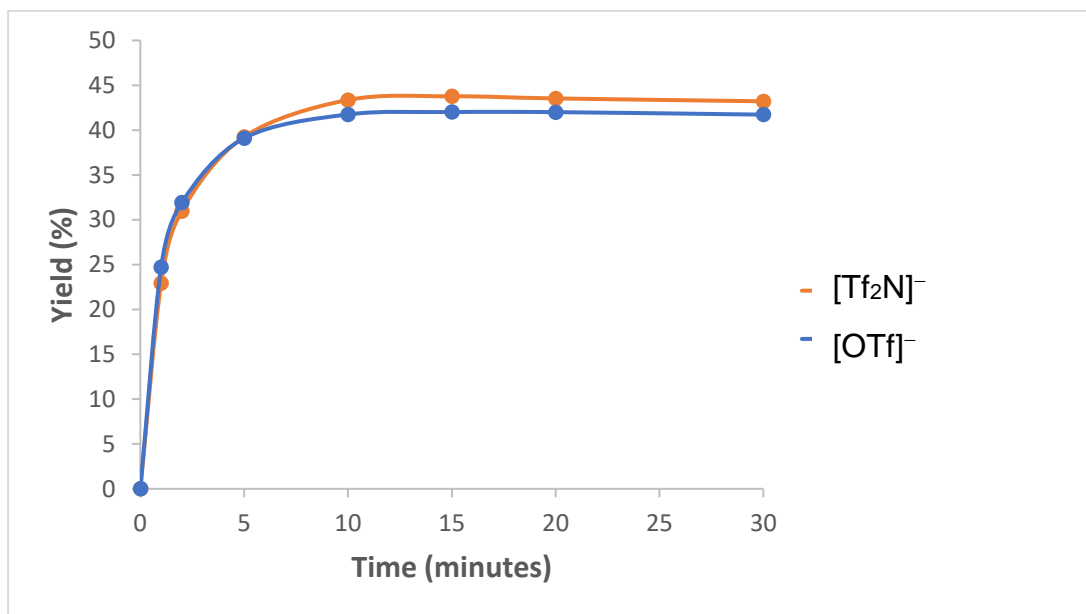
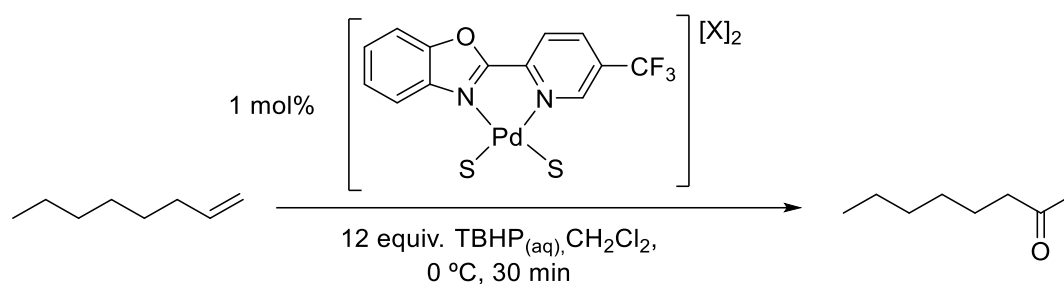


Figure S8: Comparison of [OTf]⁻ vs [Tf₂N]⁻.

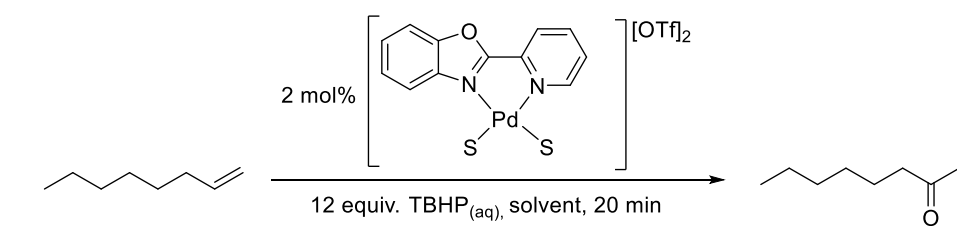
Each plot is an average of two runs.

Despite the drastic improvements in reaction rate and moderate improvements in TON achieved using these new isolated 5-CF₃ cationic complexes, under these conditions rapid catalyst deactivation was clearly still occurring. A yield of approximately 40% 2-octanone could be achieved using 1 mol% and for complete conversion a loading of 2 mol% would be necessary. This offers no substantial improvement upon the Quinox ligand framework, which also used 2 mol% for simple aliphatic alkenes such as 1-octene.

Solvent Screening and Temperature Effects

After making improvements on the catalyst portion of the system, it was decided to examine other parameters starting with the solvent. To carry out the solvent screening reactions, the underivatized [(PBO)Pd(NCMe)₂][OTf]₂ isolated complex was used at a

loading of 2 mol% (Table S2). Coordinating solvents such as alcohols and MeCN were found to be poor, giving low yields and selectivity. Non-polar solvents were generally found to be poor with hexane and ethyl acetate giving extremely low yields even upon heating to 27 °C. Toluene was found to be somewhat of an exception, giving a low yield but very high selectivity at 0 °C, with the yield improving reasonably at higher temperature, albeit with a drop in selectivity. From the solvents screened trifluorotoluene (TFT) was found to be the standout and the one solvent capable of rivalling and even surpassing the results obtained in DCM. Due to its exceptional performance, TFT was taken forward for further examination using the best performing 5-CF₃ catalyst. Toluene was also selected for further tests due to the promising selectivity and the slower reaction rate was thought to perhaps be advantageous, as slowing down the catalyst turnover slightly may reduce catalyst death.



Entry	Solvent	Conversion (%)	Yield (%)	Selectivity (%)
1	DCM	71 ^a , 70 ^b	63 ^a , 61 ^b	89 ^a , 87 ^b
2	MeOH	47 ^a , 80 ^b	10 ^a , 39 ^b	21 ^a , 49 ^a
3	EtOH	16 ^a , 27 ^b	6 ^a , 13 ^b	37 ^a , 48 ^b
4	Hexane	3 ^a , 11 ^b	2 ^a , 9 ^b	67 ^a , 82 ^b
5	EtOAc	9 ^a , 17 ^b	3 ^a , 13 ^b	33 ^a , 76 ^b
6	MeCN	10 ^a , 43 ^b	3 ^a , 12 ^b	35 ^a , 27 ^b
7	Toluene	15 ^a , 50 ^b	14 ^a , 40 ^b	93 ^a , 80 ^b
8	Trifluorotoluene	62 ^a , 88 ^b	55 ^a , 80 ^b	89 ^a , 91 ^b

(a) Reactions carried out at 0 °C

(b) Substrate added at 0 °C and stirred for 5 min before being allowed to warm to 27 °C

Table S2: Solvent screen using $[(\text{PBO})\text{Pd}(\text{NCMe})_2][\text{OTf}]_2$ as catalyst for TBHP mediated oxidation of 1-octene.

The oxidation of 1-octene was followed in toluene and TFT using the 5-CF₃ triflate catalyst at a loading of 1 mol% at both 0 °C and 27 °C. The results were then compared to those obtained in DCM under the same conditions and can be seen in Figure S9 (also Figure 5 in main manuscript) .

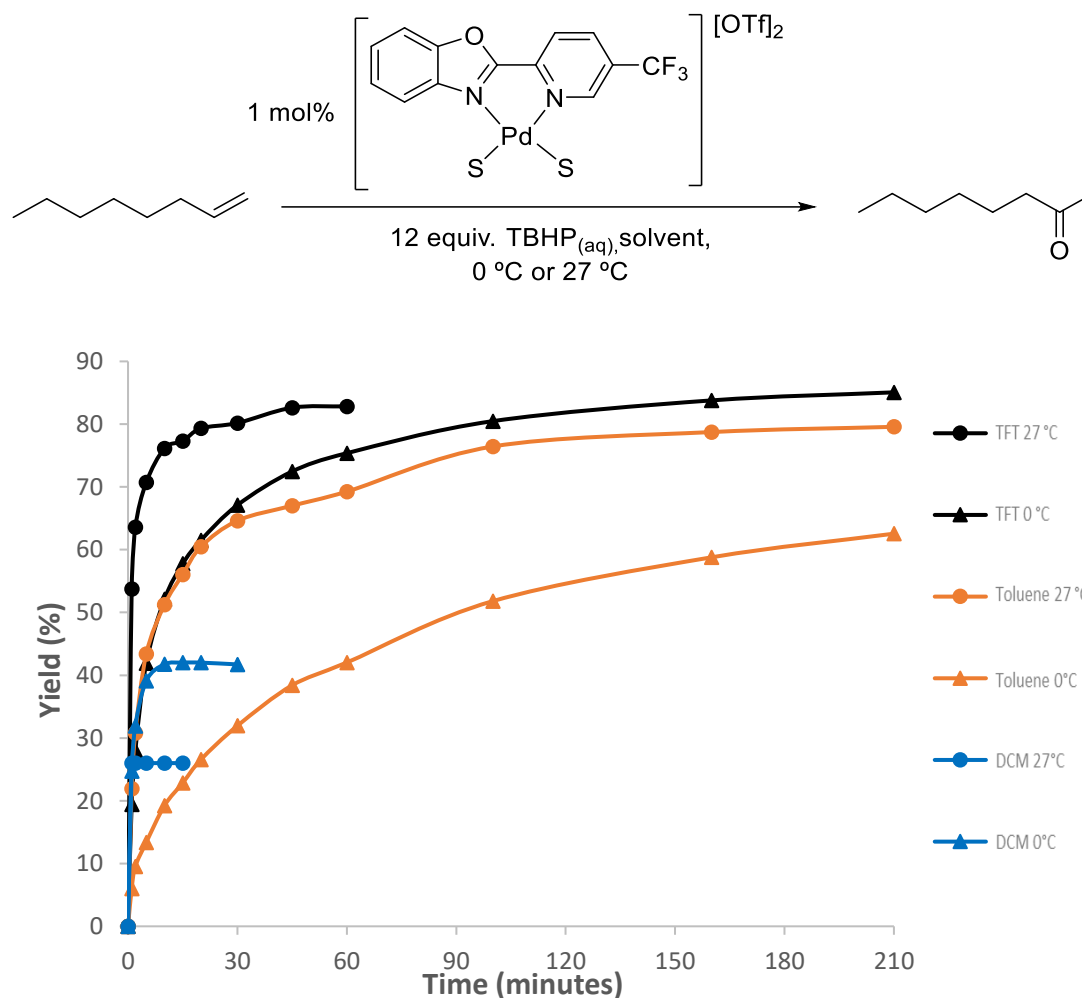


Figure S9: Comparison of TFT, toluene and DCM at 0 °C and 27 °C using 1 mol% 5-CF₃ isolated triflate catalyst. Kinetic plots an average of two runs.

At this lower 1 mol% catalyst loading it is evident that both TFT and toluene are superior reaction solvents to DCM. Using 1 mol% catalyst in both these solvents resulted in complete conversion of the starting material in all cases tested, with the reaction in toluene at 0 °C requiring overnight reaction. The reaction in TFT is significantly faster than in toluene and gives both a slightly higher yield and selectivity than toluene, with

85% of the 2-octanone attained. Impressively, in TFT at 27 °C the yield of 2-octanone produced in the reaction after only 1 minute is 54%. This is perhaps unsurprisingly exothermic (see “Notes of Safety” later) and therefore for this substrate we then carried out the majority of our studies at 27 °C.

Catalyst deactivation is much more rapid in DCM when the reaction is carried out at room temperature. The catalyst dies almost instantly and no increase in yield is seen after the first minute. Interestingly, when the reaction is performed in DCM, despite starting out as homogeneous a yellow solid, thought to be derived from the catalyst, crashes out during the reaction. In the case of the room temperature reaction in DCM this happens almost instantaneously after addition of the substrate. This phenomenon is not observed in toluene and TFT where the reaction remains homogeneous and perhaps explains their superior performance compared to DCM. The yellow solid deposited from the DCM reactions was filtered off for analysis however was found to be completely insoluble in CDCl₃, MeCN-d₃ and acetone-d₆ rendering characterization by NMR unfeasible. Stronger, more polar deuterated solvents such as DMSO were not used for fear of breaking up the suspected catalyst aggregates that had formed. The solid was also completely insoluble in both TFT and toluene which suggests that this does not form in these solvents.

The formation of insoluble, inactive μ -hydroxy bridged dimers has previously been proposed as a catalyst deactivation pathway by Sigman and co-workers, however efforts to identify these types of dimers by MS were inconclusive.⁷ The synthesis of hydroxy-bridged Pd(II) dimers was first reported by McFarland and co-workers.¹³ Reacting PdCl₂(PPh₃)₂ with two equivalents of Ag[BF₄] in moist acetone (\approx 0.5% H₂O) lead to the formation of the complex shown in Figure S10.

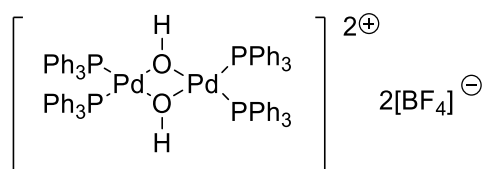


Figure S10: First example of hydroxy-bridged Pd(II) complex.¹³

This complex was found to be surprisingly stable and the bridged structure remained intact upon treatment with a variety of organic solvents. It also gave no reaction

when exposed to an excess of PPh_3 . Similar dimeric structures ligated by diimines have been synthesized by the same halide abstraction method and are now also well established.¹⁴⁻¹⁷

Vedernikov and co-workers found that the dimeric Pt(II) complex shown in Figure S11 was produced during the aerobic oxidation of Pt(II) ethylene complexes to ethylene oxide. In such reactions these dimeric structures appear to be thermodynamic final resting states.¹⁸

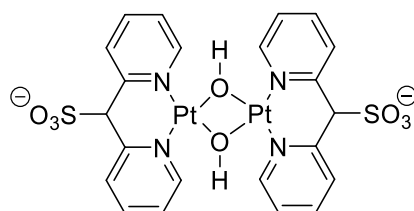


Figure S11: Dimeric Pt(II) complex produced in aerobic oxidation of Pt(II) ethylene complexes to ethylene oxide.¹⁸

Sheldon has also shown the formation of inactive μ -hydroxy bridged dimers of (bathophenanthroline)Pd(II) under aerobic Wacker conditions. In this work, the dimer is in equilibrium with the active monomeric Pd(II) species.¹⁹ Multinuclear Pd species formed under oxidative conditions have also been reported by Waymouth and co-workers.²⁰ The trimer shown in Figure S12 was observed by ESI-MS during previous work on the oxidation of styrene with aqueous hydrogen peroxide using the original [(PBO)Pd(NCMe)][OTf]₂ catalyst.²

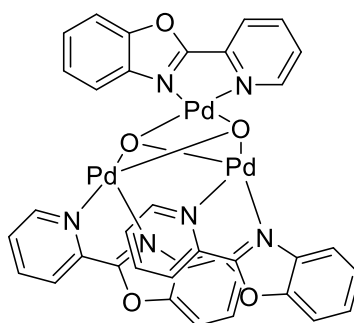


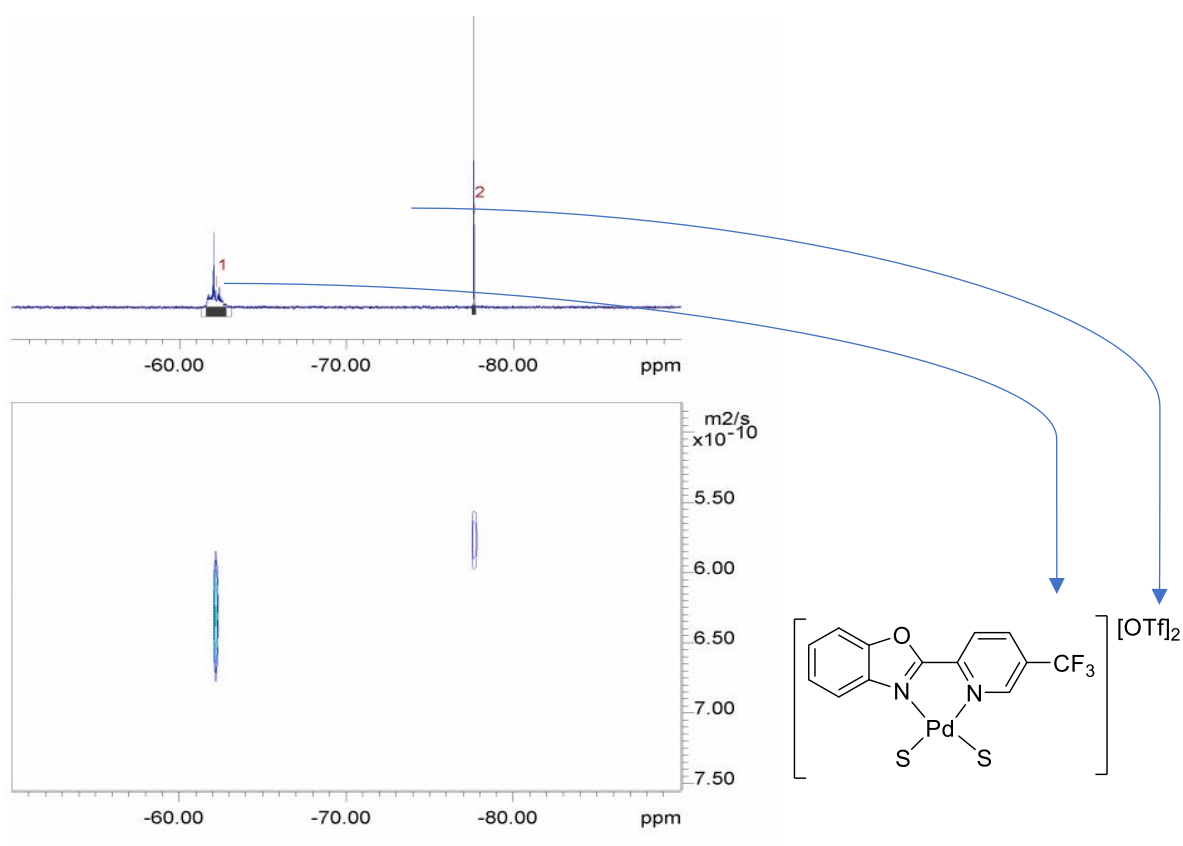
Figure S12: Trimeric oxygen bridged structure observed by ESI-MS in oxidation of styrene by aqueous H_2O_2 using [(PBO)Pd(NCMe)][OTf]₂ catalyst.²

Given the type of cationic complexes used in these Wacker reactions and the water present from the aqueous TBHP, it is plausible that these types of hydroxy dimers or larger aggregates could be forming and causing catalyst deactivation.

¹⁹F DOSY NMR in Toluene with Aqueous TBHP

Diffusion ordered spectroscopy (DOSY) NMR is a technique that measures how fast different species are diffusing in solution and gives information about molecular size. A useful feature of the 5-CF₃-PBO catalyst is that it contains a trifluoromethyl group, which allows for the use of ¹⁹F NMR. The catalyst was analysed by ¹⁹F DOSY during the reaction of 1-octene with aqueous TBHP in toluene. A DOSY spectrum was obtained for the catalyst in the toluene/TBHP mixture to obtain the diffusion speed before any reaction had taken place. Two further DOSY spectra were taken after 20 minutes and 2.5 hours once the reaction was complete.

Inspection of the ¹⁹F NMR spectra when the reaction is underway showed the formation of a plethora of peaks in the -CF₃ region, indicating the existence of numerous distinct species (Figure S13). Diffusion analysis of all individual peaks was not possible and therefore the diffusion values for 20 minutes and 2.5 hours shown in Figure S15 give the average diffusion of all these species in solution.



DOSY spectra	CF ₃ peak Diffusion (x 10 ⁻⁹ m ² s ⁻¹)	Error (x 10 ⁻⁹ m ² s ⁻¹)
Catalyst in toluene/TBHP _(aq)	0.81	0.038
After 20 minutes reaction	0.62	0.022
After 2.5 hours reaction	0.63	0.037

Figure S13: DOSY spectra after 2.5 hours reaction showing forest of peaks in CF₃ region (top). Change in diffusion coefficients of catalyst peaks throughout reaction, all CF₃ peaks in region integrated together (bottom).

On average, the diffusion of all these species formed during the reaction was found to be slower than the catalyst before the reaction began. This observation supports the formation of higher molecular weight species such as catalyst hydroxy bridged dimers and aggregates. No change in average diffusion was observed after 20-50 minutes of the reaction (the DOSY spectrum took approximately 30 minutes to obtain). This

agrees with the information from the kinetic plot for toluene at 27 °C in Figure S9 above. Looking at the kinetic plot shows that after 20 minutes reaction the curve begins to flatten out and the reaction rate slows drastically, as by this point most of the catalyst has been deactivated. The results in Figure S13 represent a 23% decrease in diffusion coefficient for the catalyst species present after the reaction has taken place. As a comparison Parvez and co-workers found a 35% drop in diffusion coefficient between the Iridium dimer and monomer shown in Figure S14 below in benzene- d_6 by ^1H -DOSY NMR.²¹

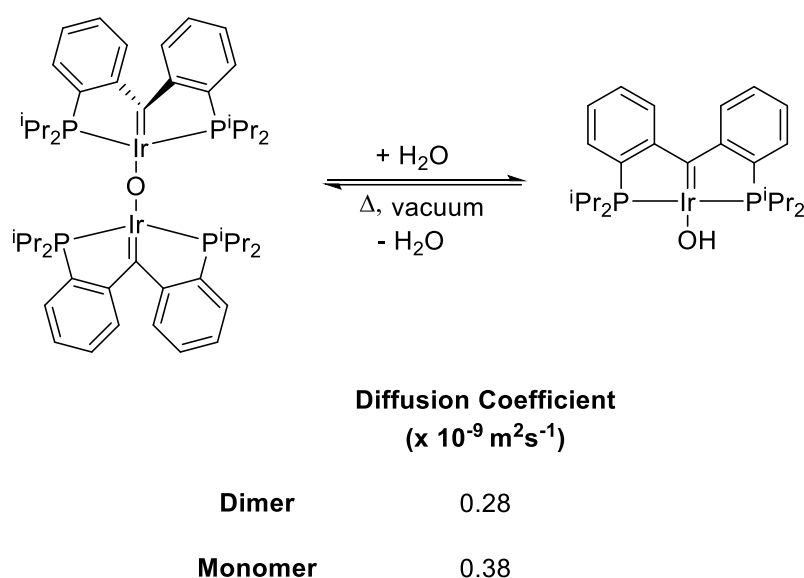


Figure S14: Iridium dimer and monomer complexes with diffusion coefficients for both species in benzene- d_6 .²¹

Individual integration of the largest CF_3 peak after 2.5 hours was carried out and found to correspond to a molecule diffusing at a much faster rate than the average ($D = 1.3 \times 10^{-9} \text{ m}^2\text{s}^{-1}$). This fast diffusion implies that this molecule is smaller than the catalyst itself and was thus suspected to be free ligand that had disassociated from the metal during the reaction. Spiking the reaction mixture with free ligand after 2.5 hours however showed that this large peak did overlap with that of the free ligand. Interestingly, this fast diffusing species was not detected in large quantities in the 20-minute DOSY spectrum, so although the average diffusion values of the species does

not change after this point, the individual components contributing to the average diffusion values does. A close-up of the CF₃ region upon completion of the reaction can be found in Figure S15.

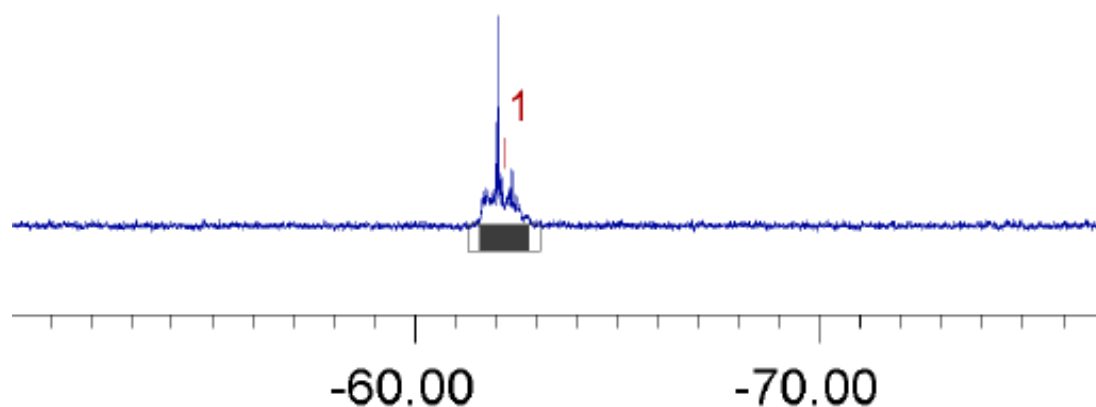


Figure S15: Expanded image of the forest of peaks in the CF₃ of ¹⁹F DOSY spectrum of complete reaction in toluene.

Using Anhydrous TBHP/organic Solvent Mixtures for Wacker Oxidation

The suspected formation of hydroxy-bridged catalyst aggregates leading to catalyst deactivation led us to try and eliminate water from these reactions. To do this, TBHP was extracted from the commercially available aqueous solution into several different organic solvents. The extracted TBHP solutions were then dried repeatedly with sodium sulphate and stored in Teflon™ FEP bottles. Before being used in reactions the TBHP/organic solvents were further dried by sitting over 3 Å molecular sieves for 30 minutes. The concentration of TBHP in the extracted solutions was determined by quantitative ¹³C NMR.

The first solvent that was tested under anhydrous conditions was toluene. Comparison with the results obtained using aqueous TBHP however showed the reaction to perform worse under dry conditions (Figure S16). Despite the two sets of conditions starting off equally in terms of rate, under the dry conditions the reaction stops at 60% yield as all the starting material has been consumed. The difference in selectivity between the wet and dry system is stark, with 91% selectivity for 2-octanone obtained under aqueous

conditions. The level of isomerization under the dry conditions is higher than the wet (5% compared to 1%) but does not account for the disparity in selectivity. Under the dry conditions after taking into consideration the isomerization, a mass balance deficit of approximately 30% remains. The methyl group of toluene is known to react with TBHP to form benzoyl radicals and this has been exploited to use toluene as a coupling partner in Pd(II) catalysed coupling reactions.^{22, 23} Under dry conditions the formation of these benzoyl radicals may be exacerbated and may be causing polymerization/oligomerization of the alkene reducing the selectivity. Sharpless and Hanson have noted the formation of a contaminant in anhydrous TBHP/toluene solutions. Using solutions that contained this impurity they observed inhibition of their desired epoxidation reaction.^{24, 25}

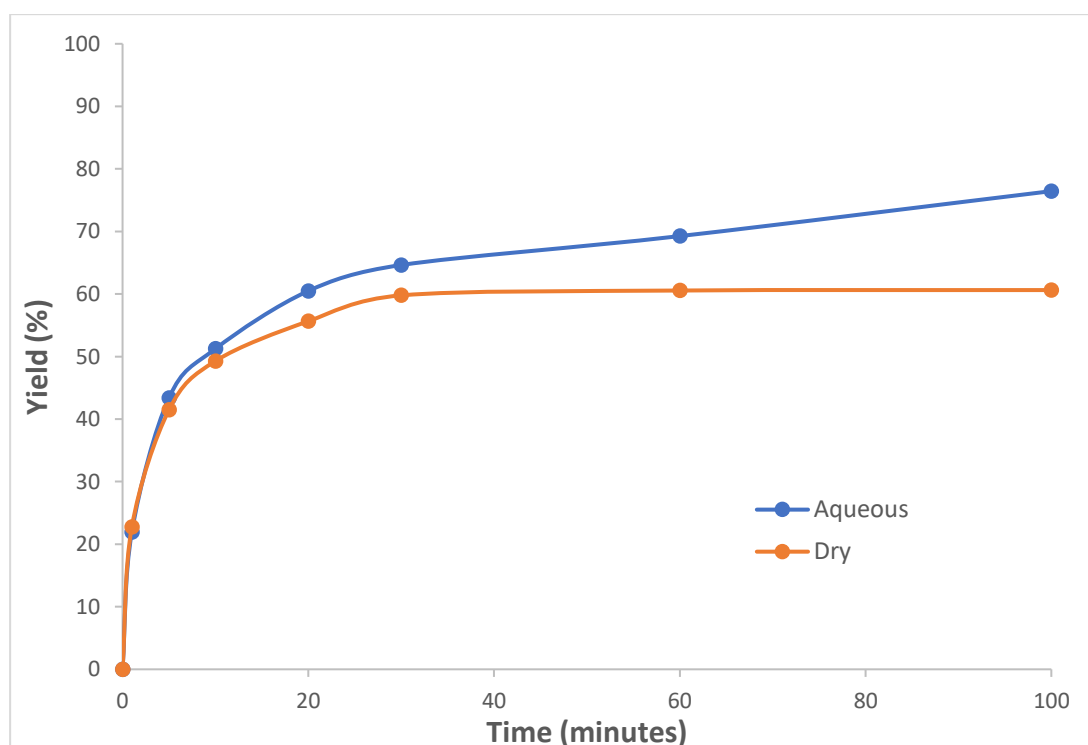
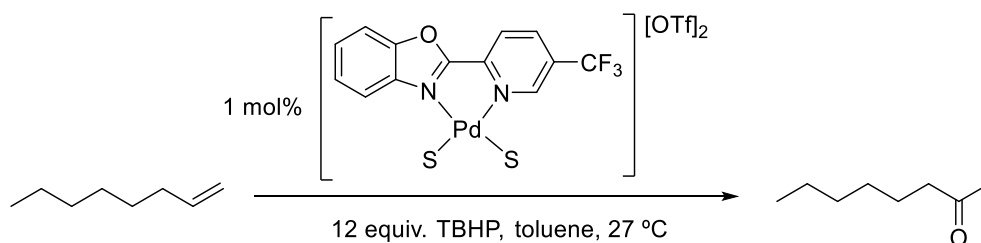


Figure S16: Toluene as solvent for 1-octene oxidation under aqueous and dry conditions.

The C-F bond is much stronger than the C-H bond and therefore should not be oxidised by TBHP. This means in TFT no radical formation should occur in either the wet or dry system and the issues found when using dry toluene should not be a factor. Indeed, when TFT was used under anhydrous conditions catalyst death was further reduced (Figure S17). Using a catalyst loading of 0.5 mol% gave almost complete conversion (93%) and a yield of 80%, the same as the yield obtained using 1 mol% catalyst under aqueous TBHP conditions. At this lower catalyst loading, complete conversion of the 1-octene was not possible when water was present and 30% of the substrate remained unreacted. This result demonstrates how water is detrimental to the reaction and points again to the formation of inactive hydroxy bridged aggregates.

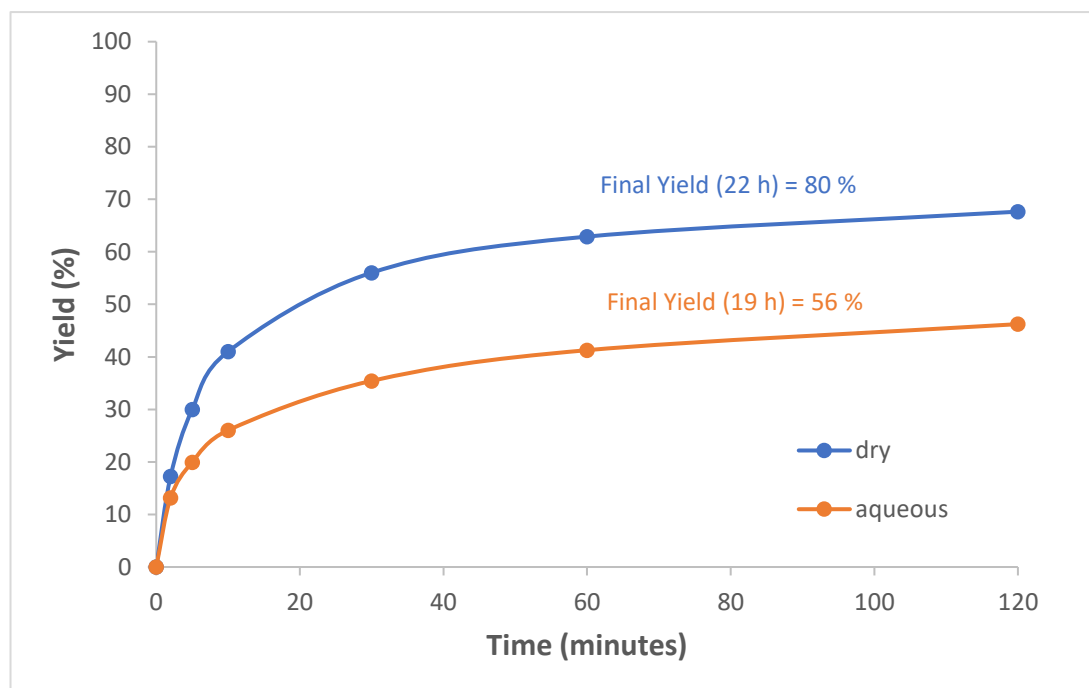
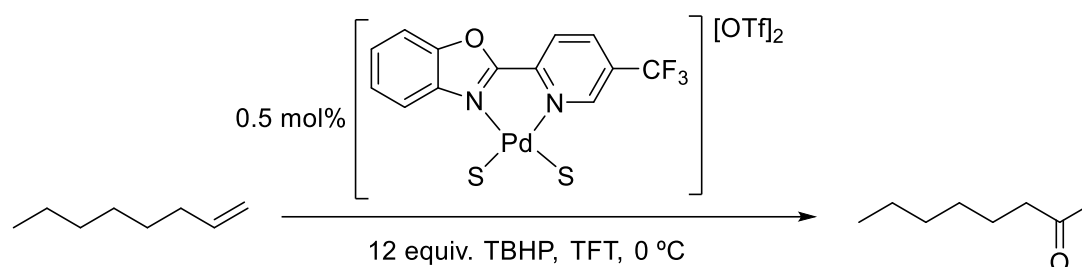


Figure S17: TFT as solvent for 1-octene oxidation under aqueous and dry conditions using 0.5 mol% catalyst loading.

Anhydrous TBHP is also commercially available as a solution in decane and this was tested as a non-aqueous source of TBHP in combination with TFT as the bulk solvent (Figure S18). Having decane as the source of TBHP negatively affected the performance of the system. When decane was used as the sole solvent with the no TFT present, the performance deteriorated even further. This shows decane is not a competent solvent for the reaction, which is in accordance with what was found for other aliphatic alkane solvents such as hexane in the initial solvent screen (Table S2).

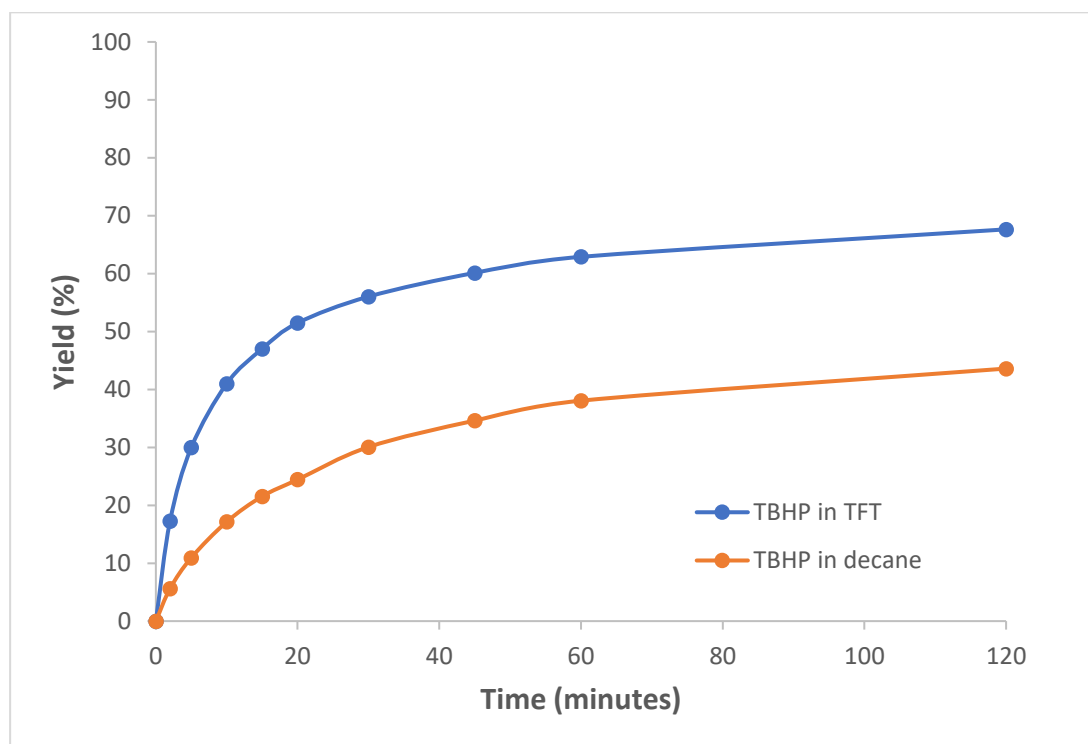
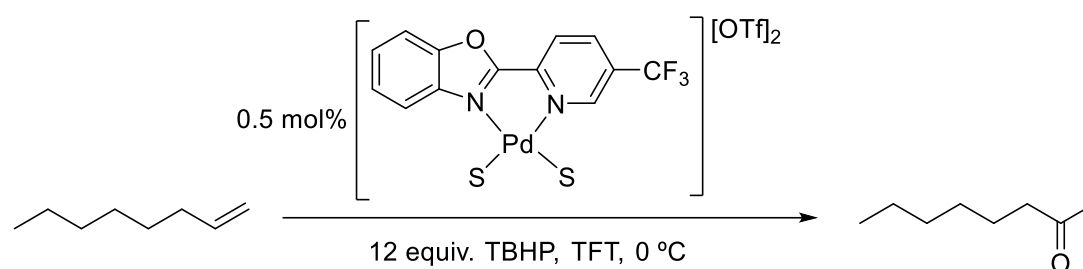


Figure S18 Comparison of decane and TFT as TBHP sources in oxidation of 1-octene.

DCM was re-examined as a solvent under anhydrous conditions and again a yellow solid was found to precipitate from the solution as was observed with aqueous TBHP. The ^{19}F DOSY analysis in toluene and improvements made in catalyst performance using anhydrous conditions with TFT do support that hydroxy bridged aggregates could be a cause of catalyst deactivation. A hydroxy-bridged aggregate formed from water however is not what is precipitating from the DCM reactions as initially proposed and some other catalyst deactivation mechanism must be aggravated in this solvent.

^{19}F DOSY Analysis of Wet vs Dry Reaction Mixtures for 1-octene Oxidation in Chlorobenzene

^{19}F DOSY analysis had previously supported the formation of larger molecular weight catalyst species during the reaction in toluene with aqueous TBHP. This technique was revisited to compare the diffusion of the catalyst species under aqueous and anhydrous reaction conditions. It was hoped that DOSY would show faster diffusing species in the anhydrous reaction compared to the aqueous indicating the prevention of catalyst aggregation.

When this was attempted using TFT as the solvent, the large solvent peak obscured the $-\text{CF}_3$ catalyst peak of interest in the ^{19}F spectrum. Efforts were made to overcome this issue using solvent suppression, however, baseline/phase issues arising from the suppressed peak meant that reliable integration of the peaks of interest would not be reliable even if they could be seen. Instead, the use of a non-fluorinated solvent that also showed better catalyst performance under dry conditions was sought.

This solvent was found in the form of chlorobenzene (Figure S19), a solvent also previously noted by Mimoun to give good results in Wacker oxidations.²⁶ Under the anhydrous conditions, 0.5 mol% catalyst loading was found to give 75% yield compared to 80% in TFT. Under the aqueous conditions the difference between the two solvents is more pronounced, with 38% yield being obtained in chlorobenzene to 56% in TFT.

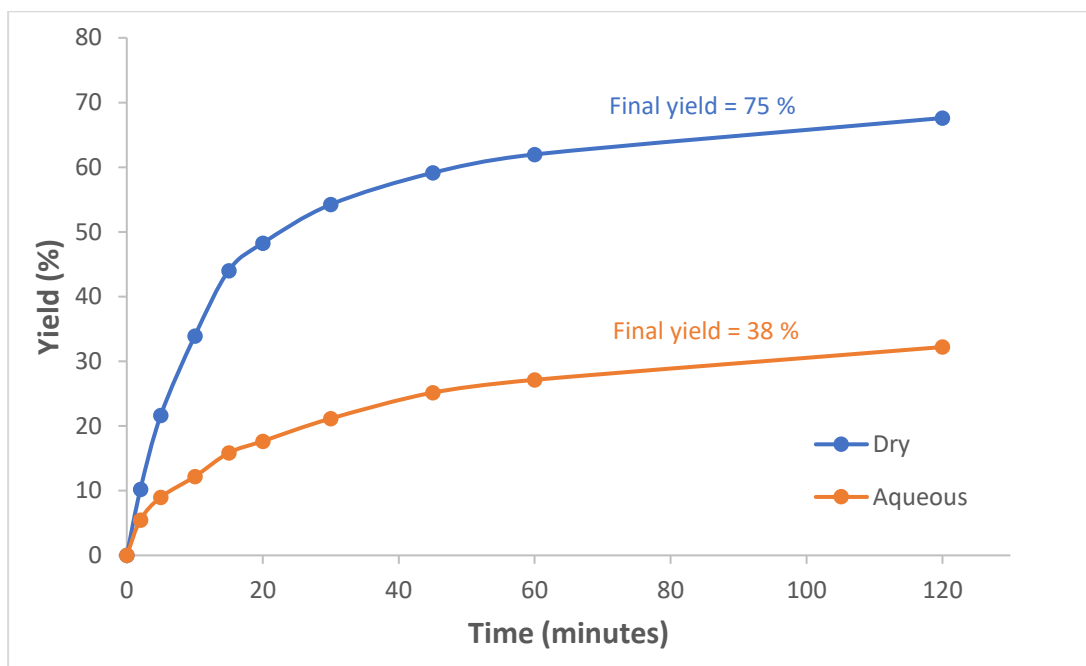
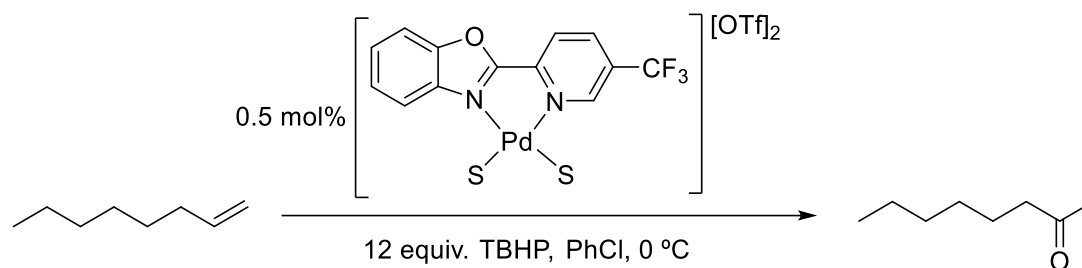
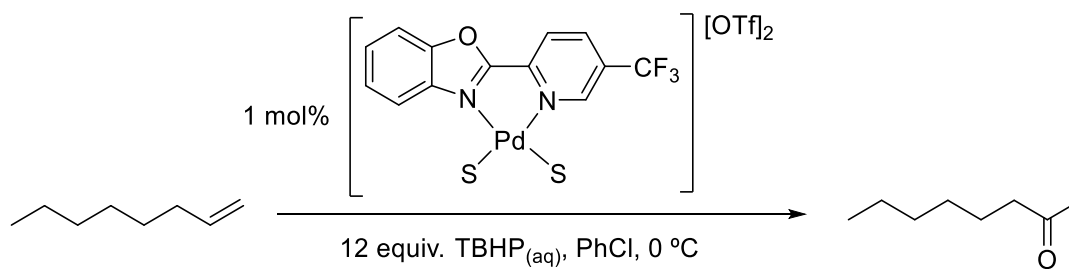
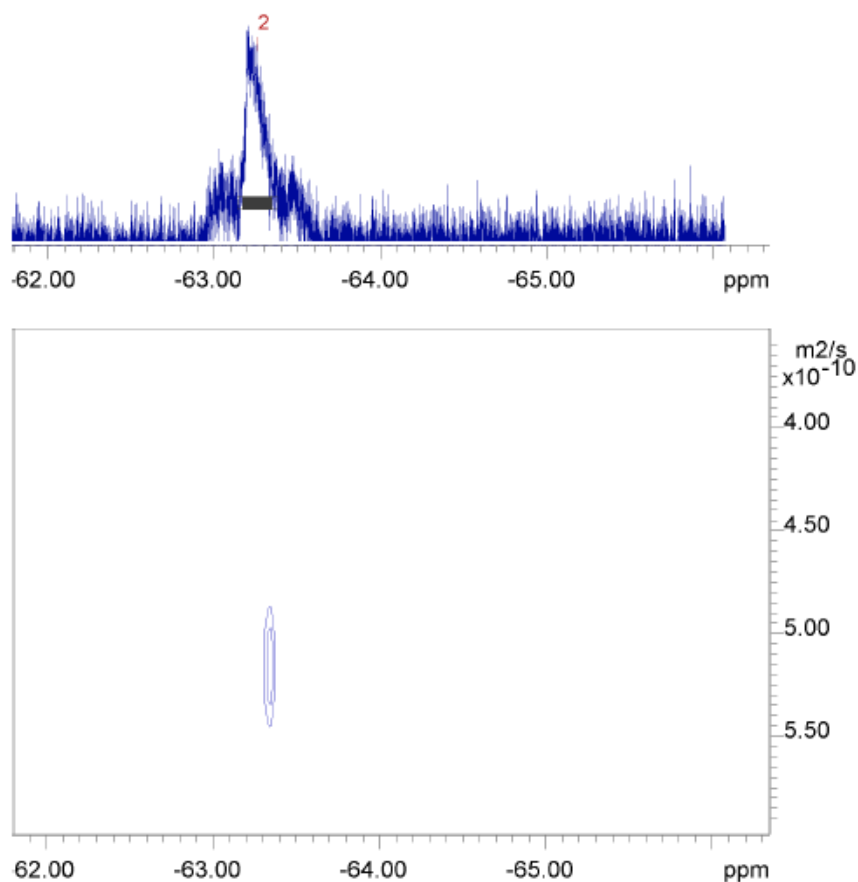


Figure S19: Chlorobenzene as solvent for 1-octene oxidation under aqueous and dry conditions using 0.5 mol% catalyst loading.

When running the ^{19}F DOSY spectra for the reaction in $\text{TBHP}_{(\text{aq})}/\text{PhCl}$ the signal to noise (S/N) ratio and resolution of the peaks was considerably worse than what was seen when using $\text{TBHP}_{(\text{aq})}/\text{toluene}$. An emulsion forms between the $\text{TBHP}_{(\text{aq})}$ and the PhCl as was observed when preparing the dry extracted solution. This emulsion is likely responsible for the drop in spectral quality. Further evidence for this was found when performing the DOSY analysis of the anhydrous PhCl reaction (see later) where S/N ratio and peak resolution were dramatically improved. The DOSY for the finished reaction required a threefold increase in the number of scans (100) to obtain a reasonable S/N ratio throughout the duration of the DOSY. If this wasn't done, the CF_3 region of the spectrum disappeared into the baseline too early into the experiment. The

diffusion coefficients before and after the reaction are shown in Figure S20 along with the DOSY spectra obtained upon complete reaction.

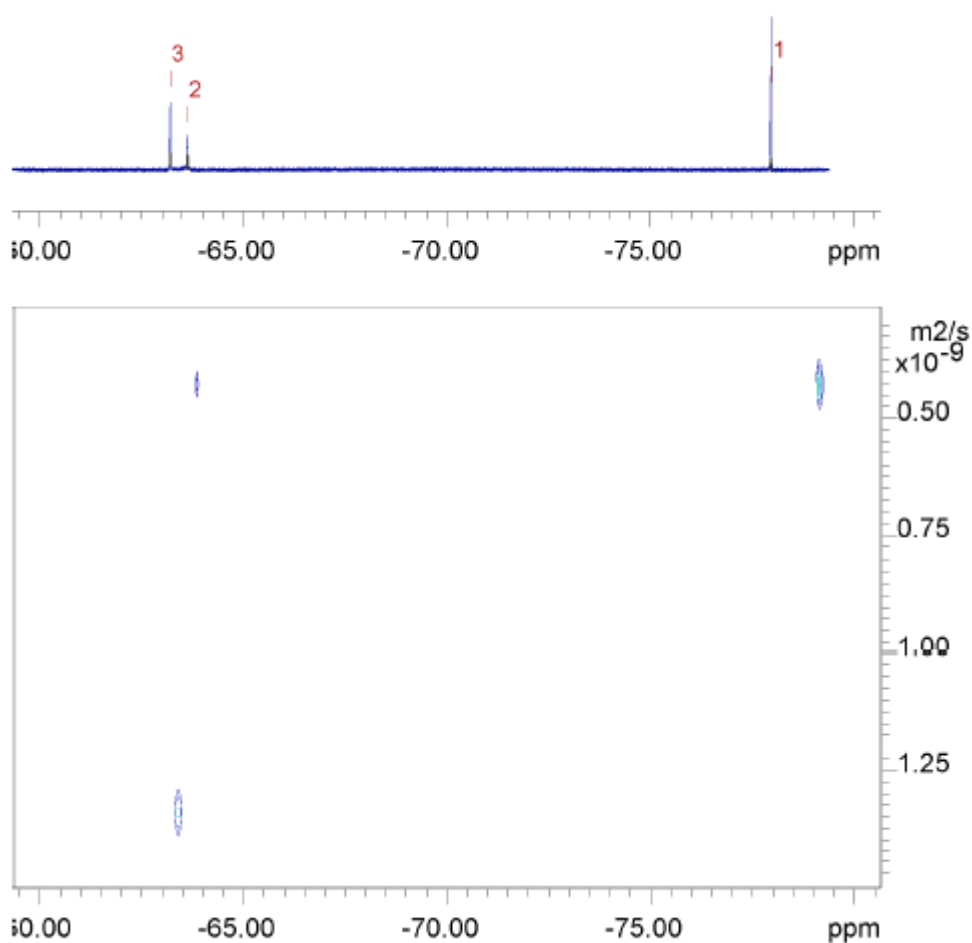
The average integration of all the species in solution after 2 hours of reaction in this instance was found to be diffusing faster than the catalyst species before the reaction had taken place. The poor resolution and S/N meant that integration of any individual peaks could not be carried out as was done with toluene. It could therefore not be determined if there was a mixture of faster and slower diffusing species at the end of the reaction as done with toluene and the presence of hydroxy bridged aggregates was inconclusive.



DOSY spectra	CF ₃ peak Diffusion (x 10 ⁻⁹ m ² s ⁻¹)	Error (x 10 ⁻⁹ m ² s ⁻¹)
Catalyst in TBHP _(aq) /PhCl	0.42	0.038
After 2 hours reaction	0.51	0.037

Figure S20: ¹⁹F DOSY spectra obtained after 2-hour reaction in PhCl. Zoomed in to the CF₃ region of interest.

^{19}F DOSY was carried out regardless on the anhydrous system, as previously stated the quality of spectra obtained under these conditions was dramatically improved. The ^{19}F DOSY of the catalyst dissolved in the anhydrous TBHP/PhCl solution showed two peaks in the CF_3 region of the spectrum before any reaction had taken place. The smaller of the two peaks diffuses 3 times slower than the larger peak (Figure S21). The catalyst was left in this anhydrous mixture overnight and analysed the following day by ^{19}F -NMR with no change in the spectrum observed.



Catalyst in dry TBHP/PhCl	CF_3 peak Diffusion ($\times 10^{-9} \text{ m}^2\text{s}^{-1}$)	Error ($\times 10^{-9} \text{ m}^2\text{s}^{-1}$)
Peak 2	0.42	0.011
Peak 3	1.32	0.039

Figure S21: ^{19}F DOSY spectrum obtained for $[\text{Pd}(5\text{-CF}_3\text{-PBO})(\text{S})_2][\text{OTf}]_2$ dissolved in anhydrous TBHP/PhCl reaction mixture.

Spiking the anhydrous mixture with the 5-CF₃ ligand showed neither peak 2 nor peak 3 corresponded to the free ligand (Figure S22). Upon addition of free ligand, peak 2 disappeared and the appearance of another peak was observed. Peak 3 did not change shift on addition of the free ligand. This observation points to ligand binding to the species represented by peak 2. If the free ligand were to dissociate from the metal, it could be oxidised to the corresponding pyridine *N*-oxide species in the presence of TBHP. The pyridine *N*-oxide of the 5-CF₃ ligand was synthesized and spiked into the anhydrous solution containing the dissolved catalyst and free ligand. The *N*-oxide was also not responsible for either peak 2 or 3 in the anhydrous solution. Addition of the *N*-oxide did not affect the chemical shifts of peak 3 or the free ligand. It did however result in the disappearance of the unidentified peak that appeared after the addition of the free ligand and formation of 3 new peaks including the free *N*-oxide species (Figure S22).

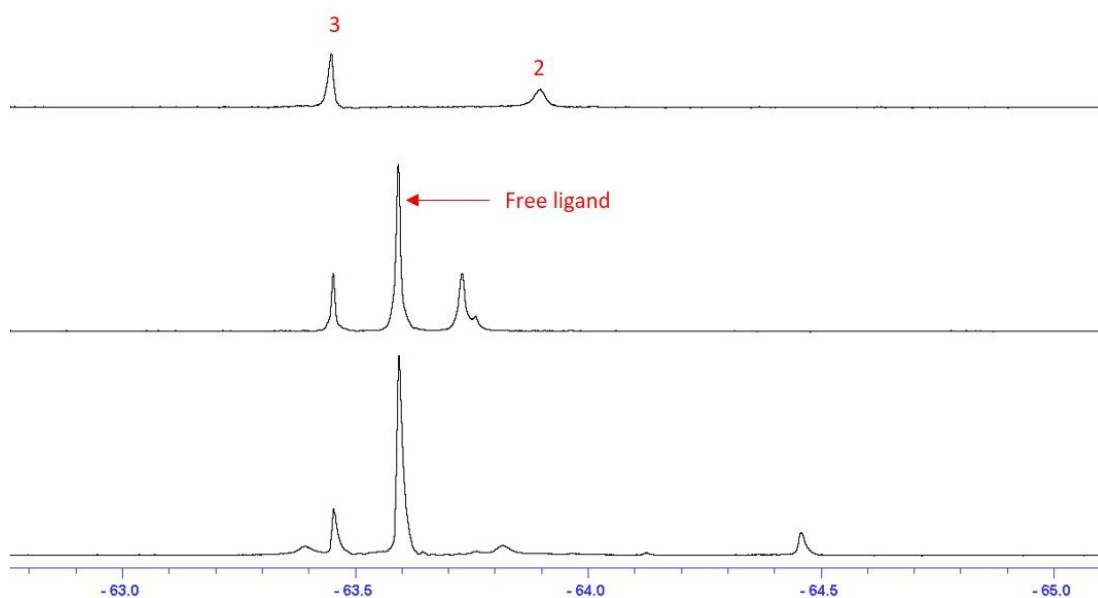
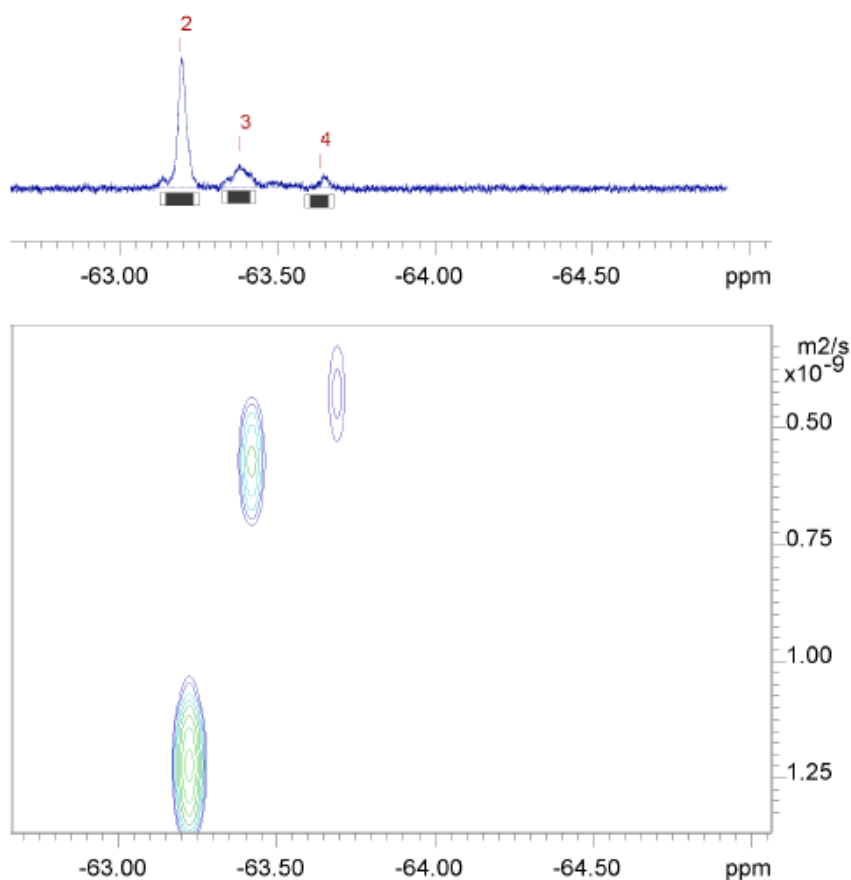


Figure S22: ¹⁹F spectra of [Pd(5-CF₃-PBO)(S)₂][OTf]₂ in anhydrous TBHP/PhCl mixture (top), spiked with free ligand (middle) and spiked with free ligand and *N*-oxide (bottom).

^{19}F -DOSY analysis of the anhydrous reaction upon completion showed the formation of many different species. There were three main groups of peaks in the CF_3 region and due to the high spectrum quality in the absence of water, all three peaks could be integrated individually (Figure S23). Peak shifting occurred during the reaction and as such none of the three peaks could unequivocally be aligned with either peak 2 or peak 3 in the initial DOSY. The peak numbers in the DOSY spectrum in Figure S23 are therefore arbitrary and do not correspond with peaks 2 and 3 in the DOSY spectrum shown in Figure S21.



Catalyst after 2 reaction in dry TBHP/PhCl	CF_3 peak Diffusion ($\times 10^{-9} \text{ m}^2\text{s}^{-1}$)	Error ($\times 10^{-9} \text{ m}^2\text{s}^{-1}$)
Peak 2	1.20	0.099
Peak 3	0.55	0.095
Peak 4	0.42	0.12

Figure S23 ^{19}F DOSY spectra obtained after complete reaction in anhydrous TBHP/PhCl.

The DOSY shows the large group of peaks diffusing approximately 2 and 3 times faster than the smaller two. Due to the small size of peak 4, the diffusion value obtained comes with a high error of approximately 35%, however still implies this peak is moving much slower than the largest group of peaks. A close-up of the CF₃ region of the catalyst after reaction can be found in Figure S24. These results indicate that even under anhydrous conditions the formation of larger more slowly diffusing species occurs. Aggregation mechanisms involving the peroxide itself and not water may be responsible for this and will be discussed in more detail later.

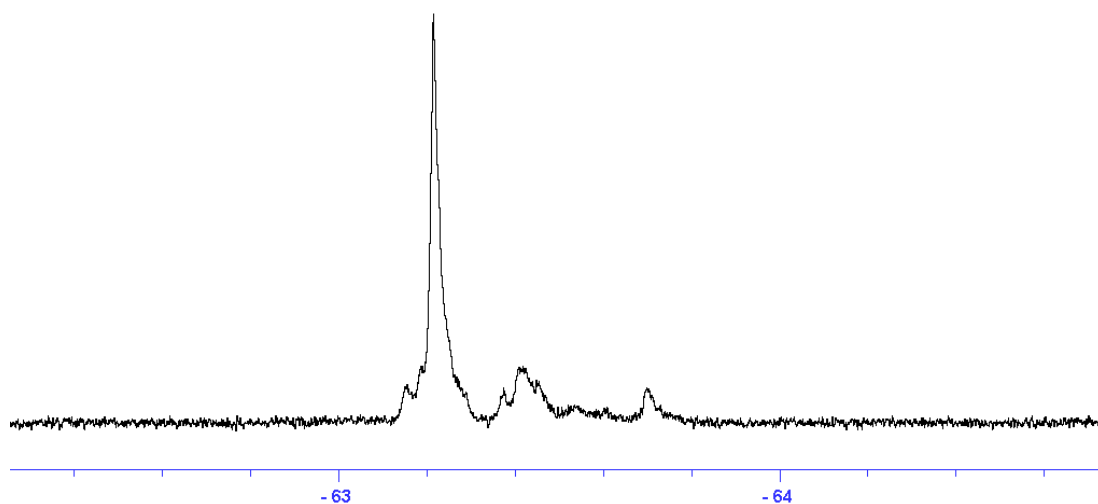
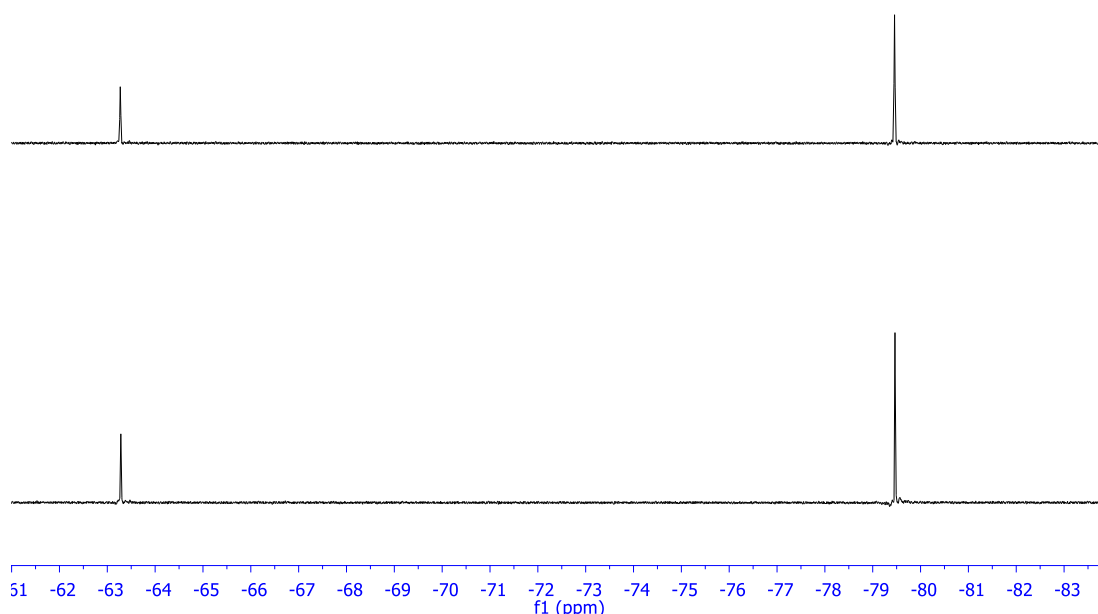


Figure S24: Zoomed in spectra of CF₃ region peaks of interest after complete reaction in anhydrous TBHP/PhCl.

Monitoring Speciation of Catalyst in Wet vs Dry Acetonitrile

Further ¹⁹F NMR studies were carried out in the absence of TBHP to monitor more directly the interaction between water and the catalyst. In the absence of TBHP, the isolated cationic complexes are soluble in a limited number of solvents, one of which is MeCN. The catalyst was weighed into two separate glass vials with one batch dissolved in MeCN that had been pre-dried with activated molecular sieves. The second batch was dissolved in untreated MeCN and spiked with a small amount of ultrapure water to mimic the amount present when using aqueous TBHP. The two

different catalyst solutions were monitored over time using ^{19}F NMR. The results using the dry MeCN are shown below in Figure S25. After 19 hours in dry MeCN solution the catalyst remains completely unchanged. ^{19}F DOSY NMR performed at the beginning and after 19 hours showed no change in diffusion coefficients for either peak in the spectra.



Catalyst in dry MeCN	CF_3 peak Diffusion ($\times 10^{-9} \text{ m}^2\text{s}^{-1}$)	Error ($\times 10^{-9} \text{ m}^2\text{s}^{-1}$)
Beginning	1.21	0.035
After 19 hours	1.17	0.030

Figure S25: ^{19}F NMR spectra of $[\text{Pd}(5\text{-CF}_3\text{-PBO})(\text{S})_2][\text{OTf}]_2$ in dry MeCN at start (top) and after 19 hours in solution (bottom) with corresponding diffusion coefficients for each peak obtained from ^{19}F DOSY NMR.

When water is present in the catalyst solution the formation of several species is observed. The ^{19}F NMR taken immediately after the addition of the water already shows

a new peak in the CF₃ region of spectrum (labelled peak 2 in Figure S26). After 19 hours in the aqueous solution the catalyst is even more changed and more peaks in the CF₃ region of the spectrum have developed. Peak 2 after 19 hours has gotten larger and this same peak remains present in the spectrum after 41 hours of the catalyst being in solution.

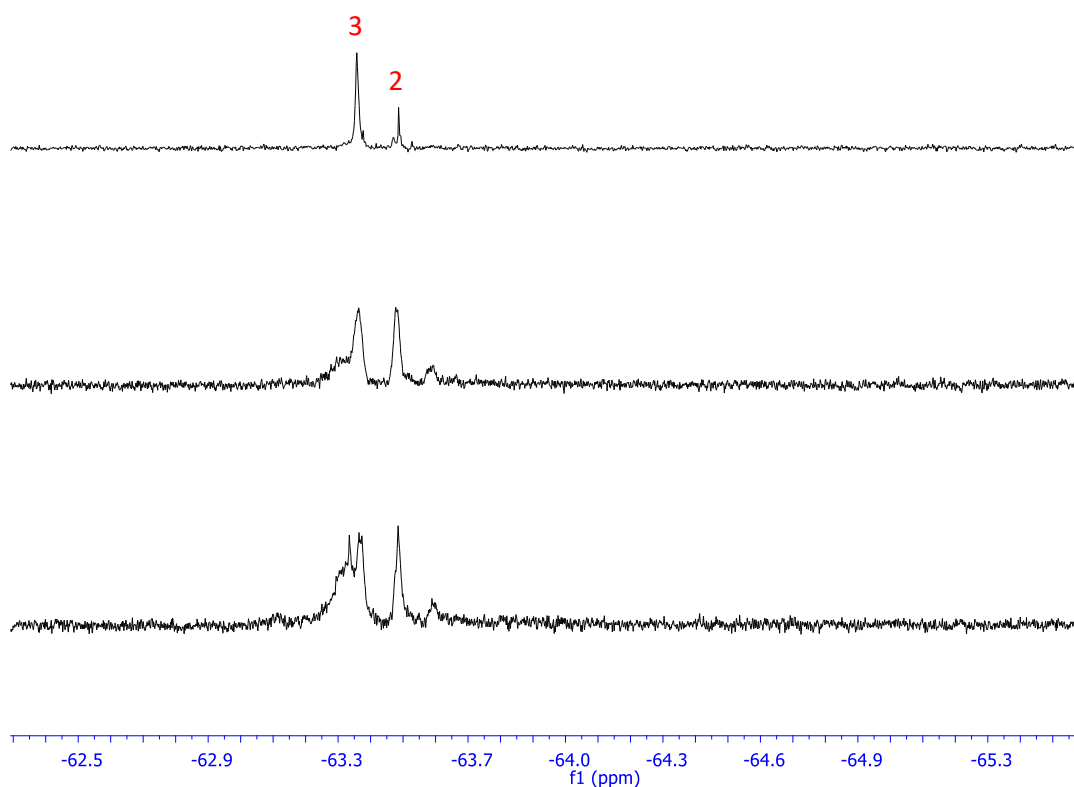
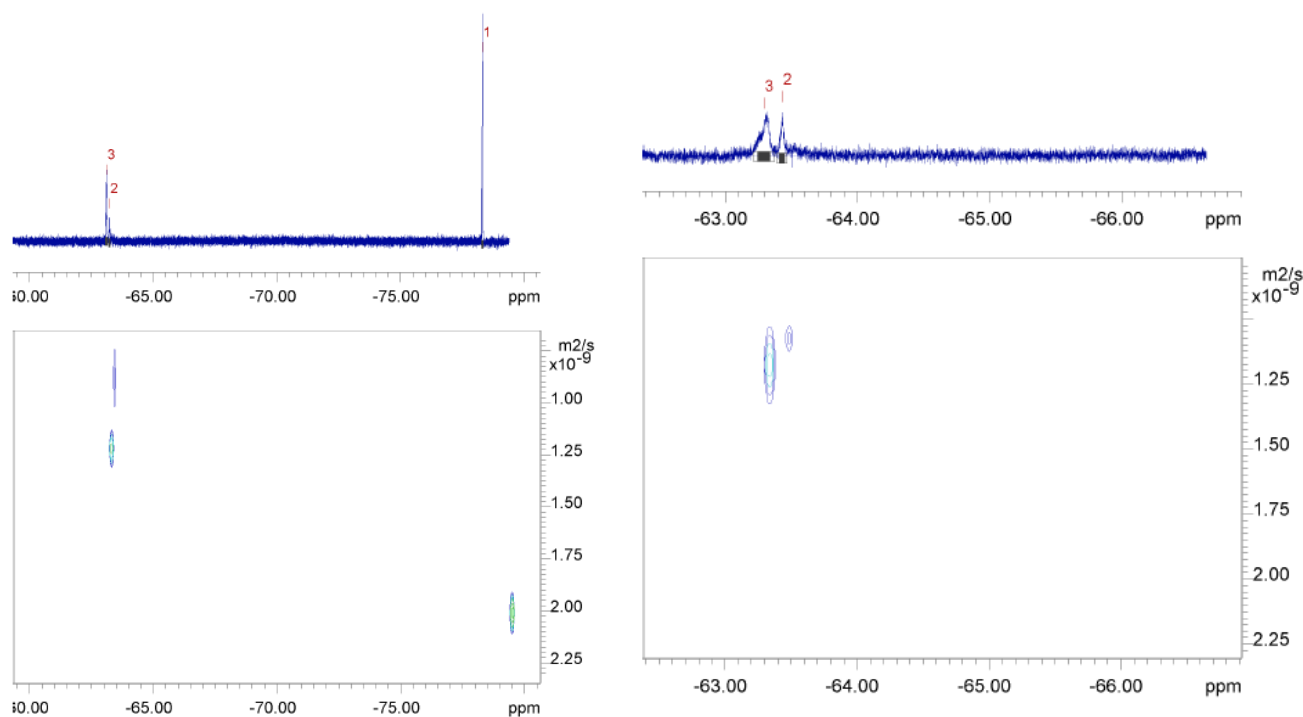


Figure S26: ¹⁹F NMR spectra of [Pd(5-CF₃-PBO)(S)₂][OTf]₂ in MeCN taken immediately after spiking with ultrapure H₂O (top), after 19 hours in solution (middle) and after 41 hours in solution (bottom). Spectra zoomed in to show peaks of interest in CF₃ region.

¹⁹F DOSY spectra of the catalyst after immediate addition of the water and after 19 hours were taken and the diffusion of the peaks compared. Immediately after water spiking, peak 2 is too small for a reliable diffusion coefficient to be obtained and efforts to do so gave results with very high error. After 19 hours in solution however once the size of peak 2 has increased, DOSY analysis shows this peak to be diffusing more slowly than the pure catalyst. The pure catalyst here refers only to the peak labelled 3

in the top spectrum of Figure S26 and the left-hand spectrum of Figure S27, as after sitting in aqueous solution over time this is no longer only the pure catalyst peak. This result suggests that peak 2 corresponds to a larger molecular species than the pure catalyst, such as a hydroxy bridged catalyst aggregate. The ^{19}F DOSY spectra and the obtained diffusion coefficients are shown in Figure S27.



Catalyst in wet MeCN	CF_3 peak Diffusion ($\times 10^{-9} \text{ m}^2\text{s}^{-1}$)	Error ($\times 10^{-9} \text{ m}^2\text{s}^{-1}$)
Immediately after adding water	1.20	0.046
Peak 2 after 19 hours	1.04	0.068

Figure S27: ^{19}F DOSY NMR of $[\text{Pd}(5\text{-CF}_3\text{-PBO})(\text{S})_2][\text{OTf}]_2$ immediately after water addition (left) and after 19 hours in aqueous solution (right).

Inhibition Studies

Mimoun has also proposed that formation of stable π -allyl complexes could be a source of catalyst deactivation in Wacker oxidations.²⁷ Although the degree of isomerization taking place in these reactions using the 5-CF₃ catalyst is minimal, it is possible that the internal alkenes formed can coordinate to the Pd catalyst preventing binding of the terminal olefin substrate. Terminal alkenes form less stable π -allyl complexes than their internal counterparts.²⁶ To test if this was a significant contributor to catalyst deactivation in the oxidation of 1-octene, the reaction was carried out in the presence of exogenously added 4-octene to act as an inhibitor. In the presence of the terminal olefin, oxidation of the 4-octene was not observed. The kinetic plot using 0.5 mol% catalyst under dry conditions shows the reaction begins to slow down noticeably once 60% yield of the 2-octanone is reached (Figure S17). Based on this, the amount of 4-octene added was 0.03 equivalents relative to the 1-octene, mimicking the isomers present at this point in the reaction. The results are shown in Figure S28 and 4-octene is not a strong inhibitor of the reaction at these concentrations. Due to the increased steric demand of the 4-octene, binding to the Pd centre is expected to be more difficult than for the terminal alkene. These results suggest that if any binding of the internal alkene is happening that it is reversible, and formation of π -allyl complexes is not a major mechanism of catalyst deactivation.

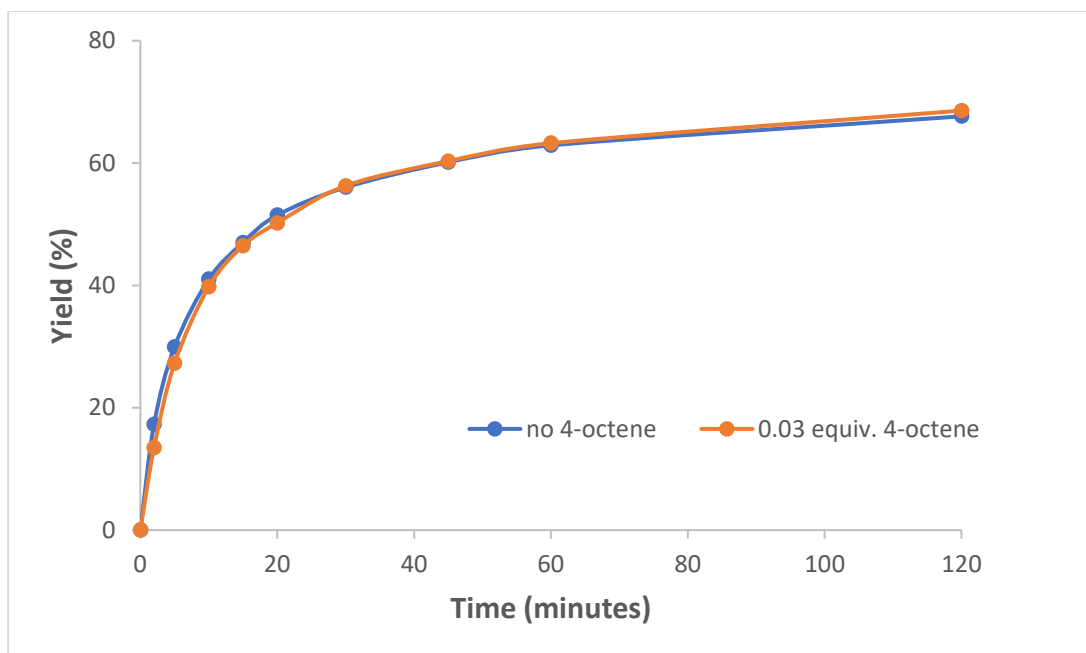
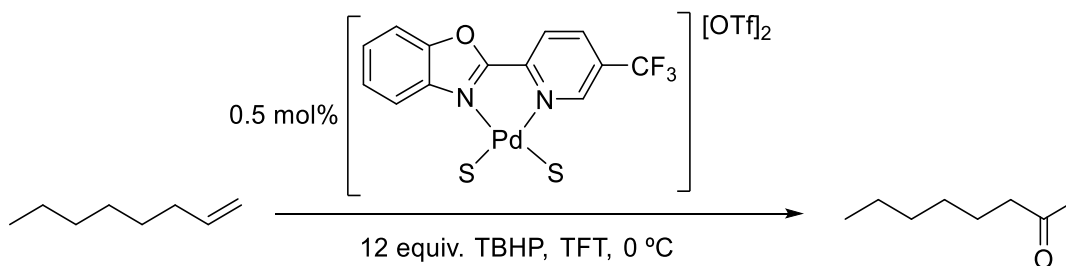


Figure S28: Comparison of 1-octene oxidation in the presence of 4-octene.

Product inhibition is another possible mechanism of catalyst deactivation. The cationic catalyst species is highly electrophilic, and this is crucial to the excellent performance of these catalysts. Competitive binding of the Lewis basic ketone product to the metal centre could be responsible for the slowdown in reaction. To test this, the oxidation of 1-octene was carried out in the presence of 2-butanone and the reaction rate monitored (Figure S29). The addition of 0.5 equivalents of 2-butanone had no effect on the rate of oxidation of 1-octene throughout the reaction and product inhibition is therefore not a cause of catalyst deactivation.

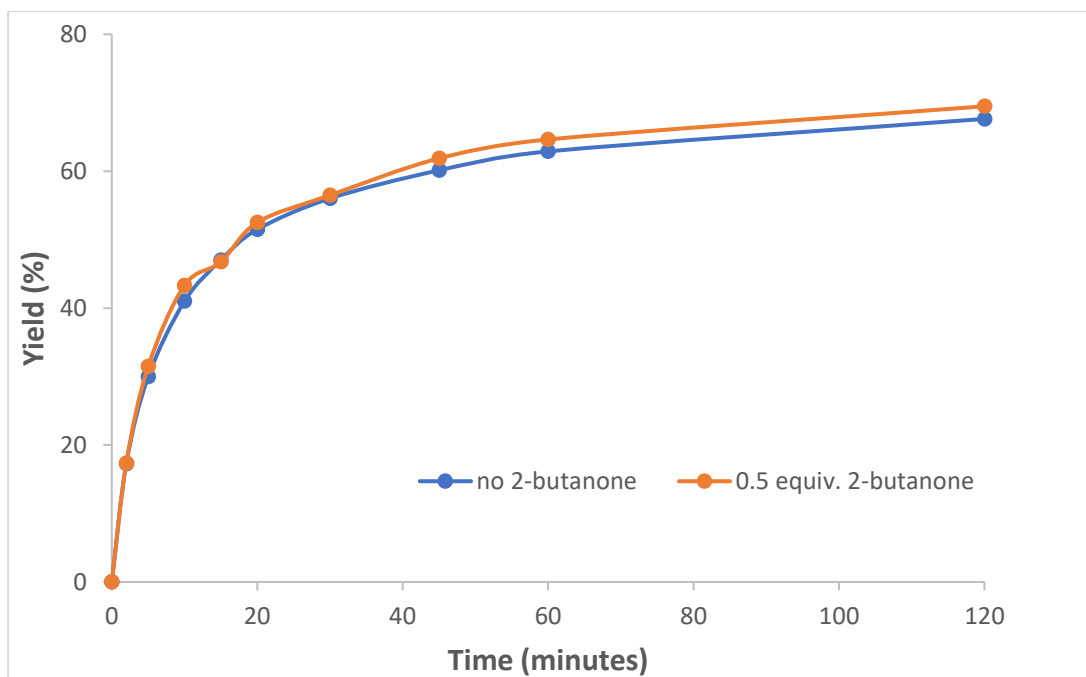
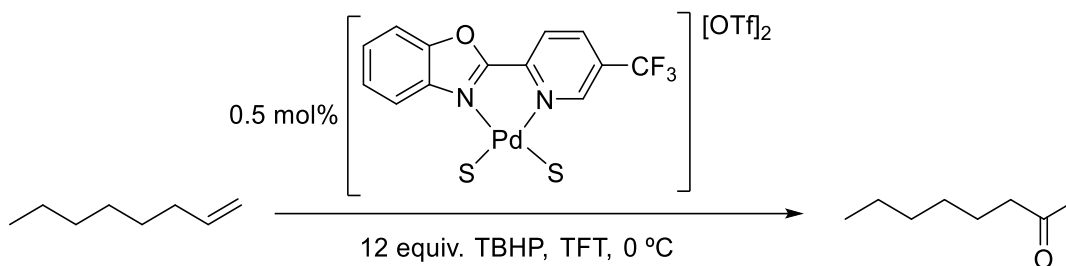


Figure S29: Comparison of 1-octene oxidation in the presence of 2-butanone.

The final component tested as an inhibitor was *tert*-butanol, one equivalent of which is produced for every molecule of TBHP that reacts to form the product. The results using this as an inhibitor are shown in Figure S30. In the presence of 0.6 equivalents of *t*-BuOH the rate of oxidation of 1-octene is marginally slowed, implying *t*-BuOH can act as a slight inhibitor of the reaction.

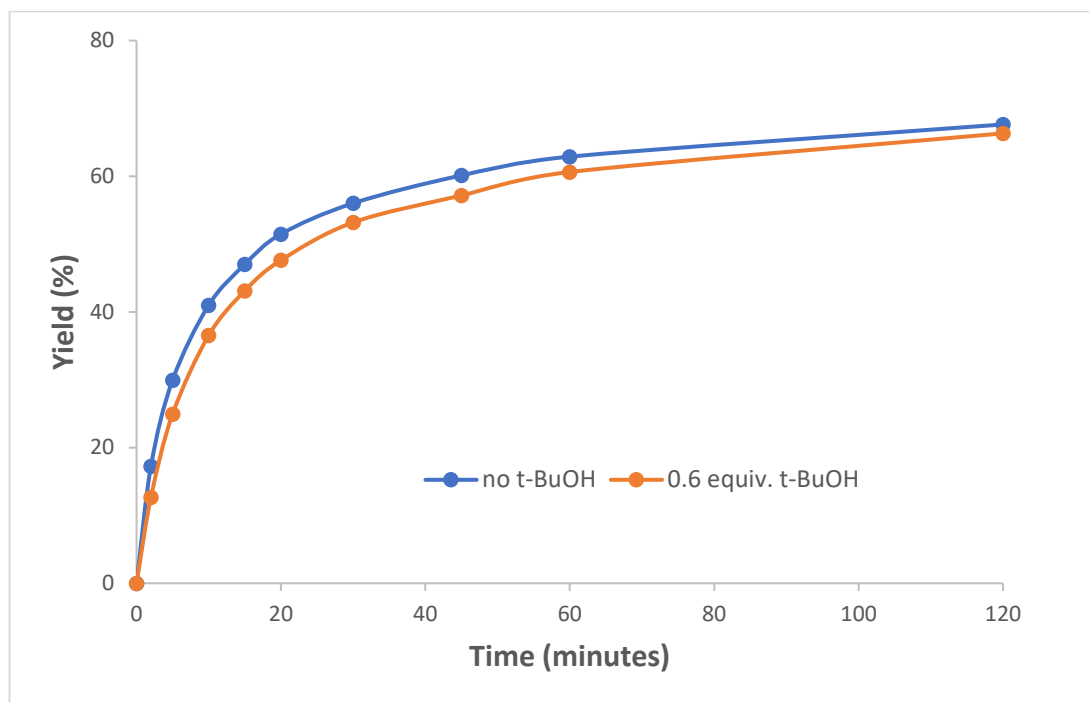
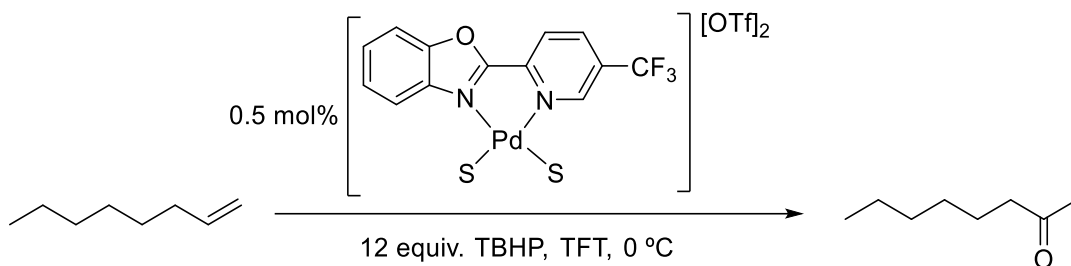


Figure S30: Comparison of 1-octene oxidation in the presence of *t*-BuOH.

Oxidation of Oct-1-en-3-yl acetate

The conditions used (and yield obtained) by Sigman and co-workers for this substrate are shown in Figure S31.

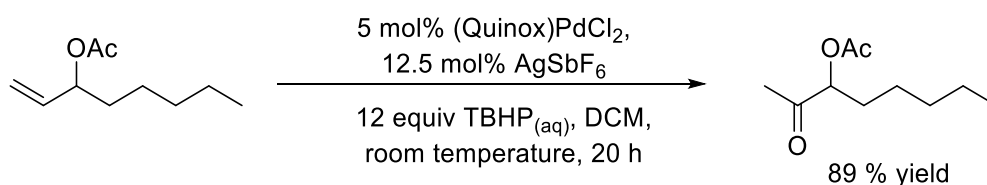


Figure S31: Sigman conditions for oxidation of using oct-1-en-3-yl acetate (Quinox)PdCl₂ and TBHP_(aq).⁴

The oct-1-en-3-yl acetate substrate is especially challenging due to substrate and product inhibition of the catalyst arising from coordination of the ester carbonyl group. In the case of the substrate, it is possible this could act as a chelating ligand, with the acetate group and the alkene interacting with the palladium. The product was also found to be an inhibitor by carrying out the oxidation of 1-octene in the presence of one equivalent (Figure S32). With one equivalent of the acetate product present during the reaction a 10% decrease in yield of the 2-octanone was obtained.

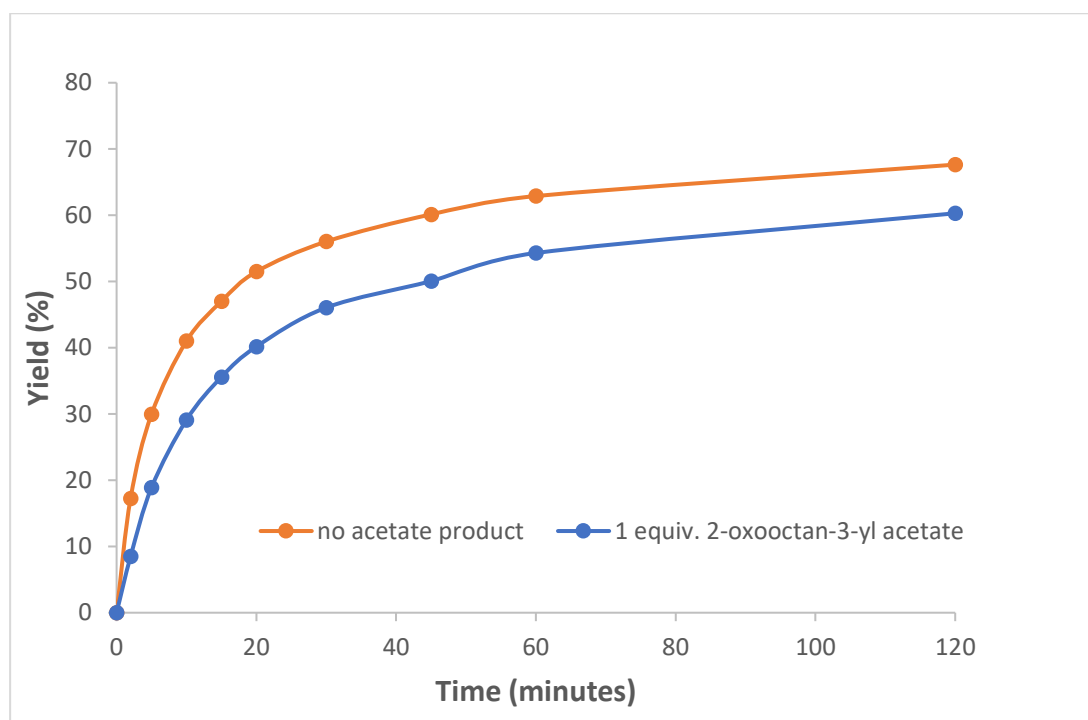
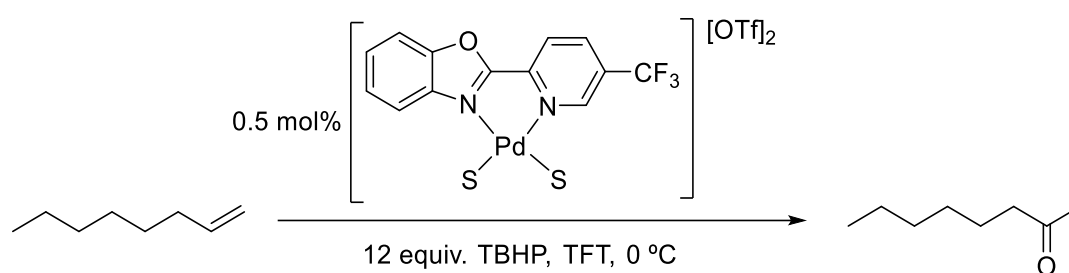


Figure S32: Comparison of 1-octene oxidation in the presence of 2-oxooctan-3-yl acetate product.

This difficult acetate substrate was initially tested using the new 5-CF₃ catalyst under both wet and dry conditions at a loading of 1 mol% (Figure S33). During the early stages, up to approximately 50% yield, there is minimal difference in the wet and dry conditions. As the reaction progresses, the difference between the two systems becomes more apparent. Under dry conditions the final yield after 24 hours is 77%, which is 15% higher than can be achieved under aqueous conditions. In both cases complete conversion of the starting material is not achieved. Substrate/product inhibition of the catalyst may be responsible for the similarity in the yields during the early stages of the reaction as there is less chance for the water to bind to the metal. This would slow the formation of inactive aggregates compared to the 1-octene substrate. The amount of catalyst inhibition present using this substrate is also reflected in the much slower rates of reaction relative to 1-octene. Although this result compares well to the Sigman Quinox catalyst system which required 5 mol% loading to obtain 89% yield.

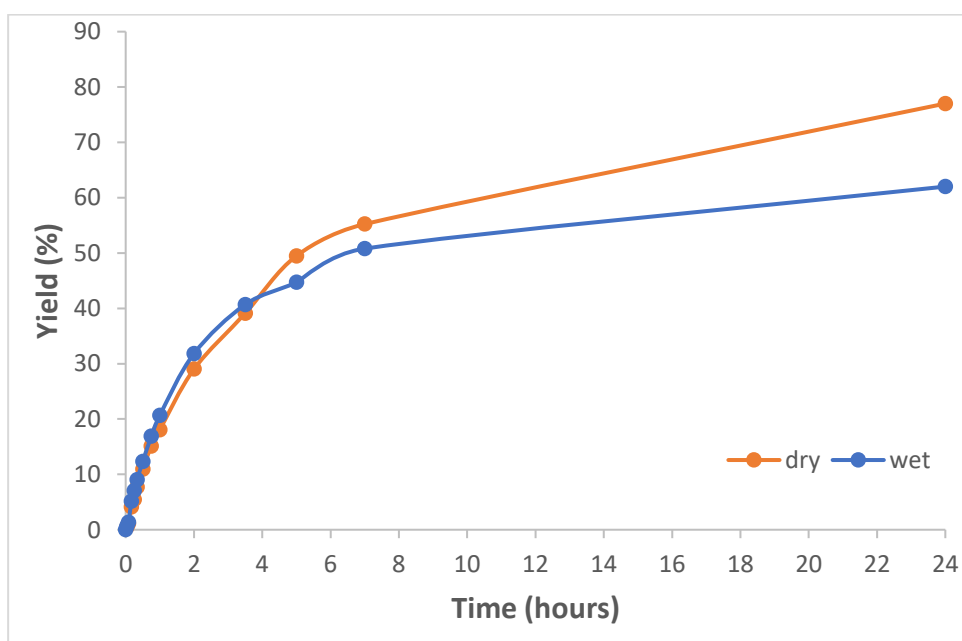
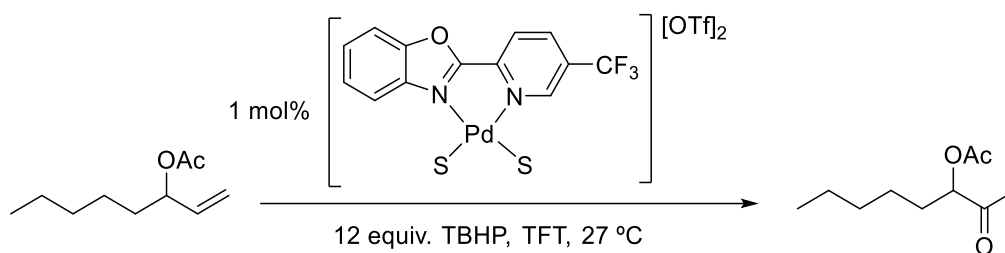


Figure S33: Oxidation of oct-1-en-3-yl acetate substrate using 5-CF₃ conditions under wet and dry conditions in TFT.

Using HFIP to Prevent Substrate/Product Inhibition

It was envisaged that 1,1,1,3,3,3-hexafluoroisopropanol (HFIP) could be used to prevent substrate/product inhibition in the Wacker oxidation of oct-1-en-3-yl acetate and improve catalyst performance. The interactions between HFIP and the oct-1-en-3-yl acetate substrate were determined by Job plot analysis (Figure S34), something which has previously been utilised in other HFIP studies.²⁸⁻³⁰ Downfield shift of the HFIP hydroxy proton was observed and the peak abscissa value was measured at a HFIP mole fraction of 0.50. This value indicates the formation of a 1:1 complex, formed through hydrogen bonding between the HFIP hydroxy proton and the ester carbonyl of the substrate.

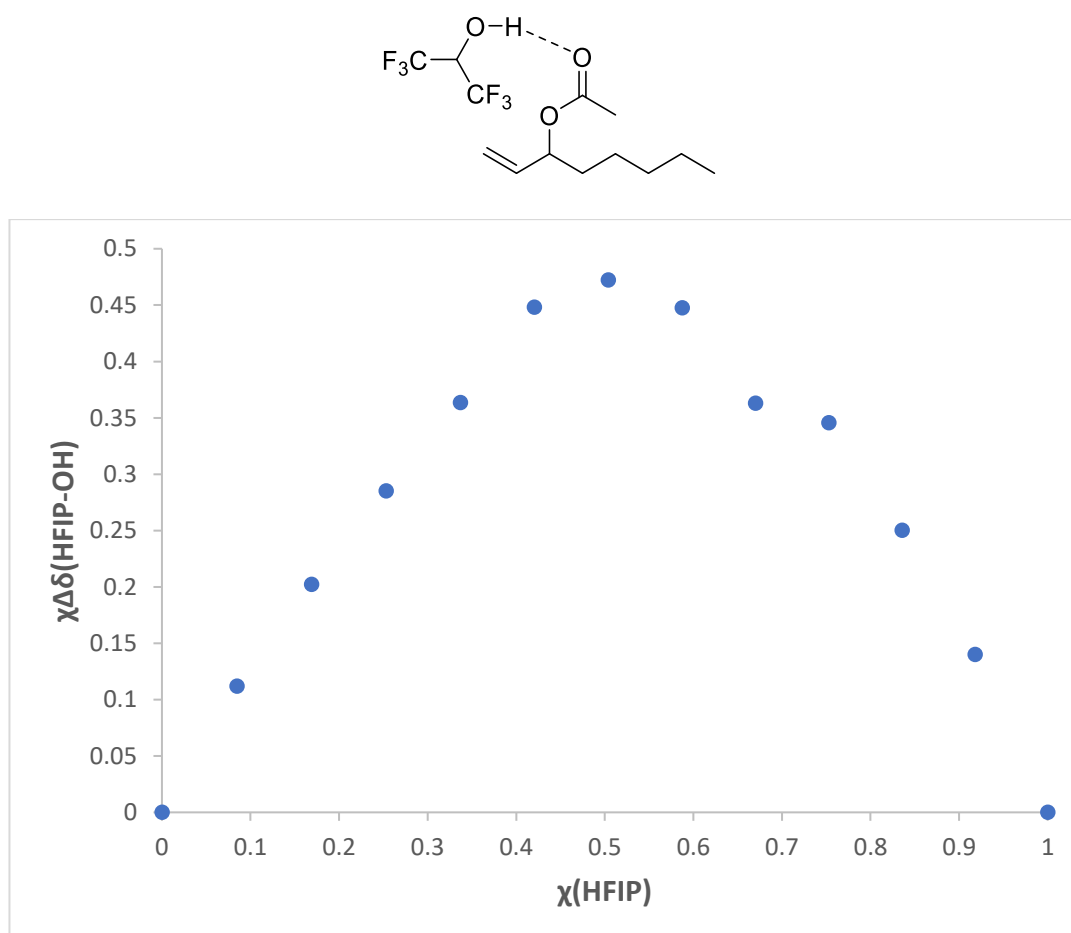


Figure S34: Job plot showing formation of 1:1 complex between HFIP and oct-1-en-3-yl acetate in CDCl₃. HFIP hydroxy proton followed.

The same Job plot analysis was done to determine the interactions between HFIP and the 2-oxooctan-3-yl acetate product (Figure S35). The product contains two carbonyl groups and therefore two possible sites of interaction for HFIP. Again, downfield shift of the HFIP hydroxy proton was observed. In this case the peak abscissa value was measured at a HFIP mole fraction of 0.58 which indicates that there is a mixture of both 1:1 and 2:1 complexes formed. Strong complexation to the more electron dense ester carbonyl occurs followed by a weaker second interaction with the ketone.

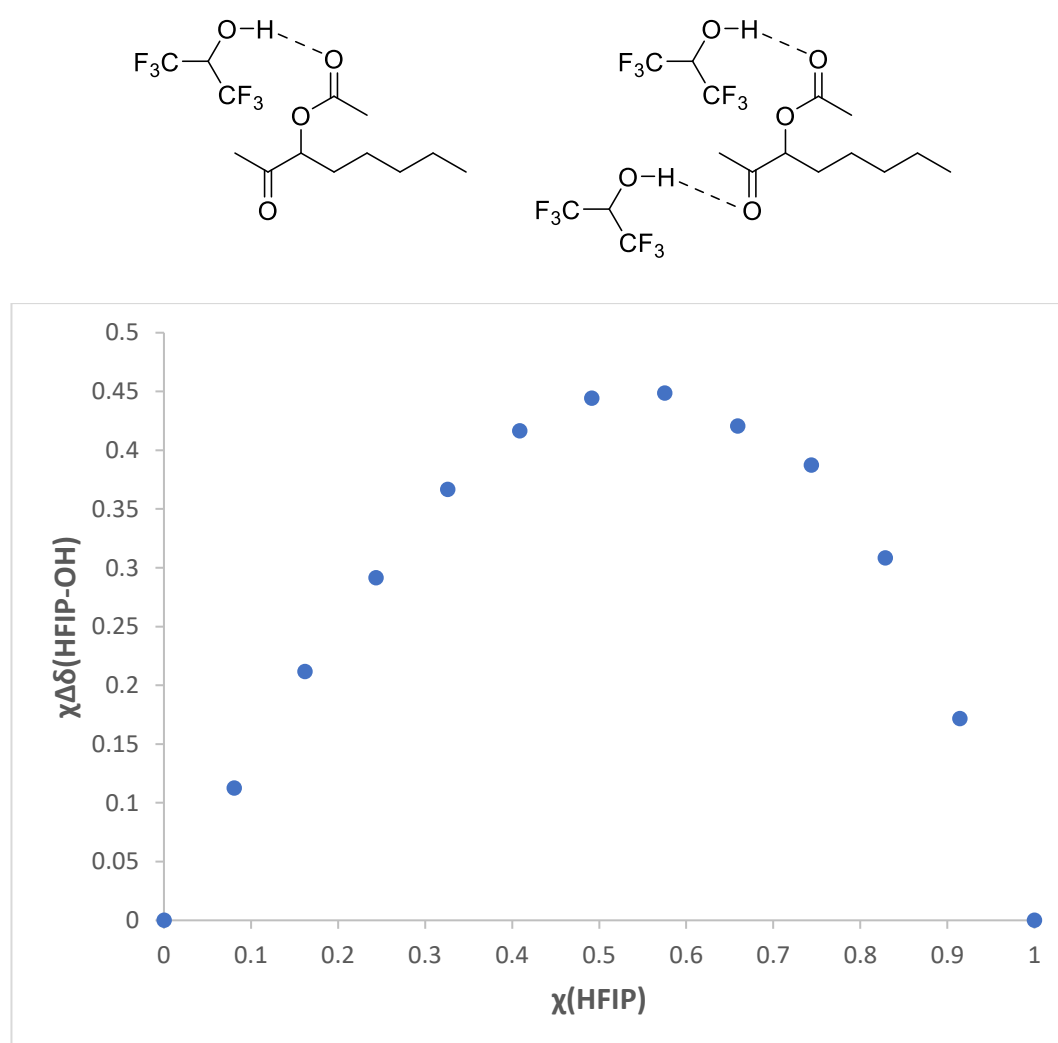


Figure 35: Job plot showing formation of a mixture of 1:1 and 2:1 complexes between HFIP and 2-oxooctan-3-yl acetate in CDCl_3 . HFIP hydroxy proton followed.

Job plot analysis confirmed that HFIP binds to both the oct-1-en-3-yl acetate substrate and corresponding ketone product and this binding could feasibly prevent substrate/product inhibition of the catalyst. To put this to the test, the Wacker oxidation of oct-1-en-3-yl acetate was carried at a catalyst loading of 1 mol% with varying equivalents of HFIP added relative to the substrate. The results of these tests are shown in Figure S36. HFIP was found perform as desired and greatly improved catalyst performance. With the addition of as little as 1 equivalent of HFIP present under dry conditions, the reaction can now be taken to completion and a yield of 90% obtained. Adding more HFIP equivalents further increases the rate of the reaction up to 20 equivalents where reductions in yield were found. Using 10 equivalents gives both high yield and exceptionally fast reaction rates, with the reaction going to completion in under 2 hours. The catalyst loading could be dropped further to 0.5 mol% using 10 equivalents of HFIP and complete conversion of the substrate still reached with a yield of 81%.

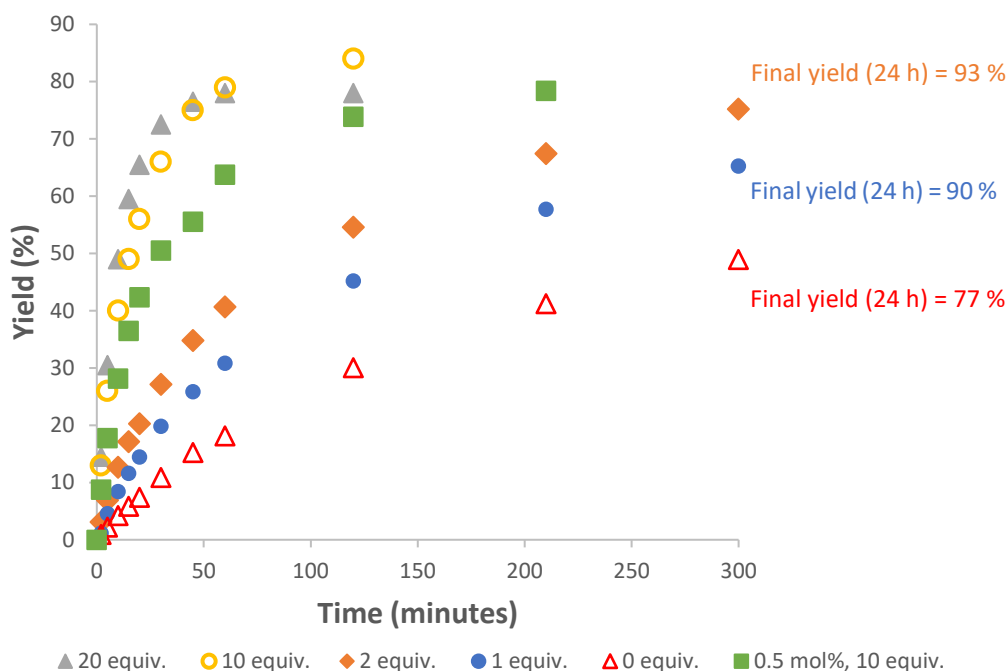
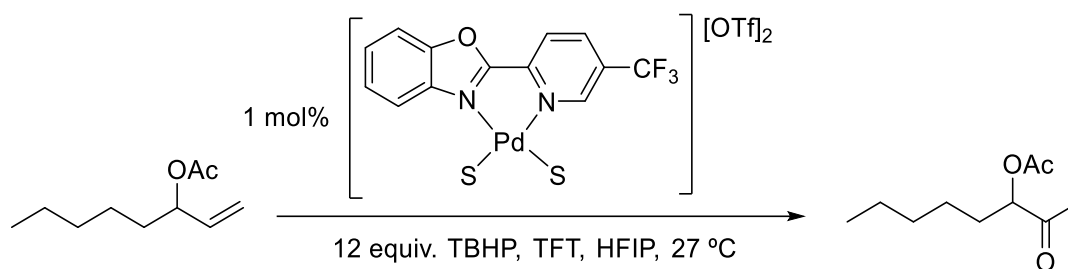


Figure S36: Using HFIP as additive in Wacker oxidation of oct-1-en-3-yl acetate. Each plot an average of 2 reactions.

HFIP was tested as an additive in reactions using 1-octene but was found to be incompatible as it led to very high levels of isomerization. Both 10 and 5 equivalents of HFIP relative to the 1-octene was found to lead to a 50/50 mixture of 2-octanone product and internal isomers. This finding is in line with other studies where HFIP has been used as both a solvent and an additive for the $\text{Pd}(\text{OAc})_2$ catalysed double bond migration of terminal alkenes.³¹

Using HFIP to Reduce Catalyst Deactivation under Aqueous TBHP Conditions

When 10 equivalents of HFIP was used in combination with aqueous TBHP, complete conversion of the oct-1-en-3-yl acetate could be achieved at a catalyst loading of 1

mol%. A yield of 95% was reached compared to the 62% previously obtained in the absence of HFIP (Figure S37). It was found that with 20 equiv. of HFIP, the aqueous TBHP was more robust/reproducible (see Figure 8 in main paper for more data).

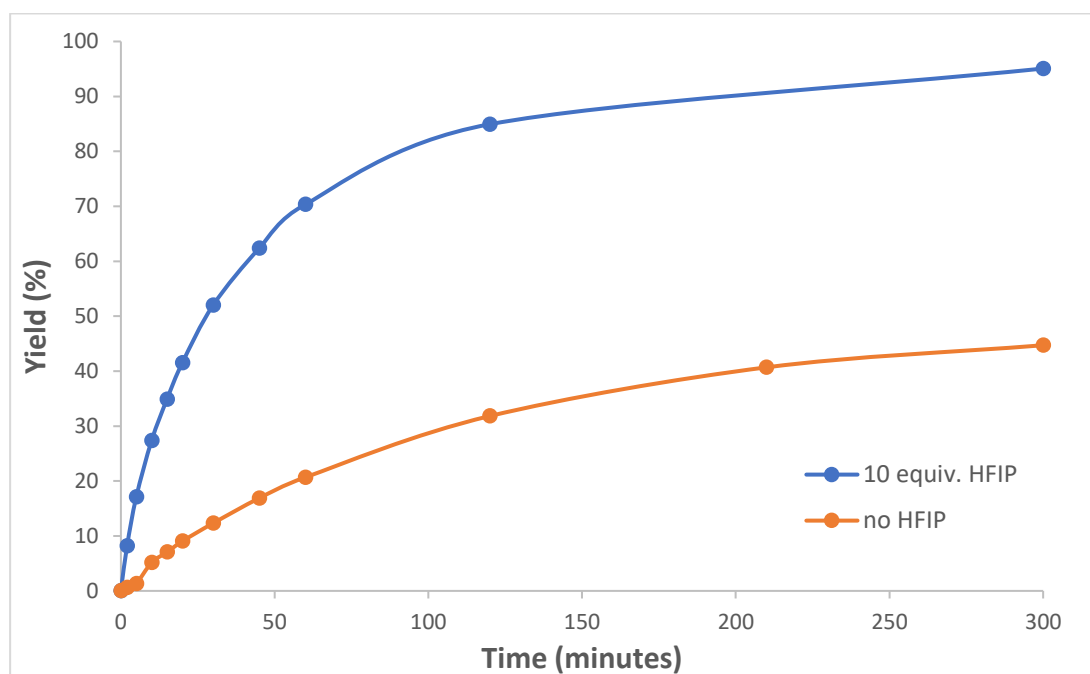
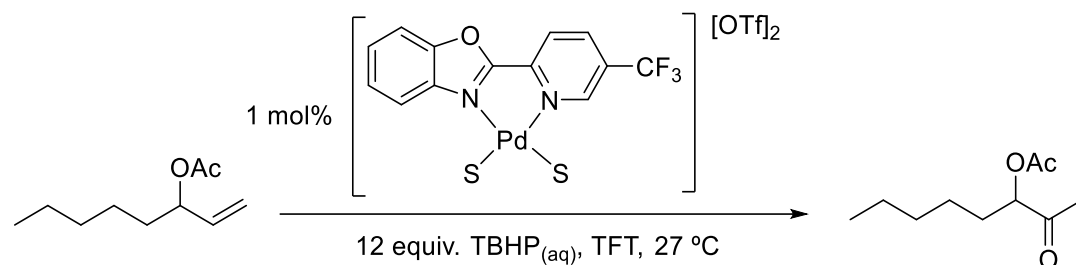


Figure S37: Wacker oxidation of oct-1-en-3-yl acetate using aqueous TBHP with and without HFIP.

In the same way that HFIP stops substrate/product inhibition by binding to the carbonyl groups present, the binding of HFIP to water could reduce its coordination to the Pd and slow the formation of inactive hydroxy species in these aqueous systems. Alternatively, HFIP could also facilitate the breakup of these hydroxy species once they have formed. Mayr and Ammer have investigated the solvent nucleophilicity of HFIP/water mixtures for the attack of benzhydrylium cations. They found that the nucleophilicity of the solvent mixtures increased as the mole fraction of water

increased, and that even the addition of as little as 10 mol% HFIP greatly reduced the nucleophilicity of pure water.³²

To investigate HFIP preventing catalyst deactivation in these ways, ¹⁹F NMR was again employed and the speciation of the catalyst monitored in wet MeCN. Firstly, the catalyst was dissolved in MeCN, spiked with water and left for 2.5 hours before HFIP (2 equivalents relative to the substrate in oxidation reaction mixtures) was added. This HFIP containing solution was left overnight and a ¹⁹F NMR spectrum taken and compared with that previously obtained for the catalyst in wet MeCN (Figure S38). Apart from peak shifting due to the presence of HFIP, the two spectra are very similar, and this suggests that HFIP is not able to break up the hydroxy bridged aggregates once they have already formed in solution.

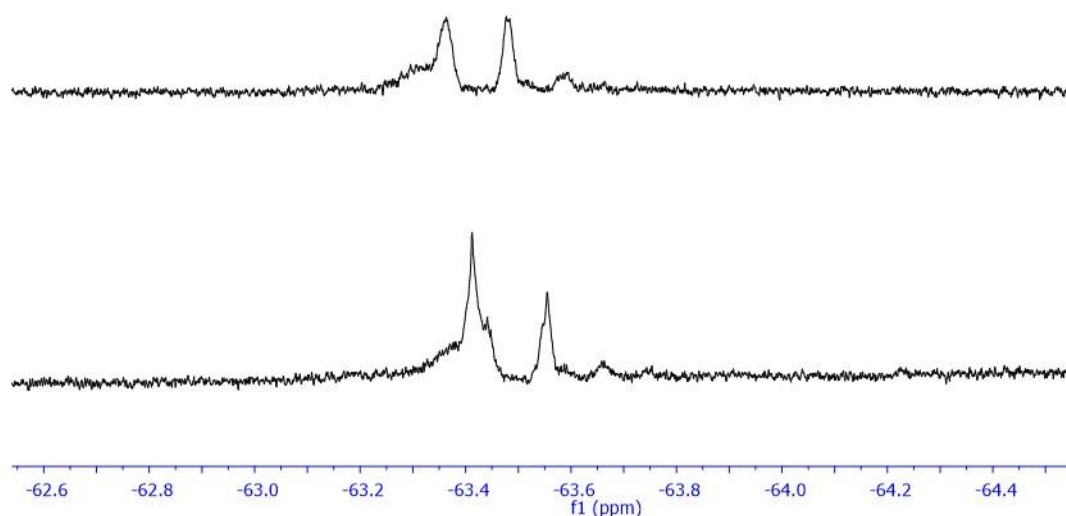


Figure S38: ¹⁹F NMR spectra of catalyst in wet MeCN after 19 hours (top) and catalyst in MeCN with HFIP added after 2.5 hours and left overnight (bottom).

The next test was to dissolve the catalyst in MeCN, spike it with water, add HFIP immediately to the solution and monitor any changes in the ¹⁹F NMR over time (Figure S39). When HFIP is present from the start, the changes in the NMR spectrum over

time are significantly reduced and the spectra obtained after 21 hours resembles the initial spectrum much more strongly than when the HFIP is not present.

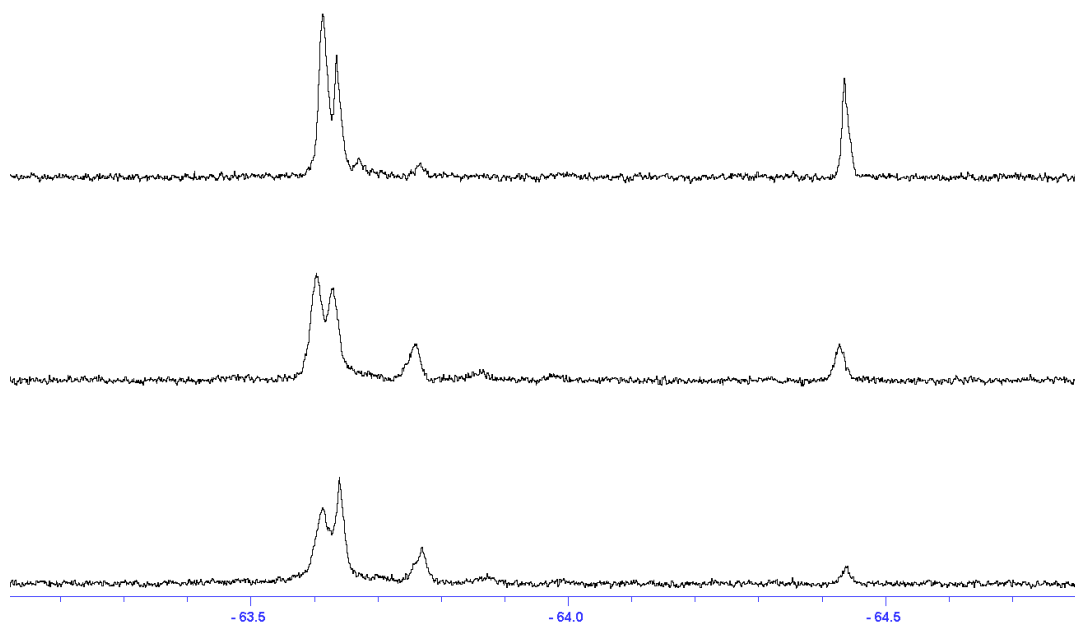


Figure S39: ^{19}F NMR spectra of catalyst in wet MeCN with HFIP present from the beginning at the start (top), after 2.5 hours (middle) and after 21 hours (bottom).

Two experiments involving the Wacker oxidation of oct-1-en-3-yl acetate were devised to further test this hypothesis. In one reaction the catalyst was stirred in TFT with aqueous TBHP for four hours before the addition of 10 equivalents of HFIP and substrate. In the other experiment the catalyst was stirred in TFT, aqueous TBHP and 10 equivalents of HFIP for 3 hours before the substrate was added. The results of these two experiments are shown in Figure S40. When the HFIP is present for the 3 hours stirring with aqueous TBHP, the rate of substrate oxidation is much higher and complete conversion of the starting material can be reached with a final yield of 91%. When the catalyst is exposed to water in the absence of HFIP for three hours, complete conversion cannot be attained at 0.5 mol% catalyst loading and a considerably lower yield of 65% is obtained. These results backed up by the ^{19}F NMR studies are consistent with HFIP reducing catalyst death caused by water in aqueous reactions, possibly by reducing binding of the water to the metal centre and slowing the formation of inactive hydroxy bridged species.

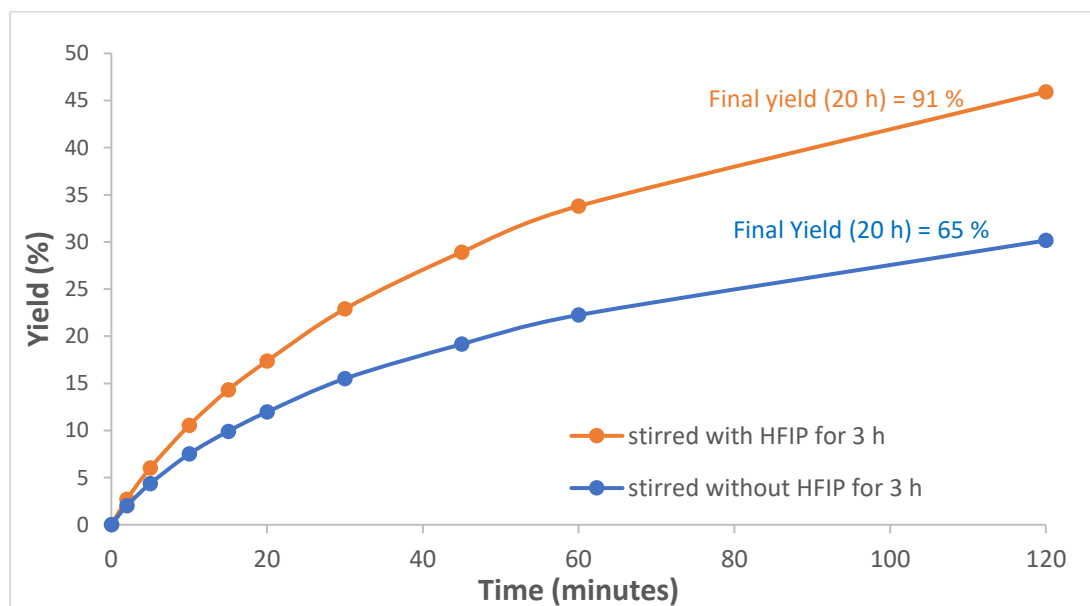
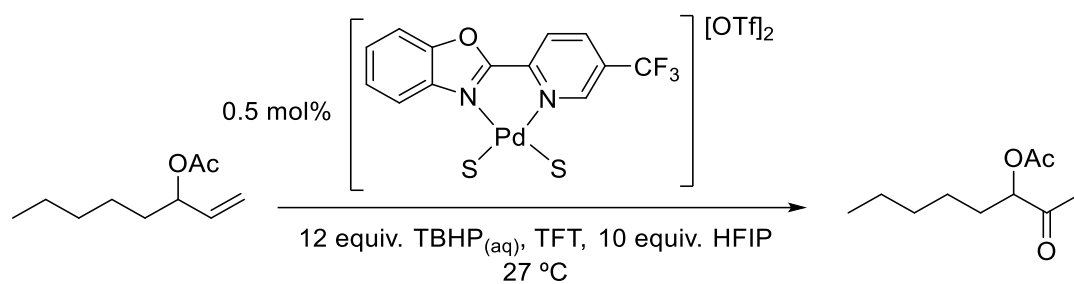


Figure S40: Kinetic plots for the oxidation of oct-1-en-3-yl acetate when the catalyst is stirred with aqueous TBHP for 3 h with and without HFIP present. Plots an average of two runs.

Comparison of 5-CF₃ Catalyst at 0.25 mol% Loading under Dry and Aqueous Conditions with HFIP

The catalyst loading was dropped even further to 0.25 mol% and the oxidation of oct-1-en-3-yl acetate carried out with HFIP under wet and dry conditions (Figure S41). Although HFIP can slow catalyst sufficiently to allow complete conversion of starting material at 1 mol% loading with aqueous TBHP, at this lower catalyst loading dry conditions are needed to obtain a complete reaction. Impressively, a yield of 92% was obtained using the anhydrous protocol, compared with a 34% yield when aqueous TBHP was employed. This result represents a 20-fold drop in catalyst loading compared to the benchmark literature conditions developed by Sigman and co-workers.

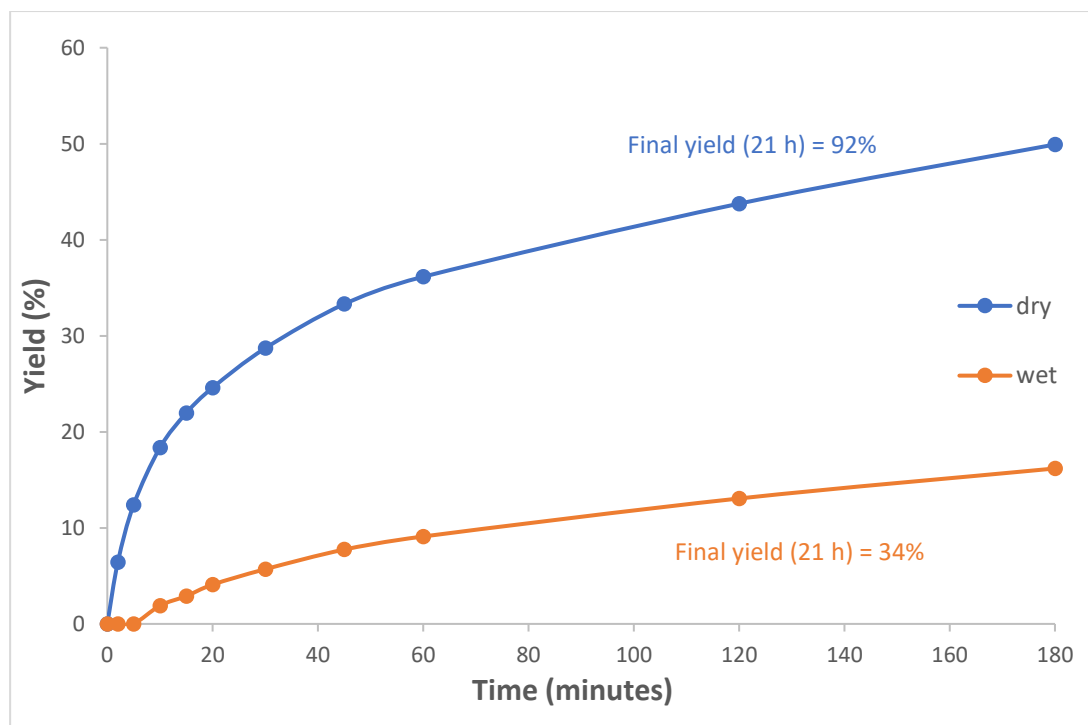
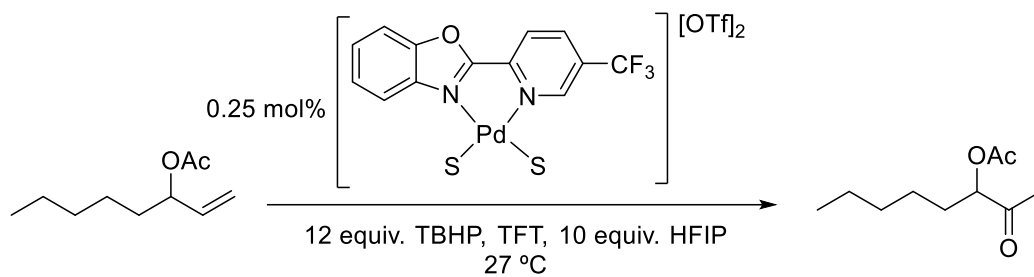


Figure S41: Wacker oxidation of oct-1-en-3-yl acetate using 5-CF₃ catalyst at a loading of 0.25 mol% under wet and dry conditions.

Re-evaluating All Second Generation PBO Catalysts in the Absence of Several Catalyst Deactivation Mechanisms

The optimised conditions greatly reduced the rate of catalyst decomposition; therefore it was decided to once again examine a range of pre-formed cationic complexes. We wanted to determine if the 5-CF₃-PBO ligand was indeed the best in terms of TON or just initial reaction rate. All ligands that were amenable to forming the pre-formed cationic triflate complexes were screened at 0.25 mol% loading and followed for 3 hours to determine rates as well as the final yield being taken (Figure S43). Structures for all ligands tested are also shown below with accompanying abbreviations used for each (Figure S42).

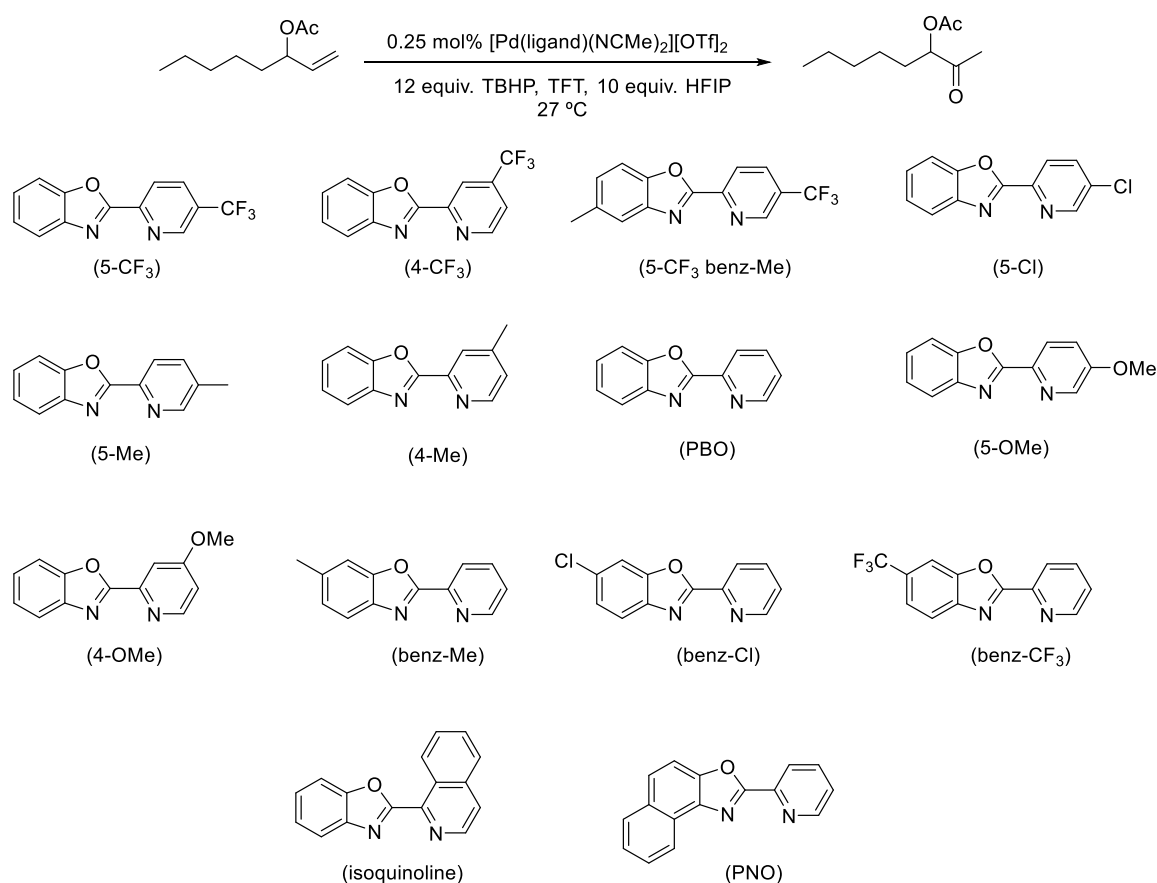


Figure S42: Ligand structures and acronyms used in Figure S45

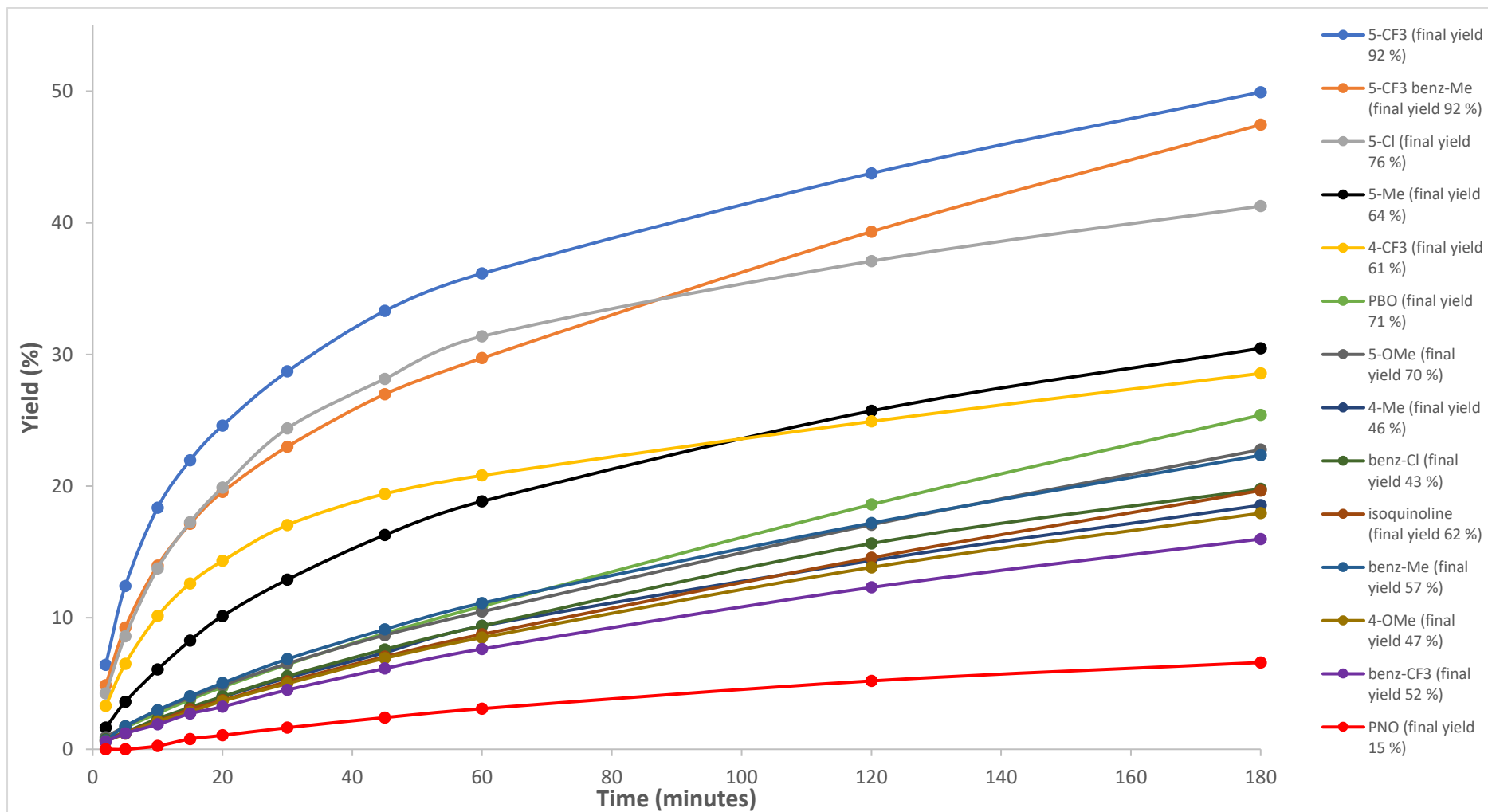


Figure S43 Screen of pre-formed cationic PBO type catalysts at 0.25 mol%. Final yields at 21 h. Kinetic plots average of two runs.

The trend of electron withdrawing groups on the pyridine moiety of the ligand giving fast reactions was again observed, with the 5-CF₃ still giving the highest rate. The 5-CF₃ was followed by the 5-Cl and the 5-CF₃ benz-Me ligands. The 5-CF₃ catalyst gave the highest yield at 92%, corresponding to a TON of 368. This TON was equalled by the 5-CF₃ benz-Me ligated catalyst. Despite starting off rapidly, the 4-CF₃ catalyst yield tailed off quickly and gave a significantly lower final TON than the other strongly electron withdrawing groups and even that of the underivatized PBO. Stability of this 4-CF₃ catalyst still appears to be an issue even under the optimized reaction conditions.

There are two notable outliers to these electronic trends, the first being the 5-OMe ligand. The OMe group is slightly withdrawing in the 5 position but the reaction rate is marginally slower than that of the underivatized PBO. Despite the poor initial rates, this catalyst gives a final yield of 70%, higher than that obtained with the 4-CF₃ catalyst. So, although this PBO catalyst is slower than the 4-CF₃ it is more stable. The other unexpected result came from the 5-Me ligand. The Me group in the 5 position is slightly electron donating but was found to give better results than anticipated. The reaction is much faster using this catalyst than the unfunctionalized PBO ligand and is only marginally slower than the 4-CF₃ catalyst before finally overtaking it around 25% yield. These outliers coupled with the 5-CF₃ ligand consistently outperforming the 4-CF₃ point to the steric bulk of the ligand in the 5 position having an influence on catalyst stability. To further probe this, the 4-Cl ligand and the 5-ethyl ligand were synthesized along with their corresponding pre-formed cationic triflate complexes (Figure S44).

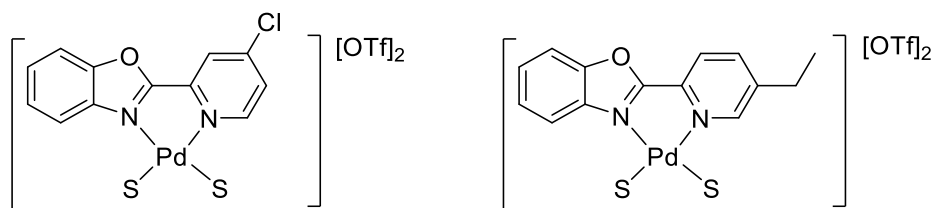


Figure S44: Structures of 4-Cl and 5-Et ligated catalysts.

The 4-Cl catalyst was the first to be tested under the 0.25 mol% conditions. Similar to the 4-CF₃ catalyst, it performed much worse than the 5-substituted counterpart. Like the 4-CF₃ catalyst, it was also found to start off much faster than the underivatized PBO but finish with a lower TON (Figure S45).

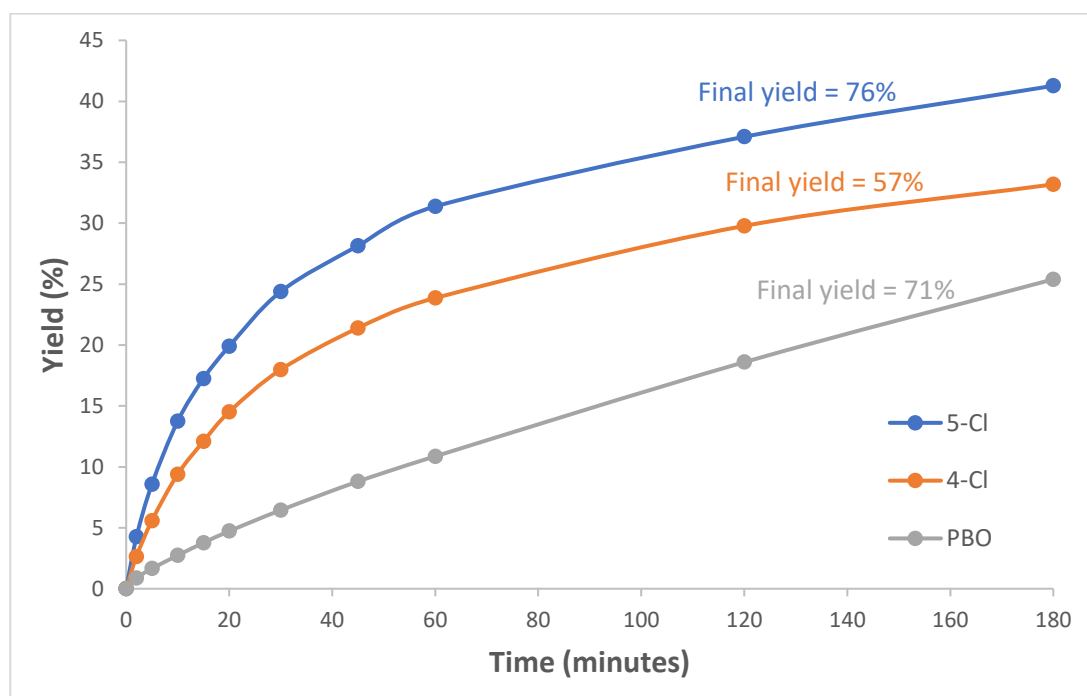
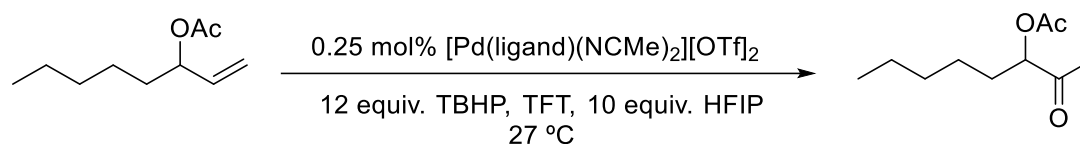


Figure S45: Comparison of 4-Cl ligand with 5-Cl and PBO ligands under optimized conditions. Kinetics plots and average of two runs.

The 5-Et group is bulkier than the 5-Me but is equivalent in its electron donating ability, with both groups having a Hammett σ of -0.07.³³ The 5-Et catalyst was found to perform even better than the 5-Me (Figure S46). Despite having the electron donating ethyl group, this catalyst gave the highest TON after the two 5-CF₃ substituted catalysts. A final yield of 84% was reached, corresponding to a TON of 336. The 5-Cl ligand gives a much faster

rate than the 5-Et as expected due to the Cl group being strongly electron withdrawing, the bulkier 5-Et group however gives a higher final yield.

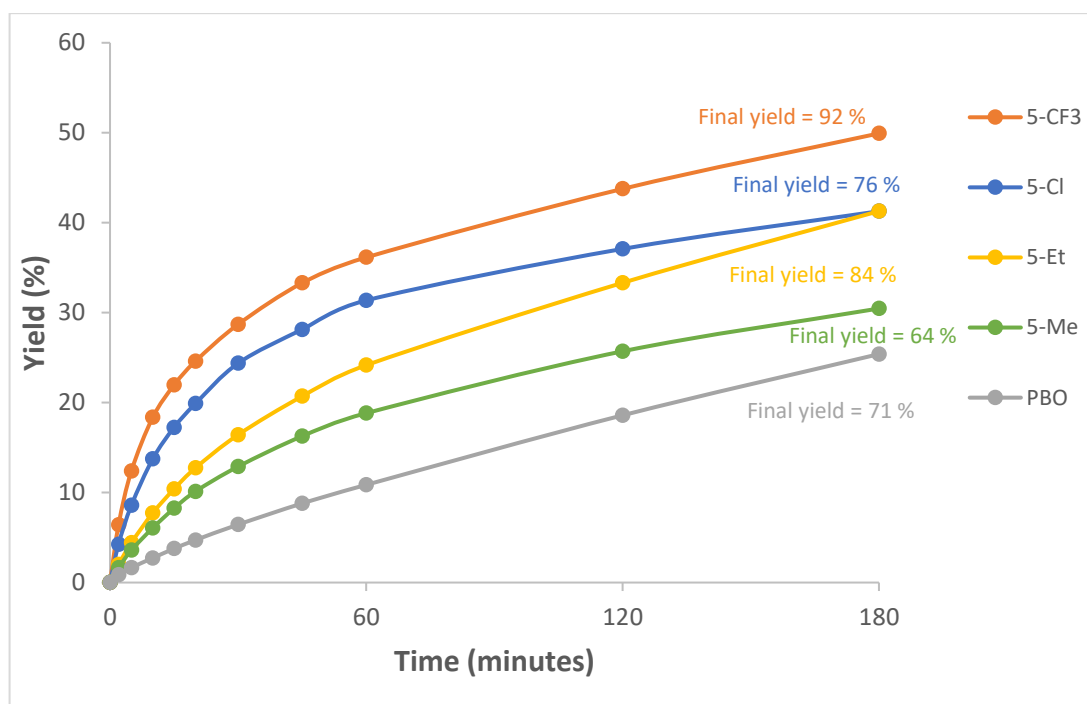
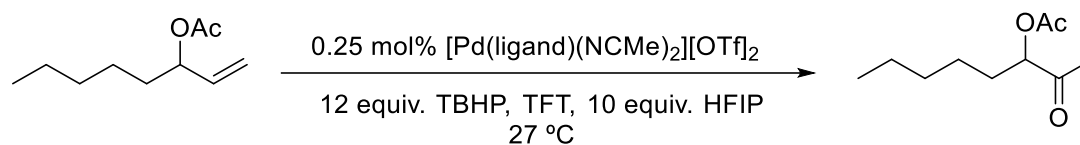


Figure S46: Comparison of 5-Et ligand with other high performing ligands.

The findings gleaned from these two newly synthesized ligands support the theory that there is a steric influence with substituents in the 5-position of the pyridine of these PBO ligands that improves catalyst stability. The 5-CF₃ catalyst can therefore be explained as the best of all those tested because the 5-CF₃ group is both highly electron withdrawing and provides a positive a steric influence.

Mechanisms of Catalyst Deactivation

Under optimized conditions for the oct-1-en-3-yl acetate substrate with HFIP, most catalysts tested are turning over at least 200 times and the major causes of catalyst death have been tackled. The inability of all catalysts to get to completion however suggests that there are mechanisms of catalyst deactivation still operating in the system. These may still be impeding the performance of even the best performing 5-CF₃ catalyst. Results from the ¹⁹F DOSY analysis of the anhydrous TBHP/PhCl as previously discussed still showed the formation of slower diffusing species by the end of the reaction. This led to the hypothesis that catalyst aggregation mechanisms through the peroxide itself acting as a bridging ligand may be responsible. Mimoun and co-workers have reported tetramer structures of the type [RCO₂PdOO-*t*-Bu]₄, formed from the treatment of the corresponding Pd(O₂CR)₂ salts with TBHP.²⁶ A single crystal of the [CCl₃CO₂PdOO-*t*-Bu]₄ variant was grown by Mimoun and co-workers and the tetramic structure in the solid phase confirmed (Figure S47). Molecular weight measurements indicated that the complexes were also probably tetramic in solution.

Dropping the amount of TBHP used in the reaction was attempted to see if this improved catalyst performance. A reaction using 3 equivalents of TBHP relative to the 1-octene substrate was performed. When any less than 3 equivalents of TBHP was used the catalyst could not be solubilized in the reaction mixture. The rate of reaction was still found to tail off at the same time as when 12 equivalents are used indicating using less TBHP not reducing catalyst deactivation (Figure S49). Slower rates and drops in yield have been found by Sigman when dropping TBHP to 4 equivalents.⁴

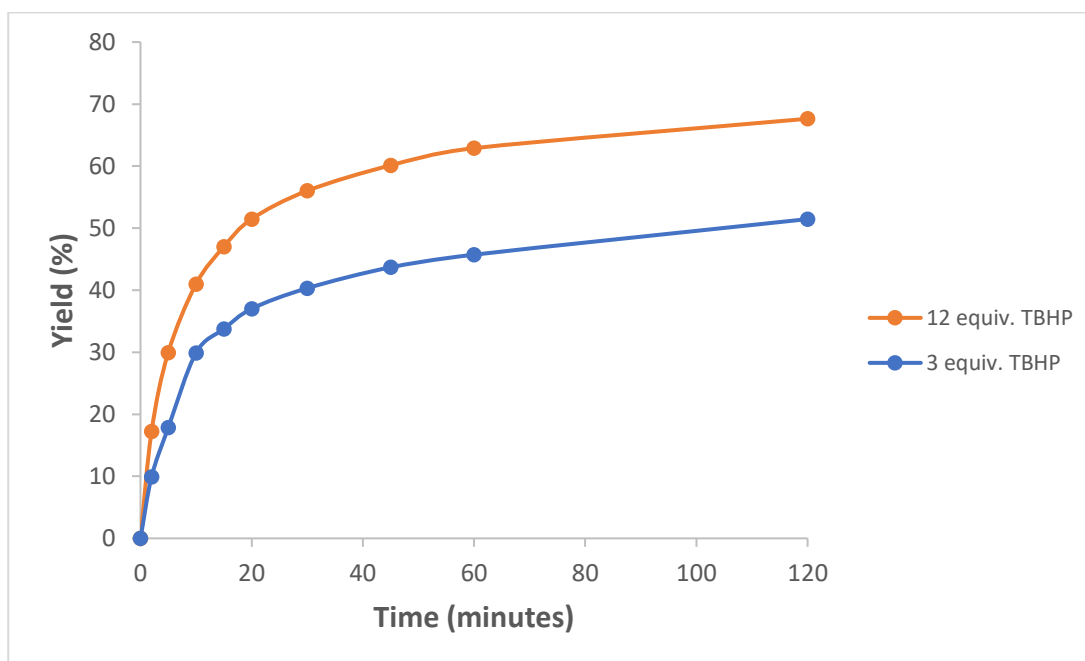
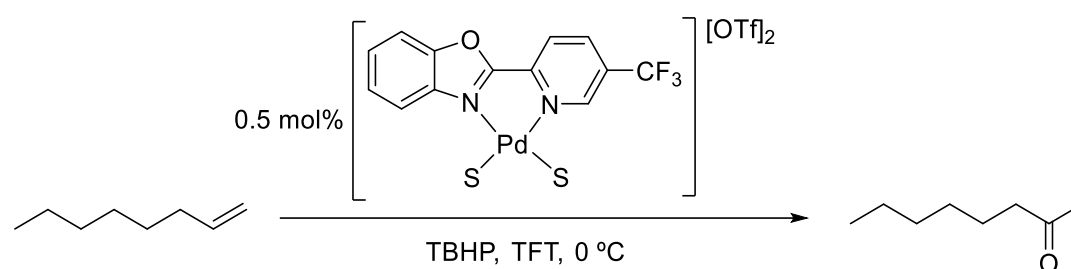


Figure S49: Oxidation of 1-octene using 3 and 12 equivalents of TBHP.

Reducing the amount of TBHP was harmful to yields and did not give any insights into the formation of peroxide bridged aggregates. Instead, the oxidation of oct-1-en-3-yl acetate was performed using 12 equivalents of TBHP at 0.5 mol% catalyst loading with 10 equivalents of HFIP with the temperature reduced from 27 °C to 0 °C. It was hoped that at lower temperature perhaps the formation of these aggregates may be less favourable and a drop off in reaction rate would not be seen until much later in the reaction. The plot obtained under these conditions is shown in Figure S50 and again the curve begins to tail off early in the reaction.

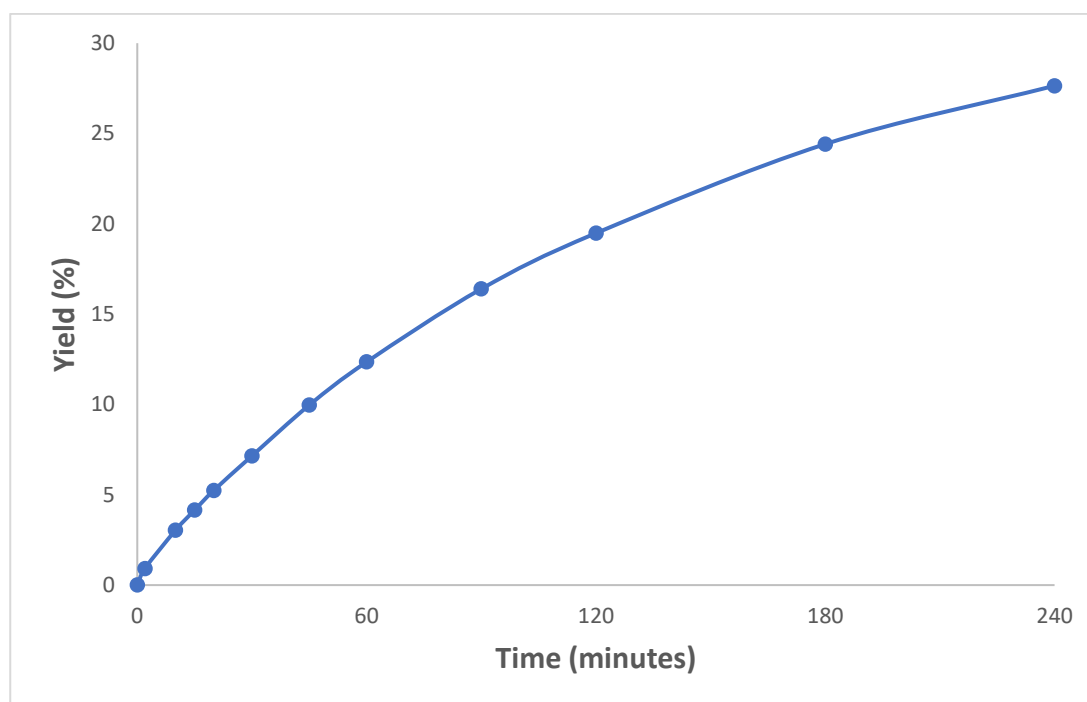
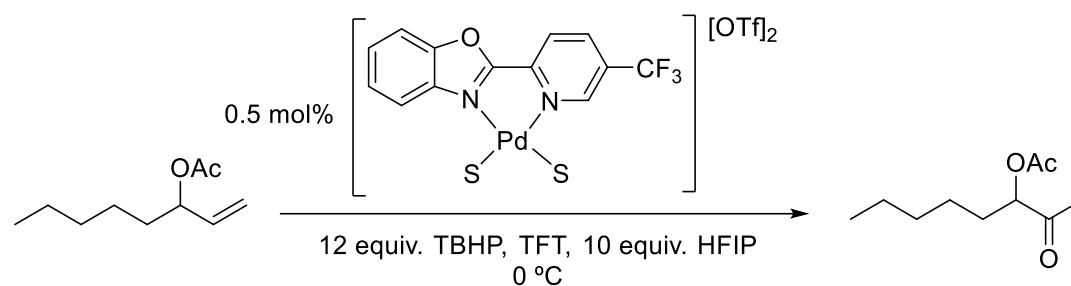


Figure S50: Oxidation of oct-1-en-3-yl acetate carried out at 0 °C.

Mass spec analysis of the post reaction mixtures did not show conclusive evidence for formation of any peroxide bridged aggregates. Attempts to precipitate aggregates in a similar fashion to that of Mimoun²⁶ were also unsuccessful.

Conversely, if large amounts of TBHP is broken down during the course of reaction, the catalyst may be starved of oxidant and this could promote deactivation pathways. To examine this possibility, the post reaction mixture for the oxidation of oct-1-en-3-yl acetate under optimized conditions was analysed by ¹³C NMR and the concentration of TBHP measured using the same procedure used to measure the TBHP concentration of the anhydrous TBHP/organic solvent solutions (see experimental section). Examination of the quantitative ¹³C NMR spectrum indicated that there remained 9.3 equivalents of TBHP in the post reaction mixture. This value represents an approximate 15% decrease from the 11 equivalents that can be expected assuming 1 equivalent of TBHP reacts to form the ketone product. This result indicates that during the reaction some TBHP may decompose. The large excess of oxidant still present however suggests that catalyst deactivation by oxidant starvation is not a problem in this system.

Comparison of 5-CF₃ Ligand vs Quinox Under Optimized Conditions

To compare between the second-generation 5-CF₃-PBO ligand and the literature benchmark Quinox, both ligands were tested for the oxidation of oct-1-en-3-yl acetate under our optimized conditions (See also Figures 8 and 9 in main manuscript). In the case of the Quinox ligand, the active cationic triflate complex cannot be isolated and it is always required to be made *in-situ* using silver salts. Nevertheless, the first comparison made was between the isolated cationic 5-CF₃ catalyst and (Quinox)PdCl₂/AgOTf under dry TFT conditions using HFIP and 1 mol% catalyst (Figure S51). Under these dry conditions Quinox was found to give only trace amounts of product. Interestingly, when the (5-CF₃-PBO)PdCl₂/AgOTf combination was used under dry optimized conditions, the same results were obtained as for the isolated cationic triflate complex. Why the Quinox ligand does not perform under anhydrous conditions while the 5-CF₃-PBO does is unclear, but presumably derives from their respective ability to form the active cationic species with silver salts under dry conditions. Our observations are in agreement with Sigman and co-

workers who have previously shown that when using Quinox, a minimum concentration of water must be present for successful catalysis.⁷

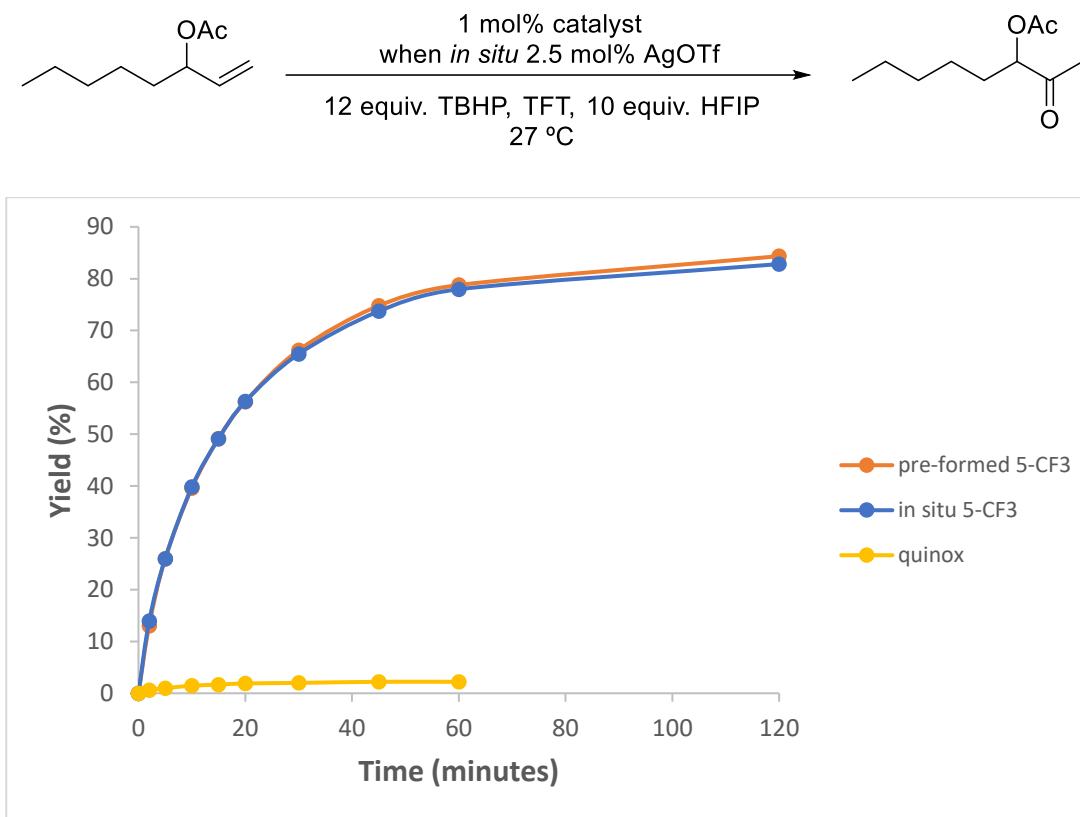


Figure S51: Comparison of Quinox and 5-CF₃ catalysts under optimized dry conditions.

Previously when using *in situ* catalyst formation with 1-octene, the presence of silver salt was found to be detrimental to the yield obtained (Figure S5). This is no longer the case under the optimized conditions using oct-1-en-3-yl acetate as substrate. As previously discussed, one of the possible reasons for the silver method reducing performance is the presence of chloride anions in solution binding to the Pd catalyst rendering it inactive. This may no longer happen as HFIP could be binding to these chloride anions³⁴ preventing them from forming inactive (ligand)PdCl₂ complexes. The chloro complex (5-CF₃-PBO)PdCl₂ was tested as a catalyst under the optimized reaction conditions with HFIP and was found to be completely inactive.

Since testing under anhydrous conditions was not feasible, a comparison between the 5-CF₃ PBO ligand and Quinox was instead done using aqueous TBHP but still using TFT as the solvent and then with HFIP as an additive. The performance of Quinox was improved compared to the original Sigman conditions simply by swapping to TFT from DCM (Figure S52). Using 1 mol% of the Quinox catalyst 43% yield of the product was obtained, implying 2 mol% could take the reaction to completion unlike the previous 5 mol% under the DCM conditions.

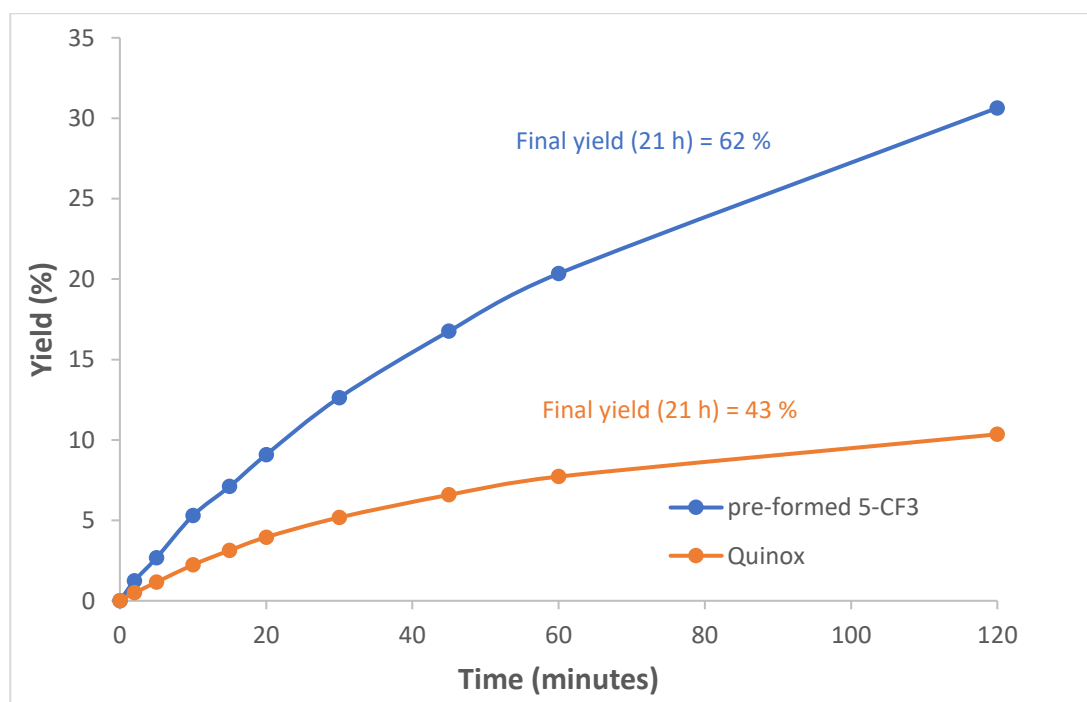
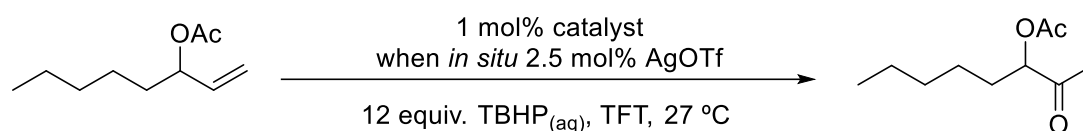


Figure S52: Comparison of 5-CF₃-PBO and Quinox using aqueous TBHP in TFT.

The addition of HFIP in combination with TFT further improves the performance of the Quinox catalyst, increasing the final yield obtainable with 1 mol% catalyst to 68% (Figure S53).

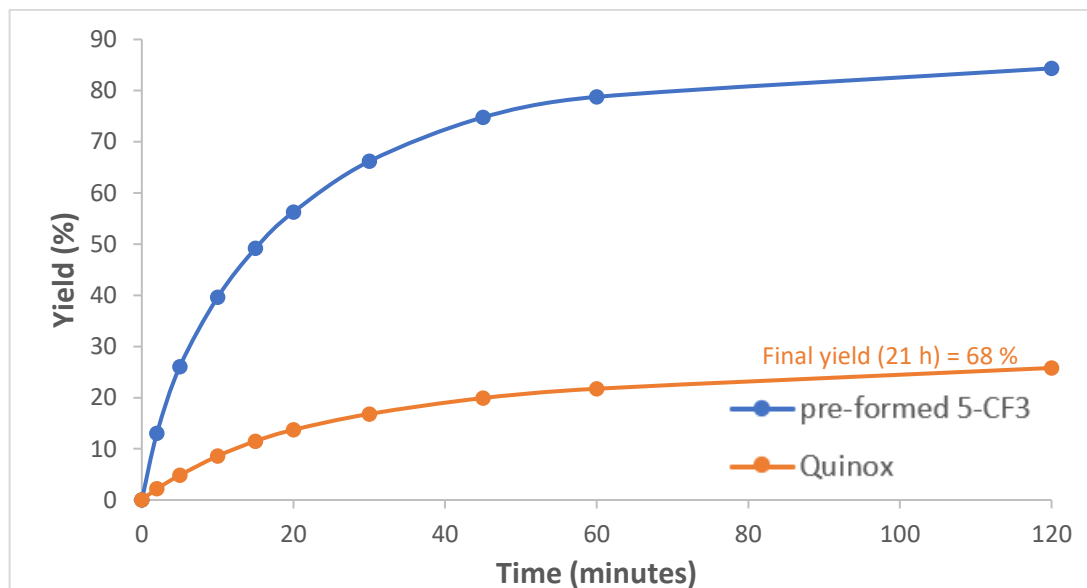
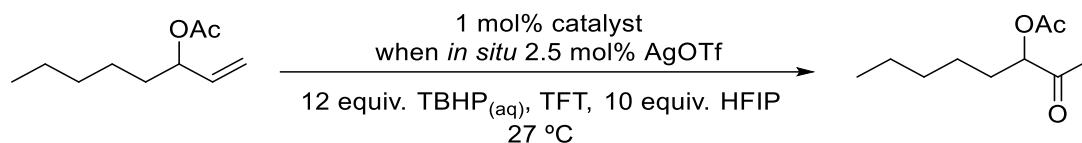


Figure S53: Comparison of 5-CF₃-PBO and Quinox catalysts with HFIP present.

The improvements of using TFT as a solvent and HFIP as an additive found in this study can be used to further improve the literature benchmark Quinox system. Figures S54 and S55 show clearly however that despite the increased performance of Quinox under these conditions, 1 mol% of the catalyst is still not able to reach complete conversion of starting material. Under all conditions tested, the newly developed second-generation 5-CF₃-PBO catalyst has significantly better performance in terms of rate and final TON when compared to the Quinox catalyst.

Experimental

General Considerations

Unless otherwise stated, all reagents were purchased from commercial suppliers and used without further purification. The aqueous TBHP used was Luperox™ TBH70X ((a 70 wt.% aqueous solution). 2-(4,5-Dihydro-2-oxazolyl)quinoline (Quinox), palladium acetate: ≥ 99.9%, trace metal basis, and palladium chloride: ≥ 99.995%, were purchased from Sigma Aldrich (Merck).

Thin layer chromatography (TLC) analysis was carried out using Merck TLC silica gel 60 sheets, and visualized with UV light, potassium permanganate or phosphomolybdic acid stain. Column chromatography was performed with Fluorochem silica gel 60 Å as stationary phase and solvents employed were analytical grade.

¹H, ¹³C and ¹⁹F NMR spectra were recorded on either a Bruker 400 MHz or Agilent ProPulse 600 MHz spectrometer at 27 °C. In cases where quantitative ¹⁹F spectra were required the D₁ relaxation delay was set to 8 seconds. Quantitative ¹³C NMR analysis of TBHP is described later.

ESI Mass spectra were performed using a Waters LCT Premier TOF spectrometer. Elemental Analysis data was obtained using a Perkin Elmer PE2400 CHNS Elemental Analyzer.

Gas chromatography analysis was carried out using Agilent 7820A series gas chromatograph. An Agilent 19091J-413HP-5 column (30.0 m Å~ 320 μ m Å~ 0.25 μ m nominal) was employed for all the separations using the following conditions: initial column temperature, 40 °C; final temperature, 200 °C; hold time, 0 min; rate of temperature ramp, 30 °C/min; injection temperature, 250 °C; injection volume 1 μL; detection temperature, 300 °C, split mode 40:1. The effluent was combusted in an H₂ /Air flame and detected using FID (flame ionization detector).

The GC yield of products and conversion of substrates were determined by using the internal standard method . The relative response factor (RF) of analytes was determined by analysing known quantities of internal standard against known quantities of pure substrate and product. Dodecane was used as the internal standard. In the case of 1-

octene and 2-octanone these are commercially available. Oct-1-en-3-yl acetate and the oxidation product 2-oxooctan-3-yl acetate were synthesized and confirmed by ^1H and ^{13}C NMR, before carrying out relative response factor calibrations.

Relative response factor (RF) was calculated by:

$$RF = \frac{Area_{internal\ standard} \times Moles_{analyte}}{Area_{analyte} \times Moles_{internal\ standard}}$$

The quantity of an analyte (substrate and product) was then calculated according to the following equation:

$$Moles_{analyte} = \frac{RF \times Area_{analyte} \times Moles_{internal\ standard}}{Area_{internal\ standard}}$$

Notes on Safety

Oxidation chemistry with peroxides requires careful consideration of safety issues. Before carrying out reactions, a full risk assessment should be carried out.

Peroxides such as TBHP can become unstable/decompose with increasing temperature and various additives such as metal ions or acids and bases.³⁵⁻³⁸ Therefore caution should be taken when designing experiments. In our case we have avoided the use of elevated reaction temperatures. We have found that our isolated dicationic Pd catalyst does not lead to rapid decomposition of the TBHP. Control experiments carried out at 27 °C stirring an anhydrous mixture of TBHP in TFT with 0.5 mol% of the [(5-CF₃-PBO)Pd(S)₂][OTf]₂ catalyst showed no decomposition of the TBHP. Monitoring the [TBHP] by quantitative ¹³C NMR showed no change after 90 mins and 24 h under these conditions.

It is advisable to carry out reactions on a small scale initially and to bear in mind that for certain substrates which are very reactive, there will be an exotherm. When carrying out our initial studies with 1-octene, reactions using proficient catalysts at loadings of 2 mol%, vigorous bubbling during the early stages of the reaction was observed, even at 0 °C. At 1 mol% loading with our optimal catalyst, [(5-CF₃-PBO)Pd(S)₂][OTf]₂, when reactions were carried out at 27 °C, there was a significant exotherm and the glass vial was hot to the touch. Therefore, many of the studies with 1-octene were focussed on using 0 °C. In the case of the oct-1-en-3-yl acetate substrate, this reacts at a slower rate and 27 °C was found to be suitable. For those interested in larger scale studies, suitable temperature control should be utilised to ensure the exotherm can be controlled and calorimetric studies would be advisable.

When using glassware such as in these studies, it is advisable not to properly stopper the vessels. For example, when using small glass vials, if lids are being used, ensure there is a hole in the lid to allow release of any pressure build up. When we carried out the larger scale reaction in a round bottom flask, we covered the flask with Parafilm™.

All reactions should be quenched at the end of the reaction to reduce the remaining TBHP. This also applies to solutions of TBHP that are to be disposed of. There are a range of potential reductants but we have used sodium thiosulfate or sodium metabisulfite, reductants that have been used by others for quenching TBHP.^{39, 40} When carrying out the quench, the TBHP solution is cooled to 0 °C and a saturated solution of the aforementioned reductant added slowly. An excess of the reductant should be employed and it is advisable to check that all the TBHP has been removed. This can be done via various means (including iodide titrations⁴¹ and peroxide test strips).

Preparation of Anhydrous TBHP solutions

Anhydrous solutions of TBHP were obtained by extraction into the corresponding organic solvents.⁴² The general procedure is as follows using TFT as representative solvent:

Into a 250 mL separatory funnel was added 120 mL of Luperox™ TBH70X solution (a 70 wt.% aqueous solution of TBHP) followed by 80 mL of TFT. The funnel was swirled gently, and the two layers were left to separate. The organic layer was collected and dried with anhydrous sodium sulfate. This drying step was repeated a further two times and the resulting TFT/TBHP solution was stored in a Teflon FEP bottle at room temperature. In the case of TFT/TBHP solutions, no change in TBHP concentration was observed after 1 month of storage under these conditions. Teflon FEP bottles are preferred over glass and PET containers. Glass should be avoided due to the small chance of pressurization. When PET containers are used slow migration of many common organic solvents (such as those used in this study) through the walls of the bottle can occur leading to concentration of TBHP.²⁵ Toluene has also been found by Sharpless and co-workers to form very stable solutions with TBHP however the formation of contaminants over time has been noted with these solutions.^{24, 25} They have also noted that the anhydrous TBHP solutions formed using chlorinated solvents such as dichloroethane and DCM are much less stable, and have observed pressurization of the containers when using these solvents due to the release of oxygen.^{24, 25, 43, 44}

The concentration of the extracted solution was obtained by quantitative ¹³C-NMR using mesitylene as an internal standard in CDCl₃. Inverse gated decoupling was used to reduce

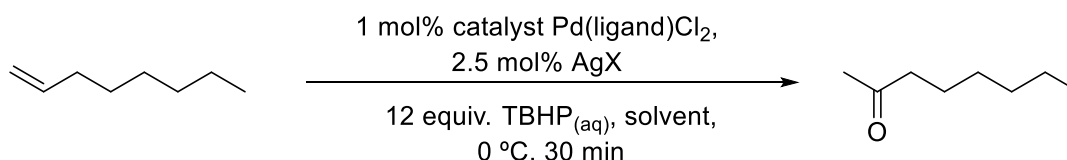
the NOE and allow for quantitative integrations. The NMR samples were typically prepared as follows:

Mesitylene (≈ 170 mg), CDCl_3 (300 μL) and 300 μL of TFT/TBHP solution.

256 scans of this concentrated solution using a D_1 delay of 115 seconds gives sharp spectra and allows for complete relaxation of all carbon nuclei, meaning any peak corresponding to TBHP can be integrated against the mesitylene standard reliably.⁴⁵ From the integrations obtained the number of moles of TBHP in the 300 μL can be ascertained and from this the concentration of the extracted TBHP solution. This approach was validated by confirming the concentration of the commercial Luperox™ TBH70X solution using CD_3CN as deuterated solvent.

Catalytic Reactions

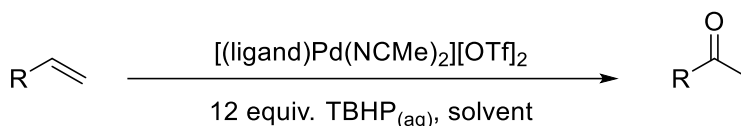
General procedure for testing ligand and cationic catalysts formed in-situ with silver salts and aqueous TBHP using 1-octene as substrate:



Into a 15 mL glass vial wrapped in aluminium foil was added pre-formed $\text{Pd}(\text{ligand})\text{Cl}_2$ complex (1 mol%), AgX (2.5 mol%) (where $X = \text{OTf}$ or SbF_6) and dodecane (approximately 60 mg) as an internal standard. Solvent was then added (7.5 mL) and the reaction stirred vigorously at room temperature for 15 minutes. After this time had elapsed the solution was cooled to $0\text{ }^\circ\text{C}$ and held at this temperature for the duration of the reaction. The temperature was accurately maintained through the use of a cooling block into which the vials were inserted, and around which coolant was pumped. Once the solution had reached the desired temperature, $\text{TBHP}_{(\text{aq})}$ was then added (70 wt% solution in H_2O , 1.5 mL, 12 equiv., 10.8 mmol) and the solution stirred for around 10 minutes. The 1-octene

substrate was then added (141 μL , 0.9 mmol, 0.1 M) and the reaction was monitored using GC by taking aliquots ($\sim 80 \mu\text{L}$) from the reaction mixture and filtering through a plug of silica using Et_2O as the eluent.

General procedure for testing ligand and pre-formed cationic catalysts using aqueous TBHP for both 1-octene and oct-1-en-3-yl acetate:



To a 15 mL glass vial equipped with magnetic stirrer bar was added catalyst $[\text{Pd}(\text{ligand})(\text{S})_2][\text{OTf}]_2$ and dodecane (approximately 60 mg) as an internal standard. Solvent was then added (7.5 mL) and the reaction allowed to reach the desired temperature before addition of $\text{TBHP}_{(\text{aq})}$ (70 wt% solution in H_2O , 1.5 mL, 12 equiv., 10.8 mmol). This solution was then stirred for around 10 minutes before the substrate was added (0.9 mmol, 141 μL for 1-octene or 175 μL for oct-1-en-3-yl acetate). It should be noted that all reactions done at 27 $^\circ\text{C}$ were maintained accurately at this temperature with a hot plate and thermocouple and were not simply carried out at “room temperature” (which can vary in significantly in Belfast depending on the time of the year).

When HFIP was used in combination with the aqueous TBHP, the volume of organic solvent used = 7.5 mL – volume of HFIP required, which maintained the total volume at 9 mL and $[\text{substrate}] = 0.1 \text{ M}$. The HFIP was added after the addition of TBHP, and then solution then stirred for 5 minutes before substrate addition.

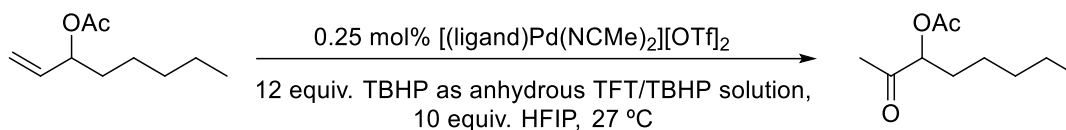
General procedure for testing ligand and pre-formed cationic catalysts using anhydrous TBHP for both 1-octene and oct-1-en-3-yl acetate

Stock solutions of TBHP in various organic solvents (TFT, DCM, PhCl, PhMe) [details of preparing anhydrous TBHP in organic solvent are described above] were diluted using their corresponding organic solvent to the desired concentration (1.44 M TBHP/organic solvent). After dilution, the solution was dried with activated 3 Å molecular sieves for 30 minutes before use. For screening in this study, substrate (0.9 mmol, 0.12 M) required 10.8 mmol of TBHP (12 equivalents), which required 7.5 mL of a 1.44 M TBHP/organic solvent solution.

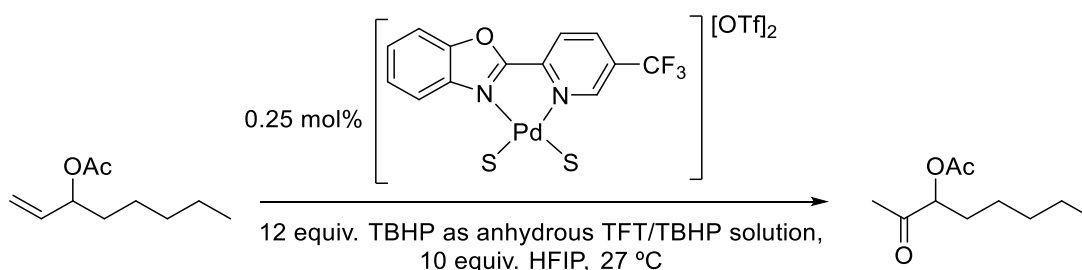
To a 15 mL glass vial equipped with a magnetic stirrer bar was added catalyst and dodecane (approximately 60 mg), followed by TBHP in organic solvent (7.5 mL, 1.44 M). This solution was heated/cooled as required to the desired temperature followed finally by addition of the substrate (0.9 mmol, 0.12 M).

For reactions involving anhydrous TBHP in conjunction with HFIP the volume of TBHP/organic solvent solution needed is again 7.5 mL – volume of HFIP required. For example, if using 10 equiv. HFIP (for 0.9 mmol of substrate = 0.95 mL HFIP) the volume of anhydrous solvent/TBHP required is therefore 6.55 mL and a 1.65 M solution of TBHP/solvent is needed. Before use the HFIP is dried overnight using activated 3 Å molecular sieves. The HFIP is used the following day after addition of the sieves and is kept over sieves for no longer than 24 hours.

General procedure for catalyst screening at 0.25 mol% catalyst loading



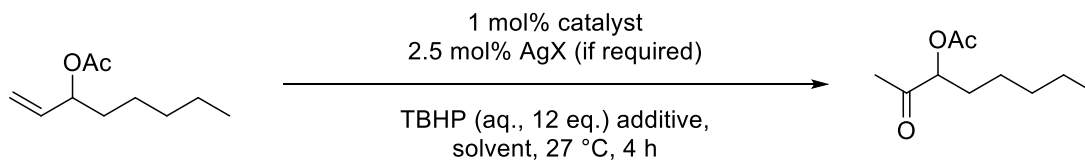
Catalyst loadings of 0.25 mol% were added by volume using freshly prepared stock solutions of catalyst in anhydrous TBHP/TFT. An example using the best performing catalyst is detailed below.



A freshly prepared catalyst stock solution was prepared by dissolving catalyst (10.2 mg, 0.0136 mmol) in a dried solution of TBHP/TFT (3.1 mL of a 1.65 M TFT/TBHP solution).

Dodecane (57.2 mg, 0.336 mmol) and a small magnetic stirrer bar were added to a 15 mL glass vial followed by a TBHP/TFT solution (6.03 mL of a 1.65 M solution). To the mixture, catalyst (0.25 mol%) was added (0.52 mL of stock solution, 1.7 mg, 0.00226 mmol) and the solution allowed to warm to 27 °C. After the addition of dry HFIP (0.95 mL, 9 mmol), the solution was stirred for 5 minutes before final addition of the substrate (175 μ L, 0.9 mmol). Aliquots of this were taken (~80 μ L) and passed through a plug of silica using Et₂O and analysed by GC.

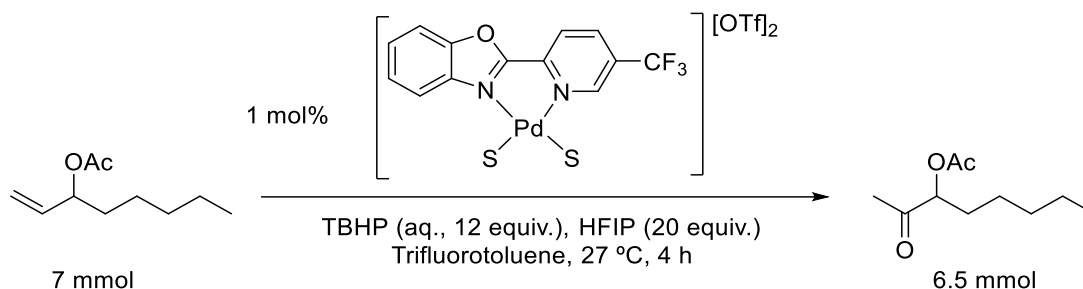
General procedure for 1 mol% catalyst loading with aqueous TBHP (Figures 8 & 9 in the main manuscript)



To a 15 mL glass vial equipped with a magnetic stirrer bar, catalyst was added (1 mol%, isolated triflate form or dichloro-complex for *in-situ* reactions) followed by dodecane (175 μ L, weight recorded) and if required, AgX (2.5 mol%). When using silver salts, vials were wrapped in aluminium foil to protect from light. Solvent was added, along with Luperox TBH70X (1.5 mL, 10.8 mmol) followed by HFIP. The reaction was stirred at 27 °C in an aluminium heating block for 2 minutes before addition of oct-1-en-3-yl acetate (175 μ L, 0.9 mmol). In sampling, a few drops of the reaction mixture were filtered through a silica plug with Et₂O and analysed by GC.

The volume of solvent added was based on desired additive content, with the total volume maintained at 9 mL for a 0.1 M reaction concentration. For example, with 20 eq. HFIP, solvent volume was calculated as 9 mL – 1.9 mL (HFIP) – 1.5 mL (aq. TBHP solution) = 5.6 mL. Due to the water sensitive nature of Ag[SbF₆], this was weighed into vials in a glovebox.

“Gram-scale” oxidation of oct-1-en-3-yl acetate



To a 250 mL round bottom flask, oct-1-en-3-yl acetate (1.1947 g, 7.02 mmol), dodecane (1.1037 g, 6.48 mmol), trifluorotoluene (45 mL), catalyst (0.0525 g, 0.070 mmol) were transferred and the mixture allowed to stir for 10 minutes at 27 °C, after which TBHP (12 mL, 84.2 mmol) and HFIP (15 mL, 140.4 mmol) were added and the flask sealed with parafilm, the reaction then left to stir at 27 °C for 4 hours. The reaction was sampled for GC analysis (a few drops passed through a silica plug and washed through with diethyl ether). The reaction mixture was then quenched (see earlier discussion in “Notes in Safety”).

The quenched reaction mixture and was transferred to a 250 mL separating funnel. The contents were diluted with diethyl ether (50 mL), the mixture extracted, and the aqueous/organic layers separated. The aqueous layer was further extracted with additional portions of diethyl ether (3 x 50 mL). The organic layers were combined and dried over MgSO₄, filtered and solvent removed by rotatory evaporation. The crude product, a brown liquid, was subjected to column chromatography using 1:15 diethyl ether - hexane eluent, gradually raised to 1:4 and isolated product fractions combined, solvent removed by rotatory evaporation and further dried under reduced pressure, the product (1.2101 g, 6.50 mmol, 93% yield) obtained as a clear liquid and analyzed by ¹H and ¹³C NMR. The yield according to GC analysis, before work-up, was found to be 97%.

Control experiments to examine the potential effect of hexafluoroacetone on catalytic reactions.

A reaction with oct-1-en-3-yl acetate (0.9 mmol) was run for 1 hour with 10 equiv of HFIP. The solution was then cooled in icebath for 5 min, and hexafluorobenzene (0.84 mmol) was added as ^{19}F internal standard. The mixture was stirred (while chilled) for 5 min, then a sample was taken for ^{19}F NMR. The NMR tube contained a capillary with d_6 -acetone to improve the shim lock. ^{19}F -NMR analysis was carried out on a Bruker 600 MHz unit, and an extended D_1 delay (8 sec) was used. As shown below, there was no signal for hexafluoroacetone. Note: signals for the ligand are masked by the trifluorotoluene signal.

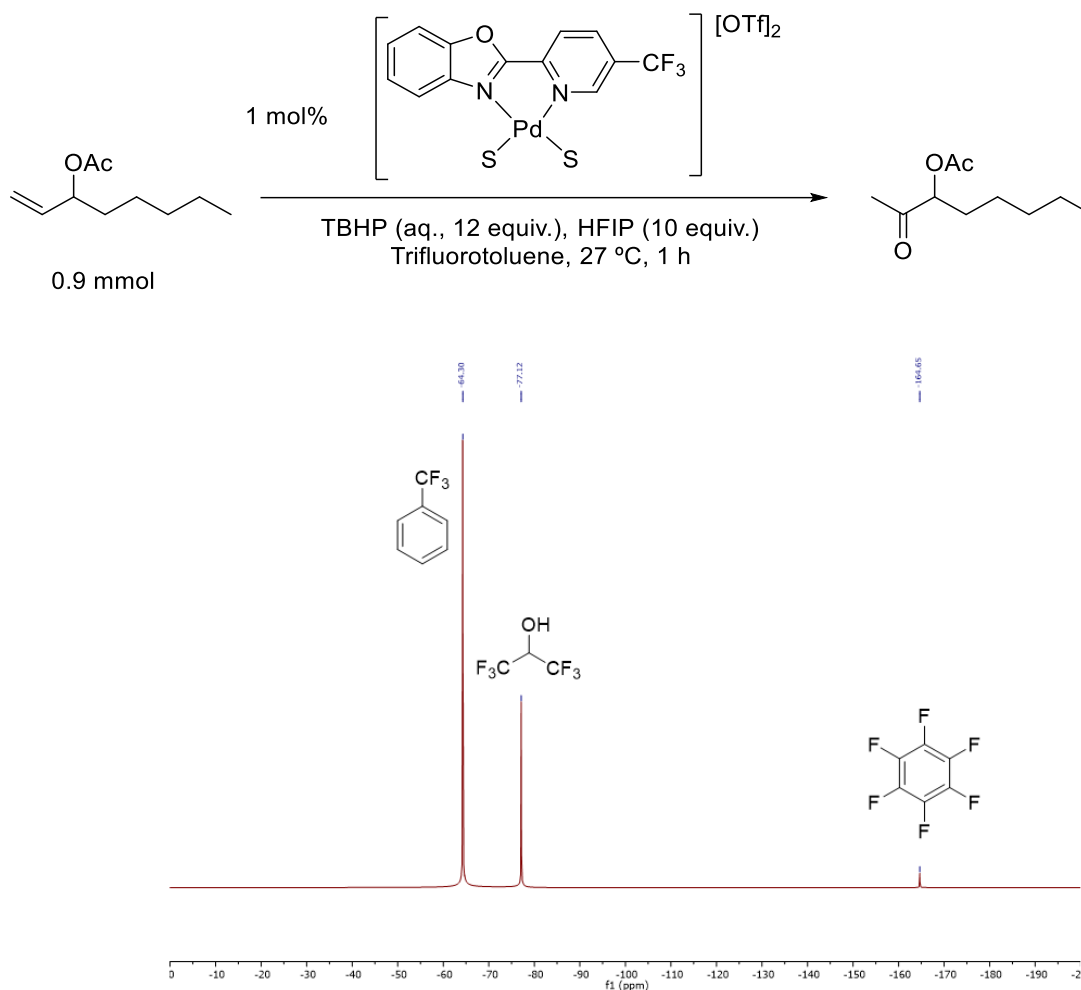


Figure S54: ^{19}F NMR analysis of a reaction mixture.

Spiking of the above reaction mixture with hexafluoroacetone trihydrate resulted in a peak at around -84 ppm. To ensure that small amounts of HFA were not being formed and having an influence we also carried out control reactions where we added 1 equivalent of hexafluoroacetone trihydrate (HFA) and found no positive influence on the reactivity, as shown below in Figure S55. In addition, ^{19}F NMR analysis of a reaction which had 1 equivalent of hexafluoroacetone trihydrate added demonstrated that the HFA was clearly visible in the spectra (Figure S56).

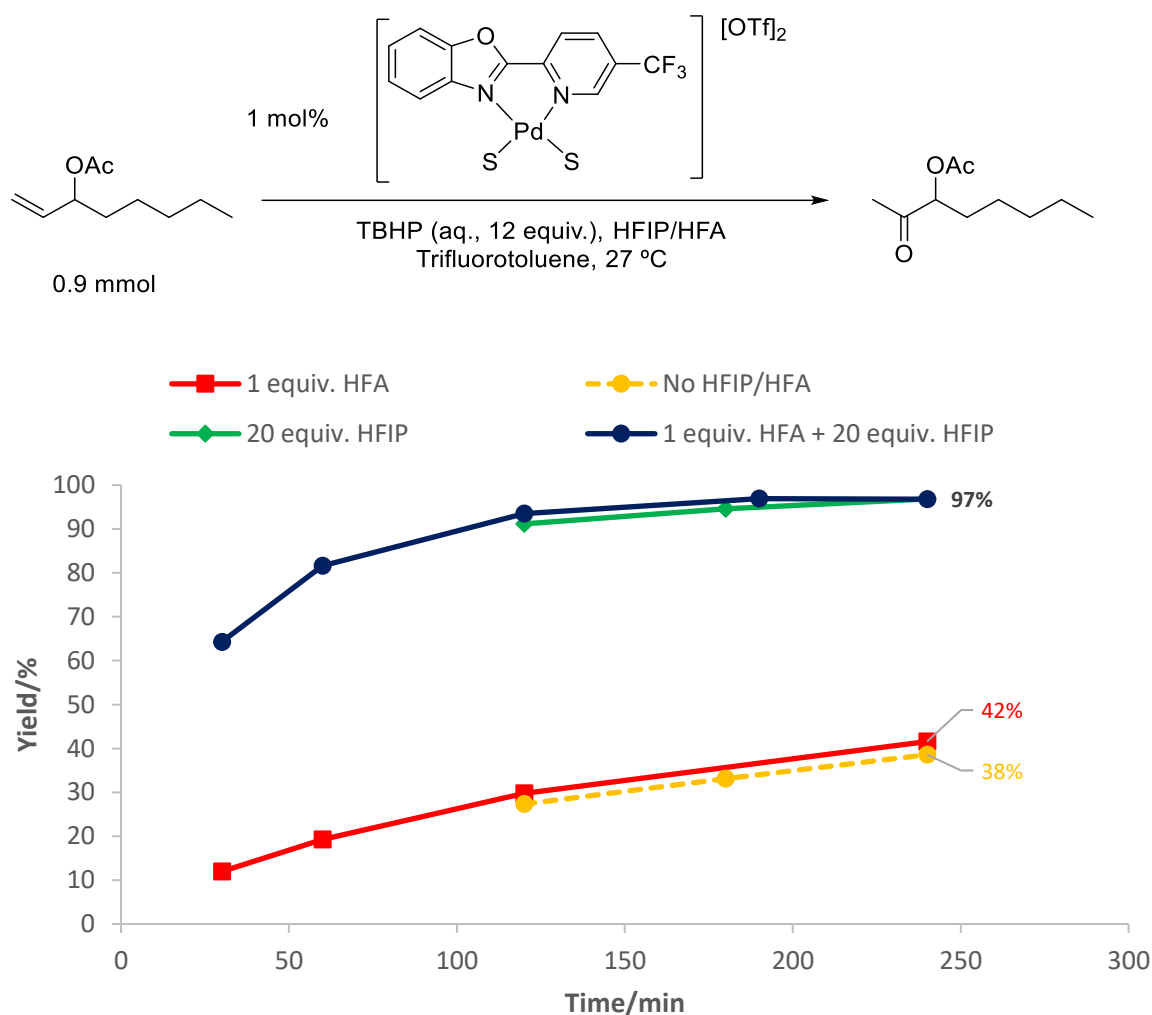


Figure S55: Control experiments to examine the potential effect of hexafluoroacetone trihydrate (HFA).

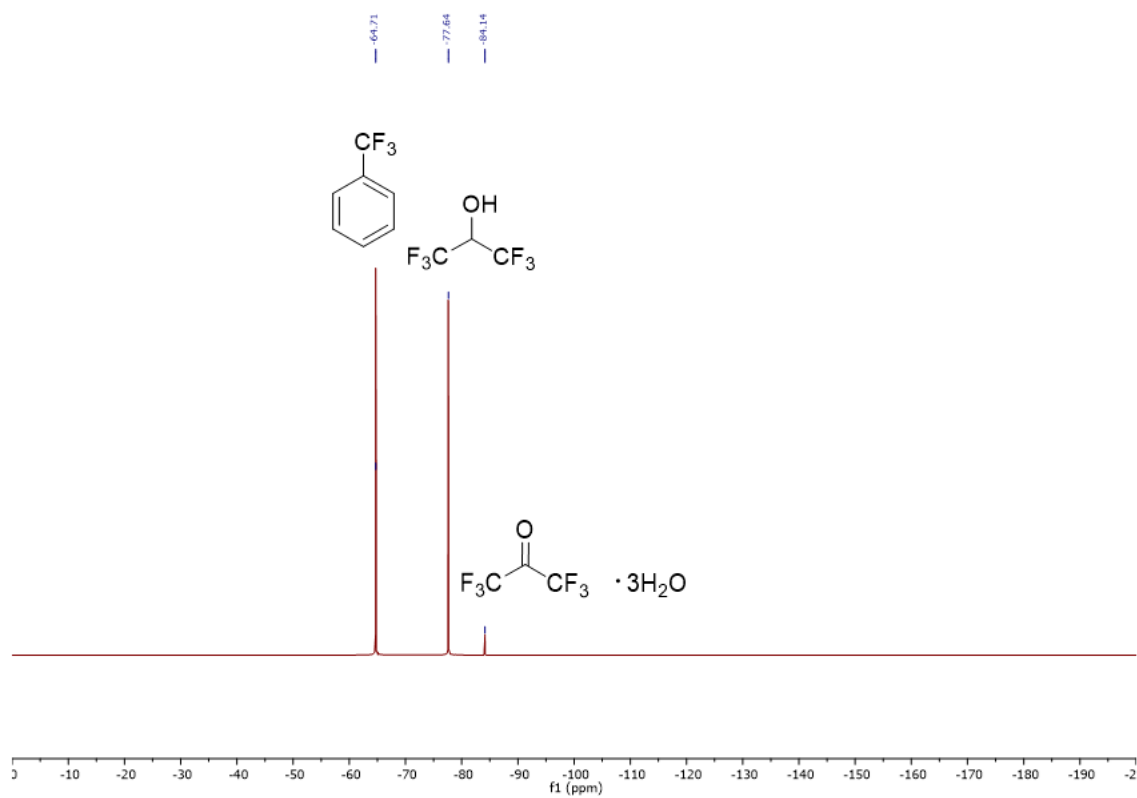


Figure S56: ^{19}F NMR analysis of post-reaction mixture where 20 equiv. of HFIP and 1 equiv. of HFA trihydrate had been added .

A Note on Reproducibility

Reproducibility is important to us and when we carried out the catalytic studies using 0.25 mol% catalyst for a range of ligands, we found no signs of any issues. As shown in Figure S45 all of the data is based on a combination of two experiments. In the case of the best catalyst (5-CF₃-PBO ligand) this was tested significantly more and by a number of the authors, over extended periods of time and no issues were observed. Indeed, these conditions were often used as a “catalyst check” when a new batch of catalyst was prepared, and consistent data was obtained. The data discussed and shown here is based on experiments that were carried out prior to the 2019 COVID lockdown and we believe that the trends shown in Figures such as Figure S45 are legitimate. When we returned to the laboratory after it had being closed for 5 months due to the lockdown, we resumed our studies and found that when using 0.25 mol% of the 5-CF₃-PBO catalyst under the anhydrous conditions, the performance was not as consistent. The evidence points towards some small amounts of impurities in the reagents sometimes having a negative effect on the performance. Indeed, when we originally carried out the 0.25 mol% studies we found that lower loadings (e.g. 0.1 mol%) led to very little activity, which is also consistent with a poisonous impurity. It is logical that any impurities which poison the catalyst can be a greater problem when using lower catalyst loadings and it seems that these impurities were in a greater concentration after the lockdown. We found no such variability when 1 mol% catalyst loading was used. Indeed, even the normally desk-bound, laboratory rusty, corresponding author was able to obtain the same results as his more skilled co-authors (Figures 8 and 9 in the main paper).

Job Plot Analysis of HFIP with Oct-1-en-3-yl acetate and 2-oxooctan-3-yl acetate using $^1\text{H-NMR}$

Commercially available HFIP was dried with activated 3 Å molecular sieves before use. CDCl_3 was passed through basic alumina before use.

0.1 M stock solutions of HFIP (85.4 mg) and oct-1-en-3-yl acetate (81.5 mg) were made up with 5.0 mL of CDCl_3 each. The total concentration of HFIP and oct-1-en-3-yl acetate was kept constant. Thirteen NMR samples were prepared with a constant volume of 0.6 mL, where the mole fractions of HFIP and oct-1-en-3-yl acetate were varied from 0.0 to 1.0 (see below). The Job plot was obtained by plotting the molar fraction multiplied by the change in chemical shift ($\Delta\delta$) of the HFIP hydroxyl proton against the mole fraction of HFIP.

This same procedure was applied to obtain the Job plot for 2-oxooctan-3-yl acetate product.

Table S3 Mole fractions and chemical shifts ($\Delta\delta$) for HFIP and oct-1-en-3-yl acetate substrate.

	Volume HFIP (μL)	mmol HFIP	Substrate Volume (μL)	mmol substrate	Mole fraction of HFIP	Mole fraction of substrate	δ HFIP OH	$\Delta\delta$	$\chi_{\text{HFIP}}*\Delta\delta$
1	600	0.06096	0	0	1	0	2.9043	0	0
2	550	0.05588	50	0.005	0.917871222	0.083333333	3.0569	0.1526	0.140067
3	500	0.0508	100	0.01	0.835526316	0.166666667	3.2038	0.2995	0.25024
4	450	0.04572	150	0.015	0.752964427	0.25	3.3634	0.4591	0.345686
5	400	0.04064	200	0.02	0.670184697	0.333333333	3.4459	0.5416	0.362972
6	350	0.03556	250	0.025	0.587186262	0.416666667	3.6664	0.7621	0.447495
7	300	0.03048	300	0.03	0.503968254	0.5	3.8415	0.9372	0.472319
8	250	0.0254	350	0.035	0.420529801	0.583333333	3.9699	1.0656	0.448117
9	200	0.02032	400	0.04	0.336870027	0.666666667	3.9837	1.0794	0.363618
10	150	0.01524	450	0.045	0.252988048	0.75	4.0315	1.1272	0.285168
11	100	0.01016	500	0.05	0.168882979	0.833333333	4.1015	1.1972	0.202187
12	50	0.00508	550	0.055	0.084553928	0.916666667	4.2286	1.3243	0.111975
13	0	0	600	0.06	0	1	0	0	0

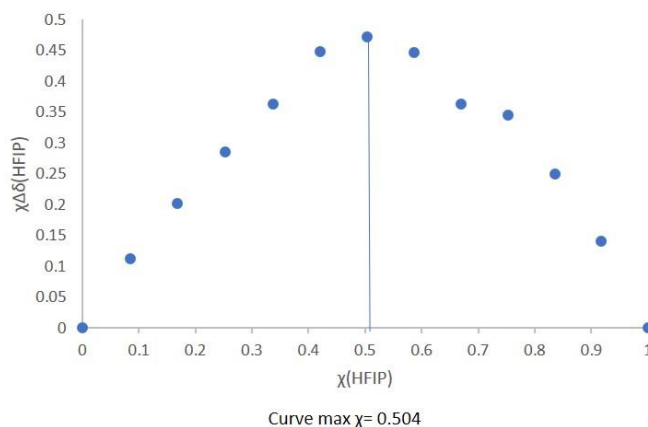
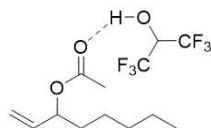
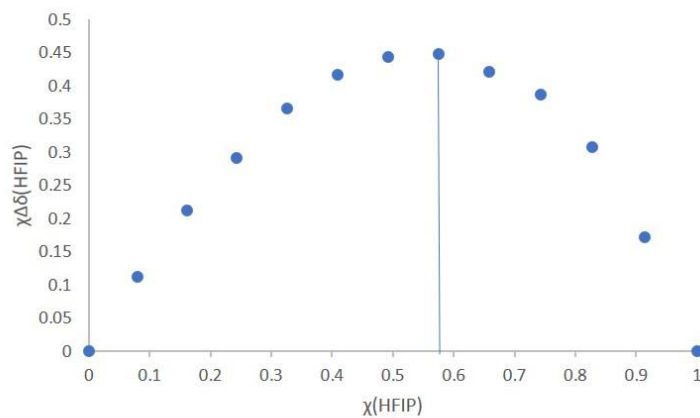
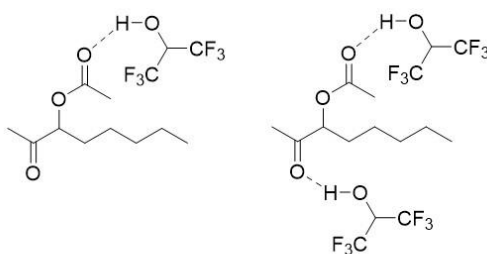


Table S4 Mole fractions and chemical shifts ($\Delta\delta$) for HFIP and 2-oxooctan-3-yl acetate product.

	Volume HFIP (μL)	mmol HFIP	Product Volume (μL)	mmol product	Mole fraction of HFIP	Mole fraction of product	δ HFIP OH	$\Delta\delta$	$\chi_{\text{HFIP}}*\Delta\delta$
1	600	0.057984	0	0	1	0	2.9325	0	0
2	550	0.053152	50	0.0049985	0.914042012	0.083333333	3.1203	0.1878	0.17165709
3	500	0.04832	100	0.009997	0.828574858	0.166666667	3.3047	0.3722	0.308395562
4	450	0.043488	150	0.0149955	0.743594347	0.25	3.4537	0.5212	0.387561374
5	400	0.038656	200	0.019994	0.659096334	0.333333333	3.5709	0.6384	0.4207671
6	350	0.033824	250	0.0249925	0.575076722	0.416666667	3.7129	0.7804	0.448789874
7	300	0.028992	300	0.029991	0.491531458	0.5	3.8367	0.9042	0.444442745
8	250	0.02416	350	0.0349895	0.408456538	0.583333333	3.9526	1.0201	0.416666515
9	200	0.019328	400	0.039988	0.325848001	0.666666667	4.0577	1.1252	0.36664417
10	150	0.014496	450	0.0449865	0.243701929	0.75	4.1294	1.1969	0.291686839
11	100	0.009664	500	0.049985	0.162014451	0.833333333	4.2403	1.3078	0.211882499
12	50	0.004832	550	0.0549835	0.080781737	0.916666667	4.3274	1.3949	0.112682445
13	0	0	600	0.059982	0	1	0	0	0



Curve Max $\chi = 0.575$

Synthesis of Ligands and Pd(II) Complexes

Synthesis of bis(acetonitrile)dichloropalladium

Bis(acetonitrile)dichloropalladium was prepared according to the literature.⁴⁶ Elemental Analysis: Predicted: C, 18.55; H, 2.33; N, 10.80; Found: C, 18.70; H, 2.22; N, 10.60

Synthesis of PdCl(C₃H₅)(dppb)

PdCl(C₃H₅)(dppb) was prepared according to the method previously described by Doucet and co-workers.⁶ An oven-dried 40 mL Schlenk tube equipped with a magnetic stirring bar under nitrogen atmosphere, was charged with [Pd(C₃H₅)Cl]₂ (182 mg, 0.5 mmol) and 1,4-bis(diphenylphosphino)butane (dppb) (426 mg, 1 mmol). Anhydrous dichloromethane (10 mL) was added, then the solution was stirred at room temperature for 20 minutes. The solvent was removed under reduced pressure to give an orange powder.

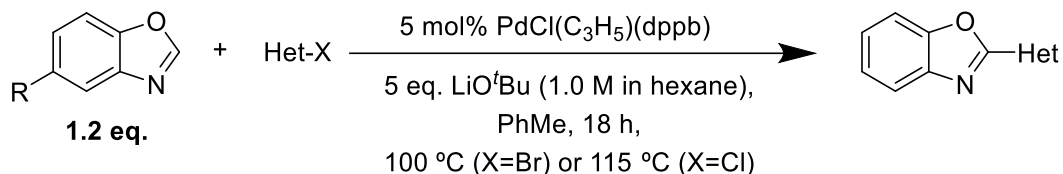
³¹P{¹H}-NMR (81 MHz, CDCl₃): δ (ppm) 18.06 (s)

It is worth noting that Jutand and co-workers have shown that this is likely a neutral complex in the form: η¹-CH₂=CH-CH₂-PdCl(dppb).⁴⁷

Pd(Quinox)Cl₂ was prepared using commercially available Quinox and via the method described by Sigman and co-workers.⁴

A number of ligands/catalysts tested in this study had previously been prepared as part of aerobic Wacker oxidation studies and the synthetic methods for these are described in that publication.³

General procedure for the one-step coupling reaction of benzoxazole with aryl pyridines:



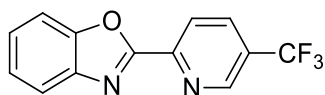
The method we used and found to be reliable, was based on a combination of conditions from previous reports.^{5, 6}

For all the following coupling reactions toluene was dried over activated 3 Å or 4 Å molecular sieves and degassed by sparging with N₂ before use.

Note: In the case of the 5-CF₃-PBO ligand, numerous batches were prepared and it was found that 1 mol% catalyst could be used and yields of 70-75 % could be obtained.

Benzoxazole (1.2 equiv.), PdCl(C₃H₅)(dppb) (5 mol%) and aryl halide (1 equiv.) were added to a 2-neck round bottom flask and a reflux condenser was attached. The system was evacuated and backfilled with N₂ three times. Toluene was then added *via* syringe followed by LiO^tBu (1.0 M in hexane) (5 equiv.). The reaction was then heated to 100 °C when X = Br and when X = Cl the reaction heated to 115 °C, and stirred vigorously for approximately 18 h. The reaction mixture was then diluted with H₂O and the organic layer collected. The solvent was then removed under reduced pressure and the crude product was purified by silica gel column chromatography.

2-(5-(trifluoromethyl)pyridin-2-yl)benzo[d]oxazole



The reaction of 2-bromo-5-trifluoromethylpyridine (686 mg, 3.0 mmol), benzoxazole (440 mg, 3.6 mmol), LiO^tBu (1.0 M in hexane) (15 mL, 15 mmol) and PdCl(C₃H₅)(dppb) (92.4 mg, 0.15 mmol) in toluene (15 mL) afforded the product as a fluffy white solid (640 mg, 80%). Columned in 15:1 Pet Ether: EtOAc.

The reaction of 2-chloro-5-trifluoromethylpyridine (182 mg, 1 mmol), benzoxazole (143 mg, 1.2 mmol), LiO^tBu (1.0 M in hexane) (5 mL, 5 mmol) and PdCl(C₃H₅)(dppb) (30.5 mg, 0.05 mmol) in toluene (5 mL) afforded the product as a fluffy white solid (200 mg, 76%). NMR analysis in agreement with literature data.⁴⁸

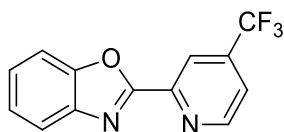
¹H NMR (600 MHz, CDCl₃) δ 9.14 – 9.03 (m, 1H), 8.50 (dd, *J* = 8.3, 0.6 Hz, 1H), 8.15 (ddd, *J* = 8.3, 1.6, 0.7 Hz, 1H), 7.93 – 7.82 (m, 1H), 7.73 – 7.67 (m, 1H), 7.52 – 7.40 (m, 2H).

¹³C{¹H} NMR (151 MHz, CDCl₃) δ 160.15, 151.21, 149.09, 147.22 (q, ³*J*_{CF} = 4.0 Hz), 141.66, 134.48 (q, ³*J*_{CF} = 3.5 Hz), 128.10 (q, ²*J*_{CF} = 33.4 Hz), 127.87, 125.36, 123.05 (q, ¹*J*_{CF} = 272 Hz), 122.23, 121.07, 111.44.

¹⁹F{¹H} NMR (376 MHz, CDCl₃) δ -62.58.

ESI-MS: [M+H]⁺: C₁₃H₈N₂OF₃ calculated m/z 265.0589, found 265.0589

2-(4-(trifluoromethyl)pyridin-2-yl)benzo[d]oxazole



2-chloro-4-trifluoromethylpyridine (182 mg, 1 mmol), benzoxazole (143 mg, 1.2 mmol), LiO^tBu (1.0 M in hexane) (5 mL, 5 mmol) and PdCl(C₃H₅)(dppb) (30.5 mg, 0.05 mmol) in toluene (5 mL) afforded the product as a white solid (243 mg, 92%). Columned in 6:1 Pet Ether: EtOAc. NMR analysis in agreement with literature data.⁴⁹

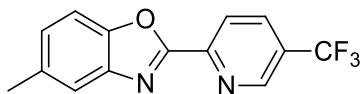
¹H NMR (400 MHz, CDCl₃) δ 9.01 (d, *J* = 5.0 Hz, 1H), 8.61 (s, 1H), 7.87 (d, *J* = 6.9 Hz, 1H), 7.69 (m, 2H), 7.45 (m, 2H).

¹³C{¹H} NMR (101 MHz, CDCl₃) δ 160.19, 151.28, 151.10, 147.36, 141.56, 139.69 (q, ²*J*_{CF} = 34.8 Hz), 126.66, 125.28, 122.41 (q, ¹*J*_{CF} = 273.5 Hz), 120.94, 120.91 (q, ³*J*_{CF} = 3.4 Hz), 119.21 (q, ³*J*_{CF} = 3.7 Hz), 111.34

¹⁹F{¹H} NMR (376 MHz, CDCl₃) δ -64.90.

ESI-MS: [M+H]⁺: C₁₃H₈N₂OF₃ calculated m/z 265.0589, found 265.0580

2-(5-Trifluoromethylpyridin-2-yl)-5-methylbenzo[d]oxazole



2-bromo-5-trifluoromethylpyridine (226 mg, 1 mmol), 5-methylbenzoxazole (160 mg, 1.2 mmol), LiO^tBu (1.0 M in hexane) (5 mL, 5 mmol) and PdCl(C₃H₅)(dppb) (30.5 mg, 0.05 mmol) in toluene (5 mL) afforded the product as a white solid (171 mg, 61%). Columned in 15:1 Pet Ether: EtOAc.

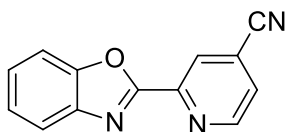
¹H NMR (400 MHz, CD₃CN) δ 9.06 (s, 1H), 8.47 (d, *J* = 8.5 Hz, 1H), 8.25 (d, *J* = 8.5 Hz, 1H), 7.65 (s, 1H), 7.63 (d, *J* = 8.5 Hz, 1H), 7.34 (d, *J* = 8.4 Hz, 1H), 2.48 (s, 3H).

¹³C{¹H} NMR (101 MHz, CDCl₃) δ 160.17, 149.45, 149.15, 147.13 (q, ³*J*_{CF} = 4.0 Hz), 141.85, 135.29, 134.36 (q, ³*J*_{CF} = 3.4 Hz), 128.05, 127.78 (q, ²*J*_{CF} = 33.4 Hz), 123.14 (q, ¹*J*_{CF} = 272.6 Hz), 122.89, 120.76, 110.72, 21.50

¹⁹F{¹H} NMR (376 MHz, CD₃CN) δ -63.22.

ESI-MS: [M+Na]⁺: C₁₄H₉N₂OF₃Na calculated m/z 301.0565, found 301.0572

2-(benzo[d]oxazol-2-yl)isonicotinonitrile



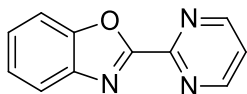
2-chloro-4-pyridinecarbonitrile (137.5 mg, 1 mmol), benzoxazole (148 mg, 1.2 mmol), LiO^tBu (1.0 M in hexane) (5 mL, 5 mmol) and PdCl(C₃H₅)(dppb) (31.3 mg, 0.05 mmol) in toluene (5 mL) afforded the product as a white solid (91 mg, 41%). Columned DCM/ 1% MeOH.

¹H NMR (400 MHz, CDCl₃) δ 9.00 (d, *J* = 4.9 Hz, 1H), 8.59 (s, 1H), 7.87 (d, *J* = 7.1 Hz, 1H), 7.72 – 7.65 (m, 2H), 7.46 (m, 2H).

¹³C{¹H} NMR (101 MHz, CDCl₃) δ 159.60, 151.26, 151.19, 147.50, 141.58, 126.93, 126.53, 125.45, 124.98, 121.92, 121.13, 115.73, 111.40.

ESI-MS: [M+H]⁺: C₁₃H₈N₃O calculated m/z 222.0667, found 222.0662

2-(pyrimidin-2-yl)benzo[d]oxazole



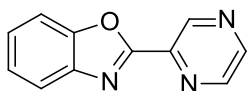
2-chloropyrimidine (115 mg, 1 mmol), benzoxazole (143 mg, 1.2 mmol), LiO^tBu (1.0 M in hexane) (5 mL, 5 mmol) and PdCl(C₃H₅)(dppb) (30.5 mg, 0.05 mmol) in toluene (5 mL) afforded the product as a light yellow solid (89 mg, 45%). Columned in 5:1 EtOAc: Pet Ether. NMR analysis in agreement with literature data.⁴⁸

¹H NMR (400 MHz, CDCl₃) δ 8.98 (d, *J* = 4.9 Hz, 2H), 7.90 (d, *J* = 7.2 Hz, 1H), 7.69 (d, *J* = 7.5 Hz, 1H), 7.49 – 7.38 (m, 3H).

¹³C{¹H} NMR (101 MHz, CDCl₃) δ 159.60, 158.02, 155.34, 151.28, 141.73, 126.99, 125.30, 121.89, 121.57, 111.45.

ESI-MS: [M+H]⁺: C₁₁H₈N₃O calculated m/z 198.0667, found 198.0663

2-(pyrazin-2-yl)benzo[d]oxazole



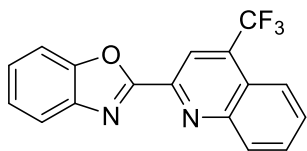
2-iodopyrazine (206 mg, 1 mmol), benzoxazole (143 mg, 1.2 mmol), LiO^tBu (1.0 M in hexane) (5 mL, 5 mmol) and PdCl(C₃H₅)(dppb) (30.5 mg, 0.05 mmol) in toluene (5 mL) afforded the product as a white solid (133 mg, 68%). Columned in 3:1 Pet ether: EtOAc. NMR analysis in agreement with literature data.⁵⁰

¹H NMR (600 MHz, CDCl₃) δ 9.60 (d, *J* = 1.5 Hz, 1H), 8.78 (dd, *J* = 2.4, 1.5 Hz, 1H), 8.75 (d, *J* = 2.4 Hz, 1H), 7.90 – 7.86 (m, 1H), 7.71 – 7.68 (m, 1H), 7.45 (m, 2H).

¹³C{¹H} NMR (151 MHz, CDCl₃) δ 159.39, 151.09, 146.16, 144.73, 144.66, 142.07, 141.62, 126.71, 125.35, 121.04, 111.33.

ESI-MS: [M+H]⁺: C₁₁H₈N₃O calculated m/z 198.0667, found 198.0662

2-(4-(trifluoromethyl)quinolin-2-yl)benzo[d]oxazole



2-chloro-4-(trifluoromethyl)quinoline (232 mg, 1 mmol), benzoxazole (148 mg, 1.2 mmol), LiO^tBu (1.0 M in hexane) (5 mL, 5 mmol) and PdCl(C₃H₅)(dppb) (30.9 mg, 0.05 mmol) in toluene (5 mL) afforded the product as a white solid (286 mg, 91%). Columned in :1 Pet ether: EtOAc.

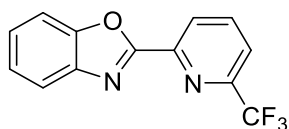
¹H NMR (400 MHz, CDCl₃) δ 8.79 (s, 1H), 8.47 (d, *J* = 8.5 Hz, 1H), 8.22 (d, *J* = 8.5 Hz, 1H), 7.98 – 7.86 (m, 2H), 7.78 (dd, *J* = 14.8, 7.3 Hz, 2H), 7.54 – 7.43 (m, 2H).

¹³C{¹H} NMR (101 MHz, CDCl₃) δ 160.65, 151.38, 148.92, 145.48, 141.74, 135.69 (q, ²*J*_{CF} = 32.3 Hz), 131.23, 131.16, 129.81, 126.84, 125.36, 124.15 (q, ³*J*_{CF} = 2.2 Hz), 123.44, 123.18 (q, ¹*J*_{CF} = 275.0 Hz), 121.07, 117.60 (q, ³*J*_{CF} = 5.4 Hz), 111.58.

¹⁹F{¹H} NMR (376 MHz, CDCl₃) δ -61.45.

ESI-MS: [M+H]⁺: C₁₇H₁₀N₂OF₃ calculated *m/z* 315.0745, found 315.0741

2-(6-(trifluoromethyl)pyridin-2-yl)benzo[d]oxazole



2-chloro-6-(trifluoromethyl)pyridine (182 mg, 1 mmol), benzoxazole (144.5 mg, 1.2 mmol), LiO^tBu (1.0 M in hexane) (5 mL, 5 mmol) and PdCl(C₃H₅)(dppb) (30.5 mg, 0.05 mmol) in toluene (5 mL) afforded the product as a yellow solid (256 mg, 97%). Columned in 8:1 Pet ether: EtOAc.

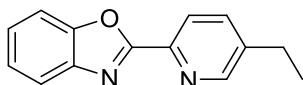
¹H NMR (400 MHz, CDCl₃) δ 8.56 (d, *J* = 8.0 Hz, 1H), 8.09 (m, 1H), 7.86 (m, 2H), 7.71 (dd, *J* = 7.0, 1.5 Hz, 1H), 7.44 (m, 2H).

$^{13}\text{C}\{^1\text{H}\}$ NMR (101 MHz, CDCl_3) δ 160.17, 151.18, 148.87 (q, $^2J_{\text{CF}} = 35.4$ Hz), 146.68, 141.61, 138.69, 126.55, 125.97, 125.16, 122.00 (q, $^3J_{\text{CF}} = 2.7$ Hz), 121.14 (q, $^1J_{\text{CF}} = 274.6$ Hz), 120.89, 111.51

$^{19}\text{F}\{^1\text{H}\}$ NMR (376 MHz, CDCl_3) δ -67.82.

ESI-MS: $[\text{M}+\text{Na}]^+$: $\text{C}_{13}\text{H}_7\text{N}_2\text{OF}_3\text{Na}$ calculated m/z 287.0408, found 287.0407

2-(5-ethylpyridin-2-yl)benzo[d]oxazole



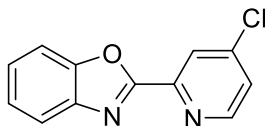
2-chloro-5-ethylpyridine (566 mg, 4 mmol), benzoxazole (572 mg, 4.8 mmol), LiO^tBu (1.0 M in hexane) (20 mL, 20 mmol) and $\text{PdCl}(\text{C}_3\text{H}_5)(\text{dppb})$ (122 mg, 0.2 mmol) in toluene (20 mL) afforded the product as a yellow solid (550 mg, 61%). Columned in 10:1 Pet ether: EtOAc.

^1H NMR (400 MHz, CDCl_3) δ 8.66 (d, $J = 1.7$ Hz, 1H), 8.29 (d, $J = 8.0$ Hz, 1H), 7.82 (m, 1H), 7.72 (dd, $J = 8.1, 2.1$ Hz, 1H), 7.66 (m, 1H), 7.39 (m, 2H), 2.77 (q, $J = 7.6$ Hz, 2H), 1.33 (t, $J = 7.6$ Hz, 3H)

$^{13}\text{C}\{^1\text{H}\}$ NMR (101 MHz, CDCl_3) δ 161.76, 151.03, 150.16, 143.72, 141.91, 141.88 136.26, 125.78, 124.82, 123.21, 120.49, 111.17, 26.17, 15.01.

ESI-MS: $[\text{M}+\text{H}]^+$: $\text{C}_{14}\text{H}_{13}\text{N}_2\text{O}$ calculated m/z 225.1029, found 225.1028

2-(4-chloropyridin-2-yl)benzo[d]oxazole



2-bromo-4-chloropyridine (577 mg, 3 mmol), benzoxazole (429 mg, 3.6 mmol), LiO^tBu (1.0 M in hexane) (15 mL, 15 mmol) and $\text{PdCl}(\text{C}_3\text{H}_5)(\text{dppb})$ (91.5 mg, 0.15 mmol) in

toluene (15 mL) afforded the product as an off white solid (346 mg, 50%). Columned in 8:1 Pet ether: EtOAc. Due to overlap, only 11 peaks are visible in ^{13}C NMR spectrum when using CDCl_3 . Both DMSO-d_6 and MeCN-d_3 give 12 peaks in the ^{13}C NMR spectrum.

^1H NMR (400 MHz, CDCl_3) δ 8.72 (d, $J = 5.2$ Hz, 1H), 8.40 (d, $J = 1.8$ Hz, 1H), 7.85 (dd, $J = 6.9$ Hz, 1.9 Hz, 1H), 7.68 (dd, $J = 7.0$ Hz, 1.8 Hz, 1H), 7.44 (m, 3H).

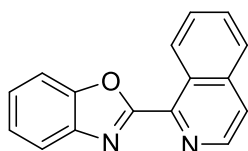
$^{13}\text{C}\{^1\text{H}\}$ NMR (101 MHz, CDCl_3) δ 160.37, 151.13, 147.41, 145.37, 141.65, 126.48, 125.75, 125.19, 123.79, 120.88, 111.32.

$^{13}\text{C}\{^1\text{H}\}$ NMR (151 MHz, DMSO-d_6) δ 160.12, 151.59, 150.48, 146.73, 144.03, 140.99, 126.59, 126.06, 125.26, 123.25, 120.46, 111.37.

$^{13}\text{C}\{^1\text{H}\}$ NMR (151 MHz, CD_3CN) δ 161.73, 152.35, 152.11, 148.54, 145.68, 142.65, 127.47, 126.84, 126.15, 124.52, 121.55, 112.23.

ESI-MS: $[\text{M}+\text{H}]^+$: $\text{C}_{12}\text{H}_8\text{N}_2\text{OCl}$ calculated m/z 231.0325, found 231.0329

2-(isoquinolin-1-yl)benzo[d]oxazole



1-chloroisoquinoline (160.6 mg, 1.0 mmol), benzoxazole (142.9 mg, 1.2 mmol, LiO^tBu (1.0 M in hexane) (5 mL, 5 mmol) and $\text{PdCl}(\text{C}_3\text{H}_5)(\text{dppb})$ (30.5 mg, 0.05 mmol) in toluene (5 mL) afforded the product as a yellow solid (163 mg, 66%). Columned in 3:1 Pet ether: EtOAc. NMR in agreement with literature.⁵¹

^1H NMR (600 MHz, CDCl_3): δ 9.75-9.71 (m, 1H), 8.78 (d, $J = 5.5$ Hz, 1H), 7.94 (dt, $J = 7.4, 3.4$ Hz, 2H), 7.85 (d, $J = 5.4$ Hz, 1H), 7.83-7.78 (m, 2H), 7.76 (dd, $J = 7.2, 1.2$ Hz, 1H), 7.46 (dq, $J = 14.8, 7.4, 1.3$ Hz, 2H).

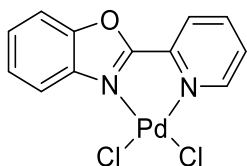
$^{13}\text{C}\{^1\text{H}\}$ NMR (151 MHz, CDCl_3): δ 161.02, 150.61, 145.01, 142.20, 142.14, 137.22, 130.79, 129.21, 127.58, 127.42, 127.38, 126.51, 125.01, 123.68, 121.05, 111.51.

ESI-MS: $[M+H]^+$: $C_{16}H_{11}N_2O$ calculated m/z 247.0871, found 247.0868

Synthesis of (ligand) $PdCl_2$ complexes

For all the following complexes of the type (ligand) $PdCl_2$, satisfactory ^{13}C -NMR spectra could not be obtained due to their low solubility in all common NMR solvents. $DMSO-d_6$ was found to sufficiently dissolve all chloro complexes such that 1H -NMR and ^{19}F NMR (where applicable) could be obtained. Due to the stability of these complexes in $DMSO-d_6$ however, mixtures of free ligand and complex are formed in various ratios, depending on the complex. Note: the solubility problem was previously found by Sigman and co-workers for $Pd(Quinox)Cl_2$,⁴ and they were unable to obtain 1H NMR. In our case, we prepared $Pd(Quinox)Cl_2$ following their procedure (and as described below) and catalytic tests with $Pd(Quinox)Cl_2$ were in good agreement with the results previously obtained by Sigman and co-workers.

(2-(pyridin-2-yl)benzo[d]oxazole) $PdCl_2$

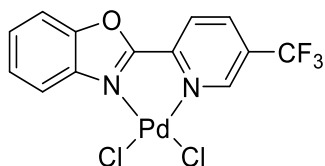


$Pd(NCMe)_2Cl_2$ (71.0 mg, 0.27 mmol) was stirred until complete dissolution in DCM (16 mL) after which time a solution of 2-(2-pyridyl)benzoxazole (53.7 mg, 0.27 mmol) was added dropwise in DCM (4 mL). The resulting mixture was stirred overnight (approx. 16 h) and the solid was collected by filtration and washed with diethyl ether before being dried under vacuum to give the product as a yellow solid (81 mg, 81%). NMR analysis in agreement with literature data.⁵²

1H NMR (400 MHz, $DMSO-d_6$) δ 9.10 (d, $J = 5.4$ Hz, 1H), 8.56 (d, $J = 8.0$ Hz, 1H), 8.45-8.34 (m, 2H), 8.04 (d, $J = 8.3$ Hz, 1H), 7.96 (m, 1H), 7.70-7.60 (m, 2H).

Elemental Analysis: Predicted: C, 38.59; H, 2.16; N, 7.50; Found: C, 38.43; H, 2.02; N, 7.28.

(2-(5-(trifluoromethyl)pyridin-2-yl)benzo[d]oxazole)PdCl₂



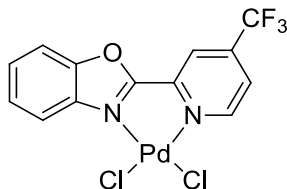
Pd(NCMe)₂Cl₂ (98.2 mg, 0.378 mmol) was stirred in DCM (24 mL) until complete dissolution was observed. After this a solution of (2-[5-(trifluoromethyl)-2-pyridinyl]-benzoxazole) (100 mg, 0.378 mmol) in DCM (6 mL) was added dropwise leading to the formation of a yellow precipitate. The reaction was stirred overnight (approx. 18 h) after which time it was filtered, washed with diethyl ether and then dried under reduced pressure to give the product as a yellow solid (128 mg, 77%).

¹H NMR (400 MHz, DMSO-d₆) δ 9.22 (s, 1H), 8.56-8.49 (m, 2H), 7.96-7.90 (m, 2H), 7.58-7.49 (m, 2H)

¹⁹F{¹H} NMR (376 MHz, DMSO-d₆) δ -61.11 (s).

Elemental Analysis: Predicted: C, 35.36; H, 1.60; N, 6.34; Found: C, 35.53; H, 1.22; N, 5.03.

(2-(4-(trifluoromethyl)pyridin-2-yl)benzo[d]oxazole)PdCl₂



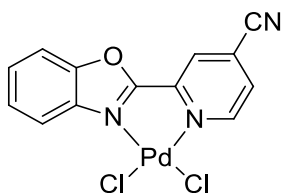
Pd(NCMe)₂Cl₂ (98.6 mg, 0.378 mmol) was stirred in DCM (24 mL) until complete dissolution was observed. After this a solution of (2-[4-(trifluoromethyl)-2-pyridinyl]-benzoxazole) (100 mg, 0.378 mmol) in DCM (6 mL) was added dropwise leading to the formation of a yellow precipitate. The reaction was stirred overnight (approx. 18 h) after which time it was filtered, washed with diethyl ether and then dried under reduced pressure to give the product as a yellow solid (115 mg, 70%).

^1H NMR (400 MHz, DMSO- d_6) δ 9.11 (d, J = 5.0 Hz), 8.56 (s, 1H), 8.06 (d, J = 4.6 Hz, 1H), 7.92 (m, 2H), 7.53 (m, 2H).

$^{19}\text{F}\{^1\text{H}\}$ NMR (376 MHz, DMSO- d_6) δ -63.57 (s).

Elemental Analysis: Predicted: C, 35.36; H, 1.60; N, 6.34; Found: C, 35.25; H, 1.28; N, 5.67.

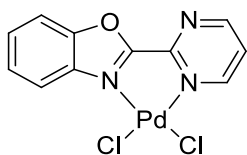
(2-(benzo[d]oxazol-2-yl)isonicotinonitrile)PdCl₂



Pd(NCMe)₂Cl₂ (58.6 mg, 0.226 mmol) was stirred in DCM (12 mL) until complete dissolution was observed. After this a solution of (2-(benzo[d]oxazol-2-yl)isonicotinonitrile) (50 mg, 0.226 mmol) in DCM (3 mL) was added dropwise leading to the formation of a yellow precipitate. The reaction was stirred overnight (approx. 18 h) after which time it was filtered, washed with diethyl ether and then dried under reduced pressure to give the product as a yellow solid (72 mg, 80%).

^1H NMR (400 MHz, DMSO- d_6) δ 9.06 (d, J = 4.2 Hz, 1H), 8.71 (s, 1H), 8.12 (dd, J = 4.9, 1.4 Hz, 1H), 7.94-7.88 (m, 2H), 7.59 – 7.47 (m, 2H).

(2-(pyrimidin-2-yl)benzo[d]oxazole)PdCl₂

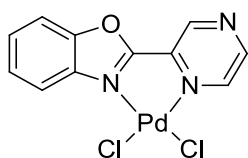


Pd(NCMe)₂Cl₂ (64.3 mg, 0.248 mmol) was stirred in DCM (12 mL) until complete dissolution was observed. After this a solution of (2-(pyrimidin-2-yl)benzo[d]oxazole) (49 mg, 0.248 mmol) in DCM (3 mL) was added dropwise leading to the formation of a yellow

precipitate. The reaction was stirred overnight (approx. 18 h) after which time it was filtered, washed with diethyl ether and then dried under reduced pressure to give the product as a yellow solid (60 mg, 65%). When trying to get an NMR in DMSO-d₆ a 1:1 mixture of catalyst and free ligand is formed.

Elemental Analysis: Predicted: C, 35.28; H, 1.88; N, 11.22; Found: C, 34.07; H, 1.76; N, 10.15.

(2-(pyrazin-2-yl)benzo[d]oxazole)PdCl₂

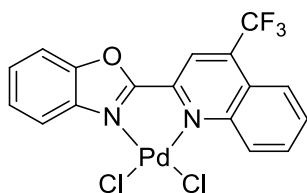


Pd(NCMe)₂Cl₂ (65 mg, 0.254 mmol) was stirred in DCM (12 mL) until complete dissolution was observed. After this a solution of (2-(pyrazin-2-yl)benzo[d]oxazole) (50 mg, 0.254 mmol) in DCM (3 mL) was added dropwise leading to the formation of an orange precipitate. The reaction was stirred overnight (approx. 18 h) after which time it was filtered, washed with diethyl ether and then dried under reduced pressure to give the product as an orange solid (67 mg, 71%).

¹H NMR (400 MHz, DMSO-d₆) δ 9.53 (s, 1H), 8.90 (m, 2H), 7.95-7.89 (m, 2H), 7.57-7.49 (m, 2H).

Elemental Analysis: Predicted: C, 35.28; H, 1.88; N, 11.22; Found: C, 34.44; H, 1.59; N, 10.88.

(2-(4-(trifluoromethyl)quinolin-2-yl)benzo[d]oxazole)PdCl₂



^1H NMR (400 MHz, DMSO- d_6) δ 8.69 (s, 1H), 8.42 (d, $J = 8.3$ Hz, 1H), 8.22 (d, $J = 8.3$ Hz, 1H), 8.09 (m, 1H), 7.98 (m, 3H), 7.56 (m, 2H).

$^{19}\text{F}\{^1\text{H}\}$ NMR (376 MHz, DMSO- d_6) δ -60.70 (s).

Elemental Analysis: Predicted: C, 41.54; H, 1.85; N, 5.70; Found: C, 41.09; H, 1.84; N, 4.57.

Synthesis of isolated dicationic Pd complexes

The synthesis and characterization of all dicationic complexes screened in this study that are not found below were previously synthesized and have already been published.^{1,3} We were unable to prepare an isolated complex with the Quinox ligand.

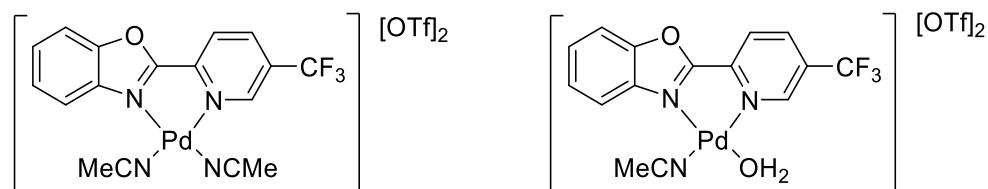
Confirming the structure *and* purity of these type of cationic complexes is challenging. In this work NMR (^1H and where possible ^{19}F) and elemental analysis were chosen. Mass spectrometry was not utilised as such complexes tend to give complex spectra and the information (although useful for some studies²) does not address the issue of purity.

The NMR spectra is useful for demonstrating the di-cationic nature of the final complexes. We have prepared isolated complexes via Pd(OAc)₂ and the absence of acetate peaks is a good indicator that the d-cationic complex has been prepared. In the case of ^1H NMR, we have often used deuterated acetonitrile as the NMR solvent and the acetonitrile peak overlaps with the acetate peak, but when other deuterated solvents (e.g. DMSO) are used these peaks are absent. In addition, with the ^{13}C NMR spectra, a Pd bound acetate would show a peak at around 23 ppm,⁵³ and this is clearly absent in our samples.

In some cases, ^1H NMR has had a good agreement for the theoretical number of acetonitrile ligands in the complex,³ with dicationic complexes containing two MeCN molecules as ligands (an integration of 6 hydrogen atoms), but in other samples this acetonitrile peak integrates for significantly less than 6. This is not unexpected, as Hii and co-workers have previously discussed.⁵⁴ Cationic palladium triflate complexes are hygroscopic and moisture from the air or in solvents can lead to water molecules displacing MeCN ligands, and it is for this reason that the structures below are shown with a generic "S" label. Complexes were found to be stable and those that had been stored for periods of time (e.g. months) showed no difference in performance compared to when

initially prepared. The methods we have used for preparing di-cationic catalysts are further supported by the analysis of complexes which have CF_3 functionalised ligands. In these cases, the di-cationic nature of the catalysts has been conclusively shown by the integration of the ligand $-\text{CF}_3$ peak against the $[\text{OTf}]^-$ or $[\text{Tf}_2\text{N}]^-$ resonance in ^{19}F NMR. For quantitative integration of these fluorine peaks the D_1 relaxation delay was set to 8 seconds. For these catalysts, a ligand to anion ratio of 1:2 was found, confirming the complex is di-cationic. In addition, we were able to obtain a crystal structure of the $(5\text{-CF}_3\text{-PBO})\text{Pd}(\text{MeCN})_2(\text{Tf}_2\text{N})_2$ complex (see later for more details).

For the elemental analysis the experimental results were compared against calculated results for the complex when it contains two MeCN ligands and the complex when it contains one MeCN ligand and one H_2O (see below for an example of the two structures).



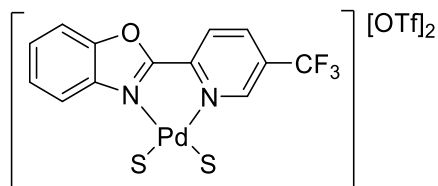
In general, the results of the ^1H -NMR and the elemental analysis are in good agreement. When the integration of the ^1H -NMR indicates one MeCN and one H_2O ligand, the obtained elemental analysis results more closely resemble this structure than the complex containing two MeCN ligands. The same is also true when the ^1H -NMR points more towards the complex with two MeCN ligands.

Despite this, the results obtained from the elemental analysis for almost all complexes have at least one element that falls outside of the error limits of most journals, an issue which has been highlighted and discussed recently.⁵⁵⁻⁵⁷ Indeed, the editors of the journal *Organometallics*, recently recognized the challenges of elemental analysis and such analysis is no longer a mandatory requirement.⁵⁸ Here we have included the data along with this additional interpretation and commentary. These discrepancies could be due to trace amounts of other molecules, including additional water, picked up from the

atmosphere. Furthermore, as has already been discussed if water is present then there is the possibility for the formation of oxygen-bridged dimers and higher order species forming. The presence of small amounts of these species in the solid phase could feasibly be throwing off the elemental analysis values.

It should be noted that across the duration of this work, multiple batches of almost all the catalysts were synthesised. In the case of the best performing catalyst, the number of batches prepared was significantly higher. The various batches all gave catalytic results that were self-consistent.

[(2-(5-(trifluoromethyl)pyridin-2-yl)benzo[d]oxazole)Pd(MeCN/H₂O)₂][OTf]₂



(2-(5-(trifluoromethyl)pyridin-2-yl)benzo[d]oxazole) (203 mg, 0.77 mmol) and Pd(OAc)₂ (173 mg, 0.77 mmol) were dissolved in MeCN (10 mL) and stirred for 1 h during which time a yellow precipitate was formed. Triflic acid (284 mg, 1.89 mmol) was then added dropwise in MeCN (4 mL) and the reaction stirred for a further 4 h. Diethyl ether was then slowly added until precipitation of a yellow solid. The solid was then filtered using a Buchner funnel and washed with diethyl ether to give the product as a yellow solid (434 mg, 75%).

¹H NMR (600 MHz, CD₃CN) δ 8.85 (d, *J* = 8.2 Hz, 1H), 8.77 (s, 1H), 8.57 (d, *J* = 8.2 Hz, 1H), 8.00 (m, 1H), 7.87 (m, 1H), 7.81 – 7.77 (m, 2H), 1.96 (s, 3H).

¹³C{¹H} NMR (151 MHz, CD₃CN) δ 164.24, 151.43 (q, ³*J*_{CF} = 3.8 Hz), 149.90, 147.07, 143.10 (q, ³*J*_{CF} = 3.5 Hz), 135.04, 131.98 (q, ²*J*_{CF} = 36.0 Hz), 131.48, 129.79, 127.33, 121.82 (q, ¹*J*_{CF} = 273.4 Hz), 120.48 (q, ¹*J*_{CF} = 320.7 Hz), 118.78, 113.93, 1.35.

¹⁹F{¹H} NMR (565 MHz, CD₃CN) δ -63.13 (s, 3F), -79.31 (s, 6F).

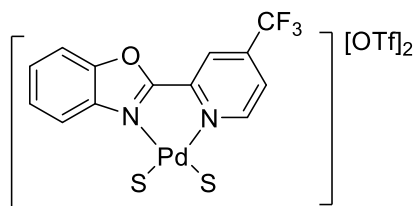
Elemental Analysis 'Batch 1': Integration value of MeCN peak by ¹H-NMR = 2.56

Element	Found (%)	Predicted [S = MeCN, MeCN] (%)	Percentage difference	Predicted [S = MeCN, H₂O] (%)	Percentage difference
C	27.96	30.39	2.43	28.05	0.09
H	1.58	1.75	0.17	1.66	0.08
N	5.96	7.46	1.50	5.77	0.19
S	8.25	8.54	0.29	8.81	0.56

Elemental Analysis 'Batch 2': Integration value of MeCN peak by ¹H-NMR = 3.08

Element	Found (%)	Predicted [S = MeCN, MeCN] (%)	Percentage difference	Predicted [S = MeCN, H₂O] (%)	Percentage difference
C	28.00	30.39	2.39	28.05	0.05
H	1.53	1.75	0.22	1.66	0.13
N	5.83	7.46	1.63	5.77	0.06
S	8.47	8.54	0.07	8.81	0.34

[(2-(4-(trifluoromethyl)pyridin-2-yl)benzo[d]oxazole)Pd(MeCN/H₂O)₂][OTf]₂



The same procedure was followed as per [(2-(5-(trifluoromethyl)pyridin-2-yl)benzo[d]oxazole)Pd(MeCN/H₂O)₂][OTf]₂ using 100 mg of ligand to obtain the product as a light yellow solid (161 mg, 57%).

¹H NMR (600 MHz, CD₃CN) δ 8.94 (d, *J* = 6.0 Hz, 1H), 8.73 (d, *J* = 2.1 Hz, 1H), 8.27 (dd, *J* = 6.0, 2.1 Hz, 1H), 8.02 (m, 1H), 7.90 (m, 1H), 7.84 – 7.81 (m, 2H), 1.99 (s, 6H).

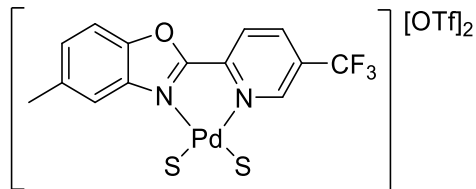
¹³C{¹H} NMR (151 MHz, CD₃CN) δ 164.85, 156.53, 150.11, 146.09, 144.69 (q, ²*J*_{CF} = 36.8 Hz), 135.37, 131.50, 129.99, 127.66 (q, ³*J*_{CF} = 3.4 Hz), 123.60 (q, ³*J*_{CF} = 3.2 Hz), 122.09 (q, ¹*J*_{CF} = 274.2 Hz), 121.89 (q, ¹*J*_{CF} = 320.6 Hz), 119.06, 114.10, 1.64

¹⁹F{¹H} NMR (565 MHz, CD₃CN) δ -65.68 (s, 3F), -79.29 (s, 6F).

Elemental Analysis: Integration value of MeCN peak by ¹H-NMR = 5.5

Element	Found (%)	Predicted [S = MeCN, MeCN] (%)	Percentage difference	Predicted [S = MeCN, H ₂ O] (%)	Percentage difference
C	28.99	30.39	1.40	28.05	0.94
H	1.86	1.75	0.11	1.66	0.20
N	6.97	7.46	0.49	5.77	1.2
S	8.00	8.54	0.54	8.81	0.81

[2-(5-Trifluoromethylpyridin-2-yl)-5-methylbenzo[d]oxazolePd(MeCN/H₂O)₂][OTf]₂



The same procedure was followed as per [(2-(5-(trifluoromethyl)pyridin-2-yl)benzo[d]oxazole)Pd(MeCN/H₂O)₂][OTf]₂ using 100 mg of ligand to obtain the product as a light yellow solid (184 mg, 67%).

¹H NMR (600 MHz, CD₃CN) δ 8.84 (d, *J* = 8.3 Hz, 1H), 8.76 (s, 1H), 8.53 (d, *J* = 8.2 Hz, 1H), 7.86 (d, *J* = 8.7 Hz, 1H), 7.68 (d, *J* = 8.7 Hz, 1H), 7.53 (s, 1H), 2.60 (s, 3H), 1.96 (s, 5H).

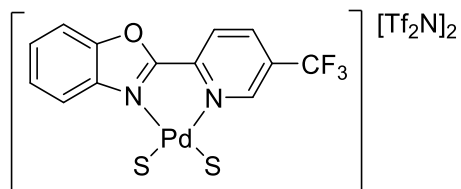
¹³C{¹H} NMR (151 MHz, CD₃CN) δ 164.26, 151.31 (q, ³*J*_{CF} = 3.9 Hz), 148.33, 147.40, 142.93 (q, ³*J*_{CF} = 3.3 Hz), 140.93, 135.34, 132.76, 131.78 (q, ²*J*_{CF} = 36.18 Hz), 127.10, 121.93 (q, ¹*J*_{CF} = 273.2 Hz), 121.76 (q, ¹*J*_{CF} = 321.0 Hz), 118.09, 113.35, 21.37, 1.35.

¹⁹F{¹H} NMR (565 MHz, CD₃CN) δ -63.13 (s, 3F), -79.31 (s, 6F).

Elemental Analysis: Integration value of MeCN peak by ¹H-NMR = 2.87

Element	Found (%)	Predicted [S = MeCN, MeCN] (%)	Percentage difference	Predicted [S = MeCN, H ₂ O] (%)	Percentage difference
C	27.87	31.41	3.54	29.14	1.27
H	1.81	1.98	0.17	1.90	0.09
N	4.39	7.33	2.94	5.66	1.27
S	8.12	8.38	0.26	8.64	0.52

[(2-(5-(trifluoromethyl)pyridin-2-yl)benzo[d]oxazole)Pd(MeCN/H₂O)₂][Tf₂N]₂



2-(5-(trifluoromethyl)pyridin-2-yl)benzo[d]oxazole (100 mg, 0.38 mmol) and Pd(OAc)₂ (85 mg, 0.38 mmol) were dissolved in dry MeCN (4 mL) and stirred for 1 h during which a yellow precipitate was formed. The solution was then cooled to 0 °C in an ice bath and trifluoromethanesulfonimide (bistriflimide) (266 mg, 0.95 mmol) was added dropwise in dry MeCN (3 mL). The reaction was stirred at this temperature for 15 min before the ice bath was removed and the solution allowed to warm slowly to room temperature. After 5 h the solution was again cooled to 0 °C and ice cooled Et₂O (approx. 100 mL) was added leading to the formation of a small amount of precipitate. The solution was placed in the freezer overnight to precipitate out the rest of the solid which was then filtered, washed with Et₂O and dried to obtain the product as a bright yellow solid (262 mg, 69%).

¹H NMR (600 MHz, CD₃CN) δ 8.86 (d, *J* = 8.2 Hz, 1H), 8.75 (s, 1H), 8.59 (d, *J* = 8.2 Hz, 1H), 8.00 (m, 1H), 7.88 (m, 1H), 7.84-7.81 (m, 2H), 1.99 (s, 6H).

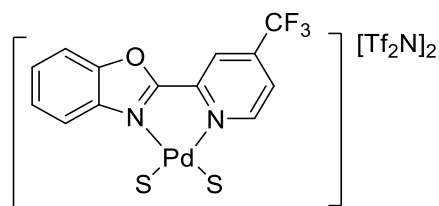
¹³C{¹H} NMR (151 MHz, CD₃CN) δ 164.24, 151.43 (q, ³*J*_{CF} = 3.8 Hz), 149.90, 147.07, 143.10 (q, ³*J*_{CF} = 3.5 Hz), 135.04, 131.98 (q, ²*J*_{CF} = 36.0 Hz), 131.48, 129.79, 127.33, 121.82 (q, ¹*J*_{CF} = 273.4 Hz), 120.48 (q, ¹*J*_{CF} = 320.7 Hz), 118.78, 113.93, 1.35.

¹⁹F{¹H} NMR (565 MHz, CD₃CN) δ -63.16 (s, 3F), -80.15 (s, 12F).

Elemental Analysis: Integration value of MeCN peak by $^1\text{H-NMR}$ = 5.58

Element	Found (%)	Predicted [S = MeCN, MeCN] (%)	Percentage difference	Predicted [S = MeCN, H ₂ O] (%)	Percentage difference
C	24.23	24.90	0.67	23.05	1.18
H	1.17	1.29	0.12	1.22	0.05
N	8.09	8.30	0.21	7.07	1.02
S	12.69	12.66	0.03	12.95	0.26

[(2-(4-(trifluoromethyl)pyridin-2-yl)benzo[d]oxazole)Pd(MeCN)₂][Tf₂N]₂



The same procedure was followed as per [(2-(5-(trifluoromethyl)pyridin-2-yl)benzo[d]oxazole)Pd(MeCN)₂][Tf₂N]₂ however upon addition of the ice cooled Et₂O the solid precipitated immediately (272 mg, 72%).

$^1\text{H NMR}$ (600 MHz, CD₃CN) δ 8.89 (d, J = 6.0 Hz, 1H), 8.74 (d, J = 2.0 Hz, 1H), 8.26 (dd, J = 6.0, 2.0 Hz, 1H), 8.02 (m, 1H), 7.90 (m, 1H), 7.84 – 7.80 (m, 2H), 1.99 (s, 6H).

$^{13}\text{C}\{^1\text{H}\}$ NMR (151 MHz, CD₃CN) δ 164.38, 156.15, 149.85, 145.62, 144.60 (q, $^2J_{\text{CF}}$ = 36.8 Hz), 135.00, 131.34, 129.75, 127.50 (q, $^3J_{\text{CF}}$ = 3.3 Hz), 123.45 (q, $^3J_{\text{CF}}$ = 3.4 Hz), 121.73 (q, $^1J_{\text{CF}}$ = 274.3 Hz), 120.48 (q, $^1J_{\text{CF}}$ = 320.6 Hz), 118.73, 113.84, 1.35.

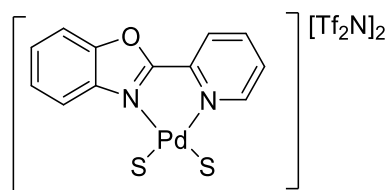
$^{19}\text{F}\{^1\text{H}\}$ NMR (565 MHz, CD₃CN) δ -65.68 (s, 3F), -80.14 (s, 12F).

Elemental Analysis: Integration value of MeCN peak by ¹H-NMR = 5.73

Element	Found (%)	Predicted [S = MeCN, MeCN] (%)	Percentage difference	Predicted [S = MeCN, H ₂ O] (%)	Percentage difference
C	24.87	24.90	0.03	23.05	1.82
H	1.27	1.29	0.02	1.22	0.05
N	8.23	8.30	0.07	7.07	1.16
S	13.1	12.66	0.44	12.95	0.15

Note: This complex and the following [Tf₂N] complex were prepared in order to try and obtain a series of crystal structures, with variation on the cation. As we had been able to crystalize the 5-CF₃-PBO complex with the [Tf₂N] anion. Unfortunately we were unable to obtain suitable crystals.

[(2-(pyridin-2-yl)benzo[d]oxazole)Pd(MeCN/H₂O)₂][Tf₂N]₂



The same procedure was followed as per [(2-(5-(trifluoromethyl)pyridin-2-yl)benzo[d]oxazole)Pd(MeCN/H₂O)₂][Tf₂N]₂ however upon addition of the ice cooled Et₂O the solid precipitated immediately (230 mg, 64%).

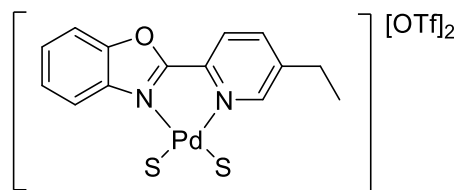
¹H NMR (600 MHz, CD₃CN) δ 8.65 (ddd, *J* = 5.8, 1.3, 0.6 Hz, 1H), 8.56 (td, *J* = 7.9, 1.3 Hz, 1H), 8.39 (ddd, *J* = 7.8, 1.5, 0.6 Hz, 1H), 8.00 (dt, *J* = 8.5, 0.9 Hz, 1H), 7.96 (ddd, *J* = 7.9, 5.8, 1.5 Hz, 1H), 7.86 (ddd, *J* = 8.6, 6.2, 2.5 Hz, 1H), 7.81 – 7.77 (m, 2H), 1.99 (s, 5H).

¹³C{¹H} NMR (101 MHz, CD₃CN) δ 165.74, 154.71, 149.91, 145.43, 144.28, 135.35, 131.56, 131.03, 129.69, 127.53, 120.78 (q, ¹*J*_{CF} = 320.7 Hz), 118.75, 114.03, 1.21.

Elemental Analysis: Integration value of MeCN peak by $^1\text{H-NMR}$ = 5.36

Element	Found (%)	Predicted [S = MeCN, MeCN] (%)	Percentage difference	Predicted [S = MeCN, H ₂ O] (%)	Percentage difference
C	25.38	25.42	0.04	23.45	1.93
H	1.37	1.49	0.12	1.42	0.05
N	8.75	8.89	0.14	7.60	1.15
S	13.55	13.57	0.02	13.91	0.36

[(2-(5-ethylpyridin-2-yl)benzo[d]oxazole)Pd(NCMe/H₂O)₂][OTf]₂



The same procedure was followed as per [(2-(5-(trifluoromethyl)pyridin-2-yl)benzo[d]oxazole)Pd(MeCN/H₂O)₂][OTf]₂ with the exception that 150 mg of ligand was used. The product was obtained as a yellow solid (162 mg, 34%).

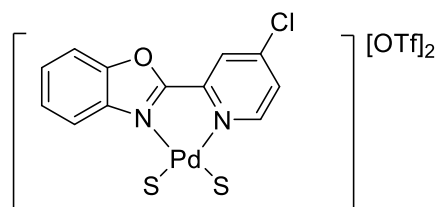
$^1\text{H NMR}$ (600 MHz, CD₃CN) δ 8.42 (d, J = 1.23 Hz, 1H), 8.41-8.39 (m, 1H), 8.31 (d, J = 8.02 Hz, 1H), 7.99-7.97 (m, 1H), 7.86-7.83 (m, 1H), 7.80-7.76 (m, 2H), 2.99 (q, J = 7.58 Hz, 2H), 1.99 (s, 3H), 1.38 (t, J = 7.58 Hz, 3H)

$^{13}\text{C}\{^1\text{H}\}$ NMR (101 MHz, CD₃CN) δ 165.71, 154.12, 149.58, 149.44, 143.52, 141.51, 135.13, 130.25, 129.19, 126.67, 121.58 (q, $^1J_{\text{CF}}$ = 320.75 Hz), 118.30, 113.55, 26.74, 14.44, 1.31.

Elemental Analysis: Integration value of MeCN peak by $^1\text{H-NMR} = 3.08$

Element	Found (%)	Predicted [S = MeCN, MeCN] (%)	Percentage difference	Predicted [S = MeCN, H ₂ O] (%)	Percentage difference
C	32.15	33.79	1.64	31.43	0.72
H	2.94	2.55	0.39	2.49	0.45
N	7.06	7.88	0.82	6.11	0.95
S	8.32	9.02	0.70	9.32	1.00

[(2-(4-chloropyridin-2-yl)benzo[d]oxazole)Pd(NCMe/H₂O)₂][OTf]₂



The same procedure was followed as per [(2-(5-(trifluoromethyl)pyridin-2-yl)benzo[d]oxazole)Pd(MeCN/H₂O)₂][OTf]₂ with the exception that 150 mg of ligand was used. The product was obtained as a light yellow solid (292 mg, 63%).

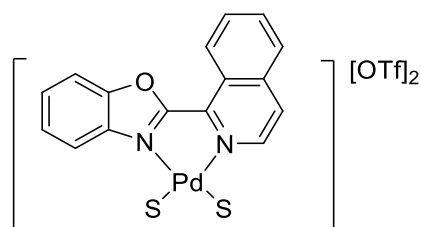
$^1\text{H NMR}$ (600 MHz, CD₃CN) δ 8.61 (d, $J = 6.3$ Hz, 1H), 8.49 (d, $J = 2.4$ Hz, 1H), 8.02 (dd, $J = 6.3, 2.4$ Hz, 1H), 8.00 (m, 1H), 7.90-7.87 (m, 1H), 7.83-7.79 (m, 2H), 1.99 (s, 5H)

$^{13}\text{C}\{^1\text{H}\}$ NMR (101 MHz, CD₃CN) δ 164.66, 154.87, 152.91, 149.73, 145.01, 135.10, 131.01, 130.99, 129.55, 127.43, 121.64 (q, $^1J_{\text{CF}} = 320.82$ Hz), 118.66, 113.73, 1.34.

Elemental Analysis: Integration value of MeCN peak by ¹H-NMR = 4.95

Element	Found (%)	Predicted [S = MeCN, MeCN] (%)	Percentage difference	Predicted [S = MeCN, H ₂ O] (%)	Percentage difference
C	28.54	30.14	1.60	27.68	0.86
H	1.91	1.83	0.08	1.74	0.17
N	7.38	7.81	0.43	6.05	1.33
S	8.28	8.94	0.66	9.24	0.96

[(2-(isoquinolin-1-yl)benzo[d]oxazole)Pd(NCMe/H₂O)₂][OTf]₂



The same procedure was followed as per [(2-(5-(trifluoromethyl)pyridin-2-yl)benzo[d]oxazole)Pd(MeCN/H₂O)₂][OTf]₂ with the exception that the scale was increased and 120 mg of ligand was used. The product was obtained as a yellow solid (238 mg, 65%).

¹H NMR (600 MHz, CD₃CN) δ 9.28 – 9.24 (m, 1H), 8.57 (d, *J* = 6.4 Hz, 1H), 8.40 (d, *J* = 6.3 Hz, 1H), 8.35 (dd, *J* = 7.7, 1.2 Hz, 1H), 8.20 (dddd, *J* = 18.3, 8.3, 6.9, 1.3 Hz, 2H), 8.13 – 8.10 (m, 1H), 7.90 (ddd, *J* = 8.5, 7.0, 1.6 Hz, 1H), 7.86 – 7.80 (m, 2H), 1.96 (s, 3H).

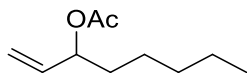
¹³C{¹H} NMR: (150 MHz, CD₃CN): δ 166.75, 150.06, 144.90, 144.13, 139.94, 136.78, 135.06, 134.25, 131.48, 130.10, 129.84, 129.43, 127.53, 125.59, 122.08 (q, ¹*J*_{CF} = 318.72 Hz), 118.91, 114.38, 1.69.

Elemental Analysis: Integration value of MeCN peak by ¹H-NMR = 2.99

Element	Found (%)	Predicted [S = MeCN, MeCN] (%)	Percentage difference	Predicted [S = MeCN, H ₂ O] (%)	Percentage difference
C	33.09	36.05	2.96	33.84	0.75
H	2.26	2.20	0.06	2.13	0.13
N	5.98	7.64	1.66	5.92	0.06
S	8.22	8.75	0.53	9.03	0.81

Synthesis of Substrates and Corresponding Products

Oct-1-en-3-yl acetate



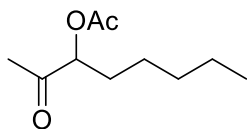
1-octene-3-ol (2.5 g, 20 mmol) was weighed into a 100 mL round bottom flask and dry DCM (40 mL) was added. The solution was stirred and DMAP (0.54 g, 4.4 mmol) was added. Once the DMAP had dissolved, acetic anhydride was added (4.1 mL, 44 mmol) and the reaction was stirred for 2 h under N₂ at room temperature. The solvent was then removed under reduced pressure and the crude mixture purified by column chromatography (95:5 Pet ether:EtOAc). The product was obtained as a clear liquid (3.2 g, 95% yield). NMR analysis in agreement with literature data.⁵⁹

¹H NMR (400 MHz, CDCl₃) δ 5.76 (ddd, *J* = 17.1, 10.5, 6.4 Hz, 1H), 5.24-5.13 (m, 3H), 2.05 (s, 3H), 1.68 – 1.50 (m, 2H), 1.34-1.22 (m, 6H), 0.87 (t, *J* = 6.4 Hz, 3H).

¹³C{¹H} NMR (101 MHz, CDCl₃) δ 170.47, 136.79, 116.59, 74.98, 34.26, 31.66, 24.83, 22.62, 21.36, 14.09.

2-oxooctan-3-yl acetate

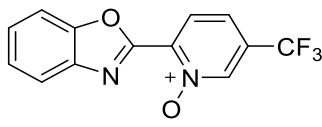
The product was made using catalytic TBHP methods described earlier. Initially unoptimized methods were used to obtain pure material for use as an analytical standard for GC analysis in our studies. After optimization, it was also prepared on a larger scale (6.5 mmol isolated). NMR analysis in agreement with literature data.⁴



¹H NMR (400 MHz, CDCl₃) δ 4.98 (m, 1H), 2.15 (m, 6H), 1.98 – 1.60 (m, 2H), 1.40-1.26 (m, 6H), 0.89 (t, *J* = 6.2 Hz, 3H).

¹³C{¹H} NMR (101 MHz, CDCl₃) δ 205.37, 170.60, 78.75, 31.37, 30.23, 26.07, 24.82, 22.36, 20.65, 13.91.

Synthesis of 2-(5-(trifluoromethyl)pyridin-2-yl)benzo[d]oxazole N-oxide



The synthesis of this compound was carried out using a modified literature procedure.⁶⁰ Ligand, 2-(5-(trifluoromethyl)pyridin-2-yl)benzo[d]oxazole (50 mg, 0.19 mmol) was dissolved in DCM and cooled to 0 °C. Urea hydrogen peroxide complex (38 mg, 0.40 mmol) was then added at 0 °C and the mixture stirred. Trifluoroacetic anhydride (80 mg, 0.40 mmol) was then added dropwise with the reaction still at 0 °C. Once addition was complete, the reaction was stirred for a further 30 min at this temperature before being allowed to slowly warm to room temperature. The reaction was monitored by TLC (8:1 Pet ether:EtOAc) and after 24 h reaction starting material still remained. Regardless, the reaction was worked up by stirring with aqueous Na₂S₂O₃ for 15 minutes before being poured into a 0.5 M HCl solution. The resultant solution was extracted with DCM and the extracted organic layer washed with saturated NaHCO₃, dried over MgSO₄ and

concentrated under reduced pressure. The crude material was purified by column chromatography (4:1 Pet ether:EtOAc) and the product obtained as an off white solid (10 mg, 20%).

^1H NMR (400 MHz, CDCl_3) δ 8.66 (s, 1H), 8.37 (d, $J = 8.4$ Hz, 1H), 7.92 (d, $J = 7.6$ Hz, 1H), 7.70 (d, $J = 8.0$ Hz, 1H), 7.54-7.43 (m, 3H).

$^{13}\text{C}\{^1\text{H}\}$ NMR (101 MHz, CDCl_3) δ 154.94, 150.48, 141.09, 140.30, 139.35 (q, $^3J_{\text{CF}} = 3.0$ Hz), 130.87 (q, $^2J_{\text{CF}} = 35.1$ Hz), 129.01, 127.30, 125.50, 121.60 (q, $^1J_{\text{CF}} = 273.5$ Hz), 121.34, 120.42 (q, $^3J_{\text{CF}} = 3.4$ Hz), 111.40.

$^{19}\text{F}\{^1\text{H}\}$ NMR (376 MHz, CDCl_3) δ -63.53.

ESI-MS: $[\text{M}+\text{H}]^+$: $\text{C}_{13}\text{H}_8\text{N}_2\text{O}_2\text{F}_3$ calculated m/z 281.0538, found 265.0550.

^{19}F DOSY Experimental Details

The reactions were run using the general procedure for both the wet and dry reactions described above. A capillary containing acetone- d_6 was used to lock and shim the sample in the NMR instrument.

For speciation tests of the catalyst in MeCN and water an acetone- d_6 capillary was again used to lock and shim sample. For the dry reaction 3.4 mg of 5- CF_3 PBO cationic triflate complex was dissolved in 3.75 mL dry MeCN (dried using 3 Å molecular sieves).

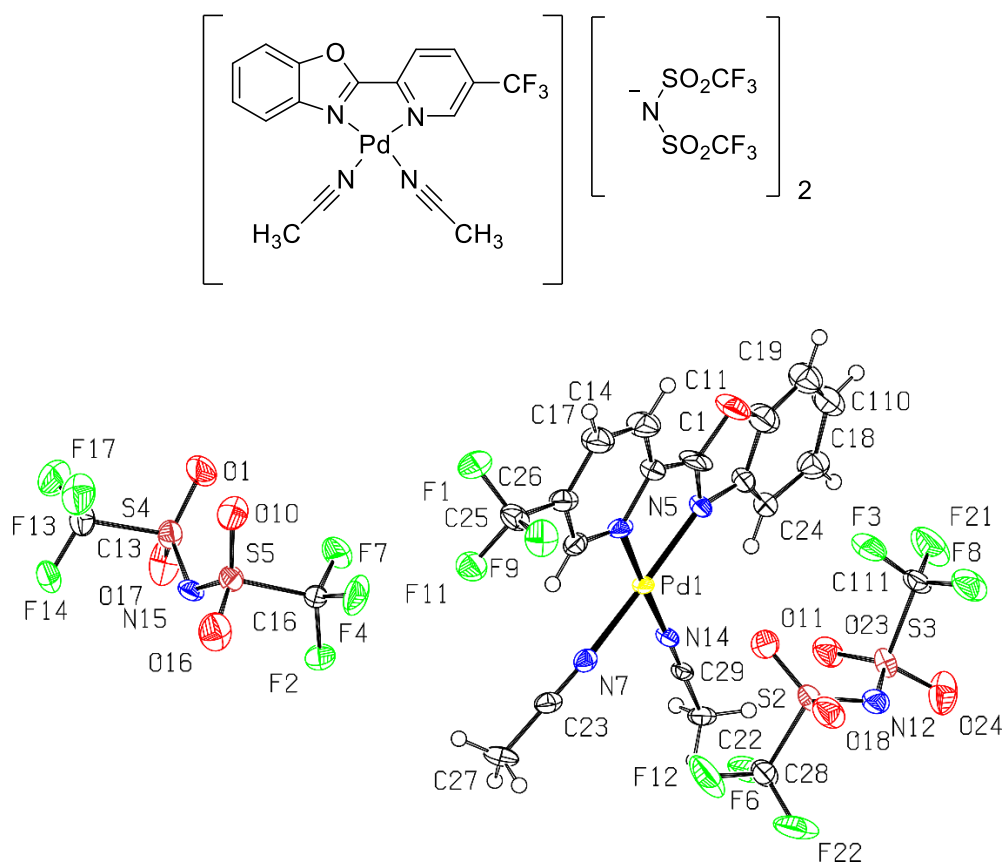
For the water spiked sample 3.4 mg of catalyst was dissolved in 4.29 mL of MeCN and followed by the addition of 0.21 mL of ultra-pure water.

Diffusion constants were measured using the following conditions:

- 8 points were taken using a linear ramp gradient amplitude from 10% to 90%
- Δ (diffusion time) = 0.0599 s
- δ (gradient pulse length) = 0.0020 s
- $\gamma = 4006.24100$ Hz/Gauss
- Peak areas were determined by manual integration of peaks of interest

X-Ray Crystallography

Crystals of $[(2-(5-(\text{trifluoromethyl})\text{pyridin-2-yl})\text{benzo[d]oxazole})\text{Pd}(\text{MeCN})_2][\text{NTf}_2]_2$ were obtained by the vapour diffusion method (vial-in-vial, MeCN & $\text{C}_5\text{F}_5\text{N}$ solvent, Et_2O anti-solvent). Low temperature⁶¹ single crystal X-ray diffraction studies were carried out using MoK_α radiation on an Agilent Supernova diffractometer equipped with an area detector and graphite monochromator. Raw frame data were reduced using CrysAlisPRO⁶² and solved using SHELXT.⁶³ Full-matrix least-squares refinement of the structures were carried out using CRYSTALS.^{64, 65} SIMU and DELU restraints were applied to sections of the benzoxazole to facilitate refinement. Hydrogen atoms were placed geometrically and refined using a riding model. **CCDC 2094910** contains the supplementary crystallographic data for this paper. These data are provided free of charge by The Cambridge Crystallographic Data Centre and copies can be obtained free of charge via www.ccdc.cam.ac.uk/data_request/cif.

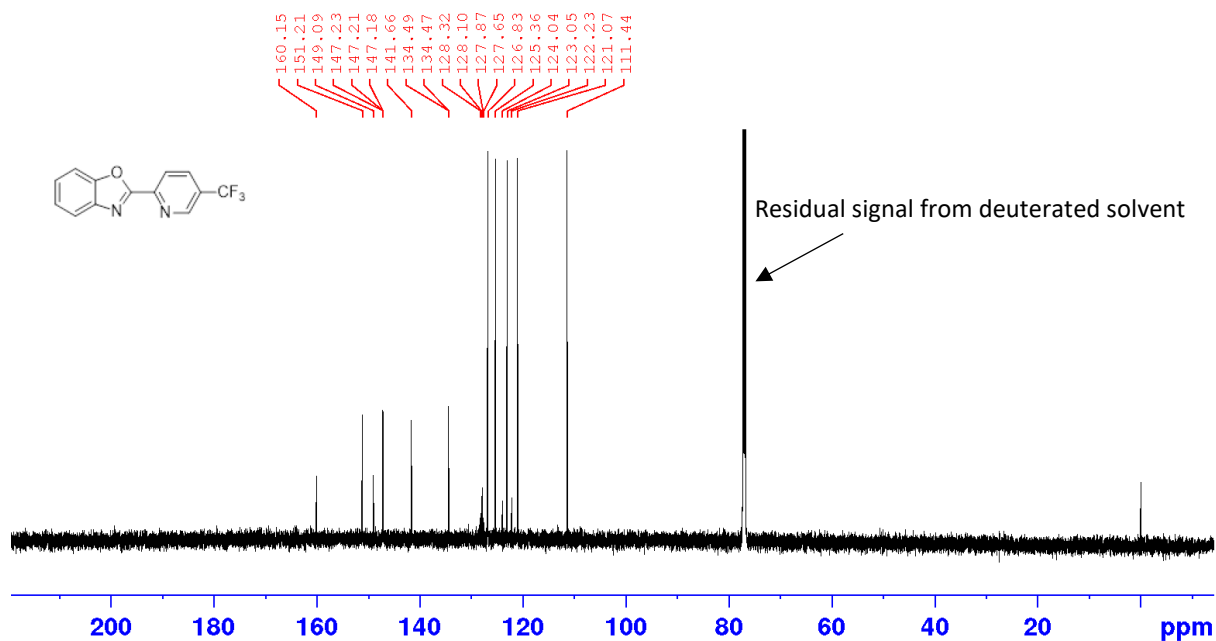
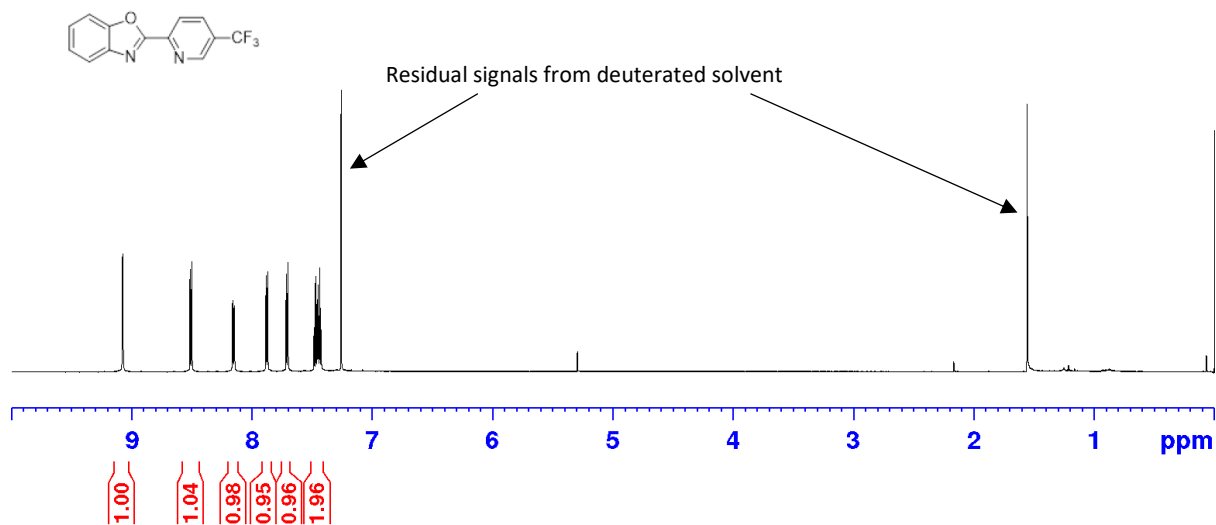


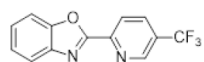
Crystal data

Chemical formula	C ₁₇ H ₁₃ F ₃ N ₄ OPd·2(C ₂ F ₆ NO ₄ S ₂)
<i>M</i> _r	1013.01
Crystal system, space group	Monoclinic, <i>Ia</i>
Temperature (K)	100
<i>a</i> , <i>b</i> , <i>c</i> (Å)	14.056499 (14), 14.319201 (14), 17.205900 (17)
β (°)	95.848 (3)
<i>V</i> (Å ³)	3445.14 (2)
<i>Z</i>	4
Radiation type	Mo <i>K</i> α
μ (mm ⁻¹)	0.92
Crystal size (mm)	0.30 × 0.20 × 0.20
Data collection	
Diffractometer	Oxford Diffraction SuperNova
Absorption correction	Multi-scan <i>CrysAlis PRO</i> ⁶²
<i>T</i> _{min} , <i>T</i> _{max}	0.72, 0.83
No. of measured, independent and observed [<i>I</i> > 2.0σ(<i>I</i>)] reflections	67479, 8852, 8549
<i>R</i> _{int}	0.000
(sin θ/λ) _{max} (Å ⁻¹)	0.693
Refinement	
<i>R</i> [<i>F</i> ² > 2σ(<i>F</i> ²)], <i>wR</i> (<i>F</i> ²), <i>S</i>	0.054, 0.132, 1.02
No. of reflections	8852
No. of parameters	505
No. of restraints	114
H-atom treatment	H-atom parameters constrained Method = Modified Sheldrick <i>w</i> = 1/[σ ² (<i>F</i> ²) + (0.05 <i>P</i>) ² + 34.38 <i>P</i>], where <i>P</i> = (max(<i>F</i> _o ² , 0) + 2 <i>F</i> _c ²)/3
Δρ _{max} , Δρ _{min} (e Å ⁻³)	2.68, -2.22
Absolute structure	Parsons, Flack & Wagner, ⁶⁶ 4157 Friedel Pairs
Absolute structure parameter	0.074 (7)

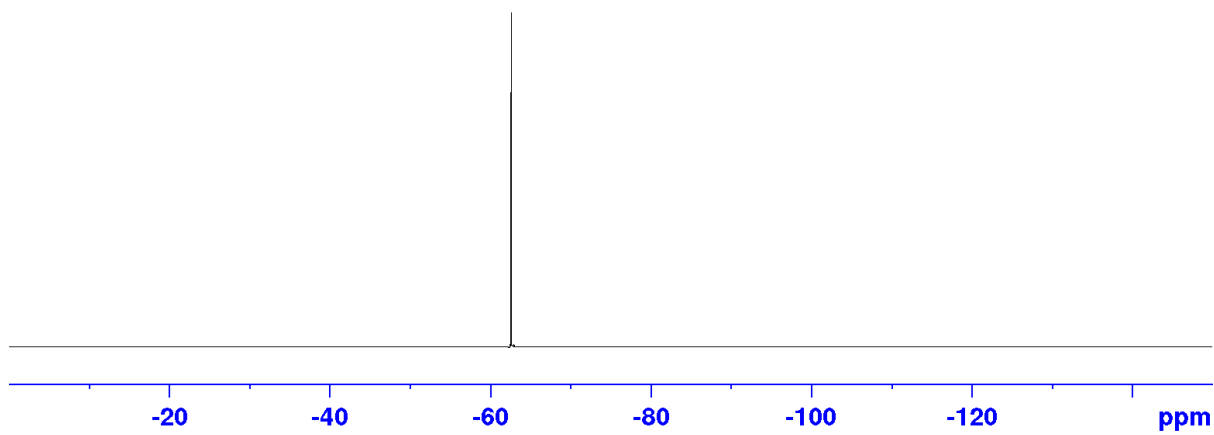
NMR Spectra

2-(5-(trifluoromethyl)pyridin-2-yl)benzo[d]oxazole: ^1H NMR (600 MHz), ^{13}C NMR (151 MHz) and ^{19}F NMR (376 MHz) in CDCl_3

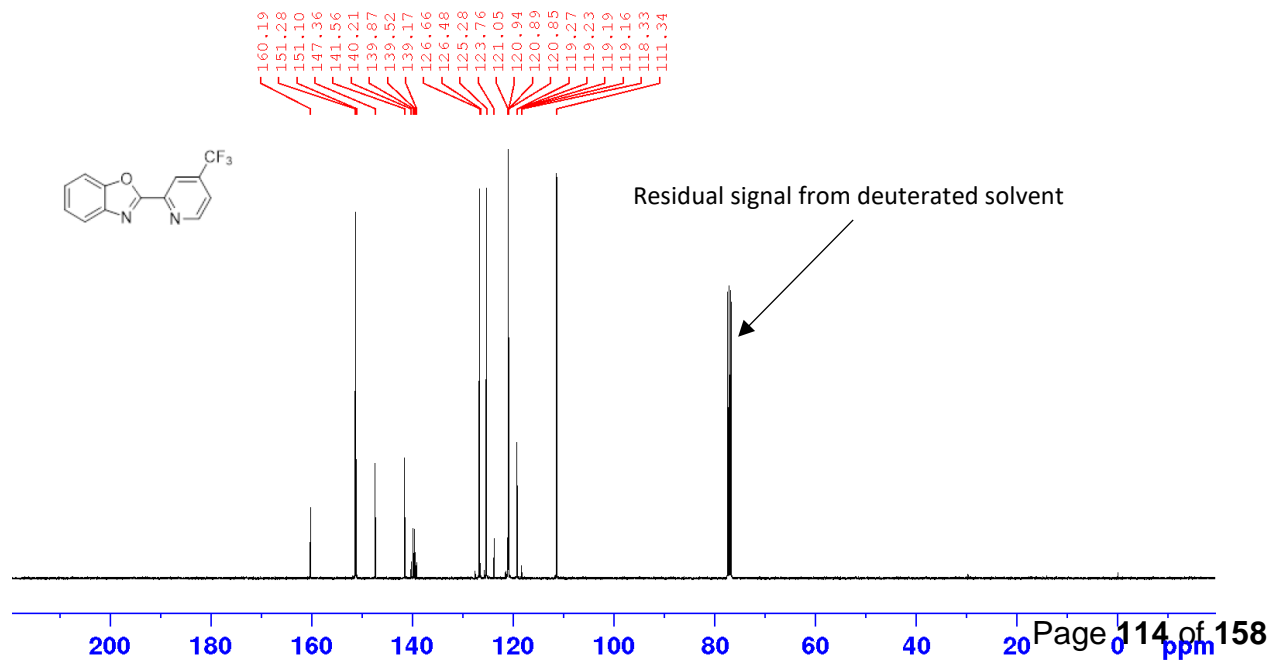
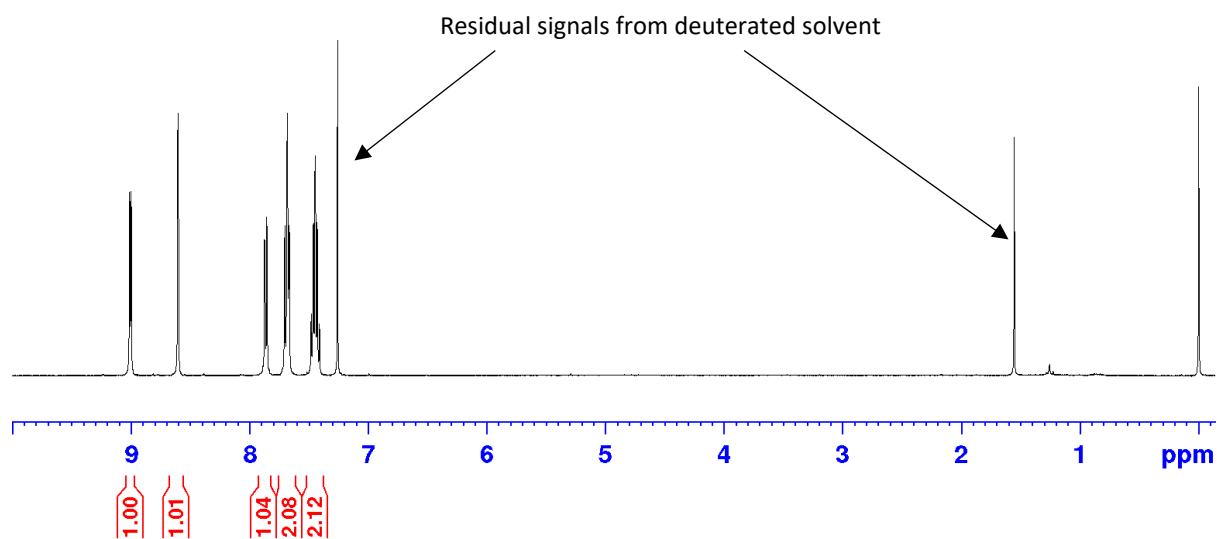
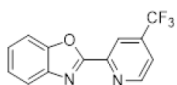


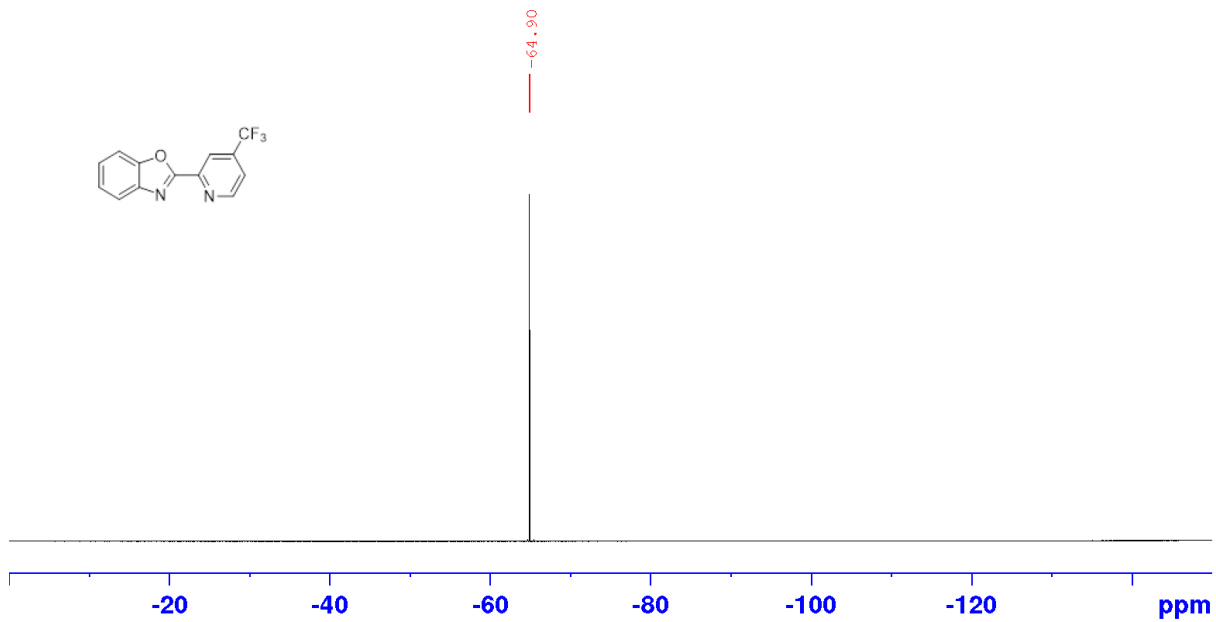
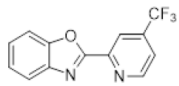


-62.57

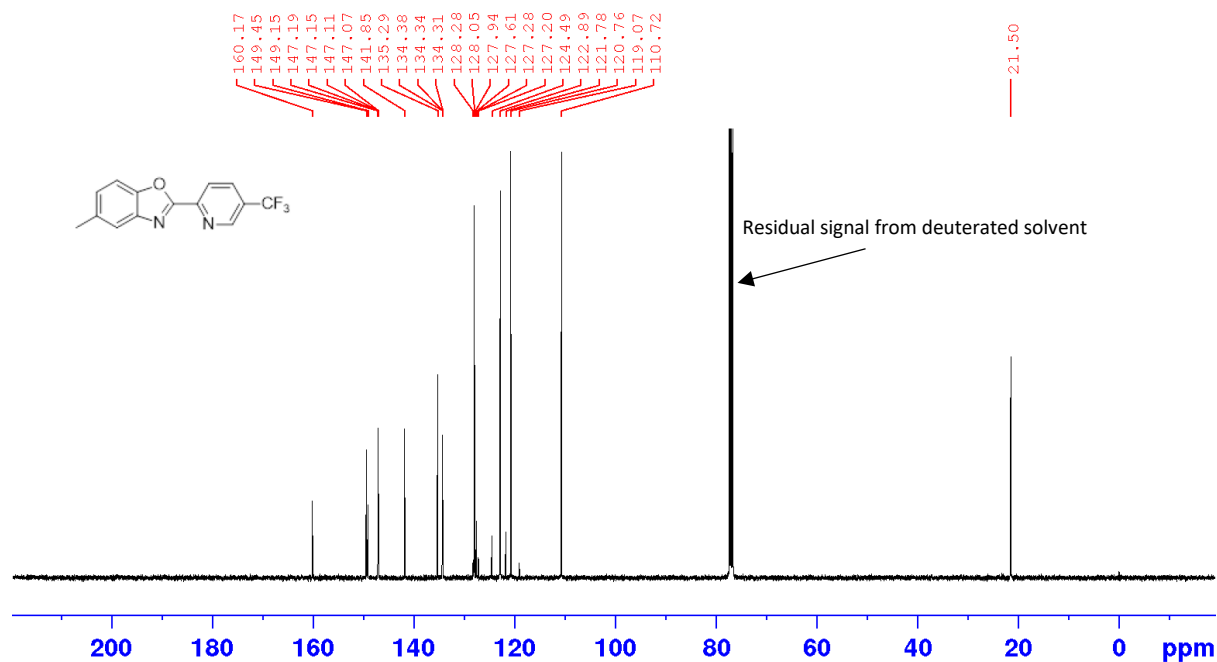
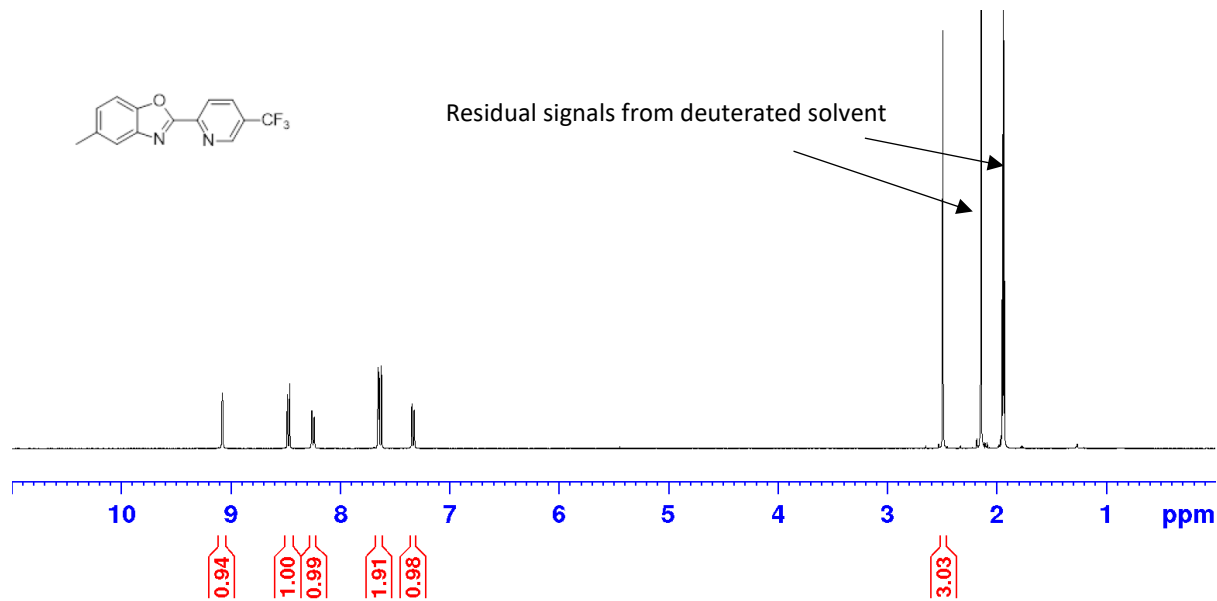


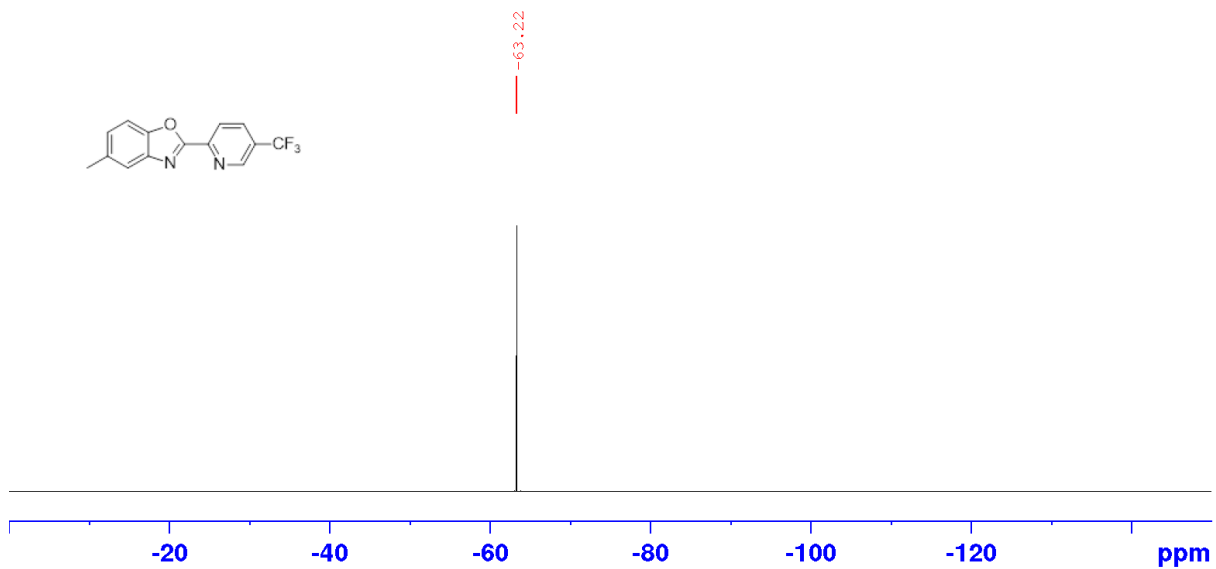
2-(4-(trifluoromethyl)pyridin-2-yl)benzo[d]oxazole: ^1H NMR (400 MHz), ^{13}C NMR (101 MHz) and ^{19}F NMR (376 MHz) in CDCl_3



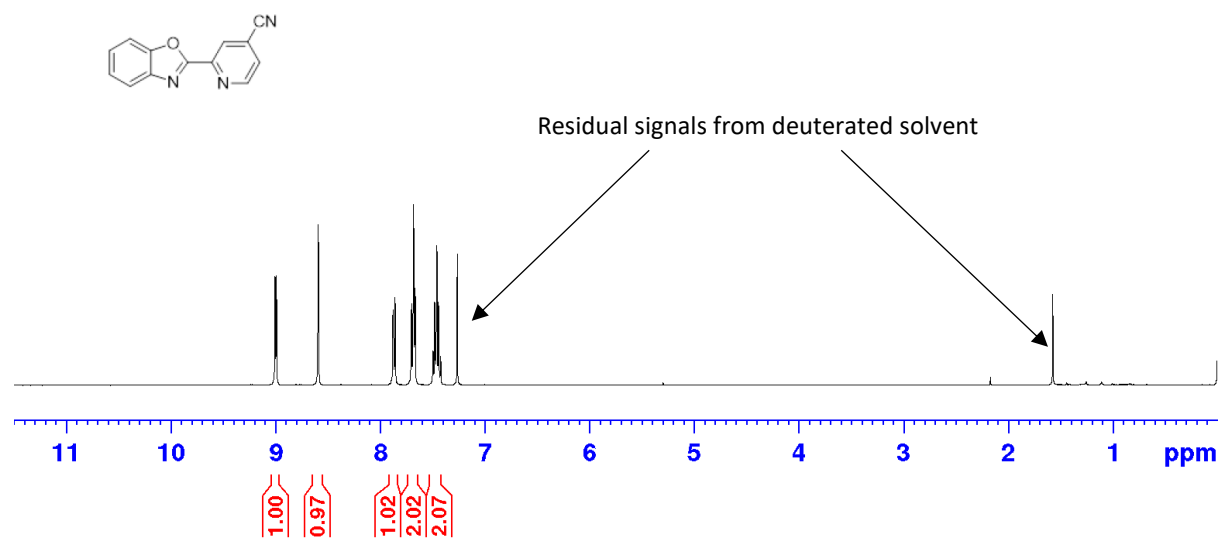


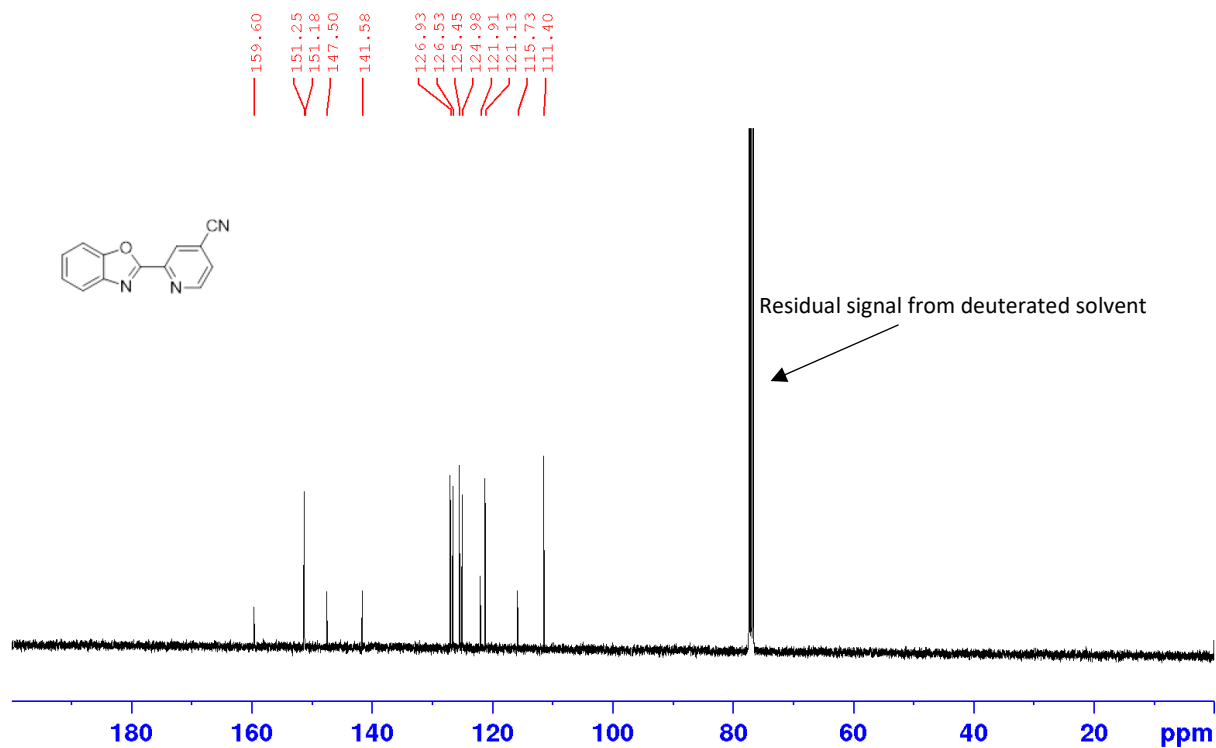
2-(5-Trifluoromethylpyridin-2-yl)-5-methylbenzo[d]oxazole: ^1H NMR (400 MHz), ^{13}C NMR (101 MHz) [in CDCl_3] and ^{19}F NMR (376 MHz) in CD_3CN



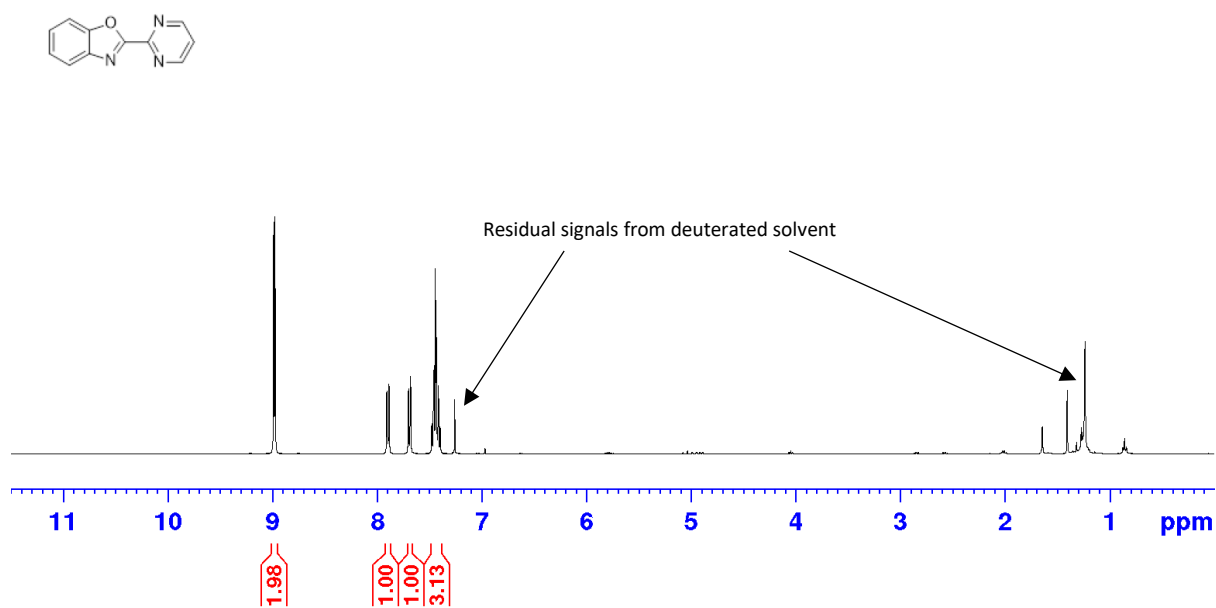


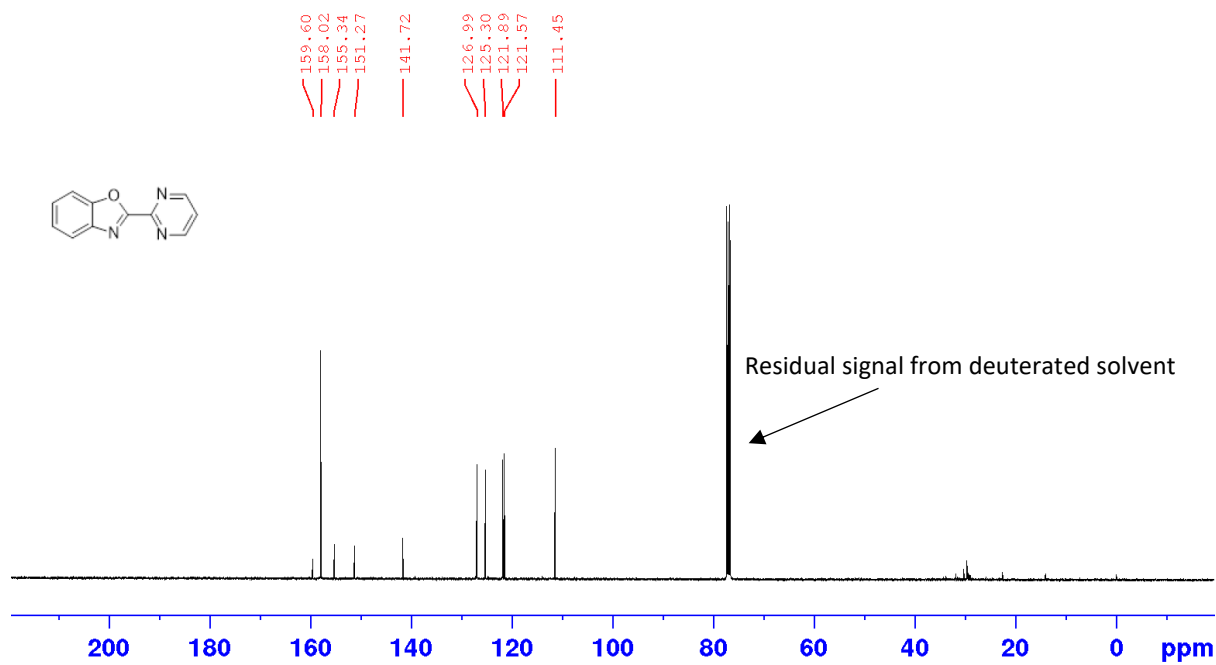
2-(benzo[d]oxazol-2-yl)isonicotinonitrile: ^1H NMR (400 MHz) and ^{13}C NMR (101 MHz) in CDCl_3



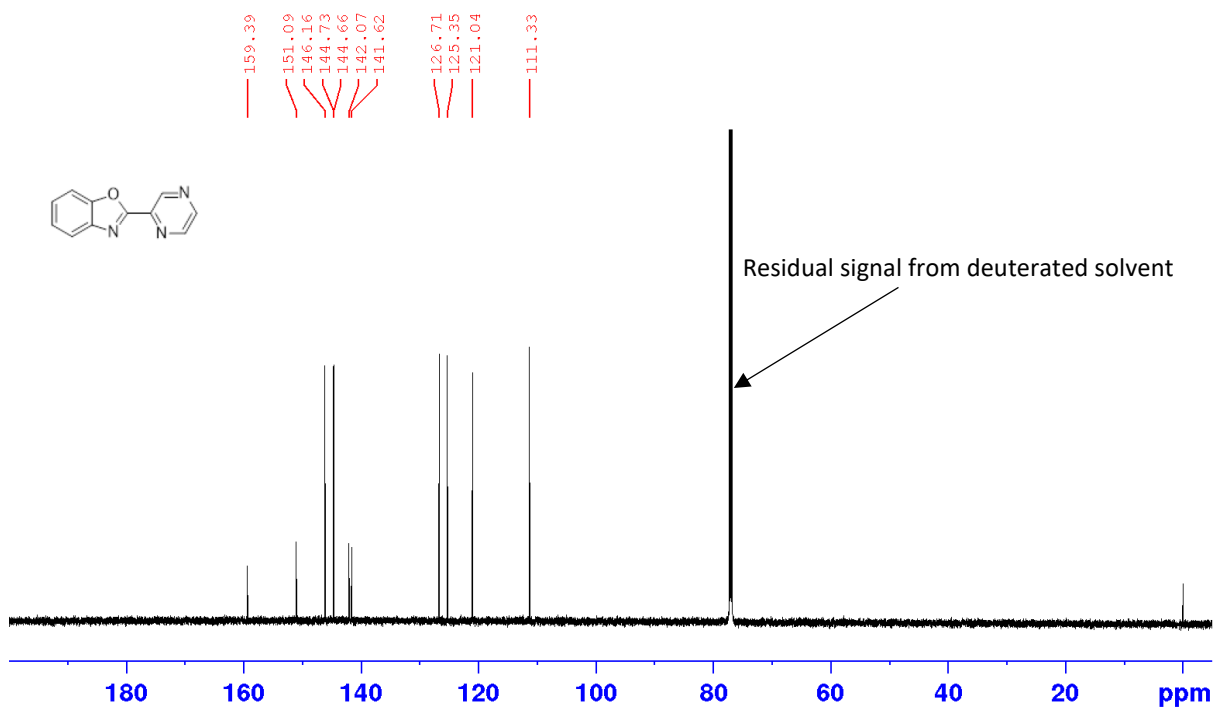
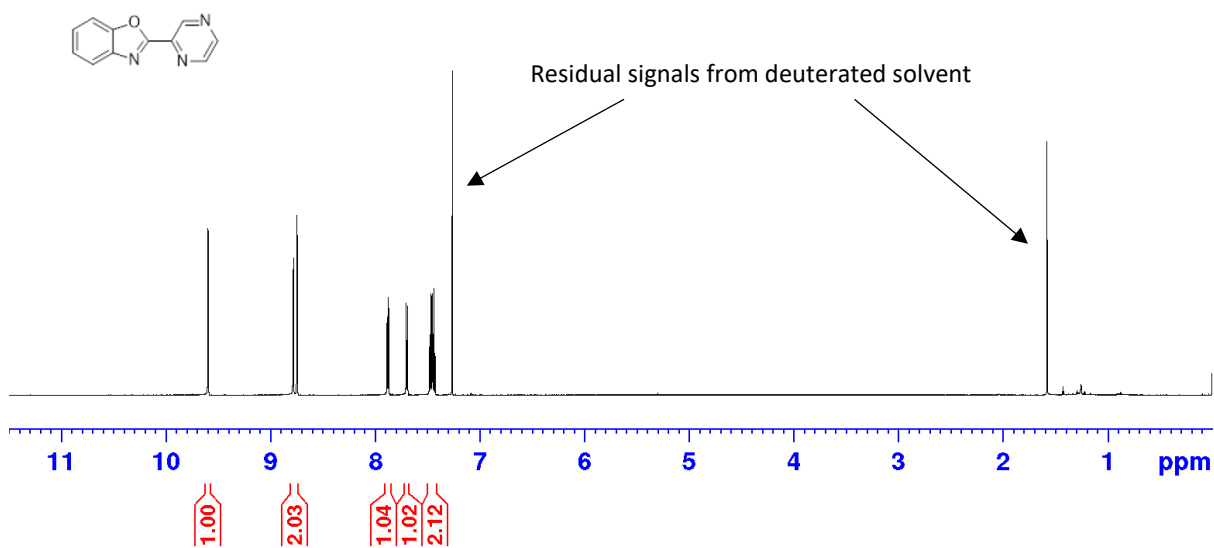


2-(pyrimidin-2-yl)benzo[d]oxazole: ¹H NMR (400 MHz) and ¹³C NMR (101 MHz) in CDCl₃

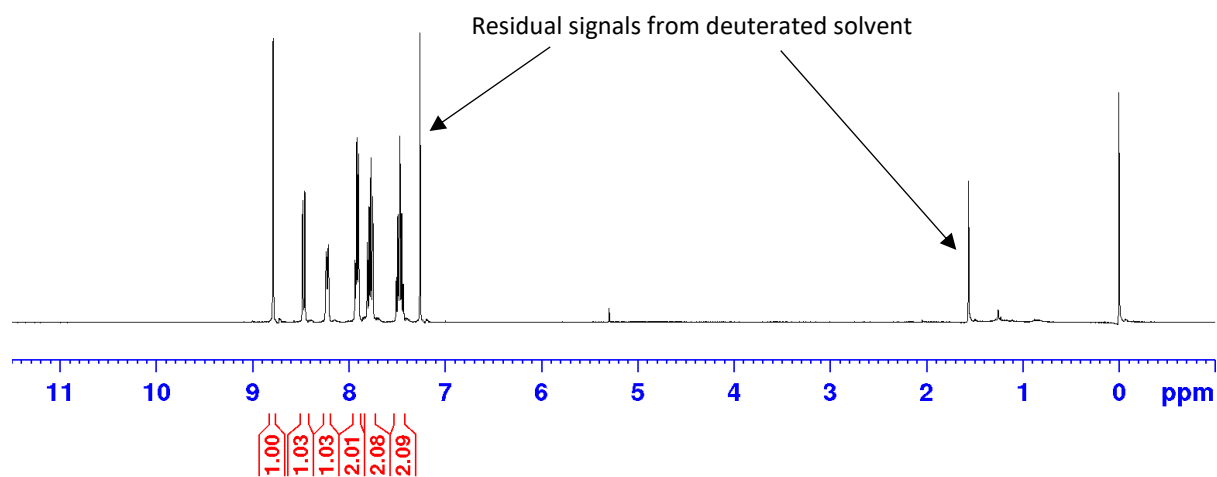
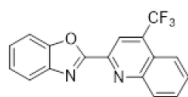


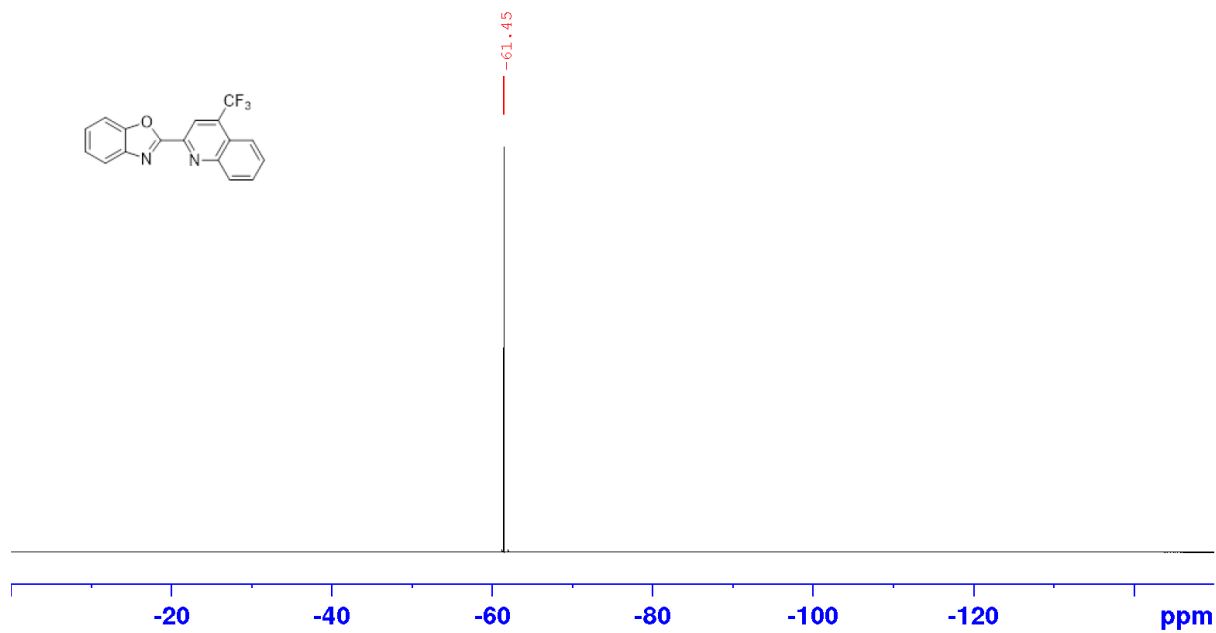
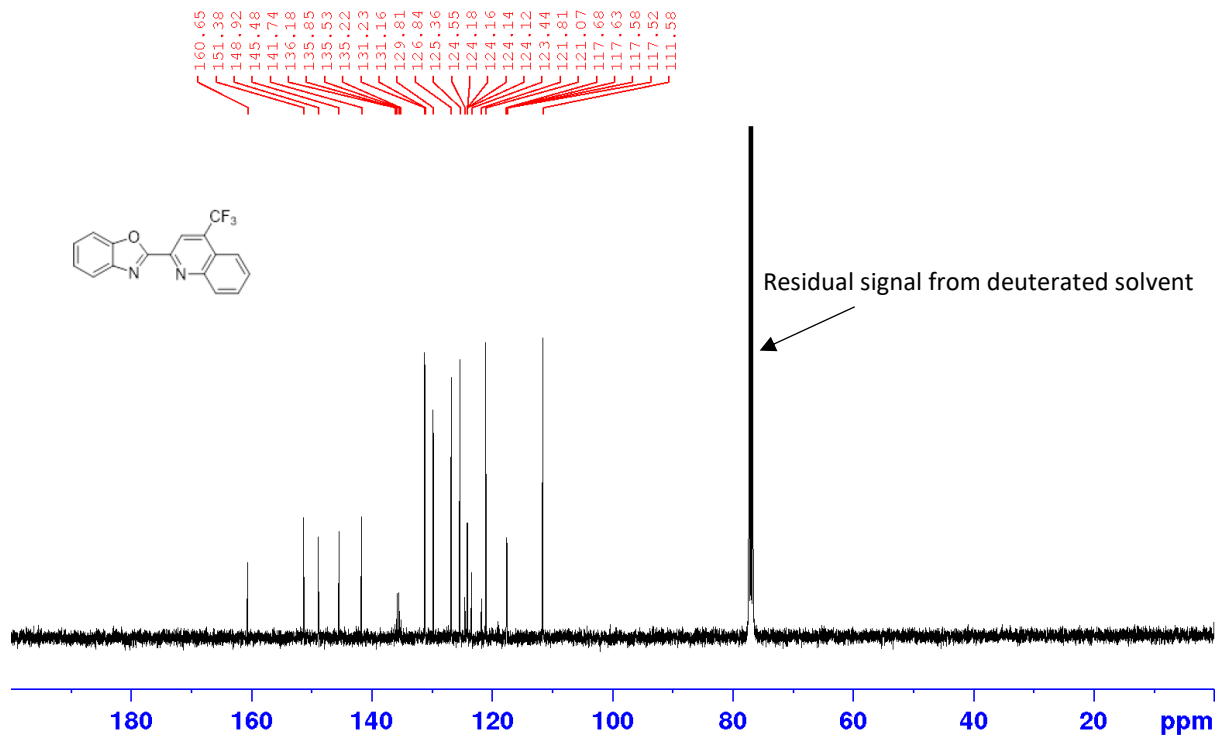


2-(pyrazin-2-yl)benzo[d]oxazole: ^1H NMR (400 MHz) and ^{13}C NMR (101 MHz) in CDCl_3

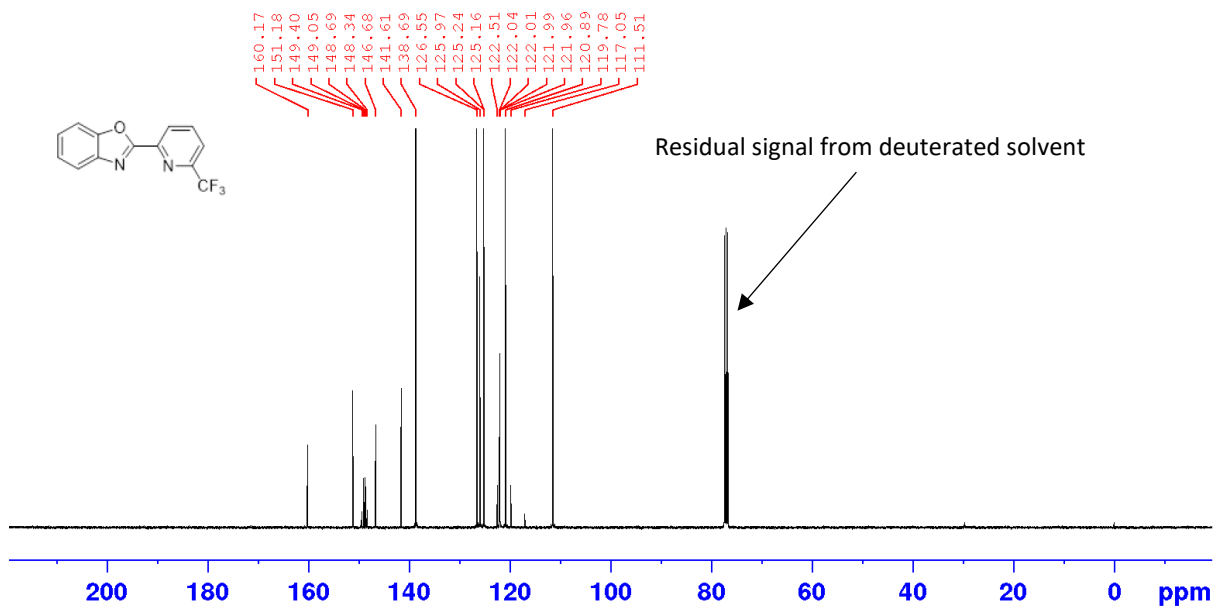
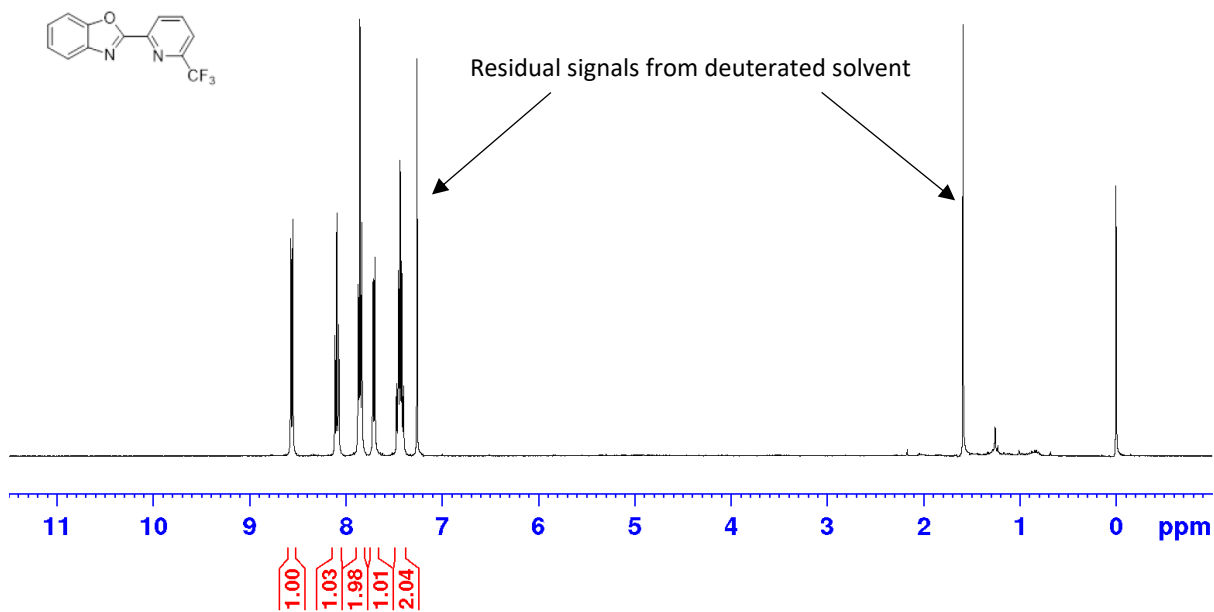


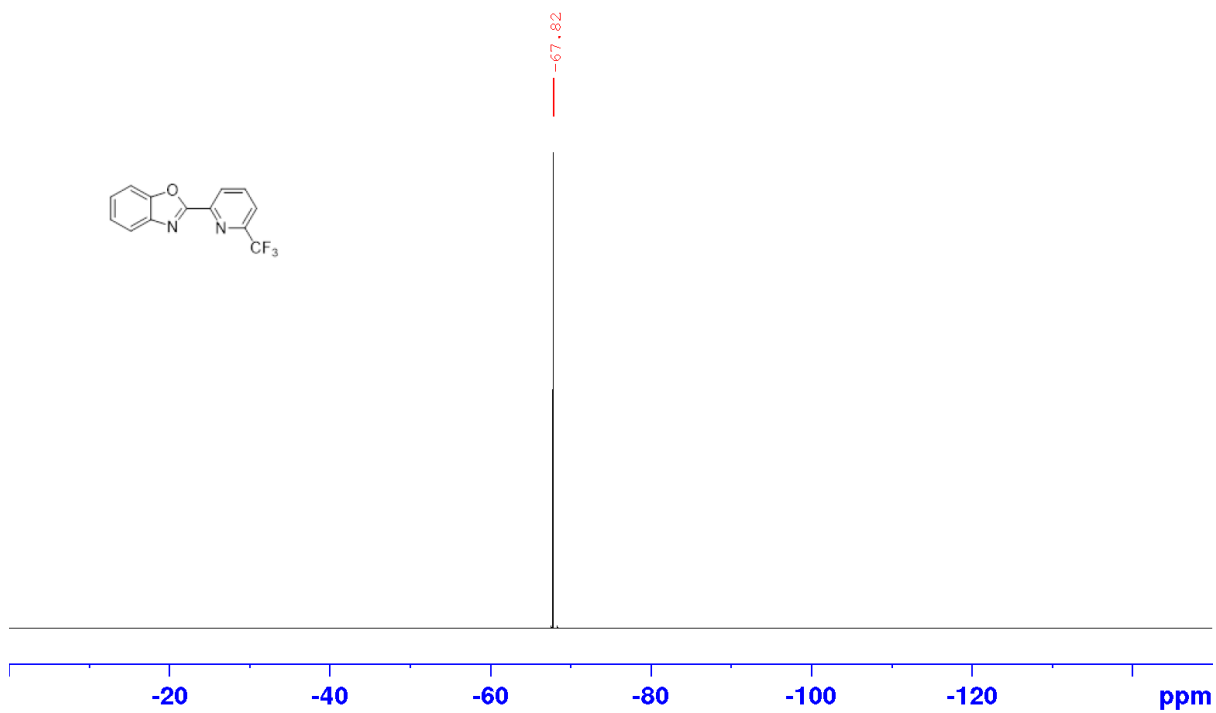
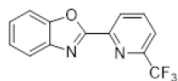
2-(4-(trifluoromethyl)quinolin-2-yl)benzo[d]oxazole: ^1H NMR (400 MHz), ^{13}C NMR (101 MHz) and ^{19}F NMR (376 MHz) in CDCl_3



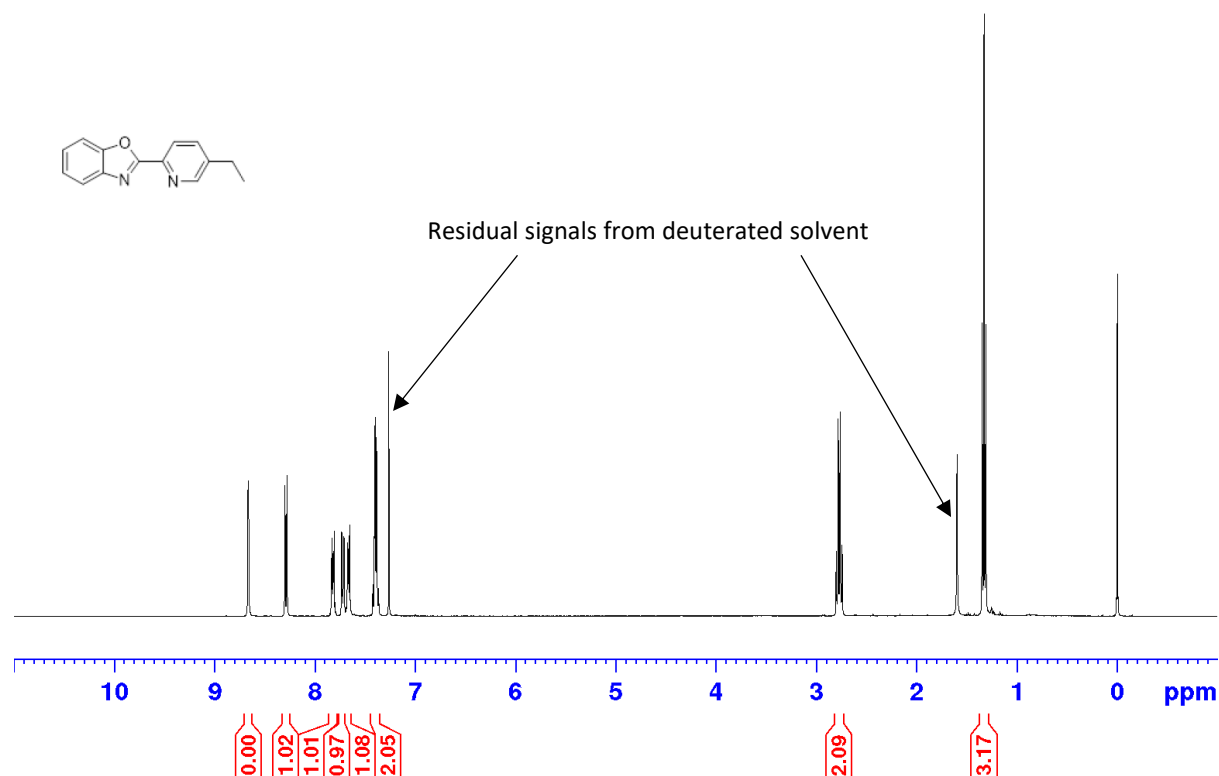


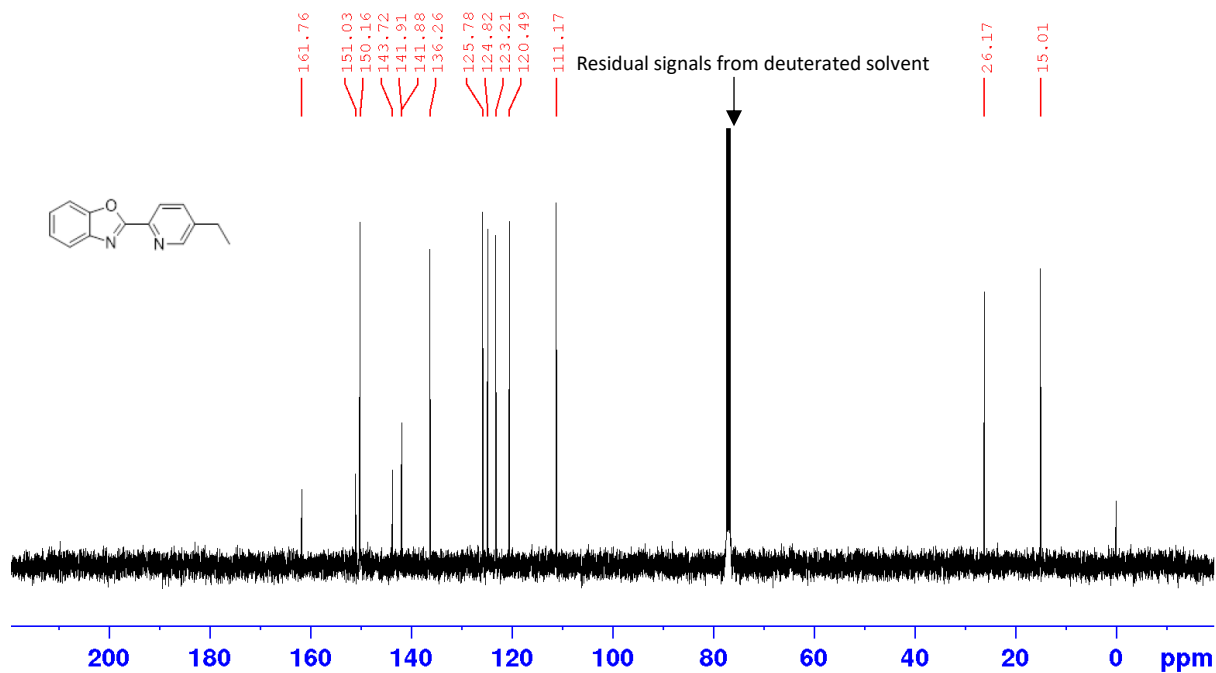
2-(6-(trifluoromethyl)pyridin-2-yl)benzo[d]oxazole: ^1H NMR (400 MHz), ^{13}C NMR (101 MHz) and ^{19}F NMR (376 MHz) in CDCl_3



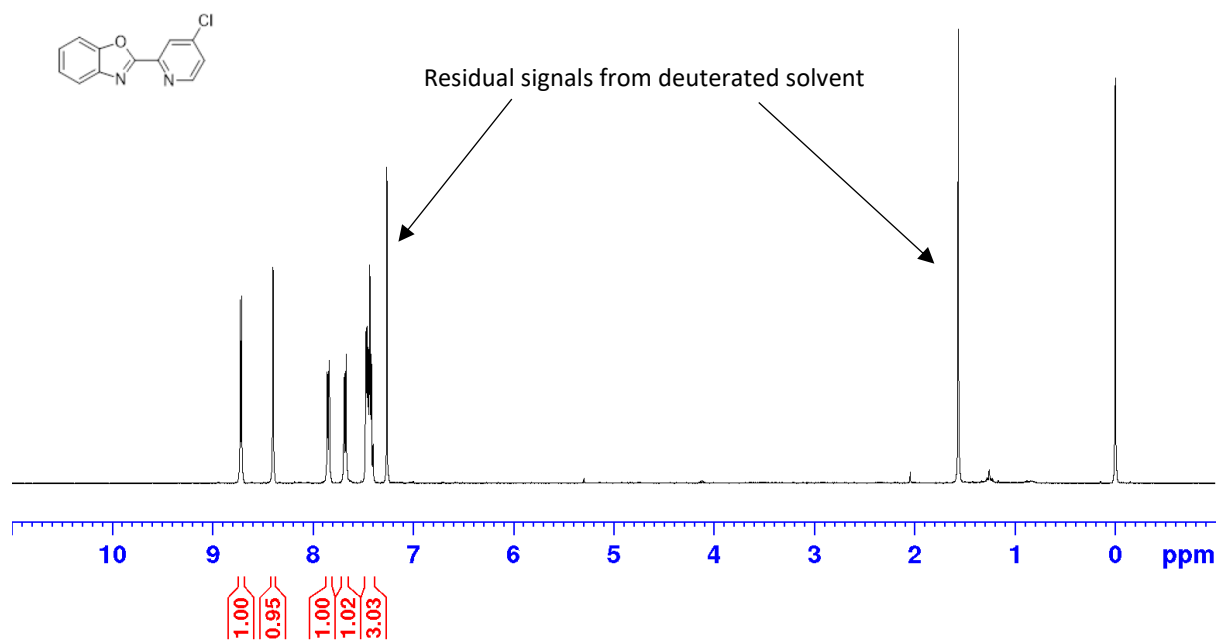


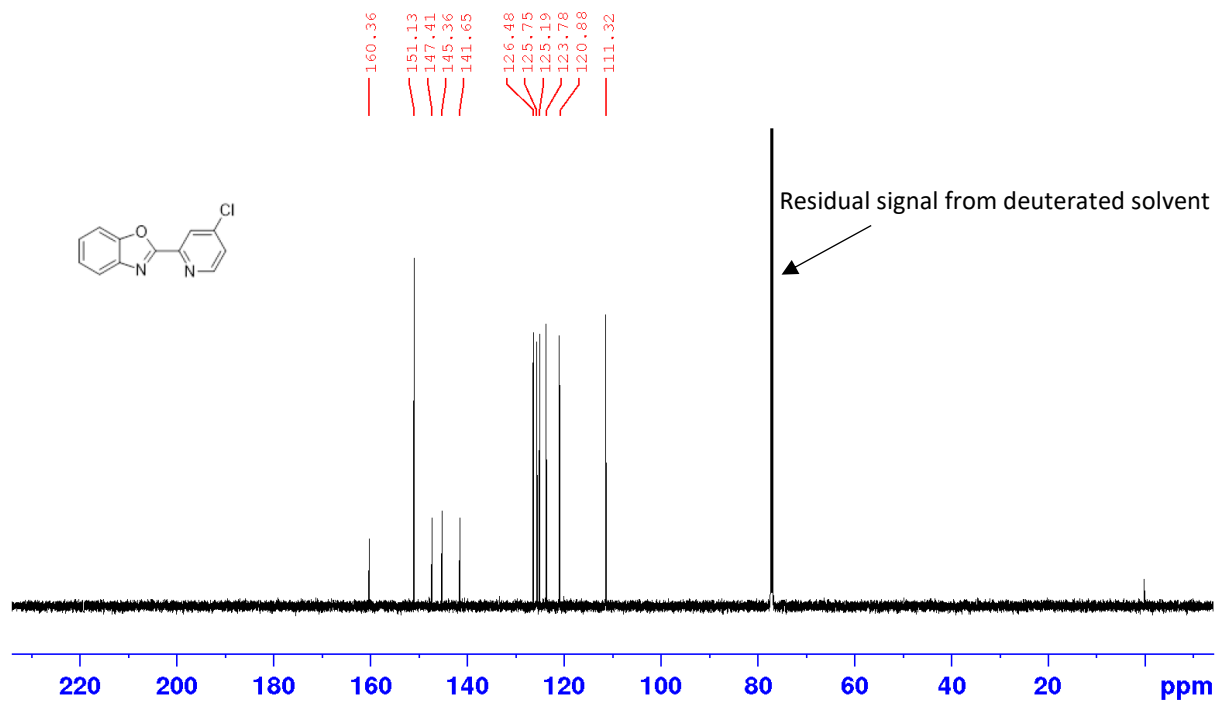
2-(5-ethylpyridin-2-yl)benzo[d]oxazole: ^1H NMR (400 MHz) and ^{13}C NMR (101 MHz) in CDCl_3



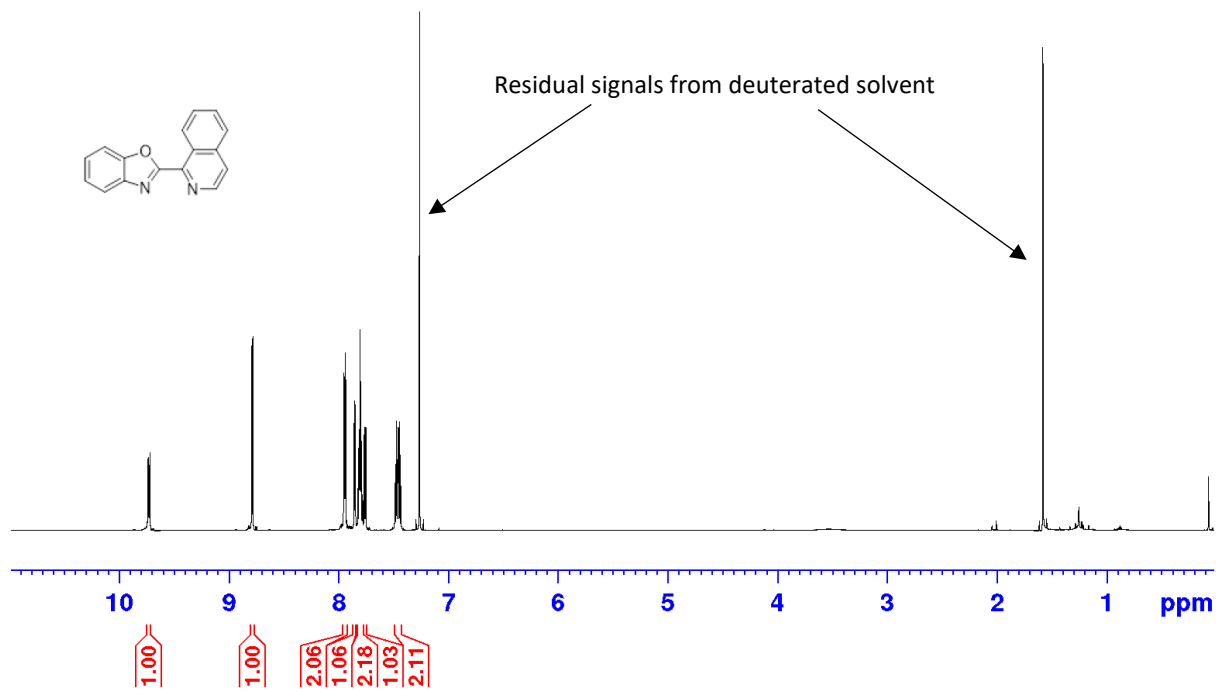


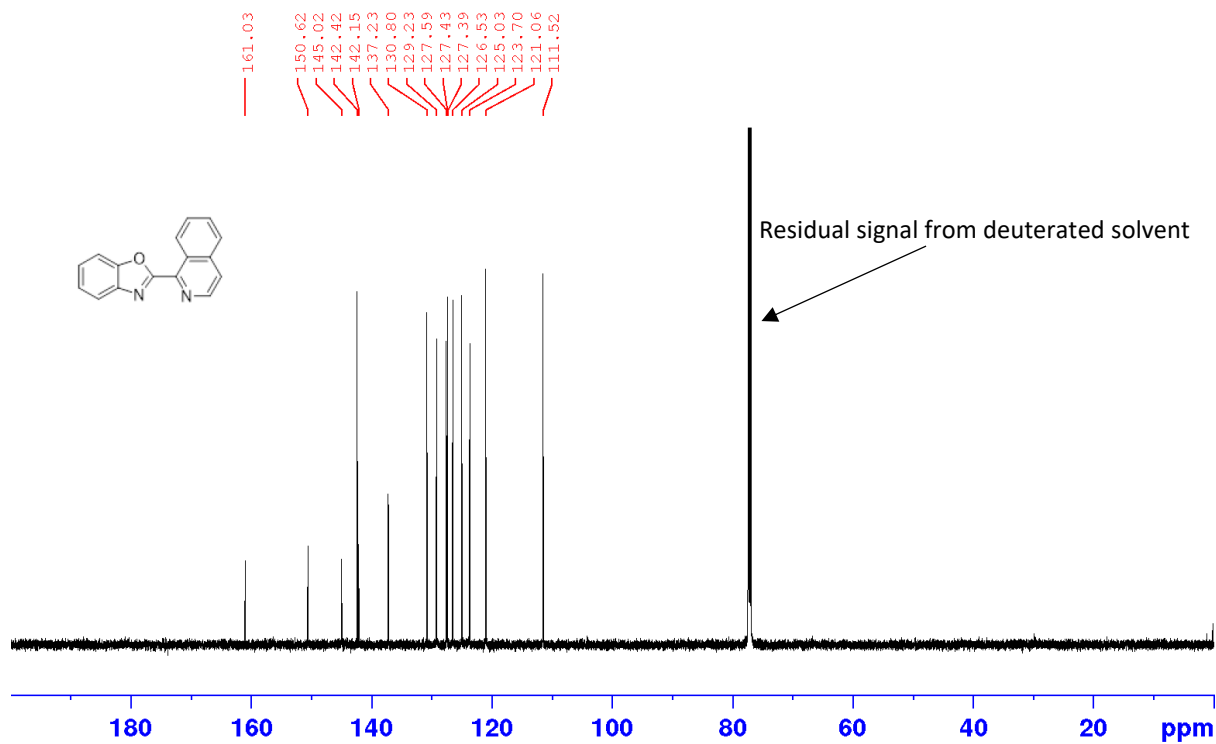
2-(4-chloropyridin-2-yl)benzo[d]oxazole: ^1H NMR (400 MHz) and ^{13}C NMR (101 MHz) in CDCl_3



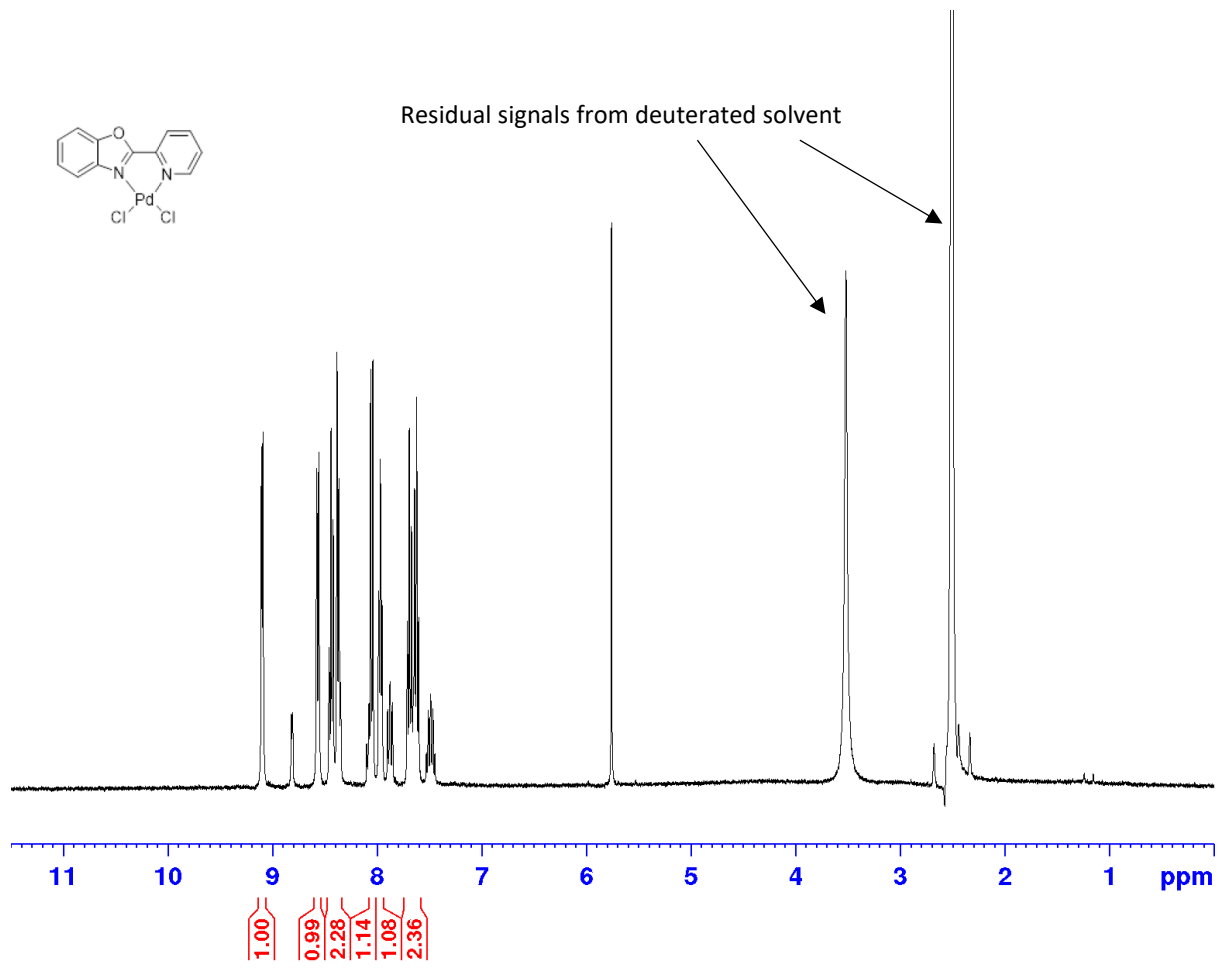


2-(isoquinolin-1-yl)benzo[d]oxazole: ¹H NMR (600 MHz) and ¹³C NMR (150 MHz) in CDCl₃

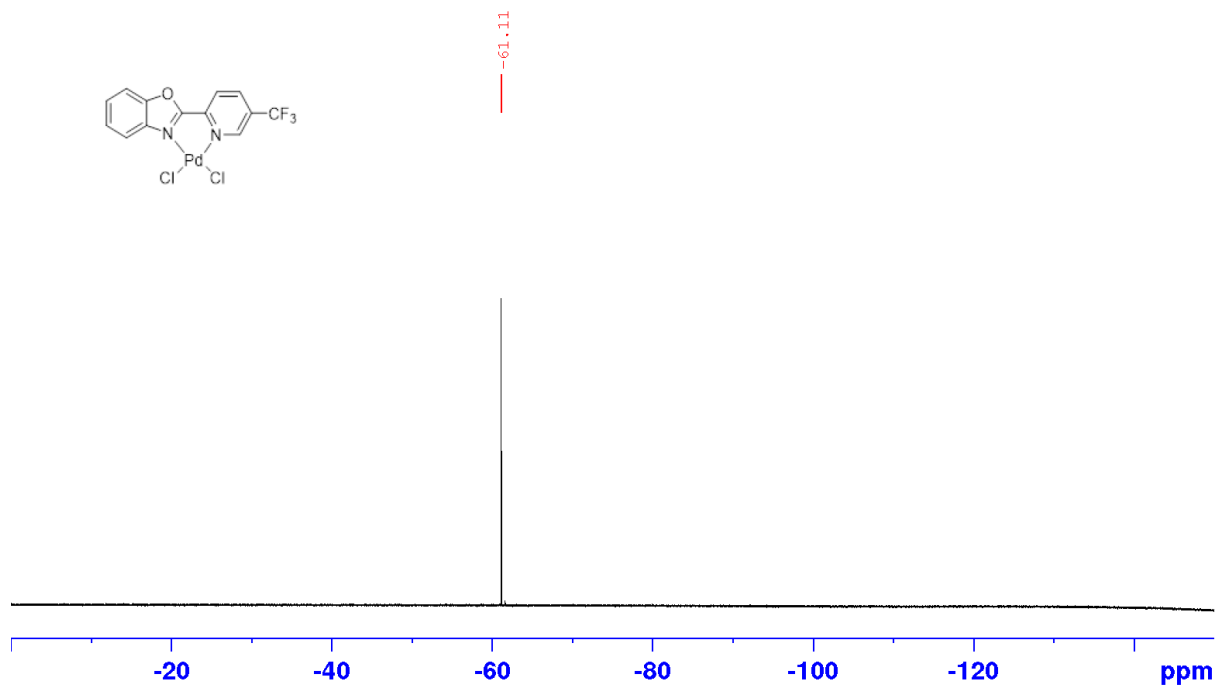
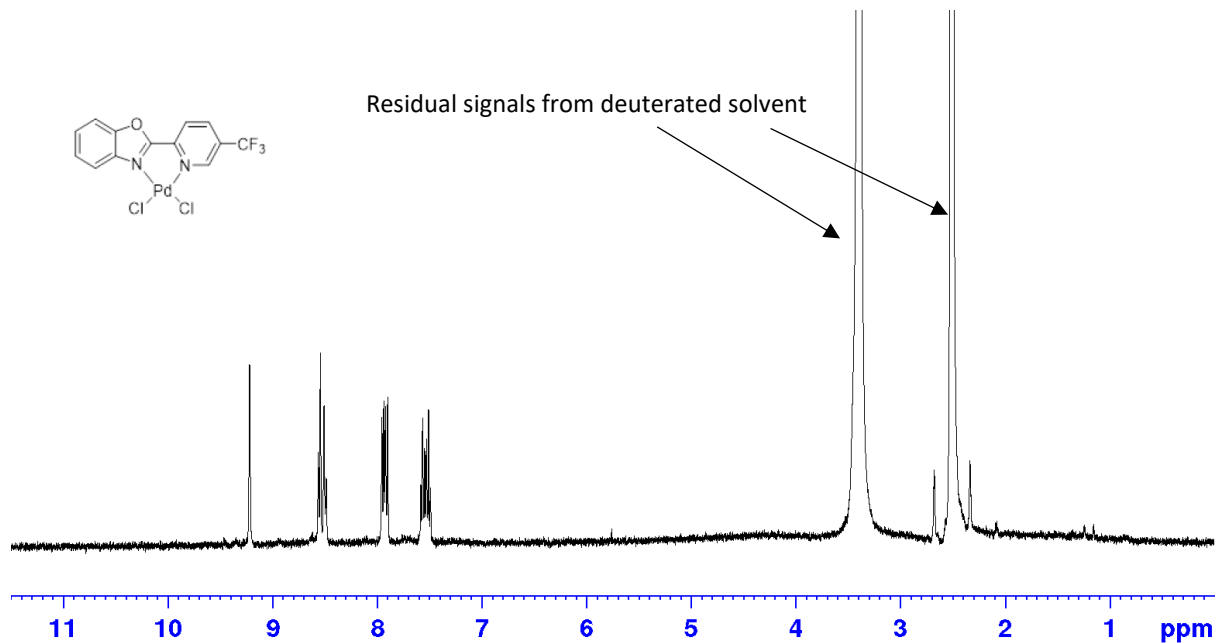




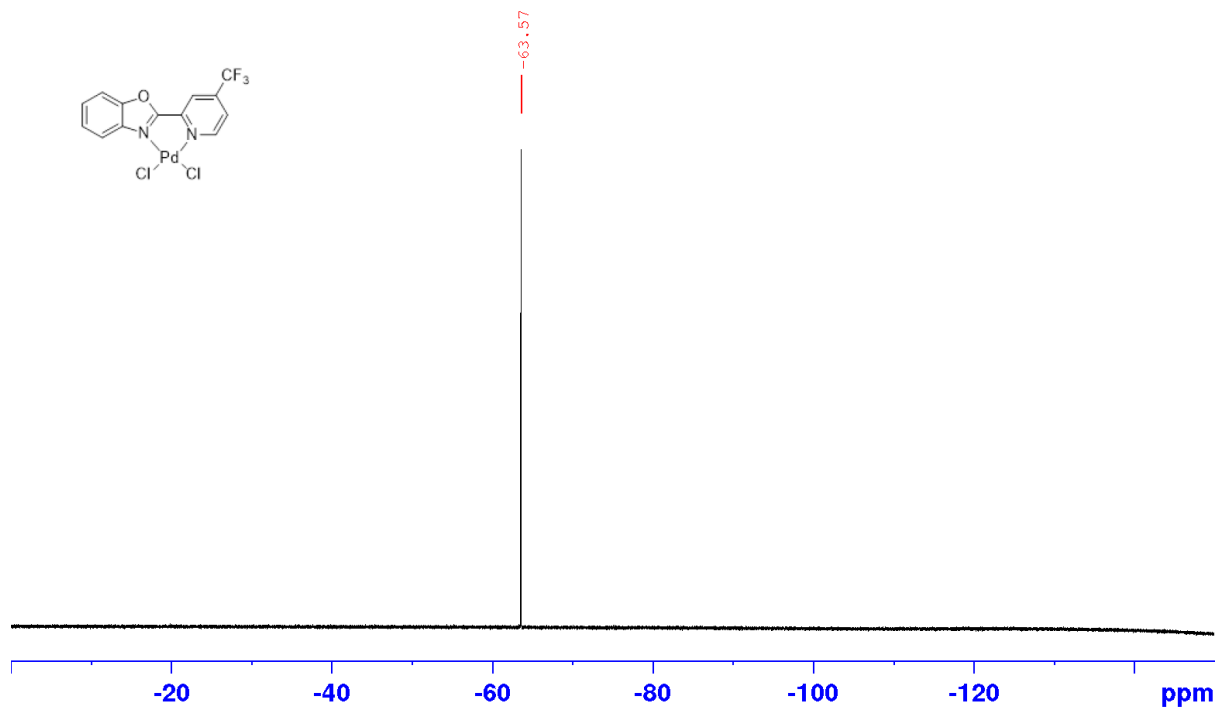
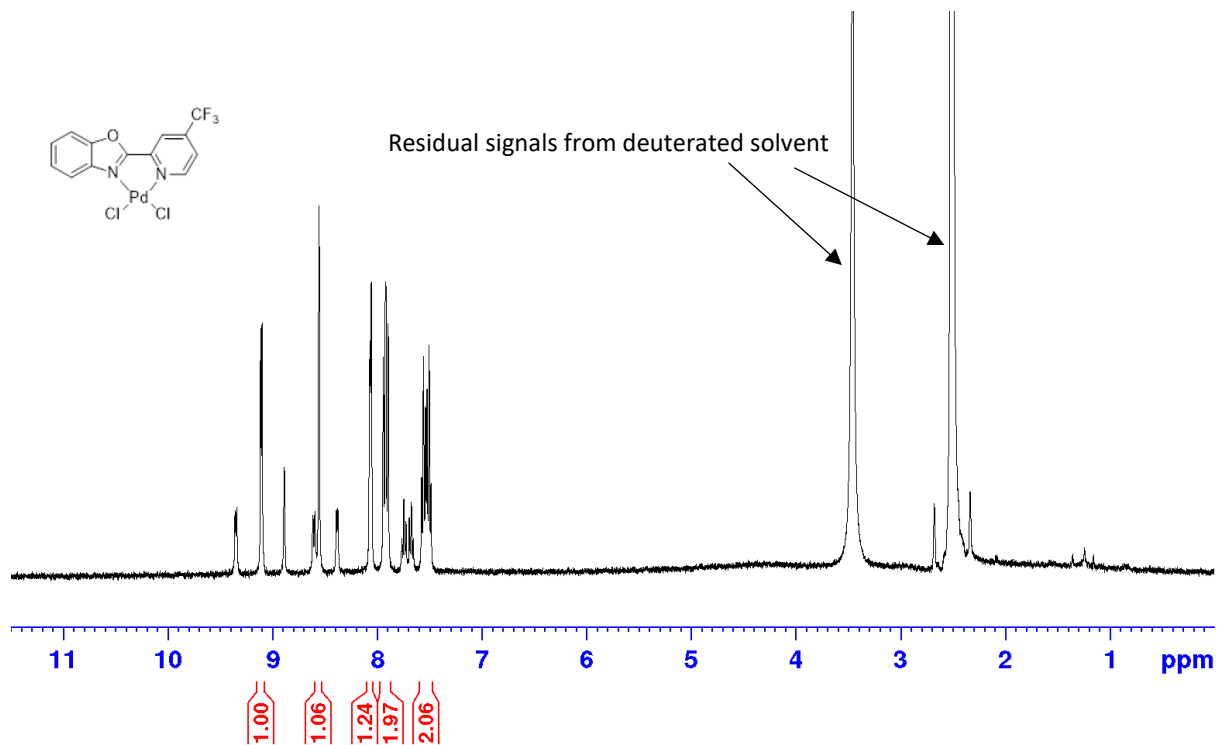
(2-(pyridin-2-yl)benzo[d]oxazole)PdCl₂: ¹H NMR (400 MHz) in DMSO-d₆



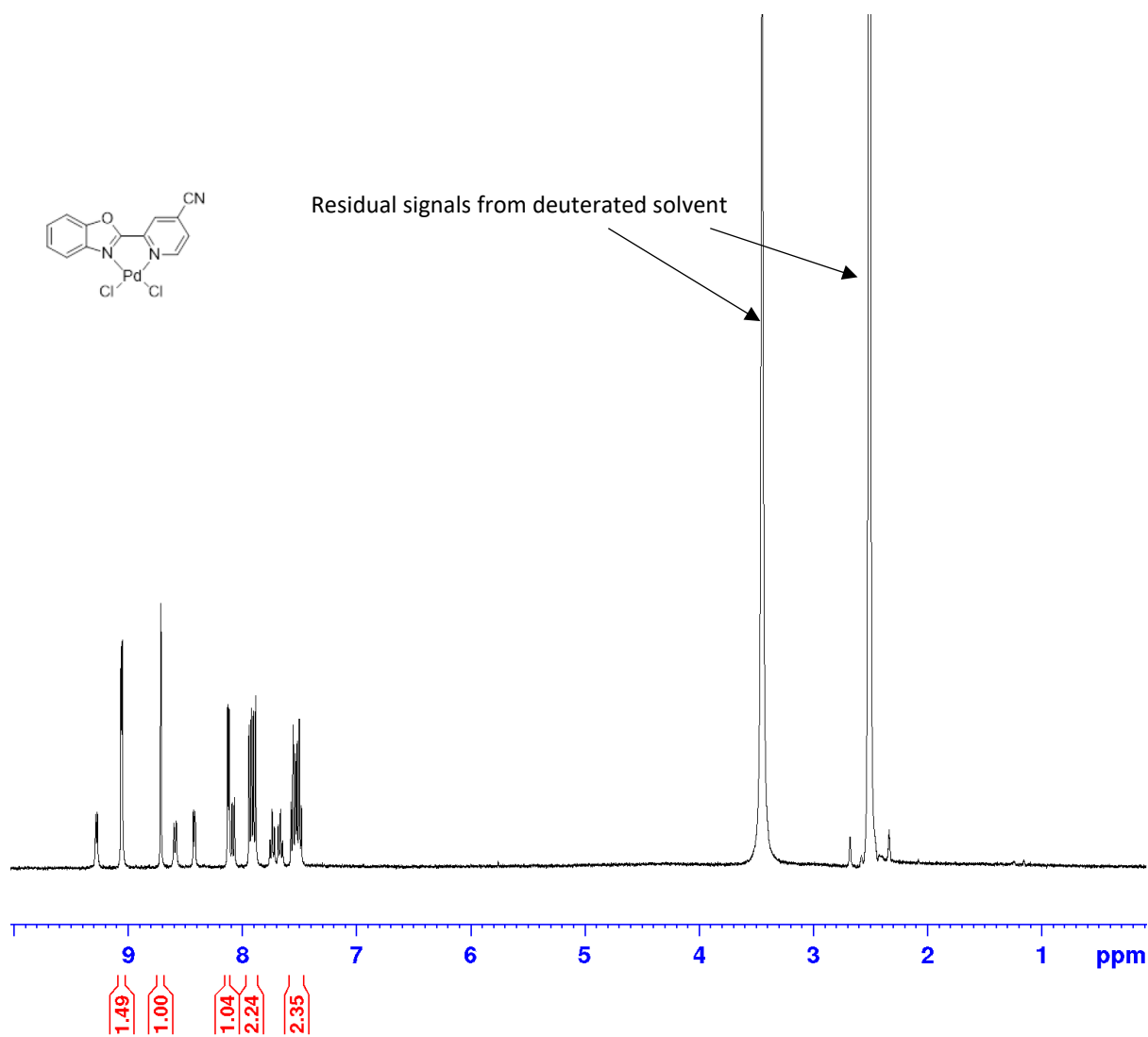
(2-(5-(trifluoromethyl)pyridin-2-yl)benzo[d]oxazole)PdCl₂: ¹H NMR (400 MHz) and ¹⁹F NMR (376 MHz) in DMSO-d₆



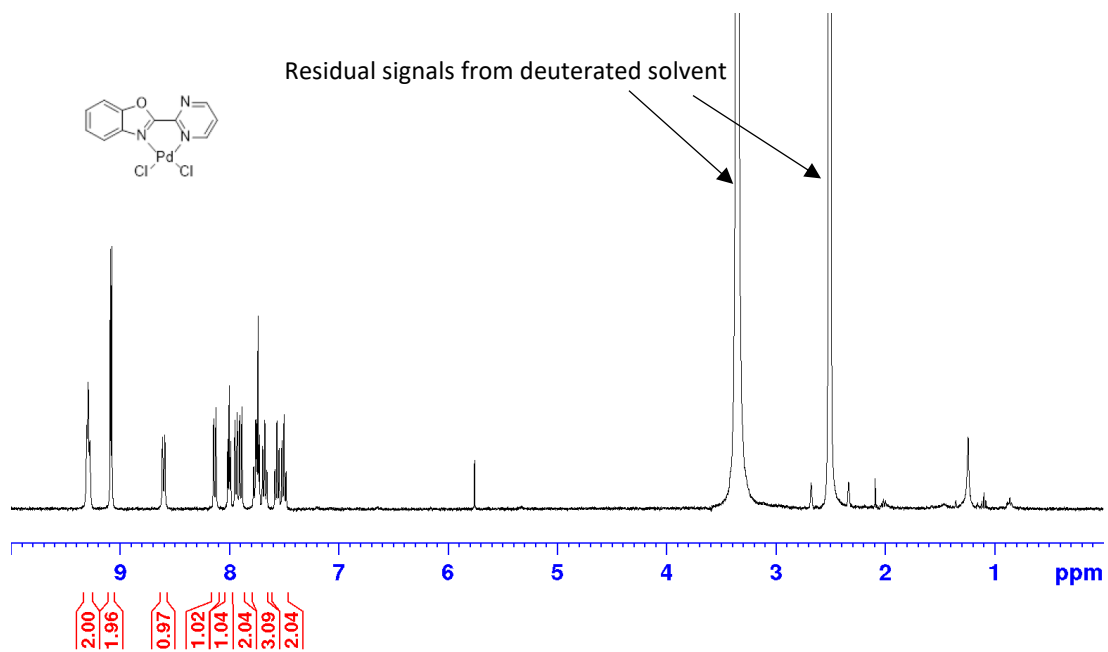
(2-(4-(trifluoromethyl)pyridin-2-yl)benzo[d]oxazole)PdCl₂: ¹H NMR (400 MHz) and ¹⁹F NMR (376 MHz) in DMSO-d₆



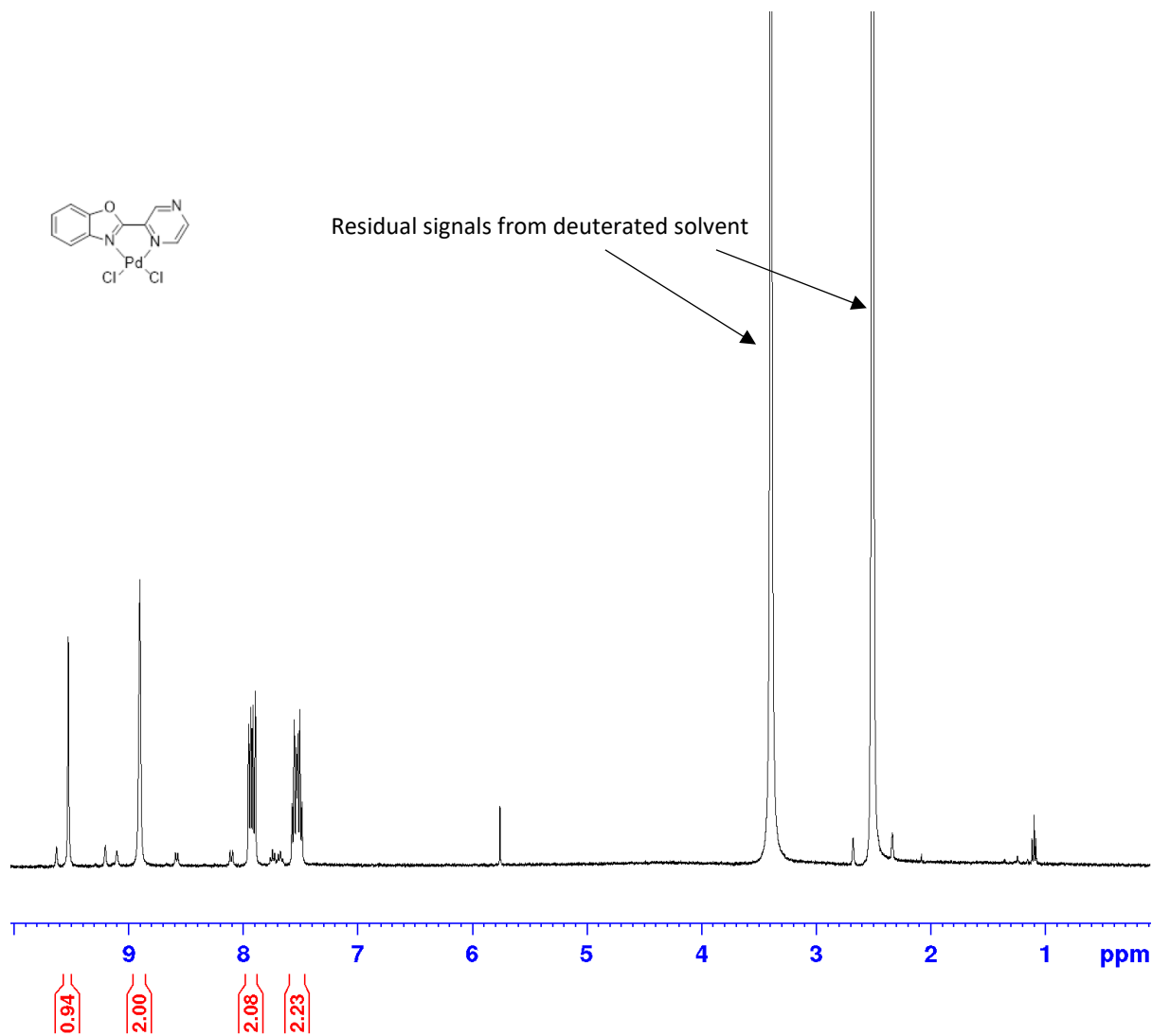
(2-(benzo[d]oxazol-2-yl)isonicotinonitrile)PdCl₂: ¹H NMR (400 MHz) in DMSO-d₆



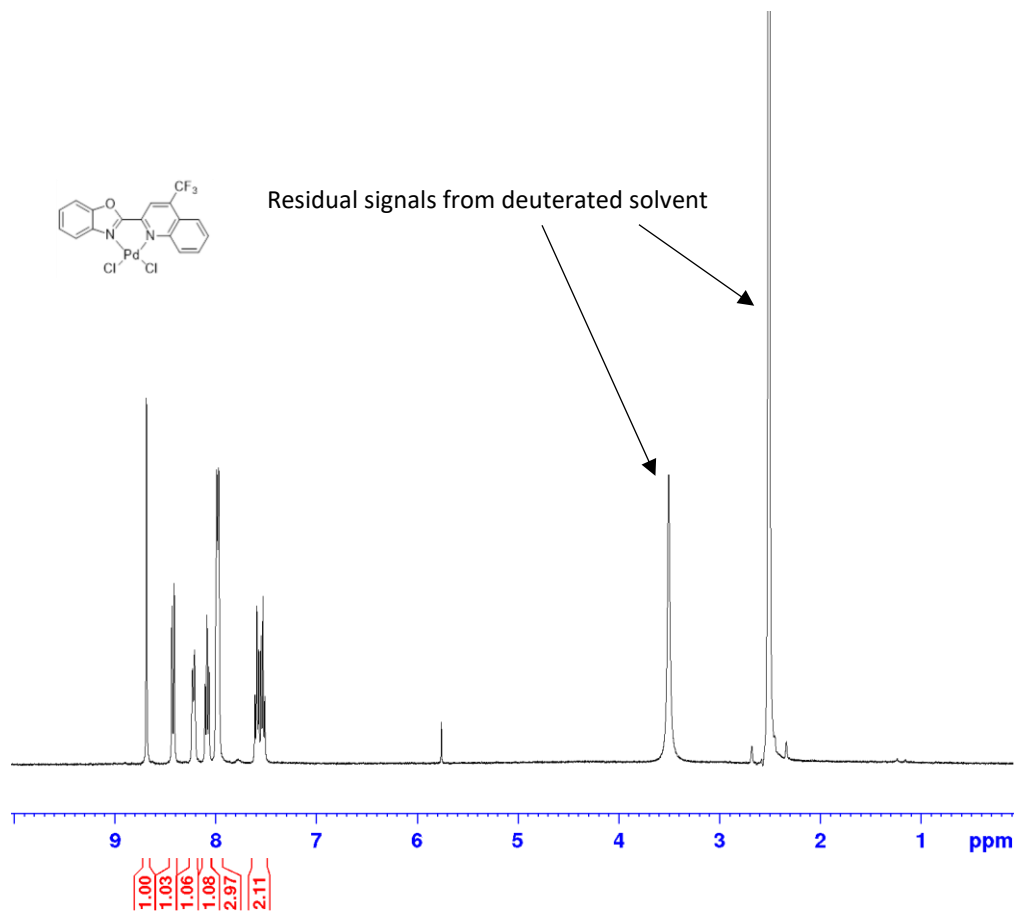
(2-(pyrimidin-2-yl)benzo[d]oxazole)PdCl₂: ¹H NMR (400 MHz) in DMSO-d₆

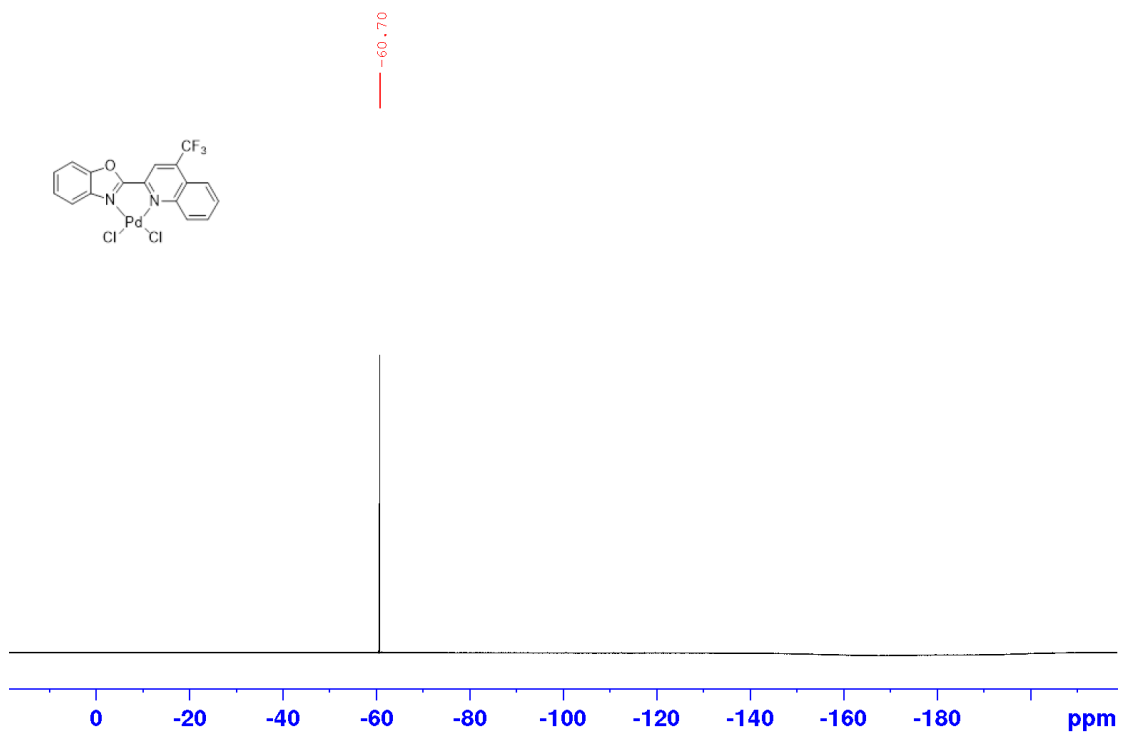


(2-(pyrazin-2-yl)benzo[d]oxazole)PdCl₂: ¹H NMR (400 MHz) in DMSO-d₆

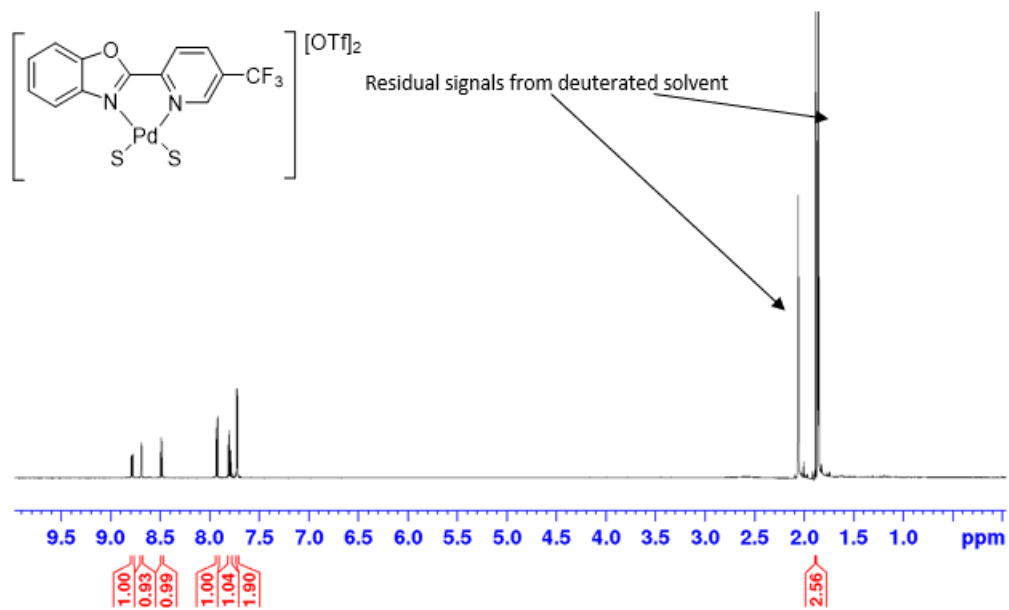


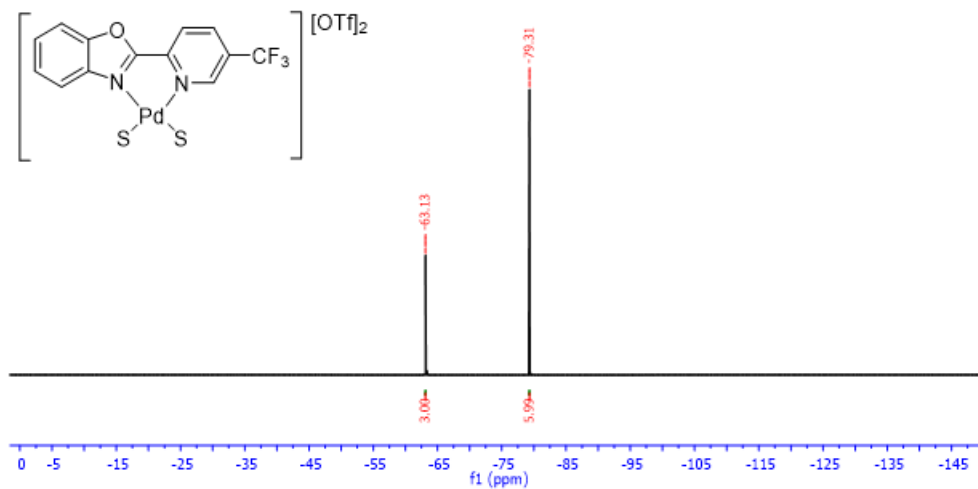
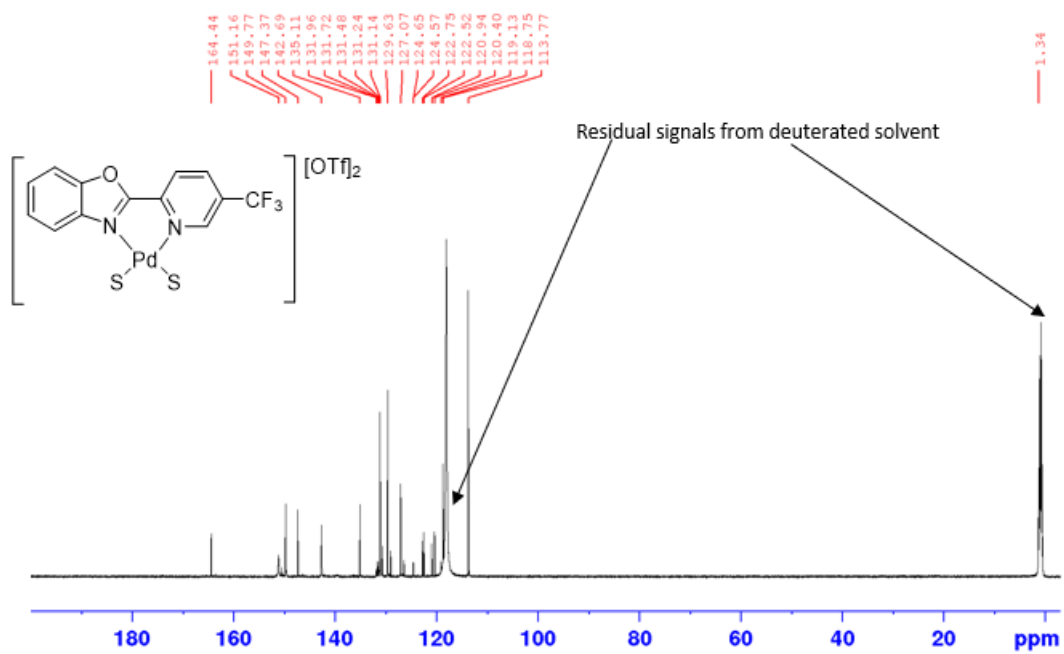
(2-(4-(trifluoromethyl)quinolin-2-yl)benzo[d]oxazole)PdCl₂: ¹H NMR (400 MHz) and ¹⁹F NMR (376 MHz) in DMSO-d₆



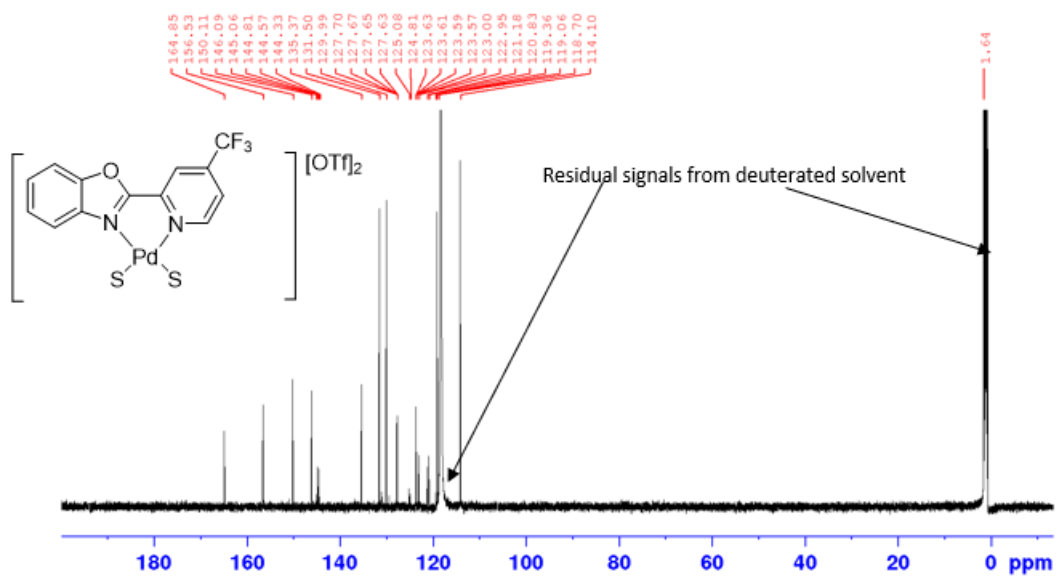
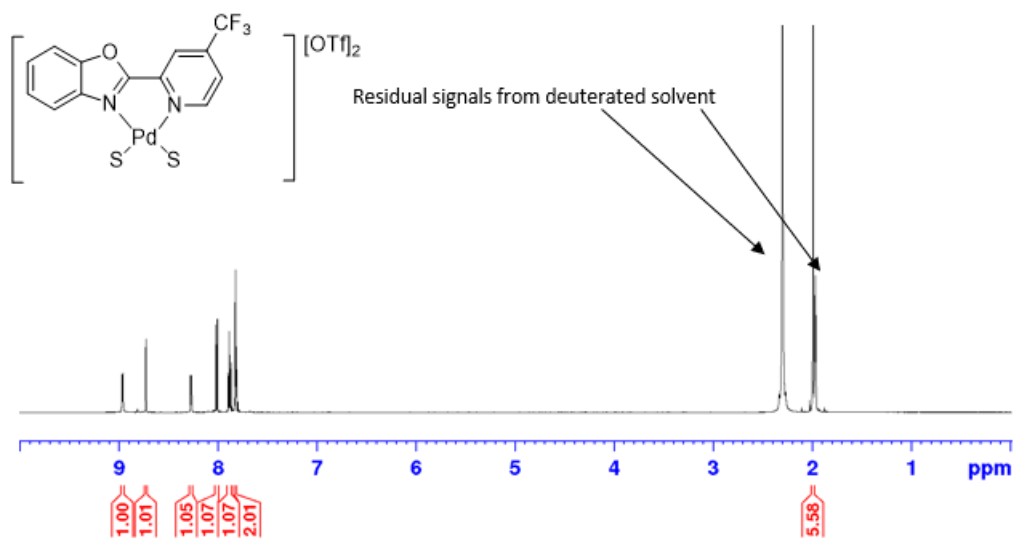


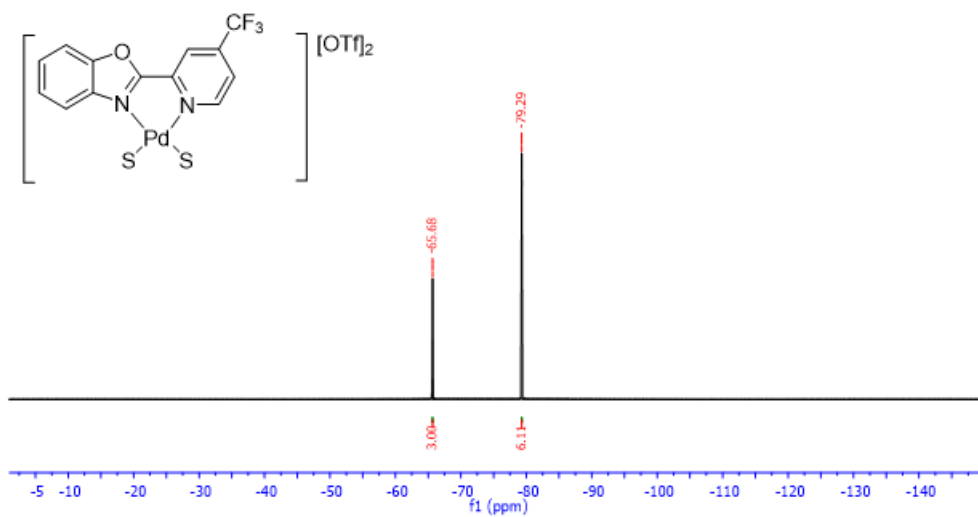
[(2-(5-(trifluoromethyl)pyridin-2-yl)benzo[d]oxazole)Pd(MeCN/H₂O)₂][OTf]₂: ¹H NMR (600 MHz), ¹³C NMR (151 MHz) and ¹⁹F NMR (565 MHz) in CD₃CN



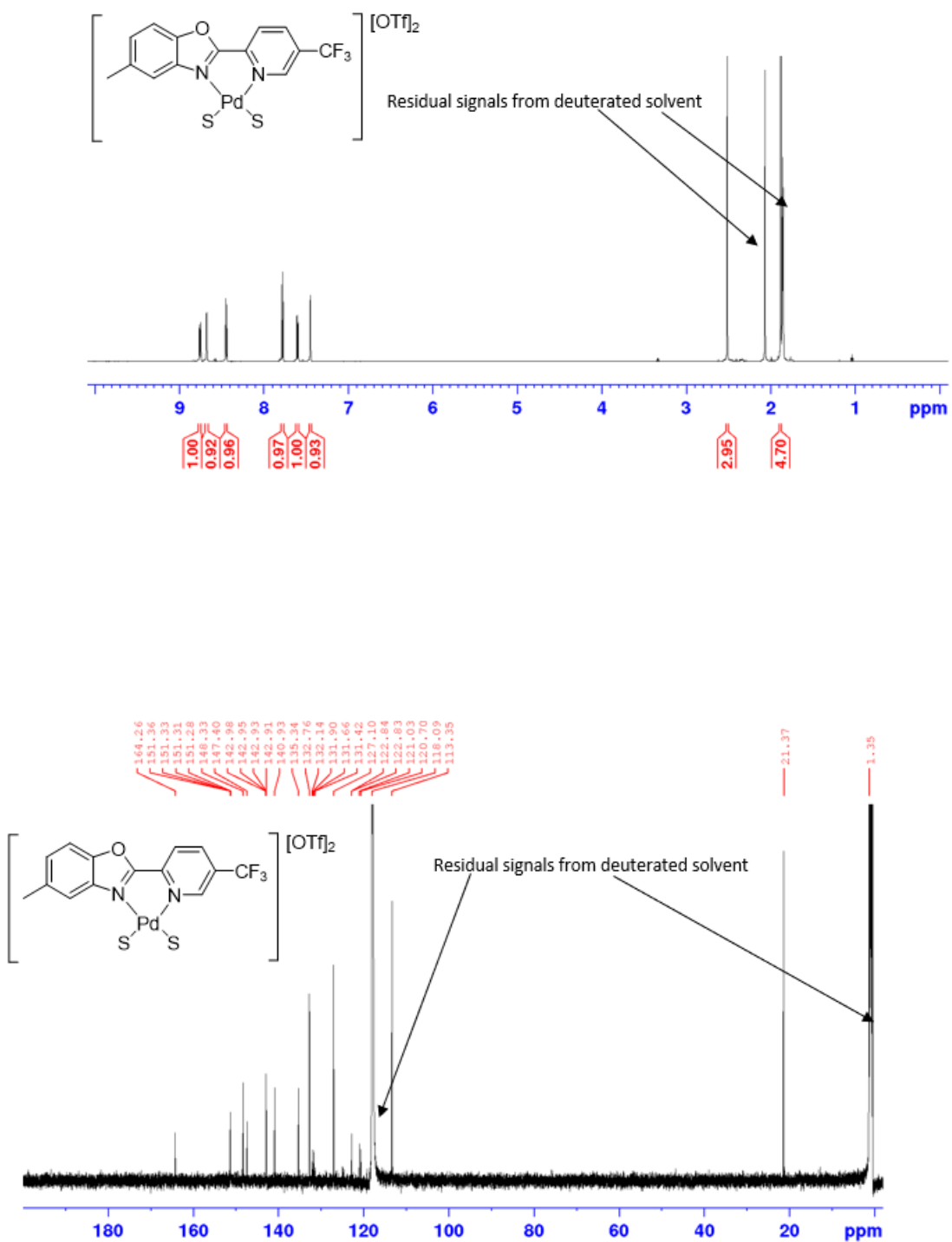


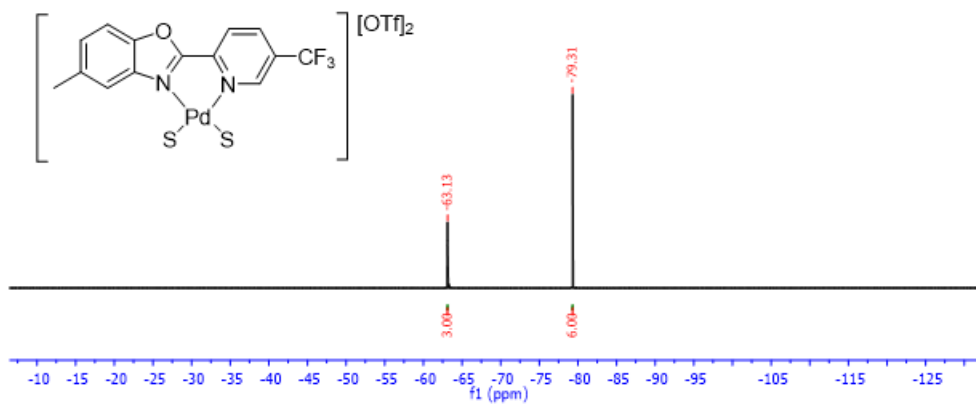
[(2-(4-(trifluoromethyl)pyridin-2-yl)benzo[d]oxazole)Pd(MeCN/H₂O)₂][OTf]₂: ¹H NMR (600 MHz), ¹³C NMR (151 MHz) and ¹⁹F NMR (565 MHz) in CD₃CN





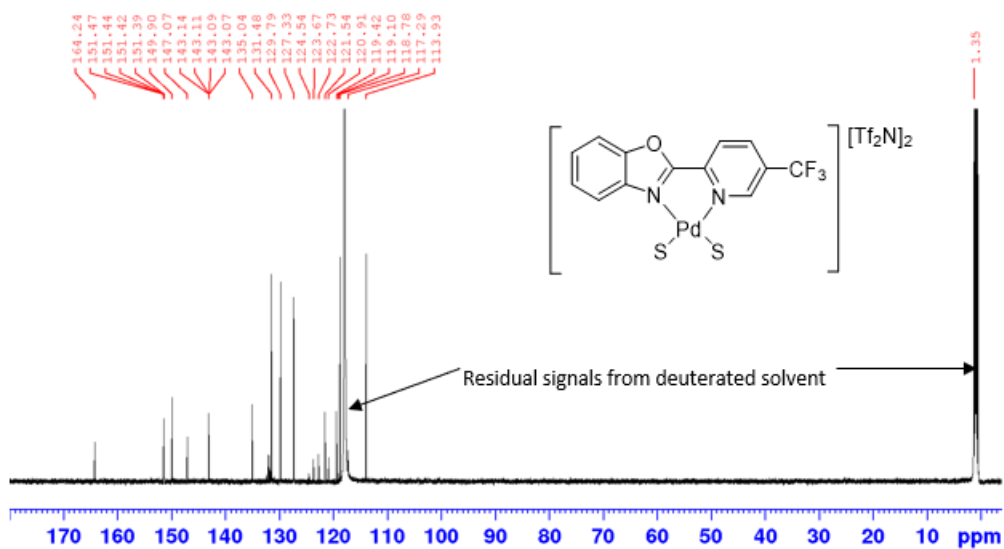
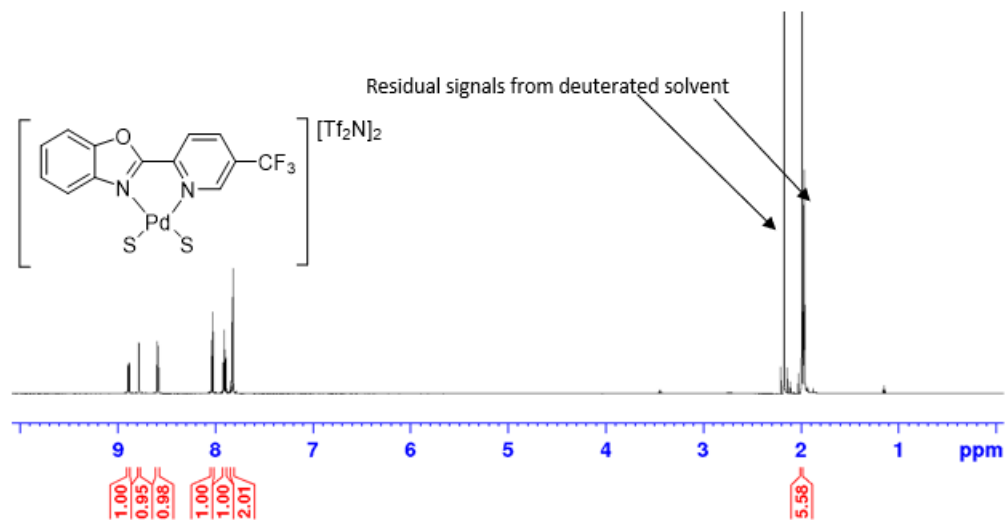
2-(5-Trifluoromethylpyridin-2-yl)-5-methylbenzo[d]oxazolePd(MeCN)₂(OTf)₂: ¹H NMR (600 MHz), ¹³C NMR (151 MHz) and ¹⁹F NMR (565 MHz) in CD₃CN

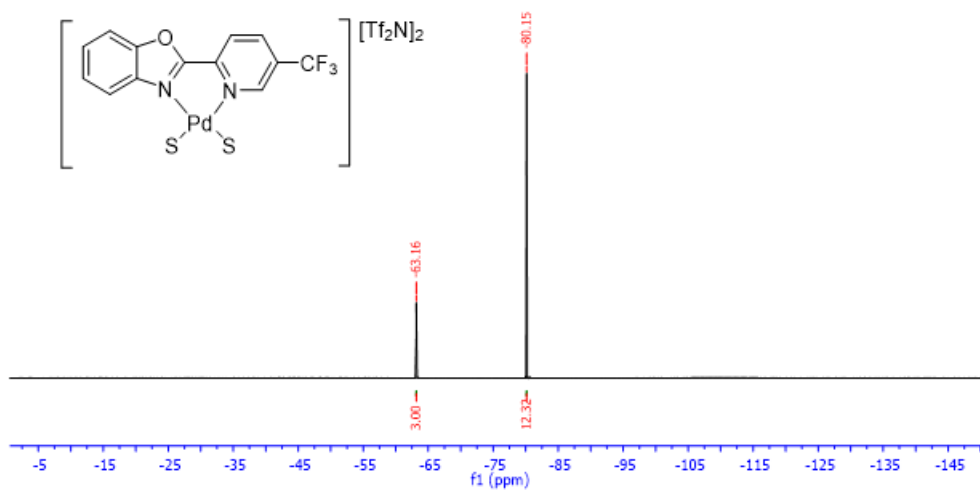




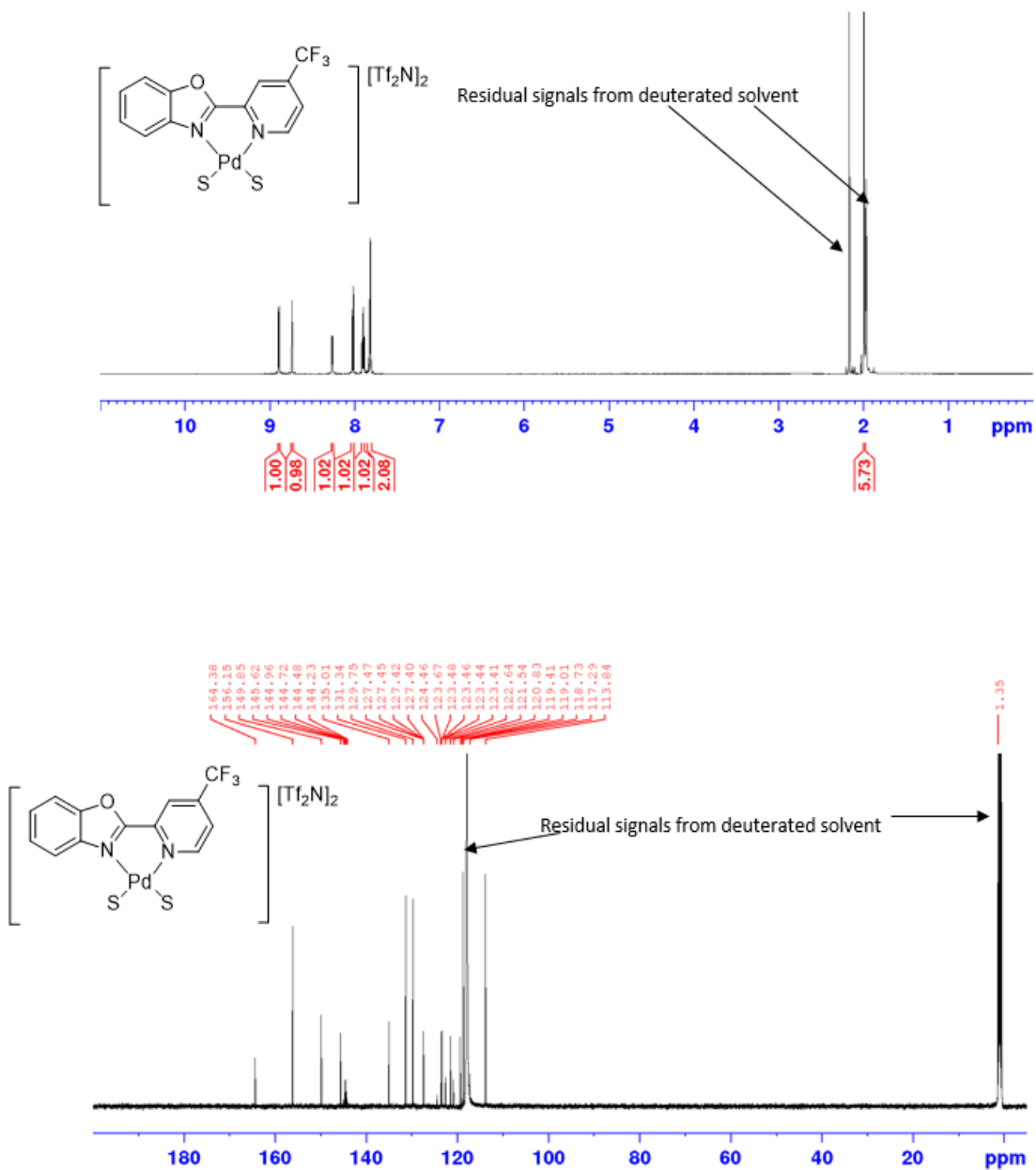
[(2-(5-(trifluoromethyl)pyridin-2-yl)benzo[d]oxazole)Pd(MeCN/H₂O)₂][Tf₂N]₂:

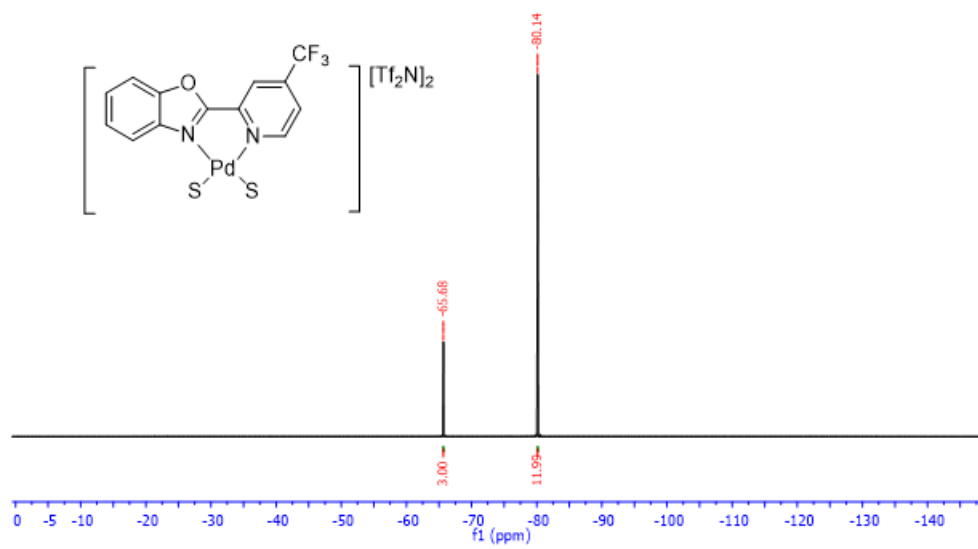
¹H NMR (600 MHz), ¹³C NMR (151 MHz) and ¹⁹F NMR (565 MHz) in CD₃CN



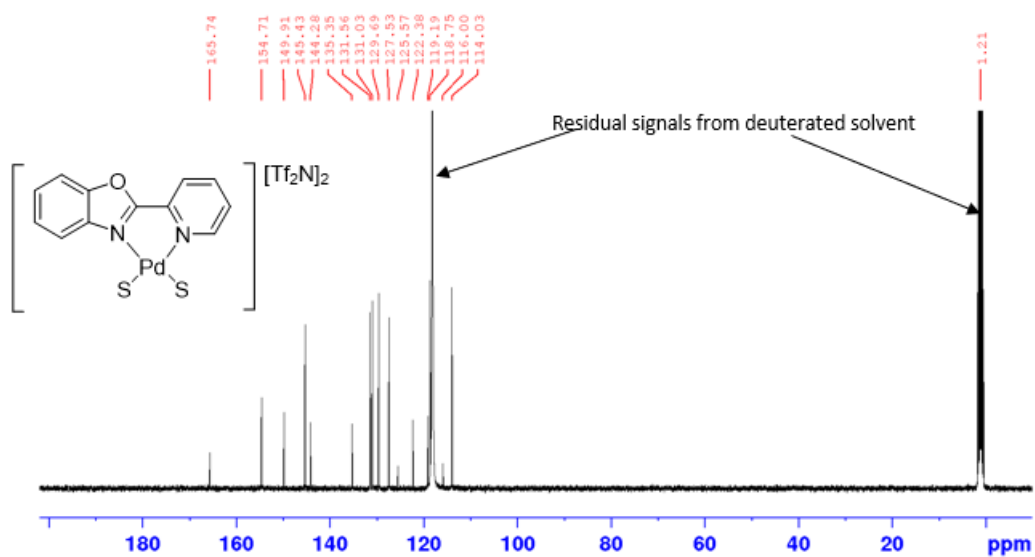
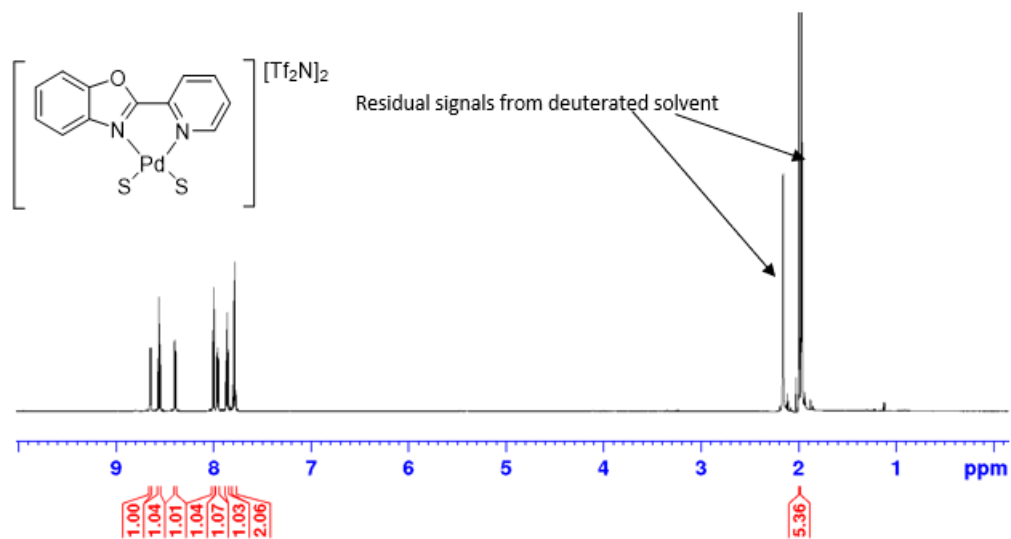


[(2-(4-(trifluoromethyl)pyridin-2-yl)benzo[d]oxazole)Pd(MeCN/H₂O)₂][Tf₂N]₂: ¹H NMR (600 MHz), ¹³C NMR (151 MHz) and ¹⁹F NMR (565 MHz) in CD₃CN

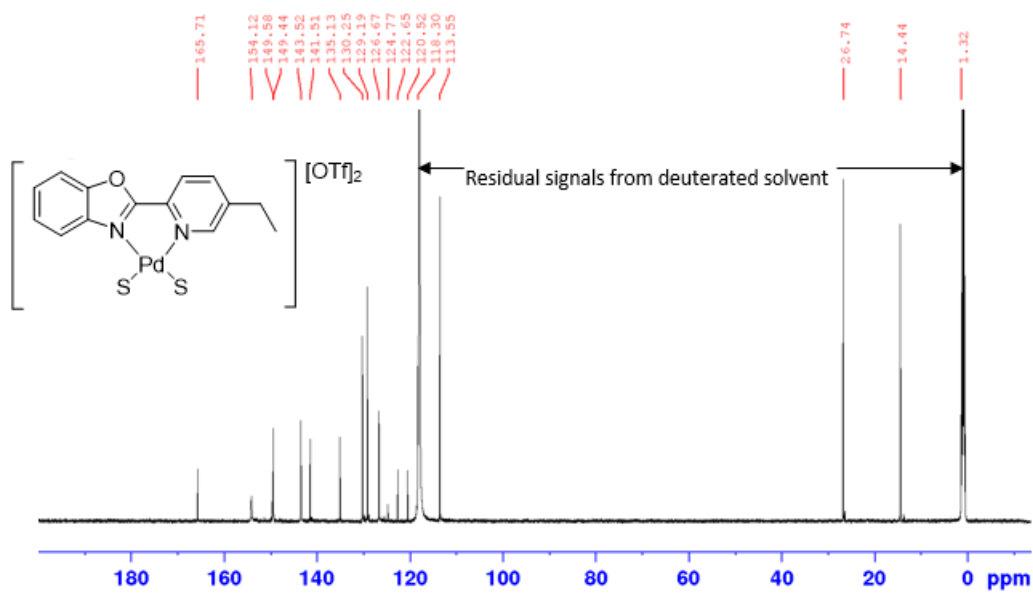
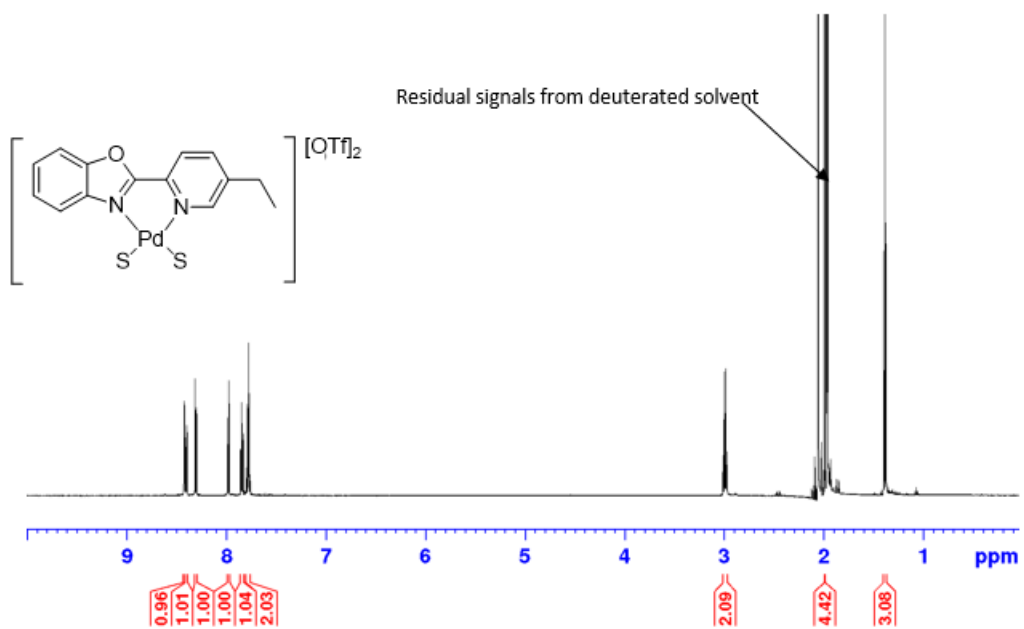




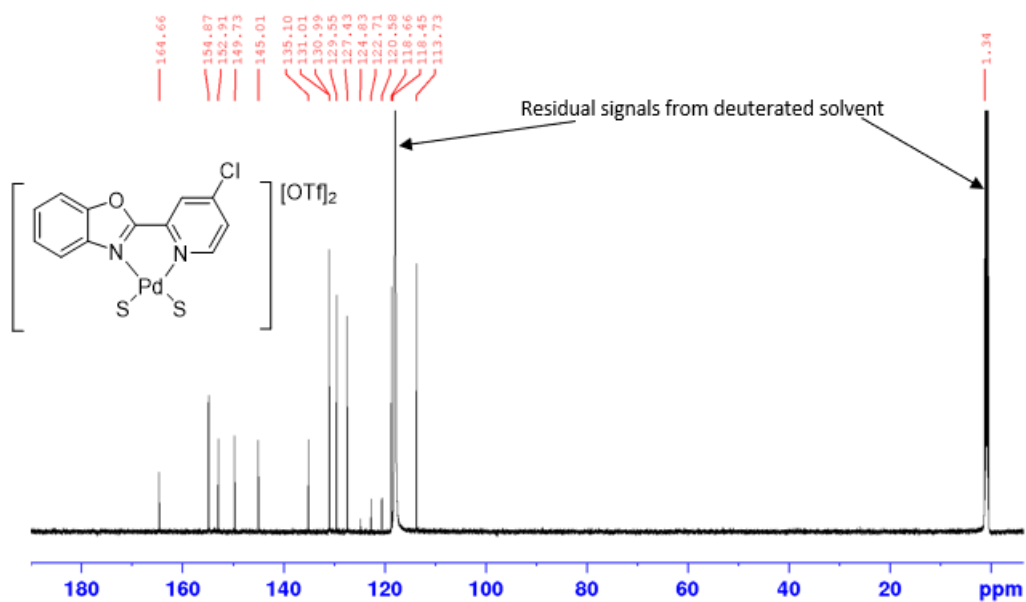
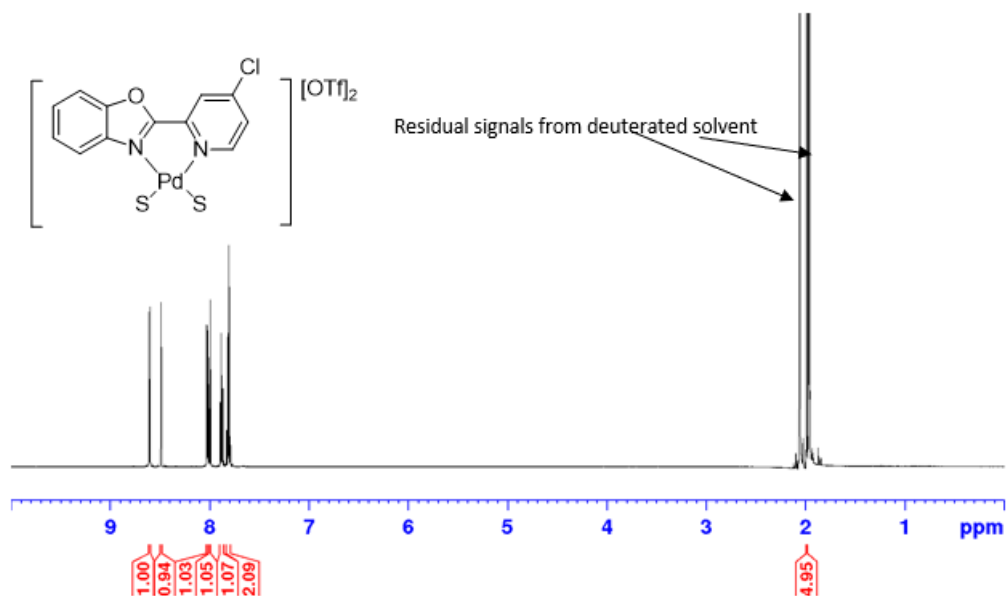
[(2-(pyridin-2-yl)benzo[d]oxazole)Pd(MeCN)₂][Tf₂N]₂: ¹H NMR (600 MHz) and ¹³C NMR (151 MHz)



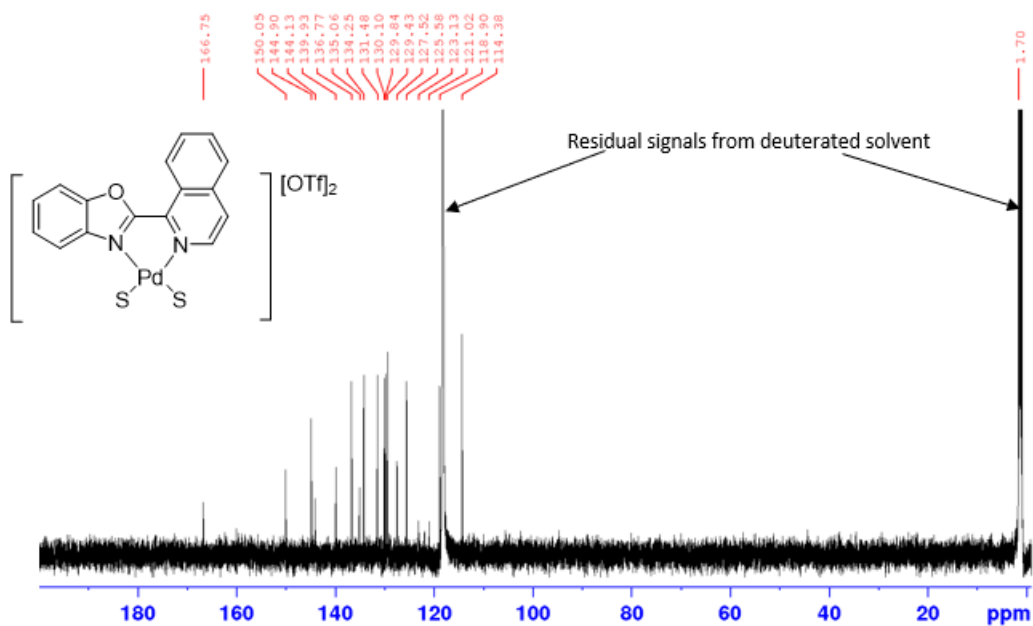
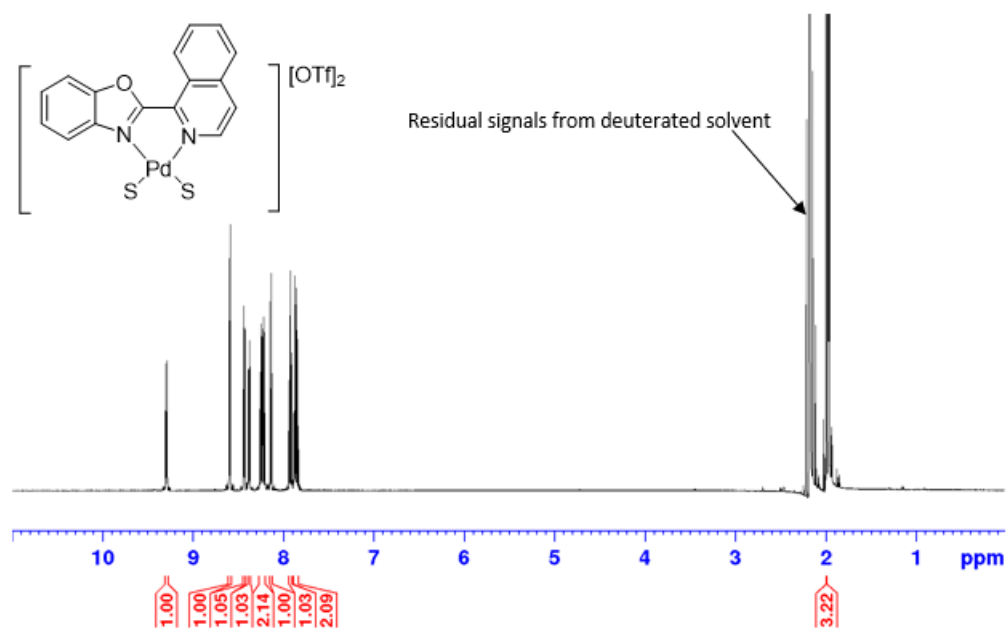
[(2-(5-ethylpyridin-2-yl)benzo[d]oxazole)Pd(NCMe)₂][OTf]₂: ¹H NMR (600 MHz) and ¹³C NMR (151 MHz) in CD₃CN



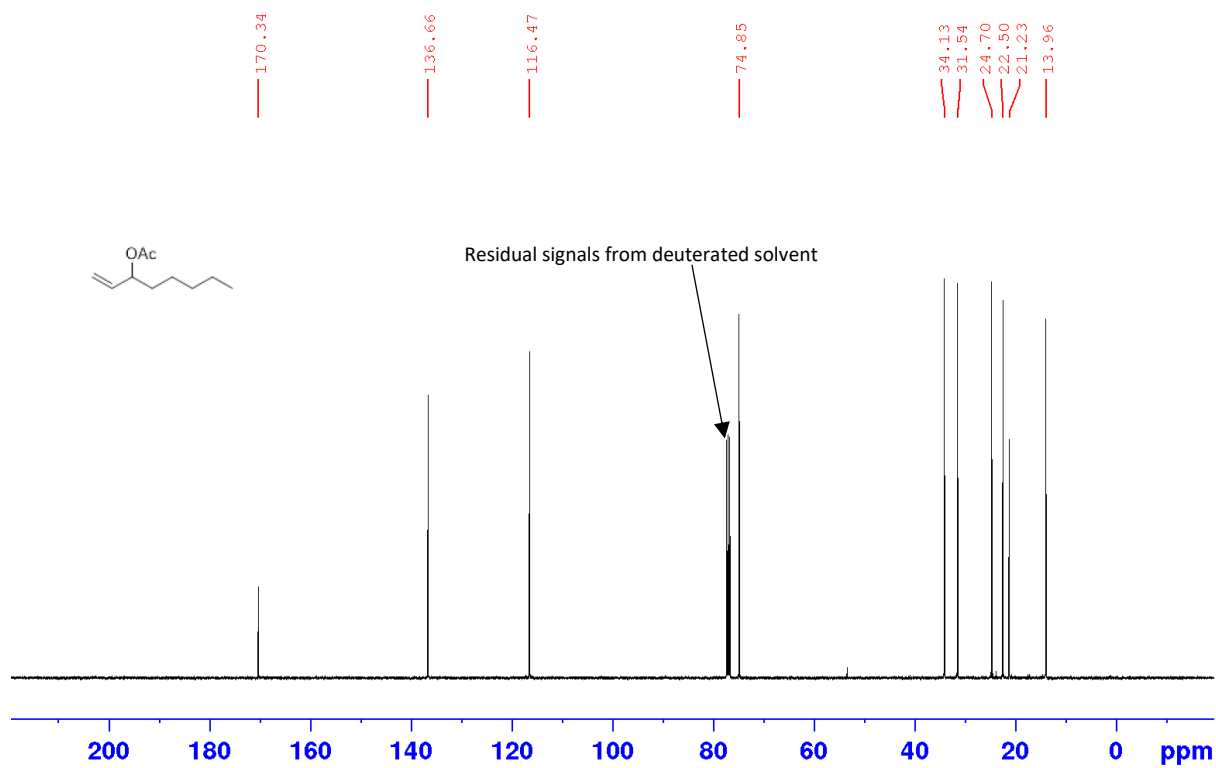
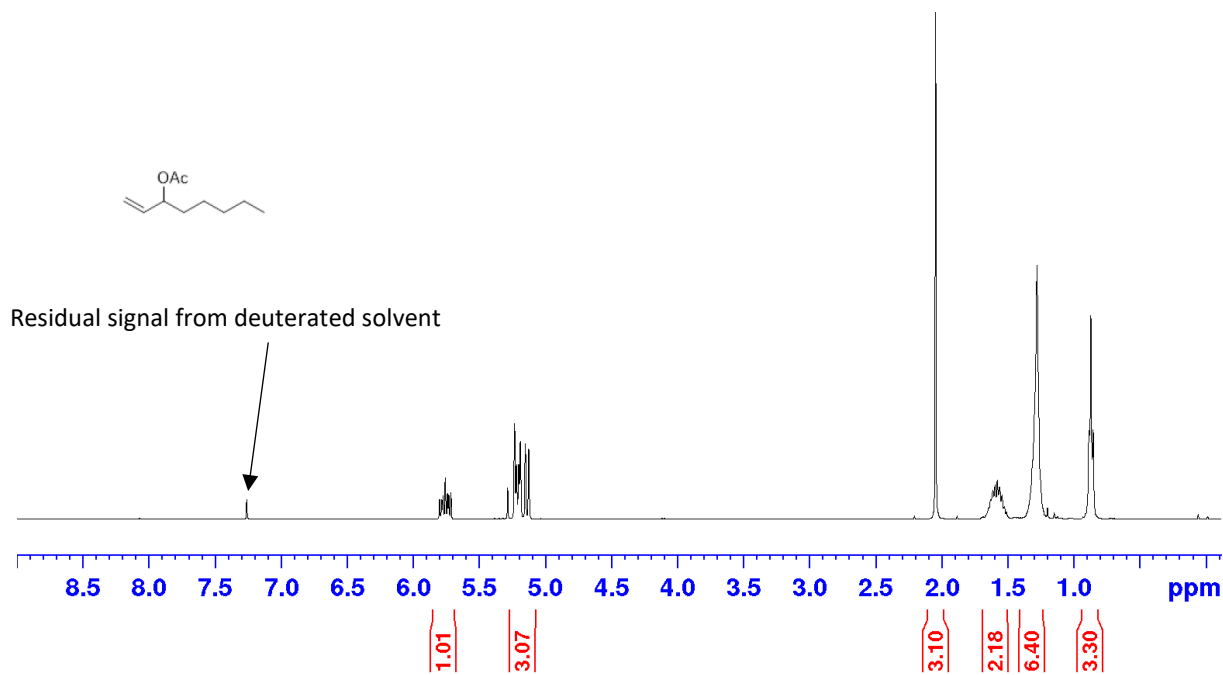
[(2-(4-chloropyridin-2-yl)benzo[d]oxazole)Pd(NCMe)₂][OTf]₂: ¹H NMR (600 MHz) and ¹³C NMR (151 MHz) in CD₃CN



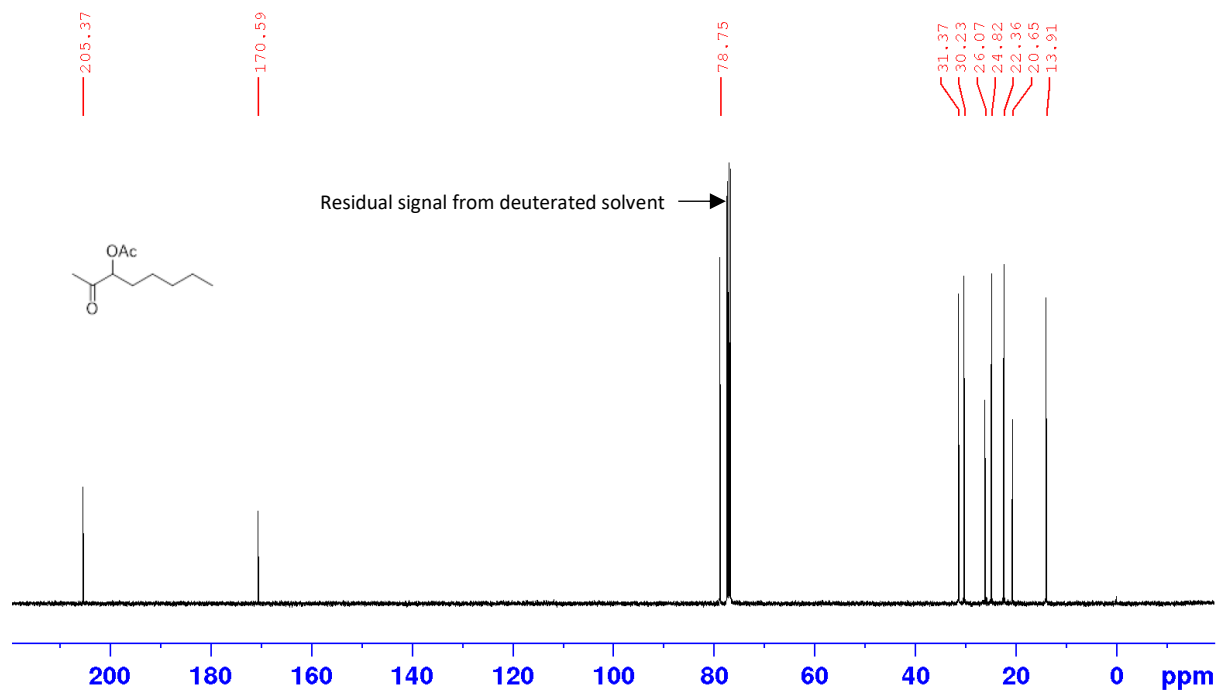
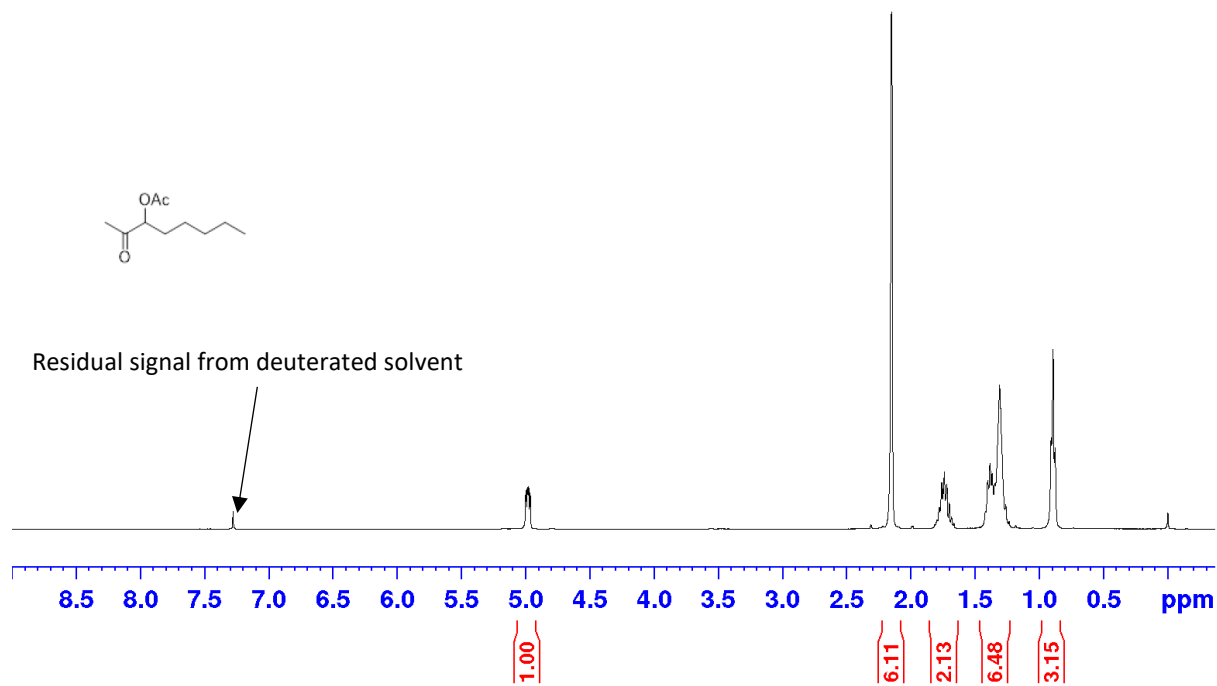
[(2-(isoquinolin-1-yl)benzo[d]oxazole)Pd(NCMe/H₂O)₂][OTf]₂: ¹H NMR (600 MHz) and ¹³C NMR (151 MHz) in CD₃CN



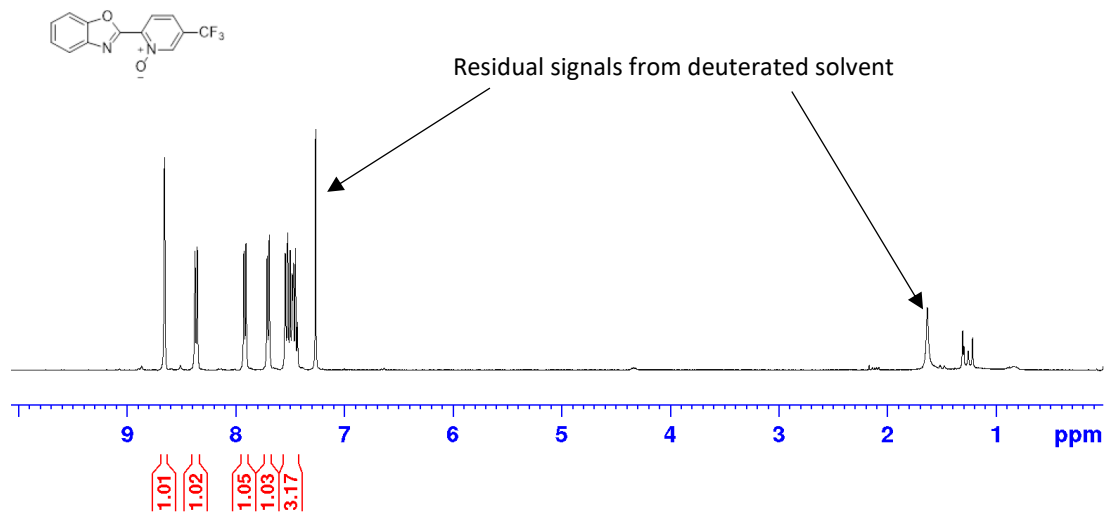
Oct-1-en-3-yl acetate: ¹H NMR (400 MHz) and ¹³C NMR (101 MHz) in CDCl₃

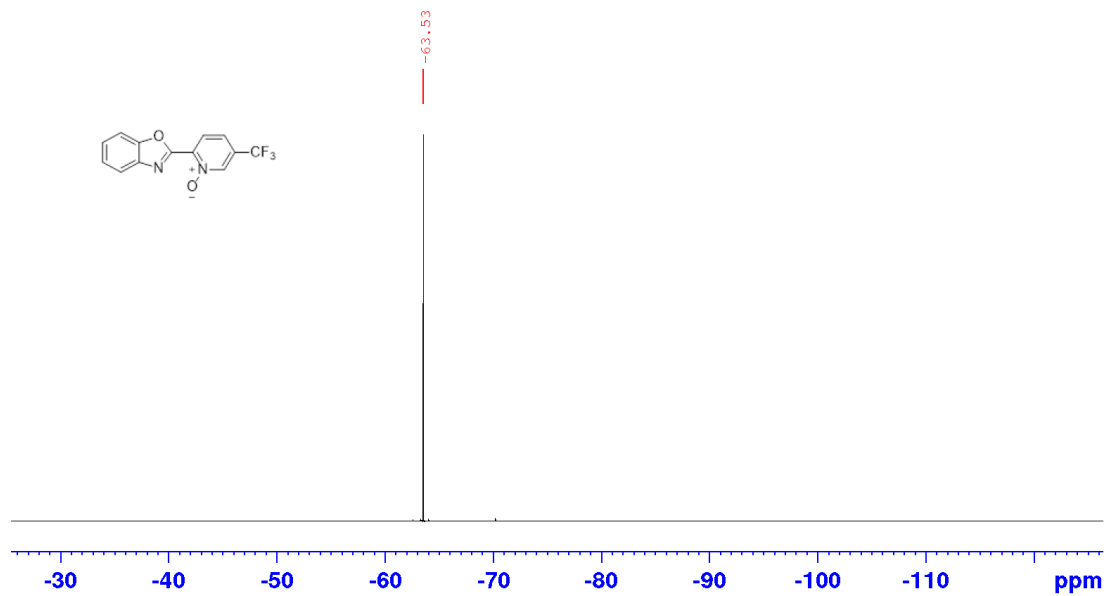
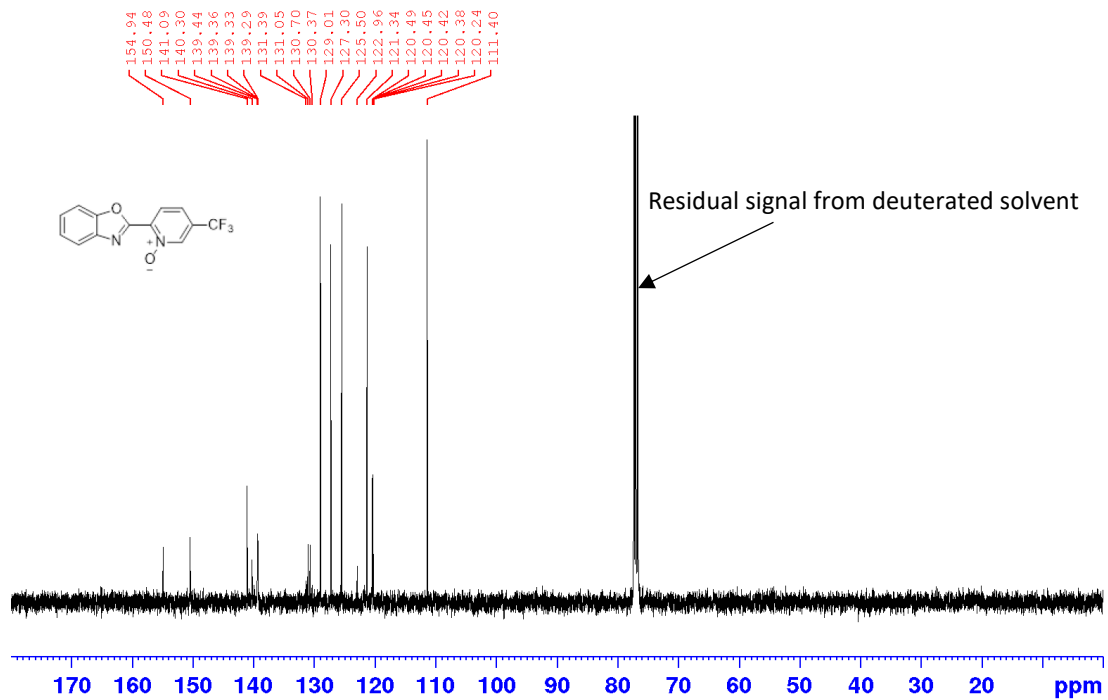


2-oxooctan-3-yl acetate: ^1H NMR (400 MHz) and ^{13}C NMR (101 MHz) in CDCl_3



2-(5-(trifluoromethyl)pyridin-2-yl)benzo[d]oxazole *N*-oxide: ^1H NMR (400 MHz), ^{13}C NMR (101 MHz) and ^{19}F NMR (376 MHz) in CDCl_3





References

1. Q. Cao, D. S. Bailie, R. Fu and M. J. Muldoon, *Green Chemistry*, 2015, **17**, 2750-2757.
2. K. L. Walker, L. M. Dornan, R. N. Zare, R. M. Waymouth and M. J. Muldoon, *Journal of the American Chemical Society*, 2017, **139**, 12495-12503.
3. H. Chai, Q. Cao, L. M. Dornan, N. L. Hughes, C. L. Brown, P. Nockemann, J. Li and M. J. Muldoon, *European Journal of Inorganic Chemistry*, 2017, **2017**, 5604-5608.
4. B. W. Michel, A. M. Camelio, C. N. Cornell and M. S. Sigman, *Journal of the American Chemical Society*, 2009, **131**, 6076-6077.
5. X.-B. Shen, Y. Zhang, W.-X. Chen, Z.-K. Xiao, T.-T. Hu and L.-X. Shao, *Organic Letters*, 2014, **16**, 1984-1987.
6. F. Derridj, S. Djebbar, O. Benali-Baitich and H. Doucet, *Journal of Organometallic Chemistry*, 2008, **693**, 135-144.
7. B. W. Michel, L. D. Steffens and M. S. Sigman, *Journal of the American Chemical Society*, 2011, **133**, 8317-8325.
8. J. E. Griffiths and G. E. Walrafen, *Inorganic Chemistry*, 1972, **11**, 427-429.
9. L. J. Gooßen, D. M. Ohlmann and M. Dierker, *Green Chemistry*, 2010, **12**, 197-200.
10. W. Zhao and J. Sun, *Chemical reviews*, 2018, **118**, 10349-10392.
11. L. Crowhurst, P. R. Mawdsley, J. M. Perez-Arlandis, P. A. Salter and T. Welton, *Physical Chemistry Chemical Physics*, 2003, **5**, 2790-2794.
12. M. J. Muldoon, C. M. Gordon and I. R. Dunkin, *Journal of the Chemical Society, Perkin Transactions 2*, 2001, 433-435.
13. G. W. Bushnell, K. R. Dixon, R. G. Hunter and J. J. McFarland, *Canadian Journal of Chemistry*, 1972, **50**, 3694-3699.
14. G. Sa´ nchez, A. Sanmarti´ n, J. n. Garcí a and G. Lo´ pez, *Transition metal chemistry*, 1997, **22**, 545-548.
15. L. J. Ackerman, J. P. Sadighi, D. M. Kurtz, J. A. Labinger and J. E. Bercaw, *Organometallics*, 2003, **22**, 3884-3890.
16. T. J. Williams, A. J. Caffyn, N. Hazari, P. F. Oblad, J. A. Labinger and J. E. Bercaw, *Journal of the American Chemical Society*, 2008, **130**, 2418-2419.
17. J. E. Bercaw, N. Hazari, J. A. Labinger and P. F. Oblad, *Angewandte Chemie International Edition*, 2008, **47**, 9941-9943.
18. J. R. Khusnutdinova, P. Y. Zavalij and A. N. Vedernikov, *Organometallics*, 2007, **26**, 2402-2413.
19. G.-J. ten Brink, I. W. Arends, G. Papadogianakis and R. A. Sheldon, *Applied Catalysis A: General*, 2000, **194**, 435-442.
20. A. J. Ingram, K. L. Walker, R. N. Zare and R. M. Waymouth, *Journal of the American Chemical Society*, 2015, **137**, 13632-13646.
21. R. J. Burford, W. E. Piers, D. H. Ess and M. Parvez, *Journal of the American Chemical Society*, 2014, **136**, 3256-3263.
22. Y. Zhao, U. K. Sharma, F. Schröder, N. Sharma, G. Song and E. V. Van der Eycken, *RSC advances*, 2017, **7**, 32559-32563.
23. P. Kumar, M. Gupta, V. Bahadur, V. S. Parmar and B. K. Singh, *European Journal of Organic Chemistry*, 2018, **2018**, 1552-1558.

24. R. M. Hanson and K. B. Sharpless, *The Journal of Organic Chemistry*, 1986, **51**, 1922-1925.
25. Y. Gao, J. M. Klunder, R. M. Hanson, H. Masamune, S. Y. Ko and K. B. Sharpless, *Journal of the American Chemical Society*, 1987, **109**, 5765-5780.
26. H. Mimoun, R. Charpentier, A. Mitschler, J. Fischer and R. Weiss, *Journal of the American Chemical Society*, 1980, **102**, 1047-1054.
27. M. Roussel and H. Mimoun, *The Journal of Organic Chemistry*, 1980, **45**, 5387-5390.
28. E. Gaster, S. Kozuch and D. Pappo, *Angewandte Chemie International Edition*, 2017, **56**, 5912-5915.
29. A. Berkessel, J. A. Adrio, D. Hüttenhain and J. M. Neudörfl, *Journal of the American Chemical Society*, 2006, **128**, 8421-8426.
30. H. F. Motiwala, C. Fehl, S.-W. Li, E. Hirt, P. Porubsky and J. Aubé, *Journal of the American Chemical Society*, 2013, **135**, 9000-9009.
31. N. Nishiwaki, R. Kamimura, K. Shono, T. Kawakami, K. Nakayama, K. Nishino, T. Nakayama, K. Takahashi, A. Nakamura and T. Hosokawa, *Tetrahedron Letters*, 2010, **51**, 3590-3592.
32. J. Ammer and H. Mayr, *Journal of Physical Organic Chemistry*, 2013, **26**, 59-63.
33. C. Hansch, A. Leo and R. Taft, *Chemical reviews*, 1991, **91**, 165-195.
34. L. Wang, Q. Yuan, W. Cao, J. Han, X. Zhou, S. Liu and X.-B. Wang, *The Journal of Physical Chemistry A*, 2020, **124**, 2036-2045.
35. Y.-W. Wang and C.-M. Shu, *Industrial & engineering chemistry research*, 2010, **49**, 8959-8968.
36. T. Willms, H. Kryk, J. Oertel, C. Hempel, F. Knitt and U. Hampel, *Thermochimica Acta*, 2019, **672**, 25-42.
37. R. Andreozzi, V. Caprio, S. Crescitelli and G. Russo, *Journal of Hazardous Materials*, 1988, **17**, 305-313.
38. Y.-W. Wang, *Industrial & engineering chemistry research*, 2012, **51**, 7845-7852.
39. B. Li, S. M. Guinness, S. Hoagland, M. Fichtner, H. Kim, S. Li, R. J. Maguire, J. C. McWilliams, J. Mustakis and J. Raggon, *Organic Process Research & Development*, 2018, **22**, 707-720.
40. M. Magosso, L. J. Hazen, M. Van den Berg and J. Van der Schaaf, *Industrial & Engineering Chemistry Research*, 2021, **60**, 15540-15548.
41. R. Mair and A. J. Graupner, *Analytical Chemistry*, 1964, **36**, 194-204.
42. V. S. Satam, S. R. Pedada, P. Kamaraj, N. Antao, A. Singh, R. M. Hindupur, H. N. Pati, A. M. Thompson, D. Launay and D. Martin, *Organic Process Research & Development*, 2017, **21**, 52-59.
43. K. B. Sharpless and R. T. Verhoeven, *Aldrichimica Acta*, 1979, **12**, 63-74.
44. J. G. Hill, B. E. Rossiter and K. B. Sharpless, *The Journal of Organic Chemistry*, 1983, **48**, 3607-3608.
45. W. W. Fleming and S. A. MacDonald, *Analytical Chemistry*, 1983, **55**, 1625-1626.
46. C. J. Mathews, P. J. Smith and T. Welton, *Journal of Molecular Catalysis A: Chemical*, 2004, **214**, 27-32.
47. T. Cantat, E. Génin, C. Giroud, G. Meyer and A. Jutand, *Journal of organometallic chemistry*, 2003, **687**, 365-376.
48. F. Derridj, J. Roger, F. Geneste, S. Djebbar and H. Doucet, *Journal of Organometallic Chemistry*, 2009, **694**, 455-465.

49. S. Yamada, K. Murakami and K. Itami, *Organic letters*, 2016, **18**, 2415-2418.
50. K. Amaike, K. Muto, J. Yamaguchi and K. Itami, *Journal of the American Chemical Society*, 2012, **134**, 13573-13576.
51. X. Chen, X. Cui, F. Yang and Y. Wu, *Organic letters*, 2015, **17**, 1445-1448.
52. S. Haneda, Z. Gan, K. Eda and M. Hayashi, *Organometallics*, 2007, **26**, 6551-6555.
53. Q. Cao, N. L. Hughes and M. J. Muldoon, *Chemistry—A European Journal*, 2016, **22**, 11982-11985.
54. K. Li, P. N. Horton, M. B. Hursthouse and K. K. M. Hii, *Journal of organometallic chemistry*, 2003, **665**, 250-257.
55. W. Kandiolter, J. Theiner, B. K. Keppler and C. R. Kowol, *Inorganic Chemistry Frontiers*, 2022, **9**, 412-416.
56. R. E. Kuveke, L. Barwise, Y. van Ingen, K. Vashisth, N. Roberts, S. S. Chitnis, J. L. Dutton, C. D. Martin and R. L. Melen, *Journal*, 2022.
57. S. Proctor, S. Lovera, A. Tomich and V. Lavallo, *Journal*, 2022.
58. F. P. Gabbaï, P. J. Chirik, D. E. Fogg, K. Meyer, D. J. Mindiola, L. L. Schafer and S.-L. You, *Journal*, 2016, **35**, 3255-3256.
59. M. de Greef and S. Z. Zard, *Organic Letters*, 2007, **9**, 1773-1776.
60. S. Caron, N. M. Do and J. E. Sieser, *Tetrahedron Letters*, 2000, **41**, 2299-2302.
61. J. t. Cosier and A. Glazer, *Journal of Applied Crystallography*, 1986, **19**, 105-107.
62. R. O. Diffractionu, *Yarnton, England*, 2015.
63. G. M. Sheldrick, *Acta Crystallographica Section C: Structural Chemistry*, 2015, **71**, 3-8.
64. P. W. Betteridge, J. R. Carruthers, R. I. Cooper, K. Prout and D. J. Watkin, *Journal of Applied Crystallography*, 2003, **36**.
65. R. I. Cooper, A. L. Thompson and D. J. Watkin, *Journal of Applied Crystallography*, 2010, **43**, 1100-1107.
66. S. Parsons, H. D. Flack and T. Wagner, *Acta Crystallographica Section B: Structural Science, Crystal Engineering and Materials*, 2013, **69**, 249-259.